GeoRS

Geopedology and Landscape Development
Research Series

VOLUME 03

Spatial and temporal development of sediment mass balances during the initial phase of landform evolution in a small catchment

Anna Schneider

Brandenburg
University of Technology
Cottbus - Senftenberg

ISSN 2196 - 4122

ISSN 2196 - 4122

GeoRS 03

Spatial and temporal development of sediment mass balances during the initial phase of landform evolution in a small catchment

Anna Schneider

GeoRS

Geopedology and Landscape Development
Research Series

VOLUME 03

Spatial and temporal development of sediment mass balances during the initial phase of landform evolution in a small catchment

Anna Schneider

Brandenburg
University of Technology
Cottbus - Senftenberg

This series is edited by
Prof. Dr. Thomas Raab

Brandenburg University of Technology Cottbus - Senftenberg
Konrad-Wachsmann-Allee 6
03046 Cottbus
Germany

ISSN 2196 - 4122
www.tu-cottbus.de/geopedologie

Geopedology and Landscape Development
Research Series
GeoRS
VOLUME 03

Spatial and temporal development of sediment mass balances during the initial phase of landform evolution in a small catchment

Raum-zeitliche Entwicklung von Sedimentmassenbilanzen während der Initialphase der Reliefentwicklung in einem kleinen Einzugsgebiet

Von der Fakultät für Umweltwissenschaften und Verfahrenstechnik der
Brandenburgischen Technischen Universität Cottbus-Senftenberg
zur Erlangung des akademischen Grades eines doctor rerum naturalium
(Dr. rer. nat.) genehmigte Dissertation

Vorgelegt von: Dipl. Geogr. Anna Schneider, geb. am 26.09.1982 aus Straubing

Gutachter: Prof. Dr. Dr. h.c. Reinhard F. Hüttl
Gutachter: PD. Dr. habil. Horst H. Gerke
Gutachter: Asst/Prof Dr. habil. Matthias Leopold
Tag der mündlichen Prüfung: 21.08.2013

Abstract

The central topic of this dissertation is the 3D spatial description of geomorphic and sediment mass balance development in initial phases of ecosystem development. The introductory chapters give an overview on the consideration of characteristics and relevance of the initial development phase in geomorphological landform development concepts and summarize the state of the art of research for experimental studies on landform development and for 3D soil-landscape modeling approaches. The central aim of the work is a 3D-spatially and temporally resolved description of the development of mass balances of the sediment solid phase during the initial years of ecosystem development and of its dependence on initial and boundary conditions in the 6 ha, artificially-created catchment 'Hühnerwasser'. This aim is approached using remotely-sensed data, methods of quantitative soil-landscape modeling and geomorphic change detection, and the application of a numerical landscape evolution model. The construction of a 3D volume model of the catchment's sediment body based on digital elevation data is described. Possibilities for the quantification of sediment mass balances and for the 3D spatial description of sediment properties within this model are discussed. Digital elevation models based on airborne and terrestrial laser scanning and photogrammetry are evaluated for their suitability for sediment mass balance quantification and reconstruction of initial morphologic development; and methods for the modification and combination of elevation data for improved sediment mass balance quantification are described. The development of the catchment's surface morphometry and of the geometry of the evolving erosion rill network is reconstructed and analysed based on aerial photographs and digital elevation models. Relations between structures of the initial surface and the developing hydro-geomorphic structures are discussed. Effects of initial surface morphology and precipitation characteristics during the initial development phase are further assessed by simulations with a numeric landscape evolution model. Results allow for a quantification of geometry and volume of the catchment's initial sediment body and for a visualization of sediment layers deposited in time intervals. It is shown that a combination of different elevation data, based on their suitability for depicting the sediment surface in areas of different morphologic and vegetation characteristics, allows for an improved quantification of sediment mass balances. Results allow for a characterization of phases of rill network growth, contraction and stabilization and suggest influences of initial morphology, precipitation characteristics, and developing structure-process-interactions on rill network geometry in the catchment. The phases of hydro-geomorphic surface structure evolution can be related to the spatial organization of surface flow patterns during initial phases of landform development.

Kurzfassung

Die vorliegende Dissertation behandelt die 3D-räumliche Beschreibung der Entwicklung von Morphologie und Sedimentmassenbilanzen für Initialphasen der Ökosystementwicklung. Die einleitenden Kapitel geben einen Überblick über die Behandlung von Charakteristika und Relevanz der Initialphase der Reliefentwicklung in der geomorphologischen Systemtheorie und über den Stand der Forschung zu empirischen Untersuchungen zur initialen Reliefentwicklung und zu Methoden der 3D-räumlichen Modellierung von Relief- und Landschaftsentwicklung. Zentrale Ziele dieser Arbeit sind die Beschreibung von Sedimentmassenbilanzen während der ersten Jahre der Ökosystementwicklung im 6 ha großen, künstlich angelegten Wassereinzugsgebiet 'Hühnerwasser' in 3D-räumlicher und zeitlicher Auflösung und die Charakterisierung der Abhängigkeit dieser Entwicklung von den Ausgangs- und Randbedingungen. Die Fragestellung wird mithilfe von Fernerkundungsdaten, Methoden der quantitativen Bodenlandschaftsmodellierung und Simulationen mit einem Landschaftsentwicklungsmodell bearbeitet. Die Konstruktion eines 3D-Volumenmodells des Sedimentkörpers des Einzugsgebiets auf Basis von Höhendaten wird beschrieben, und Möglichkeiten zur Quantifizierung von Sedimentmassenbilanzen und zur 3D-räumlichen Beschreibung von Sedimenteigenschaften in einem solchen Modell werden aufgezeigt und diskutiert. Die Eignung von digitalen Höhenmodellen aus terrestrischem und airborne laser scanning und aus Photogrammetrie sowie Möglichkeiten der Weiterbearbeitung dieser Daten zur Quantifizierung von Sedimentmassenbilanzen werden untersucht. Auf Basis von Luftbildern und digitalen Geländemodellen werden Entwicklungsstadien der Oberflächenmorphologie und der Geometrie des sich entwickelnden Gerinnenetzes und ihre Abhängigkeit von Ausgangs- und Randbedingungen charakterisiert. Der Einfluss von initialen Oberflächenstrukturen und Niederschlagscharakteristika auf diese Entwicklung wird über Simulationen mit einem Landschaftsentwicklungsmodell weiter bewertet. Die Ergebnisse ermöglichen eine Quantifizierung von Geometrie und Volumen des initialen Sedimentkörpers und eine Visualisierung von in verschiedenen Zeiträumen abgelagerten Sedimentschichten. Die beschriebenen Methoden zur Weiterbearbeitung und Kombination verschiedener Höhendaten auf Basis ihrer jeweiligen Eignung zur Darstellung der Oberfläche in Bereichen unterschiedlicher Morphologie und Vegetationsbedeckung ermöglichen eine verbesserte Quantifizierung von Sedimentmassenbilanzen für das Einzugsgebiet. Die Ergebnisse zeigen Phasen der Ausbreitung und anschließenden Stabilisierung des Netzwerks von Erosionsrinnen und deuten auf Einflüsse der initialen Oberflächenstrukturen, der Niederschlagsverteilung und sich entwickelnder Struktur-Prozess-Rückkopplungen auf diese Entwicklung hin. Die beobachteten Phasen der morphologischen Entwicklung können vor dem Hintergrund der räumlichen Organisation von Oberflächenabflussmustern und sich verändernder Randbedingungen während der Initialphase der Reliefentwicklung charakterisiert werden.

Contents

List of abbreviations and symbols

1 /2 /3D	one-/ two-/ three-dimensional
A, A_{2D}	area [m^2]
A_{3D}	total surface area of a TIN, integrating the area of all elements [m^2]
ALS	airborne laser scanning
a.s.l.	above sea level
AGL	above ground level
CA	Contributing Area [number of DEM cells]
D	diameter (CAESAR model) [m]
D50	median particle diameter (CAESAR model) [m]
DD	drainage density [km km^{-2}]
dw	depth of surface flow (CAESAR model) [m]
Dx	grid cell size (CAESAR model) [m]
dz	elevation difference, vertical distance between DEM values [m]
DEM	digital elevation model
(d-)GPS	(differential) global positioning system
E	energy expenditure for the total rill network [-]
g	gravitational acceleration (CAESAR model) [m s^{-1}]
GIS	geographic information system
IC	index of connectivity [-]
j	soil moisture storage (CAESAR model)
K	substrate hydraulic conductivity (CAESAR model) [m s^{-1}]
L	length [m]
LEM	landscape evolution model
LIDAR	Light Detection and Ranging
m	TOPMODEL parameter (CAESAR model) [-]
ME	mean error
MinQ	minimum discharge for runoff depth calculation (CAESAR model) [$m^3 s^{-1}$]
n	Manning's coefficient (CAESAR model) [-]
NE	north-eastern
P	rates of energy expenditure for a rill segment [-]
photo_	prefix for photogrammetry-based DEMs

Q	surface fraction of water discharge (CAESAR model) [m^3s^{-1}]
Qtot	total water discharge (CAESAR model) [m^3s^{-1}]
Qs	volumetric sediment transport rate (CAESAR model) [m^3s^{-1}]
R	ratio of A_{3D} to A_{2D}, used as an indicator of surface roughness [-]
r	rainfall rate (CAESAR model) [$m^{-1}h^{-1}$]
RMSE	root mean square error
RTK	realtime kinematic
S	sinuosity [-]
SDME	error standard deviation
SE	soil erosion
SPI	stream power index [-]
SW	south-western
T	t-statistic
t	time or time step
TIN	triangulated irregular network
TLS	terrestrial laser scanning
TWI	topographic wetness index [-]
U	flow velocity (CAESAR model) [m s^{-1}]
V	volume [m3]
v	settling velocity (CAESAR model) [m s^{-1}]
Var	Variance
wdet	minimum runoff depth for erosion calculation (CAESAR model) [m]
Z	local elevation value [m a.s.l.]

β	slope
ρ	density [kg m^{-3}]
σ	standard deviation
τ	shear stress (CAESAR model) [Pa]
ϕ	dimensionless bedload transport rate (CAESAR model) [-]
ψ	balance of forces moving and restraining particles (CAESAR model)

List of Figures

List of Tables

1 General Introduction

1.1 Relevance of initial conditions and the initial phase of landform development

When sediment bodies are newly exposed to the surface or to considerably differing exogenic conditions, surface development by geomorphic processes, along with other processes of ecosystem development, starts from "point zero". During this initial phase of landform development, the surface of sediment bodies is commonly liable to rapid change by accelerated geomorphic activity, as surfaces are not yet adapted to the environmental boundary conditions. Geomorphic processes acting during initial phases of landform development are affected by several initial and boundary conditions, but also cause the formation of landscape structures that constitute boundary conditions for further ecosystem development. Just as in other phases of landform development, gravitational, aeolian, and fluvial processes can shape land surfaces during the initial phase of development. However, an important characteristic of the initial phase of landform development is the highly limited influence of biota (Ballantyne, 2002; Corenblit et al., 2007; Raab et al., 2012), which implies that the sediment surface is directly exposed to the influences of meteorological forcing. Sediment redistribution in this phase is therefore mainly influenced by meteorological characteristics, by initial surface topography, and by sediment characteristics. Fig. 1.1 gives a schematic overview on controls and processes of landform development in the initial phase, as summarized in the following paragraphs.

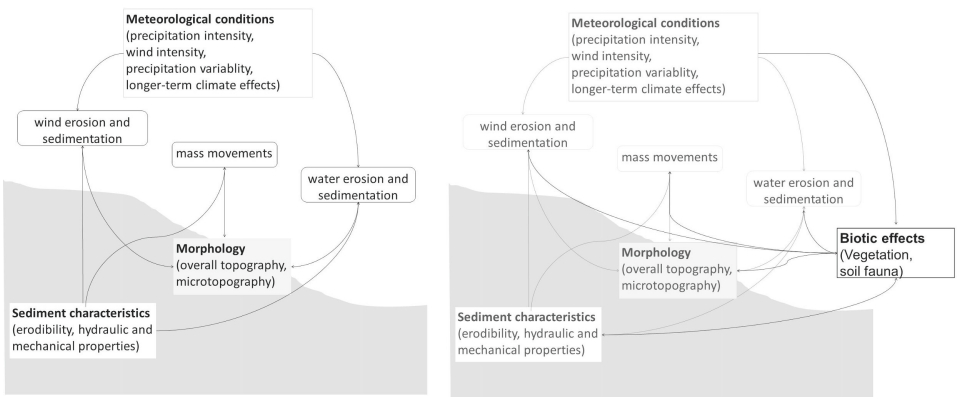

Figure 1.1: Schematic overview on major controls and processes of initial landform development with limited influence of biota (left) and added complexity with biota development (right).

Sediment erosion by wind can considerably contribute to landform development on bare surfaces. Wind erosion is directly affected by meteorological characteristics through wind velocity, and is indirectly affected through climate effects on soil structure formation and effects of precipitation characteristics on substrate moisture, which influence the sediments' susceptibility to wind erosion (De Oro and Buschiazzo, 2009; Kohake et al., 2010). The effects of sediment erosion by water on land surface development differ considerably between processes of diffusive erosion, i.e., rain splash and sheet wash, and erosion resulting from concentrated surface flow. The effects of rain splash and sheet wash are limited to a spatially distributed sediment redistribution over comparably short distances, but the relation of diffusive to convective transport can affect the geometry of developing drainage networks (McGuire et al., 2013). Sediment redistribution by water is directly influenced by precipitation intensity, and is indirectly influenced by meteorological conditions through effects on substrate hydraulic properties, which affect the generation of surface runoff, and on substrate mechanical properties which control erosion susceptibility. Initial topography affects geomorphic development at different scales: The overall slope of the surface is decisive for the occurrence and intensity of gravitational mass movement and of water erosion processes by affecting the velocity and thus the erosive power of surface flow. Local variations in topography mainly affect the erosive power of wind and water by the distribution and routing of flows, and the position of a location within the slope is relevant for the amount of accumulated flow. Microtopography and sediment characteristics affect the sediment's infiltration behavior and thus the partitioning of precipitation in infiltration and surface runoff (as shown, e.g., by Kuhn and Yair (2004) and van Schaik (2009)). Furthermore, surface development is influenced by the direct and interacting effects of a high number of sediment characteristics on the resistance of the sediment to erosional processes that have been summarized in the concept of soil erodibility, as reviewed and discussed by Bryan (2000). Small-scale sediment-water interactions, e.g., processes of soil structural breakdown, can further affect larger scale runoff-generation and hydro-geomorphic surface development (Greene and Hairsine, 2004). As summarized by Auzet et al. (2004), effects and relevance of sediment properties for erosion processes highly vary with the scale of observations.

With the establishment and growth of vegetation cover during further system development, the mainly stabilizing effects of vegetation on the surface gradually increase. During this transition period, the number of system components affecting surface development directly and by interacting effects considerably increases (Fath et al., 2004). Vegetation cover has direct stabilizing effects, e.g., by shielding the sediment surface against precipitation, by decelerating and routing surface flow or by trapping eroded and transported sediment particles. It also affects geomorphic processes indirectly, e.g., by effects of roots on sediment hydraulic and mechanical properties (Gurnell, 2013). Soil erodibility is further influenced

by effects of organic matter accumulation associated with vegetation development. A review on these key geomorphic functions of vegetation is given by Marston (2010).

In turn, the geomorphic development of land surfaces affects the evolution of hydrologic, pedologic and biologic structures in ecosystems in direct and indirect ways: The geometry of a land surface controls the accumulation and routing of water through a landscape and therefore affects the formation of groundwater bodies, streams, and standing water bodies. It further affects pedogenic and biotic processes by its influences on solar radiation at the ground surface. Geomorphic processes can cause local disruptions of soil formation when surface material is eroded or covered by sediment, leading to the formation of a pattern of soils of different maturity over a landscape, as conceptualized for hillslopes in the Catena concept (Milne, 1935). Soil development is further indirectly affected by geomorphic processes through their effects on hydraulic and biotic patterns. Soil landscape patterns constitute a persisting archive of geomorphic processes, as emphasized in the concept of soil geomorphology (Birkeland, 1984; 1990). Geomorphic structures affect the distribution and diversity of biotic ecosystem components from local to landscape scale (Nichols et al., 1998). Geomorphic processes acting during the initial phase of landform development and thus before the establishment of vegetation are of special importance in this context because they affect ecosystem development and structures both by direct effects on biota colonization and by indirect effects resulting from the influence on the developing patterns of soil in the landscape, as pointed out by Swanson et al. (1988).

It is therefore important to describe and to understand the processes and structure-process interactions during the initial phase of landform development in order to understand trajectories of longer-term landform development and the structures of 'mature' ecosystems. The possibilities to empirically study unaffected landform and ecosystem development in natural environments are rare, so that the study of initial phases of landform development has often been approached in laboratory experiments or plots on field sites (see Chapter 2.1). Such approaches cover relatively short timespans and hardly allow for studying the whole range of potentially relevant interactions between landscape components. More recently, also numerical models have been employed to study the relevance of initial conditions (Perron and Fagherazzi, 2012) or key processes of initial landform evolution (Favis-Mortlock, 1998; Istanbulluoglu et al., 2002). Such modeling studies have, as emphasized by Tucker and Hancock (2010), further increased the interest in direct observations and 'natural experiment' data. Inferring to the initial phase of landform development from developed landscapes requires relying on geoarchives or proxies for landform development processes (e.g., lake sediments, floodplain sediments, or soil profile truncation) or on the inverse approach of inferring from patterns or forms to processes. Both approaches are frequently and successfully applied in geomorphology, however, conclusions to initial conditions or

early phases of development are only possible against a background of postulated conceptual ideas on the pathways and trajectories of the system's development (von Elverfeldt and Glade, 2011), including the assumption of a largely linear behavior of the system (Murray et al., 2009).

1.2 The initial phase and trajectories of landform development in geomorphologic theory

Pathways and trajectories of landform development have been described in several concepts in geomorphologic theory, some of which address the legacy of initial conditions and the initial development phase. Most of these concepts on landform development were formulated in deductive approaches based on observations in mature landscapes.

The early concepts of Gilbert (1877), which are regarded as the beginning of modern process geomorphology (Pazzaglia, 2003), emphasize the interactions of geomorphic forms and processes and consider effects of geologic heterogeneity, as an initial condition, on geomorphic processes. During the subsequent decades, geomorphologic theory focused on chronological or cyclic models of long-term landscape evolution (Davis, 1899; Penck and Penck, 1924) which describe a flattening of landscapes over time in several stages depending on exogenous and endogenous forces and do not emphasize the relevance of initial conditions. Beginning with the concept of dynamic equilibrium introduced by Hack (1960), systems approaches were established in geomorphology. Similar to theory development in physics, chemistry, biology and ecology, conceptual ideas and models for the geomorphic development of land surfaces developed from ideas of classical mechanics and thermodynamics to open-systems, non-equilibrium, chaos and complexity theory (Huggett, 2007). A fundamental characteristic of geomorphologic systems theory is the consideration of the geographical context, i.e., the location in the three dimensions of space for each point in a landscape, as pointed out by Phillips (2006). Geomorphologic theories thus need to consider initial and boundary conditions in their spatial and temporal variability, similar to landscape ecological theories that consider, as defined by Risser (1983), "the development and dynamics of spatial heterogeneity, spatial and temporal interactions and exchanges across heterogeneous landscapes, influences of spatial heterogeneity on biotic and abiotic processes, and management of spatial heterogeneity".

Geomorphologic system concepts mostly assume that landform development is oriented towards a state in that processes compensate each other through negative feedbacks and in that no long-term net change in system components occurs. This state is commonly referred to as 'dynamic equilibrium' (Ahnert, 1994) or 'steady state' (Chorley and Kennedy, 1971), although there is a large variety of definitions and extensive discussion on these terms

(Phillips, 1992; von Elverfeldt, 2012; von Elverfeldt and Glade, 2011). Most equilibrium concepts suggest that the equilibrium or steady state is not influenced by the initial conditions but adapted to the forces acting on the landscape (Chorley, 1962). The state in that process rates change towards dynamic equilibrium or steady state is commonly referred to as 'disequilibrium'. The initial phase of landform development, however, is regarded as showing nonequilibrium tendencies, i.e., a development "directed away from equilibrium" (Ahnert, 1994), in which positive feedbacks cause a self-reinforcement of processes and thus a progressive differentiation of landforms. This phase of landform development is accordingly associated with a divergent development, i.e., an increase in relief by surface dissection (Huggett, 2007). The initial development phase was mainly considered to be a subphase of a differing development direction within the overall tendency towards the steady state condition (Ahnert, 1994). Besides concepts for landform development oriented from nonequilibrium to equilibrium states, concepts for landform development in consequence of alternating activity and stability phases induced by changing climatic conditions and for the transition between these phases were formulated (Rohdenburg, 1971). Mechanisms that cause the transition from the non-equilibrium conditions of the initial phase to the overall development towards equilibrium, however, were hardly addressed in detail. The idea that landform development results in similar landscape characteristics for different initial conditions has been described with the term and concept of equifinality. This term is used in different senses in geomorphology, as summarized by Beven (1996): in the broader sense, the equifinality concept in geomorphology describes the possibility that similar landforms can develop from different initial conditions by different processes, while in the narrower sense, it states that similar landforms are produced by similar processes, irrespective of the initial conditions (Culling, 1957).

Several conceptual models for mechanisms governing the trajectories of landform development have been described: Systems approaches oriented on classical mechanics and thermodynamics state that the development towards the equilibrium state is governed by proportional and linear response of geomorphic processes to the influence of external forces, constrained by internal resisting forces and the conservation of energy and mass. Open-geomorphic systems approaches (Hack, 1960) describe a development towards equilibrium including feedback processes by which landscape elements adjust to each other. Phillips (2011) states that geomorphic 'pseudo-equilibrium states' result from system development following the principles of gradient selection (i.e., processes act along existing structures and enforce these structures by positive feedbacks) and of threshold-mediated modulation (i.e., the direction of development can be inversed by threshold behavior when the system reaches the borders of a possible range). Concepts of complex and nonlinear system development explicitly assume that a system's response is not proportional to the forces applied

but is a result of complex process interactions (Murray et al., 2009). Phillips (2003) defines several types of complex nonlinear dynamics, including fractals, multiple equilibria, and self-organization; and describes several sources for nonlinearity, including thresholds, multiple modes of adjustment, and self-reinforcing positive feedbacks. Beven (1996) states that the analysis of nonlinear dynamic systems suggests that there is not necessarily a relaxation back to the original system state after changes in behavior have been caused by perturbations, which implies that there is not one single development trajectory and equilibrium state. The idea of multiple possible trajectories of system development has also been addressed in other concepts. Within the concept of evolutionary geomorphology, which focuses on the initiation and development of landform structures and process domains, Thornes (1983) describes bifurcation states at which system development can follow one of several possible trajectories towards different equilibrium states. Based on observations and models of vegetation development and erosion processes in water-limited systems (Kirkby, 1995; Thornes, 1985), Phillips (2003) further describes mechanisms of landform differentiation in consequence of the bifurcation of trajectories, stating that under unstable conditions, systems will 'tip' to different states and development pathways in response to small and short-term disturbances. With this 'tipping', the system or a local subsystem passes a threshold, enters one of several possible new regimes and can evolve further along differing pathways. Self-similarity of geomorphic patters resulting from such a differentiation has often been related to the fractality concept (see Baas, 2002). The concept of self-organization, which "refers to the formation of patterns attributable to the internal dynamics of a geomorphic system" (Phillips, 2006), has been related to erosion rill formation (Favis-Mortlock, 1998; Favis-Mortlock et al., 2000), sand dune formation, fluvial landscape dissection, or coastline formation (see Murray et al., 2009). Self-organization in landform development has been described as a source for the generation of systemic orderliness by locally decreasing entropy (Favis-Mortlock et al., 2000) to maximize total energy dissipation and equalize energy expenditure for the system (Leopold and Langbein, 1962; Rodríguez-Iturbe et al., 1992).

Within the context of nonlinear and complex systems theory, the relevance and characteristics of the initial development phase have been approached in more detail. Taking on the high sensitivity for initial conditions described in chaos theory, it is supposed that nonlinear systems can show sensitivity to initial conditions and small perturbations (Beven, 1996; Culling, 1987) and that systems can move towards one of several possible equilibrium states that may or may not depend on initial conditions (Perron and Fagherazzi, 2012). Summarized in the statement that "geography matters, and history matters", Phillips (2006) presumes an influence of the initial conditions and the initial phase of geomorphic development, stating that "geomorphic systems 'remember' initial variations and perturbations".

The relevance of initial conditions in landform development became a focus of increasing interest in the context of research on prediction in geomorphology and on the development of numerical landform evolution models, where it was recognized that insufficient knowledge of initial conditions can limit the quality of predictions and the possibilities to compare predictions and observations (Church, 2003). In this context, Church (2003) states that nonlinearities in landform development may amplify small initial differences so that the trajectory of landscape evolution considerably differs from predictions not considering the initial conditions; but that despite these differences, statistical properties can be identified that allow to measure landscapes irrespective of the effects of the initial conditions. Similarly, Perron and Fagherazzi (2012) review results of different modeling approaches and conclude that initial conditions influence the exact arrangement of landform components, but not the general statistic characteristics of a landscape. Based on further simulations, they also showed that initial conditions can persist through landform development as landforms evolve towards one of multiple equilibrium stages.

1.3 Transdisciplinary concepts on initial landform and ecosystem development

Concepts of geomorphic development have largely been developed based on the same fundamental theories as concepts of ecosystem development founded in ecology and landscape ecology. However, most concepts focus on the development of either the geomorphic or the biotic system components.

Generally, while geomorphologic theory mainly describes the system's response to boundary conditions or driving forces, ecological system development theory places a stronger focus on the development of process-interactions within the ecosystem. While geomorphologic theory focused on the development towards equilibrium for different landform units, ecosystem development theory describes a development away from thermodynamic equilibrium for the overall ecosystem by the increase of biomass and species' internal organization, as described in the maximum exergy dissipation hypothesis (see Fath et al., 2004). Concepts of ecosystem development have emphasized that systems become more energetically efficient and minimize entropy production and that systems maximize energy throughflow, power (or exergy) storage and retention time (Fath et al., 2004; Jorgensen et al., 2000; Odum, 1969). As compared with geomorphology, there is a stronger focus on inherent dynamics of patterns in landscape ecology (Bürgi et al., 2004), where pattern development and interactions were further conceptualized, e.g., in models of hierarchical dynamics of landscape patches (Wu and Loucks, 1995).

In a review of studies on vegetation-geomorphology interactions, Marston (2010) states that a "lack of attention to vegetation among early geomorphologists is evident as one reviews

the history of geomorphology". Early concepts integrating landform and biotic development mainly focused on uni-directional effects of geomorphic processes on vegetation or vice versa (see Viles, 1988), and hardly considered specific characteristics of the initial development phase. In concepts of landform evolution, changes in vegetation cover have mainly been regarded and implemented as the effects of disturbances. These disturbances in vegetation cover were generally related to geomorphic instability, and a gradual increase in geomorphic stability was correlated to a gradual increase in vegetation cover after a certain time or response (Knox, 1972). Effects of biota on geomorphology have been addressed in the concept of ecosystem engineers (Jones et al., 1994). Concepts of 'ecogeomorphology' (Fisher et al., 2007; Reinhardt et al., 2010) have explicitly focused on bi-directional linkages and feedbacks between biota and geomorphology on a landscape scale (Corenblit et al., 2011). Based on an integration of concepts and theories from geomorphology and ecology, co-evolution of morphology and biota was described, e.g., within the framework of complexity theory (Stallins, 2006). Several bio- or ecogeomorphic concepts have explicitly addressed the co-evolution of biota and landforms over the progress of ecosystem development (Corenblit et al., 2011). For the analysis of development dynamics of biogeomorphic systems after disturbances, Brunsden and Thornes (1979) have proposed the 'transient forms ratio', which describes the relation of the relaxation times of biogeomorphic structures and the recurrence of disturbance events. In a concept of fluvial biogeomorphic succession, Corenblit et al. (2007) described several phases of the progressing shift from the dominance of geomorphic factors to the dominance of vegetation effects and related them to the formation of characteristic morphological patterns in fluvial landscapes. Also models for the spatial differentiation of landform and vegetation cover in water-limited systems explicitly focused on interacting development of landform and biota (Kirkby, 1995; Saco et al., 2007; Thornes, 1985). Based on geomorphic studies that integrate ecological or evolutionary biology concepts, Corenblit et al. (2011) describe a biogeomorphologic macroevolutionary conceptual framework that considers feedbacks between geomorphic and ecologic evolutionary processes for different spatial and temporal scales.

2 State of the art of research and methodology

2.1 Field and physical experiment studies on the initial phase of landform development

The initial phase of geomorphic development has been studied intensively for deglaciating landscapes, i.e., in the field of paraglacial geomorphology (introduced by Ryder (1971) and Church and Ryder (1972)). The paraglacial period has been defined as "the period of readjustment from a glacial to a nonglacial condition" (Ballantyne, 2002). For paraglacial landform development, Ballantyne (2002) reviews studies on gravitational, aeolian and fluvial processes, integrating a wide range of methods. Generally, however, structures and processes of the initial phase of landform development and the relevance of initial conditions for landform development have received relatively little attention in geomorphologic studies, considering the high process intensity, the high rates of change in geomorphic structure and the potential relevance for further system development. One reason for the scarcity of empirical studies certainly is the fact that observations of initial phases of landform development under natural conditions are only possible in the rare cases when surface exposure to exogenic conditions takes place naturally. Besides studies of deglaciated or paraglacial landscapes (Curry et al., 2006; Mercier et al., 2009), possibilities to study initial surface development have been found on the upraised bed of Hegben Lake, USA (Morisawa, 1964) and in coastal areas following sea level change (Bowman et al., 2011; Hesp, 2002). Field studies have also been carried out on anthropogenic land surfaces in post-mining areas (Hancock et al., 2008; Nyssen and Vermeersch, 2010; Ritter and Gardner, 1993), in which, however, surface development is affected by reclamation measures. Other studies focused on short-term development in landscapes where a repeated surface rejuvenation takes place, as in volcanic areas (Salvany et al., 2012), fluvial systems (Larsen and Harvey, 2010) or tidal flats (Temmerman et al., 2007). Also studies in pro-glacial systems have focused on processes of initial landform development, but are limited to the specific conditions of environments largely controlled by glacier-hydrological processes (Russell et al., 2001). Studies on initial landform evolution have dealt with the development of drainage systems (Bowman et al.,

2011; Morisawa, 1964; Ritter and Gardner, 1993), foredune initiation (Hesp, 2002), hillslope erosion (Hancock et al., 2008; Nyssen and Vermeersch, 2010; Salvany et al., 2012), and fluvial channel erosion (Larsen and Harvey, 2010; Temmerman et al., 2007). Other processes of initial ecosystem development, e.g., colonization by vegetation and initial soil formation, have been studied in natural systems, e.g., on volcanic deposits (Bishop, 2002), newly emerged volcanic areas (Fridriksson, 1987), or in deglaciated areas (Chapin et al., 1994).

Studies on experimental plots can contribute significantly to the understanding of geomorphic processes that are active during the initial phase of landform development; however, experiments on plots in natural environments have hardly been carried out with an explicit focus on the initial phase or the influences of initial conditions. Several experiments in experimental plots or flumes under laboratory conditions have addressed specific processes of initial geomorphic development, and experiments under laboratory conditions have been designed to study questions of landform development in downscaled physical models of landscapes. As summarized by Paola et al. (2009), such geomorphic experiments have focused on landform development in erosional landscapes, depositional systems, alluvial fans, deltas and rivers. Drainage system evolution has been studied in several physical model experiments since the works of Parker (1977) and Schumm et al. (1987). Physical experiments have addressed the sensitivity of erosional landscapes on initial conditions and effects of initial relief on drainage network patterns (Hancock and Willgoose, 2001; Hasbargen and Paola, 2000; Pelletier, 2003). The effects of vegetation cover on flow structures and morphodynamics in river channels were studied in a number of flume experiments (Gurnell, 2013; Tal and Paola, 2010); however, those physical experiments that focused on larger-scale landform or drainage network development have hardly included representations of vegetation cover development. Dynamical scaling of the components of physical experiments (e.g., fluid flow, sediment transport) is necessary to allow for quantitative interpretations of the results, however, possibilities of scaling are limited, e.g., for flow dynamics, fine scale topography, or time (Paola et al., 2009). The value of physical models is mainly seen in the possibilities to obtain detailed observations of geomorphic processes and feedback mechanisms in longer-term landscape development, as stated, e.g., by Douglass and Schmeeckle (2007).

Research on mature landforms and ecosystems is carried out on a number of projects based on the long-term monitoring of extensively instrumented sites, such as the network of environmental observatories TERENO (Bogena et al., 2012) or the network of Critical Zone Observatories CZO (Anderson et al., 2008). Constructed hydrological catchments that are instrumented and monitored similar to such sites can serve as large-scale physical experiments that allow for the observation of hydrological processes for defined boundary conditions (Kendall et al., 2001) and for the study of ecosystem structures and processes begin-

ning with the initial development phase, as approached for the 'Hühnerwasser' catchment (Gerwin et al., 2009b)

2.2 Three-dimensional digital modeling of soil and landform development

2.2.1 Overview and classification of approaches

The integrative analysis of soil, landform and ecosystem evolution can be facilitated by digital representations or models. Models that aim at describing the relationship between geomorphic, pedologic and ecologic structures need to capture the spatial variations of landscapes by a digital representation of the three dimensions of space and the dimension of time. Approaching landform or landscape modeling in a spatially explicit way is of special importance for studies that focus on the highly dynamic development of landform structures during the initial development phase.

Similar to the broad notion of the terms 'modeling' and 'model' in science, also methods of spatially-explicit landscape modeling comprise many different approaches, methods and levels of abstraction. Different classifications have been proposed for these approaches. Pazzaglia (2003) distinguishes three classes of models of landscape evolution, i.e., qualitative landscape models, which describe long-term landform change over large areas and "are not rooted in the principles of physics"; physical models, which are representations of landforms, often at differing scales; and numeric surface process models, which represent major processes acting on landscapes by mathematical proxies. According to Gaucherel and Houet (2009), cartographic or interpolation approaches simulate the spatial distribution of landscape variables using spatial patterns, mainly through the representation and analysis in Geographical Information Systems (GIS). Gaucherel and Houet (2009) recommend to only refer to those approaches as 'landscape models' when they highlight changes in land use or forms and thus include a temporal aspect besides the two-dimensional (2D) or three-dimensional (3D) spatial representation of landscape elements. They further distinguish process-explicit models, which reproduce one or several specific processes to represent a landscape, and neutral models, which deliberately formulate only the minimum set of rules required to produce patterns to be used as objects of comparison against observations from real landscapes (Pearson and Gardner, 1997). Grunwald (2009) distinguishes modeling and mapping methods, and defines modeling as the "use of mathematical equations to simulate and predict real events and processes", and mapping methods as approaches that emphasize "to 'make a map' or 'to depict something on a map'".

2.2.2 Digital soil mapping and quantitative soil landscape modeling

Digital soil mapping has been defined as the "computer-assisted production of digital representations of soil type or soil properties, which involve the creation and population of spatially-explicit information by the use of field and laboratory methods, coupled with spatial and non-spatial soil inference systems" (Grunwald, 2009) or as "the creation and population of spatial soil information systems by numerical models inferring the spatial and temporal variations of soil types and soil properties from soil observations and knowledge and from related environmental variables" (Lagacherie, 2008). Methods of digital soil mapping have been extended to include the representation of soil in 3D space. The extensive review of digital soil mapping studies by Grunwald (2009) shows that although digital soil mapping research is conducted over a wide range of spatial scales, a 3D representation of the soil system in digital maps was approached in few studies. Several methods have been described that extend 2D cartographic approaches to include representations of the third dimension of space and/or the temporal dimension. Many approaches on 3D soil mapping are based on geostatistics and attempt a description of the spatial variability of soil properties (see Delarue et al., 2009). Some studies include a 3D representation of volumes of soil horizons and a separate characterization of properties for different horizons (Cosandey et al., 2003; Delarue et al., 2009; Grunwald et al., 2000; Mendonca Santos et al., 2000). Generally, the possibilities for such approaches are growing with the proceeding development of 3D GIS (Abdul-Rahman and Pilouk, 2008; Coors and Zipf, 2005).

Moore et al. (1993) states that most attempts to characterize the spatial variability of soil attributes have concentrated on the characterization of patterns by sampling and interpolation approaches; however do not consider processes of pedogenesis and have thus missed to link patterns to processes. Methods of quantitative soil landscape modeling approach this linkage. In addition to soil sampling and statistical modeling methods for soil property mapping, quantitative soil-landscape modeling includes a representation of surface topography in digital elevation data and employs methods of digital terrain analysis to predict and analyze soil patterns over landscapes based on the variability of morphologic parameters (Thompson et al., 2006). Quantitative soil landscape modeling therefore can integrate a number of methods, from field sampling and remote sensing to statistical modeling and digital terrain analysis using GIS (Gessler et al., 2000). Thompson et al. (2006) summarize the most important methods in soil-landscape modeling, which comprise the analysis of digital elevation models (DEMs), the gathering of georeferenced soil data, and the development of quantitative empirical models. Methods of geomorphometry, defined as "the science of quantitative land-surface analysis" (Pike et al., 2009), are central to quantitative soil landscape modeling. With the increasing availability of digital elevation data, geomorphometry

mainly focuses on "the extraction of measures (land surface parameters) and spatial features (land surface objects) from digital topography" (Wilson, 2012). A land surface parameter, in this context, is defined as "a descriptive measure of surface form (e.g. slope, aspect, topographic wetness index)", while a land surface objects is "a discrete surface feature (e.g. watershed boundary, cirque, alluvial fan, drainage network)" (Wilson, 2012). Thresholds of land surface parameters, e.g., relations of local slope and contributing area, have frequently been employed for the differentiation of geomorphic process domains or land surface objects (Dietrich et al., 1992; Montgomery and Dietrich, 1989; Willgoose, 1994).

Carbonneau et al. (2012) emphasize the need to integrate a representation of non-smooth landscape structures as recognized and modeled in landscape ecology theory (Wiens, 2002) into geomorphologic landscape modeling approaches. As an example for such a representation, they describe a 'riverscape model', i.e., a quantitative documentation and analysis of a river landscape, which is based on an integration of spatially explicit elevation data, aerial photographs and first and second order variables derived from these datasets. Soil landscape analysis and predictive terrain analysis aim at identifying correlations between terrain attributes and measured soil attributes to conclude on effects of landscape structure on pedogenic processes (Sommer, 2006). However, most studies gather elevation data and soil information for one stage of soil landscape development, which implies that recent topography is employed as a proxy for all states of morphologic development that have influenced soil formation over time. The effects of initial morphology and of the highly dynamic evolution of morphology and sediment redistribution patterns of the initial development phase, which can affect the spatial variability of soil attributes, cannot be assessed in such approaches.

Methods for the 3D spatial description of surface and subsurface topology and geometry were further developed in the field of 3D geo-database research (see Breunig and Zlatanova, 2011). Breunig and Zlatanova (2011) point out that 3D geometric models more and more integrate different topographical features (such as geology, landforms, buildings, etc.); however, most approaches to 3D spatial modeling were described for geological applications. Methods and software applications for 3D geologic modeling of geometrically complex surfaces and the construction of volumetric models of stratigraphy were developed. 3D modeling applications were, on the one hand, developed based on GIS systems, with a focus on the spatial representation, analysis and manipulation of 3D geographic data; and, on the other hand, based on Computer Aided Design (CAD) systems, with a stronger focus on geometric aspects of models and on visualization (Abdul-Rahman and Pilouk, 2008). 3D geologic modeling mainly aims at visualizing geological structures in order to allow for improved understanding and interpretation. Geometric models are mainly constructed based on borehole and geophysical data using geostatistical methods or specific interpolation methods,

e.g., the Discrete Smooth Interpolation method implemented in the 3D modeling application GOCAD by Mallet (1997, 2004). GOCAD (Geological Objects CAD) was developed for modeling the geometry of geological objects (Renard and Courrioux, 1994) and includes basic GIS functionalities, i.e., the possibility for analyses and manipulation of attributes assigned to the modeled objects. A high number of GOCAD applications focus on the modeling of geologic faults (Renard and Courrioux, 1994; Zanchi et al., 2009) or folds (Bistacchi et al., 2011; Bistacchi et al., 2008; Schober and Exner, 2011). Applications have aimed at the visualization of complex geometry (Renard and Courrioux, 1994), at volume quantifications for geologic strata (Zanchi et al., 2009) and at geothermal and mining exploration (Bar et al., 2011; Sprague et al., 2006). GOCAD has also been employed for the reconstruction of palaeosurfaces and quantification of sediment thickness for pleistocene deposits based on borehole data (Lang et al., 2012; Meinsen et al., 2011) and for the visualization and analysis of archaeological excavations (Feine, 2007; Losier et al., 2007). Applications of 3D geological modeling methods for analyses of soil landscape development, however, have hardly been described.

2.2.3 Methods of sediment budgeting and geomorphic change detection

For a spatially distributed assessment of sediment redistribution and its effects on soil landscape patterns, reconstructions of initial landscape morphology and of initial soil thicknesses have been employed. These so-called soilscape models are mainly derived from depths of soil profile truncation deduced from soil profile mapping and from quantifications of colluvial and alluvial deposits (Förster and Wunderlich, 2009; Houben et al., 2006; Rommens et al., 2005; Verstraeten et al., 2009). They are based on the assumptions of homogeneous thicknesses of soil and parent material cover for a state of landscape development unaffected by erosion (Houben et al., 2006; Rommens et al., 2005) and of a clear alternation of phases of geomorphic stability and soil formation and phases of geomorphic instability and soil erosion. To reconstruct spatial patterns of sediment redistribution, sediment budgets have been constructed using, e.g., a combination of soilscape models and DEMs of the recent surface (Förster and Wunderlich, 2009; Notebaert et al., 2009; Seidel and Mäckel, 2007). Sediment budgets have also been established based on tracer applications or morphologic and sedimentologic field mapping (see Hinderer, 2012). The sediment budget has been defined as "the accounting of sources, sinks and redistribution pathways of sediments in a unit region over unit time" (Slaymaker, 2003). It is thus a mass balance approach and based on the principle of mass conservation, stating that sediment production equals sediment yield together with changes in storage. Sediment budgeting aims at a quantification and description of the input, output, and storage as well as of the transport of sediment within a geomorphic system (Reid and Dunne, 2003) and requires the delineation of this system,

the identification of processes and locations of erosion and deposition as well as transport pathways, the quantification of each component in space and time and the construction of a balance between sediment production, deposition and sediment yield (Marston and Pearson, 2004).

A further step towards the integration of the temporal component in soil landscape models is the analysis of change in morphologic parameters and its effects on soil landscape structures. Including a representation of dynamic landform development in soil-landscape evolution modeling was approached using geomorphic change detection by differencing two or more DEMs of an elevation data time series, which can be considered a "rudimentary form of spatially distributed dynamic geomorphological analysis" (James et al., 2012). DEM differencing has been applied to identify areas of geomorphic change or stability, to reconstruct process rates, or to establish sediment budgets (see James et al., 2012). Methods of geomorphic change detection are continuously improved and facilitated by the increasing availability of high-resolution digital elevation data. However, possibilities for an integration of geomorphic change analysis and pedogenesis in soil landscape models are limited because of the large timescales that are relevant for pedogenesis, so that integrative quantitative soil and landform modeling has rarely been approached. Chronosequence studies can be employed as 'false time series' (Schaaf, 2001), but have hardly been implemented in 3D soil landscape modeling. Sommer et al. (2008) propose that soil landscape models describing different stages of development can be further improved by analyzing geomorphic change from a time series of DEMs that describe surface development beginning with the initial state and by implementing measurements of dynamic processes of initial soil landscape development.

2.2.4 Numerical landform evolution models

Numerical models describe landscape evolution "by representing a geomorphic process, multiple processes, or landscape characteristics as mathematical expressions" (Pazzaglia, 2003). Numerical models focusing on the redistribution of sediment over landscapes and thus on landform development were developed before two different research backgrounds: On the one hand, soil erosion models were developed mainly for applications in agricultural lands and taking into account land use and vegetation cover characteristics. On the other hand, geomorphologic landscape evolution models (LEMs) were developed with a strong focus on the development of surface morphometry over long timescales. As pointed out by Tucker and Hancock (2010), the majority of these geomorphologic models focus on fluvial landscapes, including representations of tectonic uplift, weathering, mass movements and hillslope erosion. The spatial and even more the temporal scales of the majority of applications differ considerable between these two types of models, and relatively few attempts

(Coulthard et al., 2012) have been made to bridge the two areas of modeling.

Beginning with and based on the Universal Soil Loss Equation (USLE), a number of soil erosion models were formulated that are based on empirical parameters but do not implement physical processes (Kinnell, 2010). Later, several spatially-distributed soil erosion models were developed which combine physical process representation and empirical parameters (e.g., LISEM (DeRoo et al., 1996)), are physically-based (e.g., EROSION3D, (Schmidt et al., 1999)) or make use of fuzzy-logic approaches (e.g. FUDSEM (Cohen et al., 2008)). Reviews on soil erosion models are given by Aksoy and Kavvas (2005) and Merritt et al. (2003). As pointed out by Cohen et al. (2008), the possibilities for the prediction of erosion over large areas and long time periods with soil erosion models are still limited. Soil erosion models often do not include a temporally dynamic representation of variables as vegetation growth (Jetten et al., 1999) or a dynamically changing topography, so that the representation of feedback effects over the landscape is limited. Many models (e.g., WEPP (Laflen et al., 1997), KINEROS (Smith et al., 1995)) require an ex ante differentiation of process regimes, e.g., of hillslope and channel areas.

The development of early mathematical models of larger and longer-scale landform development was focused on hillslopes, spanning the length from an upslope divide to a stream at the downslope end (see Lawrence 1996). The models are mainly based on the principle of conservation of mass, quantified in the continuity equation in the form

$$\frac{\delta z}{\delta t} = U - \nabla \cdot \tilde{q}_s$$

, where z is the surface elevation, $\tilde{q}_s$ is the sediment flux vector, and U is the uplift rate.

Sediment redistribution by gravity-driven processes is often described using the diffusion equation

$$\tilde{q}_s = -K\frac{\delta z}{\delta x}$$

, where $\tilde{q}_s$ is the volumetric sediment transport rate per unit contour length, K is a constant with units of a diffusion coefficient [L^2/T], and x is the distance from the divide; assuming a linear dependence of transport on slope. Sediment transport by water is mainly modeled based on transport laws in the form of

$$\tilde{q}_s = k(\tau - \tau_c)^n$$

, where $\tilde{q}_s$ is the volumetric sediment transport rate per unit width, k and n are parameters, τ is the boundary shear stress and τ_c is the critical boundary shear stress for sediment entrainment. Sediment transport modeling is often simplified by using the contributing area

for water flux and extended by empirical constants in the form of

$$\tilde{q}_s = dCA^m \beta^n$$

, where CA is the contributing area, β is the local slope, and d, m and n are parameters. These transport laws are, in many LEMs, employed for surface wash transport and fluvial channel transport, so that the fluvial erosion of hillslopes is treated as a downscaled version of channel erosion (Dietrich et al., 2003; Willgoose, 2005). Transport functions were further specified, e.g., to differentiate between diffusive and advective transport, between detachment- and transport-limited conditions, and between different grain-size classes; or to include discontinuities and threshold processes (Dietrich et al., 2003; Martin and Church, 1997). Lawrence (1996) lists a number of reasons for which full mathematical solutions to these governing equations are hardly possible, ranging from the multidimensional nature of land surfaces, the nonlinear characteristics of development and the spatially non-uniform behavior of processes, to the physical discontinuities of land surfaces. Numerical landscape evolution simulation models therefore mainly work by repeatedly applying rules that are derived from the functions to a grid of data points representing a land surface for several time steps and continuously adapting the elevation of these points. Recent reviews on numerical landscape evolution models are given by Coulthard (2001), Willgoose (2005), and Tucker and Hancock (2010). As pointed out by Tucker and Hancock (2010), most of these models are centered around a fluvial transport module. The models' focus is mainly on surface elevation change; however, some models allow for the simulation of sediment deposition in different layers, approaching the actual 3D modeling of landscape evolution. Most LEMs distinguish between a layer of unweathered, unerodible bedrock and a layer of soil or regolith and include a representation of 'soil production' by weathering based on rates of conversion from bedrock to soil (Tucker and Hancock, 2010). Integrated modeling of physical and chemical weathering and soil transport was attempted, e.g., by Minasny and McBratney (2006) and Yoo et al. (2007). Minasny et al. (2008) developed a mass balance model for soil landscape evolution that integrates representations of transport processes, soil thickness development by physical and chemical weathering, and soil organic carbon evolution. From simulation results, Minasny et al (2008) distinguished between three classes of soils developed for different topographic positions, i.e., residual, transportational, and depositional soils.

Most applications of LEMs have focused on long periods of surface development. Several applications for relatively short-term development were described for the SIBERIA model, which was frequently applied to simulate surface development in post-mining landscapes (Hancock et al., 2008; Willgoose et al., 1992). The possibilities of assessing the relevance of initial conditions for large-scale landform development using LEMs were discussed by Perron and Fagherazzi (2012).

3 Scope of the thesis

3.1 Project context, aims and objectives

This dissertation was accomplished within the Transregional Collaborative Research Centre 38 (SFB TRR 38), which investigates relevant structures and processes during the initial phases of ecosystem development. The central objects of the SFB TRR 38 were the identification of structures and processes as well as structure process-interactions that govern the initial phase of ecosystem development and the characterization of the initial ecosystem development phase in contrast to more mature development phases. For this purpose, the artificially-constructed hydrological catchment 'Hühnerwasser' was established and its development was investigated starting from 'point zero'.

The dissertation was part of the SFB TRR 38 subproject C5, which was focused on the development of a structure and process model. The objective of this project was to establish a 3D model of the Hühnerwasser catchment that allows to describe, integrate, analyze and visualize information on catchment structures and to establish mass balances of ecosystem components for the initial stage and for later stages of development. Within this research framework, the dissertation focuses on the 3D representation and characterization of the catchment's sediment body and on the development of sediment mass balances as affected by geomorphic evolution of the catchment's surface. The central questions approached in this work were:

- How can the geometry of the catchments sediment body be described in a 3D spatial model?
- How does the structure of the sediment body's surface change during the progress of ecosystem development?
- Which processes are essential for the evolution of geomorphic structures?
- How do structures and processes interact?

Based on the central hypothesis of the SFB TRR 38, which states that the initial phase of ecosystem development determines the development and defines the developing states of ecosystems, the main hypotheses of this dissertation were:

- During the initial phase of ecosystem development, the evolution of geomorphic patterns is affected by initial structures of the sediment's solid phase.
- Geomorphic development during the initial phase leads to a diversification of surface structures.
- Geomorphic patterns established during the initial development phase are constitutive for structures of the developing ecosystem.

The central aim of the work was to develop a 3D model of the development of mass balances of the sediment solid phase during the initial phase of ecosystem development in order to assess the effects of initial conditions on this development and to describe the pathways of development. The following objectives were formulated to approach this aim:

- to describe stages of surface morphology development during the initial development phase in the Hühnerwasser catchment
- to quantify sediment mass balances for development phases in the catchment
- to analyze and describe the modification and diversification of surface morphology during the initial development phase
- to analyze the effects of initial conditions and boundary conditions acting during the initial phase on morphologic development

Regarding the scale of analysis, the study was carried out in order to analyze the first five years of development for the total catchment area and to assess relevant structures as far as possible from datasets that cover the total area. A methodological framework for approaching these objectives and tasks was given by the concept of the project and the study site, which necessitated basing the model construction and analysis on remotely-sensed and basic monitoring data. The main tasks of the dissertation and the approaches to these tasks were:

- **the establishment of a 3D volume model of the catchment's sediment body for the initial and later stages of development**
  A volume model representing the initial state was constructed from geometric information on the catchment's delineating surfaces, and basic information on sedimentary structures was assigned to the volume model (Chapter 4).
  A method to extend the volume model by integrating surface geometric information for later stages of development was developed, so that the developed surface geometry and layers of sediment accumulated during different time intervals are represented. Simulations using a numeric landscape evolution model were employed to generate a representation of the internal structure of newly deposited sediment layers (Chapter 5).

- **the establishment of 3D sediment mass balances for the developing sediment body**
  Different types of remotely-sensed elevation data were evaluated for their suitability of the establishment of sediment mass balances at the scale relevant in the artificial catchment, and methods to modify elevation data for improved mass balance quantification were developed and evaluated (Chapter 6).
- **the characterization of the effects of initial and boundary conditions and of developing structure-process interactions on geomorphic development of the sediment body**
  Morphologic development was analysed based on a DEM and aerial photograph time series and discussed in relation to relevant initial conditions (Chapter 7).
  A numeric landscape evolution model was evaluated and applied to assess the effects of initial surface topography and precipitation characteristics on geomorphic development in the catchment (Chapter 8).

3.2 The constructed catchment Hühnerwasser as a study site for initial landform development

The study area of this work was the artificially created hydrological catchment 'Hühnerwasser' (translated as 'Chicken Creek'). The catchment is located in the post-mining recultivation area of the open-cast mine Welzow-South in the Lusatian lignite mining district, approximately 150 km south of the city of Berlin (Germany) (Fig. 3.1). The catchment was constructed between 2004 and 2005 by the company Vattenfall Europe Mining AG (Cottbus, Germany) to restore the former headwaters of the Hühnerwasser stream that had previously been removed in the course of open-cast lignite mining operations (Kendzia et al., 2008). It forms the central study site for research projects on different aspects of initial ecosystem development within the Collaborative Transregional Research Center (SFB/TRR) 38.

The catchment's lower boundary in vertical direction is formed by a clay liner of 1-3 m thickness, which acts as a hydraulic barrier for seeping water. Above this clay lining, quaternary sediments were deposited with a varying thickness of up to 4 m (Fig. 3.2) to form the porous medium (i.e., the water the storage layer). The catchment was formed as a relatively small longitudinal hillslope of about 150 m*450 m (Fig. 3.1). Surface elevation varies between 125.5 m a.s.l. and 140 m a.s.l. (Gerwin et al., 2009b). The slope has a convex longitudinal profile with inclinations of about 1% -3% in the upper and middle slope area and about 5% - 8% in the lower slope area (Fig. 3.2). The backslope is composed of two parallel parts facing together with an inclination of 0.2 - 1.2°. Surface runoff therefore accumulates in the central area of the slope. In the central slope area, a subsurface clay wall and a trapezoidal surface structure were constructed to form an artificial spring area; and at the lowest point of the

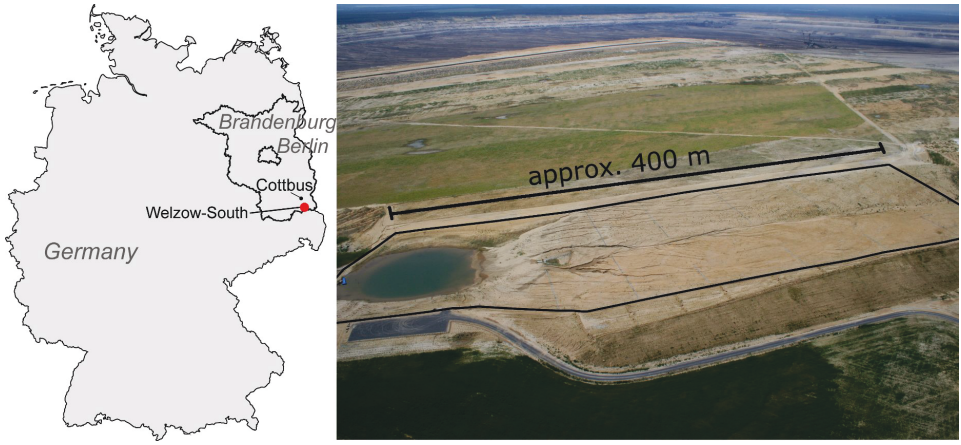

Figure 3.1: Location of the study site in the recultivation area of the open-cast mine Welzow-South, Brandenburg, Germany (left) and aerial photograph of the catchment surface, taken in June 2007 (right). The black line in the photograph marks the location of a fence delineating the monitoring area. Schneider et al., 2013.

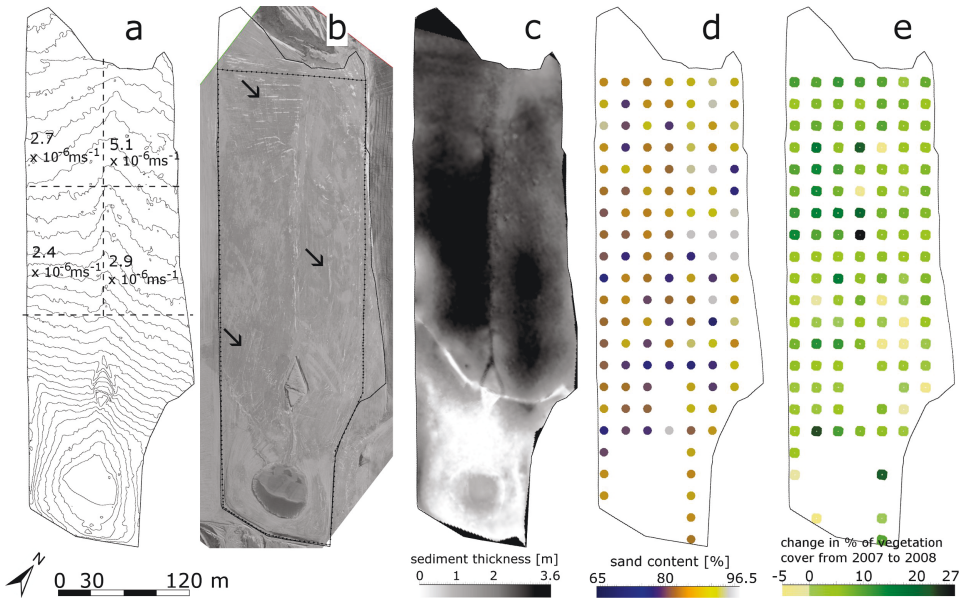

Figure 3.2: Overview on catchment surface characteristics. The solid black line marks the demarcation of the surface catchment area. a) Initial topography, indicated by 0.5 m contour lines of a photogrammetry-based DEM from November 26, 2005, and hydraulic conductivity for the surface for four sectors (conductivity data from Gerwin et al., 2009b). b) Aerial photograph (© VEM AG) of the surface on November 26, 2005. The dotted line marks the fence around the monitoring area. Noticeable small-scale surface structures remaining from the construction works are marked by arrows. c) Sediment thickness determined from DEMs of the surface in November 2005 and the clay layer. Black areas are no data areas not covered by the clay layer DEM. d) sand contents in 0-30 cm depth as determined from sampling in a 20 m grid (data from Gerwin et al., 2009b). e) Change in percent of accumulated vegetation cover for 25 m^2 plots from 2007 to 2008 (data from Zaplata et al., 2010). Schneider et al., 2013.

catchment, a hollow has been shaped to initiate the development of a pond that collects outflow from the catchment. The surface catchment area was delineated by creating a rampart around its borderline. The construction of the catchment ended in September 2005 after the surface was leveled using steel rails pulled by tractors. Small structures formed by this machinery remained in some areas (Fig. 3.2b, Gerwin et al., 2010). The catchment was then left to undirected succession, and disturbance by larger animals was prevented by fencing of the monitoring area (Fig. 3.2). The rampart delineating the surface catchment area was modified at the backslope in November 2009, and the topography of the easternmost part was modified in September 2006 and February 2008, resulting in the formation of a subcatchment outside of the fenced area (Gerwin et al., 2010).

The sediment textures are sands to loamy sands with silt contents ranging between 2 and 25 % and clay contents between 2 and 16 % (Gerwin et al., 2009b). The organic carbon content of the unweathered sediments is mostly below 1.6-2.2 mg g^{-1}. Infiltrometer measurements for four sectors of the slope revealed hydraulic conductivity values at saturation in the range of 2-5*10^{-6} m s^{-1} (Gerwin et al., 2009b) (Fig. 3.2), values which are relatively low for coarse-textured porous media (Bear, 1988). The spatial distribution of substrate properties is governed by technogenic structures (Maurer et al., 2011), which limited the identification of spatial auto-correlation patterns (Papritz et al., 2011). A rapid formation of physical and biological soil crusts was observed. Spröte et al. (2010) described an irregular pattern of crust cover, which was also suggested by a surface classification from aerial photography by Maurer and Gerke (2011). Also the colonization of the bare soil by higher plants started relatively quickly after finishing the construction works (Gerwin et al., 2009b) although the catchment is surrounded by a sparsely vegetated post-mining area of about 50 km^2 (Kendzia et al., 2008) that is a poor source of plant seeds. After about 3 years of development, the area around the pond was covered by relatively dense riparian vegetation. The slope area became colonized by grasses and shrubs and several specimens of Robinia pseudoacacia. Zaplata et al. (2011) observed a rapid increase of vegetation cover during the first years (Fig. 3.2e) and a spatial differentiation between the SW and NE part and backslope and footslope area.

Climate in the Lusatian region is temperate subcontinental. For the period 1961 to 1990, the mean annual precipitation was 563 mm and the annual average temperature was 8.9°C at the meteorological station of the German Weather Service (DWD) located in Cottbus (see Gerwin et al. (2009b)). High intensity rainfall events mainly occur in the summer months. Precipitation is recorded directly in the Chicken Creek catchment since October 2005 (Biemelt and Nenov, 2010). A number of 42 rainfall events with intensities > 4 mm h^{-1} and 8 events with intensities > 10 mm h^{-1} were measured between November 2005 and August 2008. The highest intensities in each year (from 2006 - 2008) were 14.6 mm h^{-1}

in June 2006, 24.8 mm h^{-1} in May 2007, and 19.1 mm h^{-1} in August 2008 (Biemelt et al., 2011). These storm events mainly occurred in the summer months. Annual precipitation for 2006, 2007, 2008 and 2009 was 403 mm, 667 mm, 660 mm and 665 mm, respectively (Biemelt et al., 2011); with strong variations between individual months. Mazur et al. (2011) characterized the catchment's hydrological regime as dominated by precipitation-induced surface runoff events. Surface runoff also occurred in consequence of snowmelt and rain on frozen soil during the winter months. Surface runoff triggered the development of erosion rills; and a progressing rise in groundwater levels, superposed by seasonal fluctuations, has been observed (Mazur et al., 2011). The major erosion rill has cut down to the groundwater level in the lower parts of the slope, which resulted in low permanent flow of about 0.01 l s^{-1} (Biemelt et al., 2011) in this rill.

3.3 Terminology and Definitions

3.3.1 Temporal definition of the initial development state for the Hühnerwasser catchment

Modeling and analysis of landform development in the Hühnerwasser catchment in this work was centrally based on aerial photographs and elevation data which were available for specific dates representing development states of the catchment surface. An elevation model based on stereo-photographs recorded on November 26, 2005 was employed to represent the initial state of surface development. Generally, the initial state or 'point zero' of development for the Hühnerwasser catchment was defined to be in September 2005, after the final leveling and homogenization of the surface and at the date of the fencing of the monitoring area (Gerwin et al., 2010). Based on a comparison of the available aerial photographs from mine-surveying recorded closest to this date (i.e., at September 9, 2005, and November 26, 2005), elevation data derived from the DEM recorded at the later data were regarded to best represent the initial surface. The photographs show that the surface was still modified after September 9; i.e., the clay layer below the central weir and around the pond was not covered by sediment on September 9, but a continuous sediment cover is observable in this area for November 26. Furthermore, tracks of construction machinery are clearly observable in the photograph for September 9, whereas the surface appears more homogeneous on the photograph of November 26. However, the photograph of November 26 also suggests that the incision of the major erosion rill in the SW part of the catchment and sediment redistribution below the central weir had already commenced before this date. Signs of hydro-geomorphic structure formation are only observable in the lowest parts of the slope, whereas linear structures in the upper slope areas are clearly similar to tracks of construction machinery observable in earlier photographs and are therefore not interpreted as signs of beginning rill incision.

3.3.2 Dimensionality

As pointed out by Jones et al. (2008), there is little consensus regarding the semantics of dimensionality in the description of geospatial data. Different applications of the terms one-, two- and three-dimensional arise from the existence of different valid ways of considering dimensionality. For example, while data points are generally zero-dimensional, their location is commonly described in three dimensions using x-, y- and z-coordinates. In most studies, the term '1D' is used to denote measurements carried out at one point in a landscape (e.g., borehole data), while '2D' is used to denote horizontally-projected representations of land surfaces in maps or representations of vertical cross-sections (Jones et al., 2008). For irregular surface data as represented in gridded or triangulated elevation models, the terms '2.5 D' and '3D' have been used. Most DEM data types, however, do not allow for representing multiple elevation values or z-coordinates at one location, defined by x- and y-coordinates, so that a representation of complex 3D geometries is not possible. Furthermore, elevation models do not allow for a description of volumes contained within boundary surfaces. Based on a review of definitions and usage of dimensionality terms, Jones et al. (2008) suggest to refer to mapping and cross section data by using ´2D' and to differentiate between the term 'surface 3D', to be used for elevation models, and 'volumetric 3D', to be used, e.g., for subsurface structure data based on geophysical methods. Alternatively, the dimensionality of modeled objects can be denoted based on the dimensions of modeled objects that are depicted in the model, or, as defined by Losier et al. (2007), on "the portion of space occupied by an object or its geometric representation". Because major parts of this work focus on the construction of models that allow for describing sediment structures in the three dimensions of space, based on point datasets or surface datasets, the latter definition is followed here. Consequently, datasets representing surfaces are referred to as '2D (elevation or surface) models' and datasets representing volume bodies are referred to as '3D (volume) models'.

3.3.3 Landforms and landscape elements

The term 'structure' is used in a general sense in this work, denoting any non-homogeneous and non-random spatial distribution of non-process ecosystem components, and any spatially delimitable, relatively homogeneous element within this distribution. This use follows the general understanding of spatial structure in ecology as "a distribution of constituent parts that differs significantly from complete spatial randomness" (Cutler et al., 2008). It is not used to imply any assumptions on the processes or mechanisms that generated this distribution. Landscape regions or areas that can be delineated based on specific structures as a result of structure-generating processes, and the representations of such areas in landscape models, are referred to as 'units' in this work. This general term is used in order to integrate

delineations based on anthropogenic and on natural structures, and on subsurface and surface structures. The geomorphic units that are in the focus of hydro-geomorphic analyses and considered in elevation data evaluation in this work are features resulting from the erosion of sediments by concentrated overland flow along the slope of the catchment and from the deposition of these sediments at the lowest areas of the slope. Linear erosion features, following Evans and Taylor (1995), can be classified into several forms, depending on size and strength of water flow, from 'traces' and 'discontinuous' rills to continuous erosion rills and (ephemeral) gullies. The distinction between 'rills' and 'gullies' was mainly drawn by the possibility to remove rills by tillage operations (FAO, 1965), or by a critical cross-section of 930 cm^2 (Poesen et al., 1996). Because this work focuses on the dynamic evolution of topography and erosion features in an area left to undirected succession, a differentiation based on a critical size or effects of agricultural operations is not practicable. The term 'erosion rills' or 'rills' is therefore used for referring to all linear erosion features, irrespective of their size. Erosion rills in the Hühnerwasser catchment terminate and pass into sedimentation areas at several points at the base of the slope. The rills thus do not, sensu strictu, form one single network; however, discharge from these rills is routed to one common point at the outlet of the catchment. For this reason and for simplicity reasons, the entire complex of erosion rills that are connected to the sedimentation area is referred to as a 'rill network' throughout the following work.

Sediment deposited at the lower parts or base of slopes as a result of mass movement and unconcentrated overland flow is generally described with the term 'colluvial', while the term 'alluvial' is used to denote material transported or deposited by running water (Soil Science Glossary Terms Committee, 2008). The term 'colluvium' is also used to describe any correlate sediment of soil erosion, not distinguishing between erosion by unconcentrated and concentrated flow; and to describe the correlate sediments of anthropogenically induced soil erosion (Leopold and Völkel, 2007). Landforms resulting from the deposition of sediment by streams are correspondingly termed alluvial fans, while steeper landforms resulting from the deposition of material transported by gravity-driven processes are commonly termed debris cones. Fan-shaped colluvial deposits have also been termed colluvial fans (Innes, 1985; Moller et al., 1995). For the Hühnerwasser catchment, it can be presumed that processes of sediment redistribution by concentrated overland flow, occurring as ephemeral and as continuous runoff along the erosion rills, were dominant in generating the fan-shaped sediment deposits at the lower slope area. Deposited sediment in the Hühnerwasser catchment emanated from the base of several gullies in the catchment, so that a sediment body consisting of several intersecting fan-shaped deposition areas emerged. Because the deposition areas of sediment emanating from specific erosion rills cannot be differentiated, the term 'alluvial fan' will be used to describe the entire sediment body deposited at the base of the slope in this work.

4 3D initial sediment distribution and quantification of mass balances of an artificially-created hydrological catchment based on DEMs from aerial photographs using GOCAD

The material presented in this Chapter was published as Schneider, A., Gerke, H. H., Maurer,T., 2011. 3D initial sediment distribution and quantification of mass balances of an artificially-created hydrological catchment based on DEMs from aerial photographs using GOCAD. Physics and Chemistry of the Earth (Special Issue: Hydrological Observations) 36 (1-4), 87-100.
doi: 10.1016/f.pce.2010.03.023.

4.1 Abstract

The spatial distribution and properties of parent material components form the starting point for any soil and ecosystem. Initial phases of ecosystem development are predominantly characterized by the redistribution of sediment components. To improve the understanding of soil-landscape development, the initial sediments need to be quantified in space and time. This study aims at developing and testing methods for the quantification of initial sediment mass balances in the three dimensions of space and in time. The initial mass balance and composition of parent material in an artificially created hydrological catchment were quantified from a 3D model of the catchment's water storage layer. Multidate DEMs were constructed from photogrammetrically derived elevation data after the assessment and improvement of elevation data quality. Three-dimensional models of volume change were constructed from the DEMs. Regions of significant volume change were identified. Mass changes were calculated from the volume changes in combination with bulk density information. Based on information about the catchment's construction, mass changes were separately analysed in subregions of the models. Terrain attributes were com-

puted to characterize surface structure and to examine correlations with mass change. From the 3D model, an initial sediment volume of 122608 m^3 was quantified. A variation of about ± 12300 m^3, due to uncertainty in DEMs from aerial photographs, was calculated. The 3D model indicates differences in sediment properties between the western and eastern part of the catchment, which are most probably resulting from the dumping of two separate material deliveries during the construction. Models of volume and mass change are constructed for three time periods of catchment evolution. Spatial variations in volume and mass change are observed. The total mass balance reveals a considerable mismatch between the detected amounts of erosion and sedimentation, which gives reason to closely examine the quality of the DEMs. Terrain attributes of four elevation models reflect the diversification of surface structures. Correlations between volume change and surface structures show that erosion processes are dependent on initial surface structures and that these structures, in turn, are enhanced by the processes of sediment redistribution. Although there is a considerable uncertainty in the observed mass changes, the 3D modelling approach allows a first approximation of the initial, mostly erosion-affected, surface structural dynamics of the artificial catchment. The comparison of multi-date elevation data allows a critical evaluation of the quality of models of change obtained from repeated topographical surveys.

4.2 Introduction

The solid phase represents the starting point for any geo-hydrological system (i.e., a system characterized by dynamic interactions between geological, geomorphological, and hydrological processes). Rocks or sediments are the mineral parent material from which soils develop by processes of pedogenesis (Scheffer et al., 2008). The solid phase of the sediments provides the initial structure and material components and forms the spatial frame for ecosystem development in a geographic and landscape context. Soil and ecosystem development starts wherever buried sediments get exposed to surface conditions or where sediments are newly exposed to differing environmental boundary conditions. Also in disturbed landscapes, where ecological development starts at point zero (Hüttl and Gerwin, 2005), soil formation begins on recently exposed, modified, or 'fresh' sediments. Here, the spatial distribution and mineralogical properties of the solid sediment components form the initial condition of the system that determines the further soil and ecosystem development (Hüttl and Weber, 2001; Schlichting, 1993; Sommer et al., 2008). Physical, chemical, and mineralogical properties of parent material constituents and their spatial distribution predetermine the soil that can develop (Wysocki et al., 2005). The components of primary sediments as one of Jenny's main factors of soil genesis (Jenny, 1941) need to be quantified to improve the understanding of relationships between parent material and developing

soil patterns (Shaw et al., 2004). The soil system can be described as a four-dimensional continuum, characterized by a spatial variability in all the dimensions of space (Delarue et al., 2009) as well as variability in time (Schlichting, 1993): The spatial distribution of sediment components is not stable, but the properties of the system are changing by spatially distributed processes of sediment component rearrangement. One of the most important processes that considerably alter the sediment distribution and form the system's structures in initial phases of ecosystem development is the redistribution of sediment components due to erosion and sedimentation (Biemelt et al., 2005; Hancock et al., 2008). This redistribution furthermore creates new areas of initial conditions as it limits soil development (Nicolau, 2002). The development of the soil system is influenced by an interaction of pedochemical and geomorphic processes in all the dimensions of space and time and requires to be studied by multi-dimensional, soil-geomorphic approaches, as stated by Birkeland (1990).

Three-dimensional (3D) soil-landscape models of established systems have been developed, mostly based on a combination of geostatistical interpolation of soil sampling data and topographic attributes derived from digital elevation data (Delarue et al., 2009; Grunwald et al., 2000; Mendonca Santos et al., 2000; Park and Vlek, 2002). Sommer et al. (2008) modelled soil-landscape development in spatial and temporal resolution based on topography and parent material as the initial conditions. The redistribution of sediment components due to erosion and sedimentation processes has been monitored and analysed by a variety of methods. Traditional methods for measuring soil and parent material redistribution like the use of erosion pins or detailed field assessment (Casalí et al., 2006; Vandekerckhove et al., 2001) have been complemented by remote sensing techniques and the use of DEMs constructed from GPS (Global Positioning System) field surveys (Ramos et al., 2008) or photogrammetry (Martinez-Casasnovas et al., 2003; Nachtergaele and J. Poesen, 1999). DEMs constructed from sequential aerial photographs have been used to map volumetric changes and to measure erosion processes in actively eroding, established gully systems (Betts and DeRose, 1999; Betts et al., 2003) or in cultivated catchments (Vandaele et al., 1996). The determination of DEMs of difference from multi-date elevation models, obtained by repeated topographic surveys, has mainly been used for detailed monitoring and modelling of sediment redistribution in gravel-bed river systems (Brasington et al., 2000; Lane et al., 2003; Milne and Sear, 1997) or experimental drainage basins (Brasington and Smart, 2003). The uncertainty inherent in such models of morphological change has been analysed (e.g., Brasington et al. (2000), Lane et al. (2003)) and has mainly been dealt with by defining minimum levels of change detection based on statistical theory of error propagation (Lane et al., 2003; Taylor, 1997).

However, initial structures of primary sediments and changes in mass balances during the

earliest phases of system development have hardly been visualized and quantified in 3D. A combination of sediment volume change with sediment composition and 3D distribution of sediment, including the heterogeneity of the material, has rarely been attempted. Most studies are spatially limited to the monitoring of processes on eroding hillslopes and do not include the monitoring of sedimentation areas. Therefore, complete catchment mass balances are hardly quantified, which reduces the possibilities of methodical validation. Artificially-created watershed-systems, for which the construction and the initial parent material properties have been documented and multi-temporal information on the development of surface structures exists, offer a chance to further evaluate the approach of constructing 3D models of change. Out of the few systematically observed artificial systems (e.g., Elshorbagy and Barbour, (2007), Kendall et al., (2001), Nicolau, (2002)), the hydrological catchment 'Hühnerwasser' ('Chicken Creek') is exceptional with respect to size and monitoring intensity (Gerwin et al., 2009a). In the catchment, the structures and processes of initial ecosystem development have been intensively monitored since completion of the construction works (Schaaf et al., 2008).

The main objectives of our research are the 3D quantification of sediment mass distribution and parent material composition for characterizing the starting point of ecosystem development and the quantification of further alterations in mass balances. This study aims at the quantification of spatial and temporal dynamics of erosive mass relocations during the first years of development of the 'Chicken Creek' catchment and at the exploration of their interdependencies with surface structures and sediment properties. We describe an approach to determine volume and mass changes during the initial development phases of the artificially created hydrological catchment by constructing, analysing, and discussing 3D models of change.

4.3 Material and Methods

4.3.1 Data base

The construction of the artificial catchment has been monitored by a series of aerial photographs, which depict the successive dumping and spreading of the clay and storage layer's material on the site. The catchment's surface was repeatedly recorded by photogrammetric analysis of aerial photographs during and after the construction. Surface elevations were obtained in a 1 m by 1 m grid by automated digital photogrammetry in the mine surveying department of Vattenfall Europe Mining AG, Cottbus, using the software packages Match-T and DTMaster (inpho GmbH). Orthophotographs were taken with a digital camera (DMC01-0007 Z/I Imaging Intergraph) at a flight altitude of about 1250 m. Ground resolution is about 0.16 m (Dominik, 2007). Based on flight altitude and camera parameters,

Dominik (2007) calculated a vertical accuracy of ± 0.147 m. This value corresponds with the achievable accuracy of elevation values of 0.02 - 0.03 % of aircraft altitude (Fryer et al., 1994). The initial structure of the surface was recorded in November 2005 after completion of the construction works; the surface was recorded again in May 2006, November 2007, and August 2008. Additional topographic data with a vertical accuracy of about ± 0.02 m was obtained using Trimble R8 differential GPS (d-GPS) (Trimble, Sunnyvale) running in realtime kinematic (RTK) mode (Fig. 4.1). On a 20 m by 20 m grid, the surface elevation of 121 data points was measured with d-GPS in October 2008, another 81 coordinates located along the borderline of the catchment area were obtained in July 2008 (M. Dimitrov and R. Nenov, personal communication, 2009).

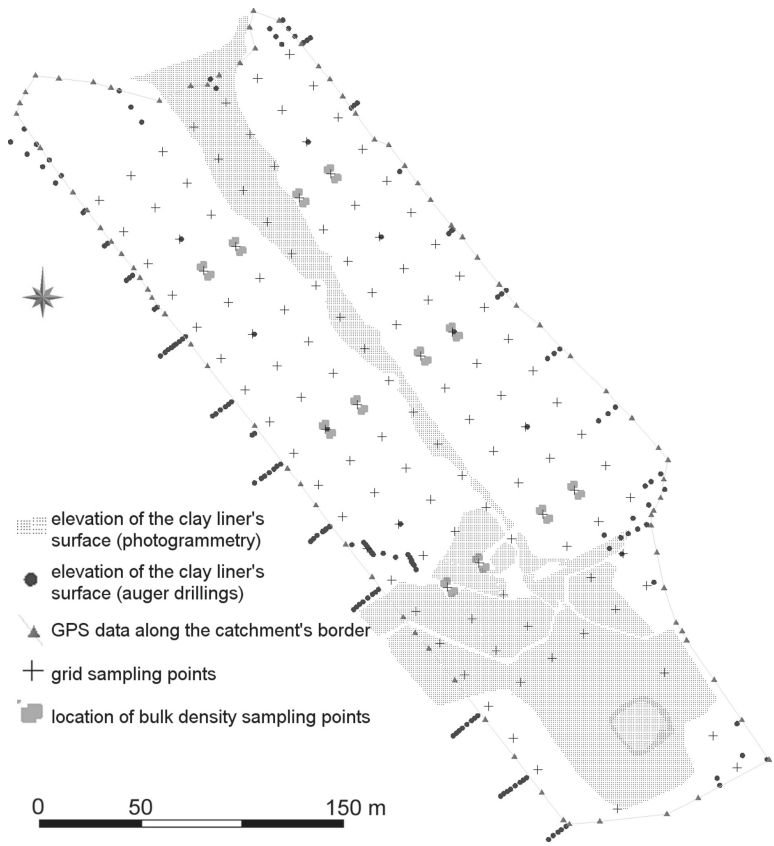

Figure 4.1: Basic elements of the data base used to construct the 3D-models. Surface elevation data from repeated photogrammetric surveys is processed in the area marked by the connection of GPS data along the catchment's borderline. The closely spaced bulk density sampling points are depicted in more detail in Fig. 4.5.

The surface area of the bottom clay liner could not completely be recorded in aerial photographs because, as a result of the rapidly progressing catchment construction, parts of the clay liner were already covered by quaternary sediments at the time of the survey flights. Thus, an additional 155 manual auger drillings (Fig. 4.1) were carried out to determine the elevation of the clay liner in the regions not identified by the aerial photographs. At 137 auger-hole positions, the clay liner was encountered in less than 2 m depth; coordinates were recorded using tape measure and d-GPS. Another 20 point coordinates of the clay layer's surface were available from observations during the installation of piezometer tubes for measuring the ground water level (D. Biemelt, personal communication, 2009). Soil physical and chemical data was from 301 disturbed samples from a 20 m by 20 m grid, taken in depth intervals of 30 and 50 cm down to the clay liner between October 2005 and April 2006 (Gerwin et al., 2009b). Additional bulk density data of the soil near the surface (0 - 3 cm) was from 192 locations sampled in August 2008 (A. Dümig, personal communication, 2009). Spatial data were processed using the Software package GOCAD Suite 2.5.2 (Paradigm Ltd., George Town). TIN elevation models and gridded 3D models are constructed from point coordinate data, sediment properties are then assigned to these models. To prepare raw elevation data for modelling in GOCAD, we used Surfer Version 8 (Golden Software, Inc., Golden). The program SAGA (SAGA User Group Association, Göttingen) was used to calculate terrain parameters from elevation models. Basic statistics were obtained using statistics options in GOCAD and the program SPSS Version 17.0.0 (SPSS Inc., Chicago).

4.3.2 Accuracy assessment and correction of errors in elevation data

To assess and improve the accuracy of the digital elevation data derived from photogrammetric measurements, we considered the following three possible types of errors, following Temme et al. (2008):

(1) Artefacts, in our case, mainly resulted from the unintentional recording of vegetation or monitoring devices installed in the catchment. To remove this type of outliers in surface elevation data, a threshold filter was applied in Surfer to replace elevation data points that differ more than 0.3 m from the average of the surrounding elevations with the arithmetic mean of surrounding elevations in a 5 m by 5 m window. The threshold value was iteratively adjusted to ensure that only individual outliers are affected by the filter procedure.

(2) Random errors can occur as a result of imprecise pixel matching (Wise, 2000) or limited quality of the original orthophotographs. We assume that the potential random error in the processed data set equals the accuracy in elevation (Z) values σ_z = 0.147 m.

(3) Systematic errors can occur when the general elevation level is shifted. These errors are often not detectable in elevation data without statistical procedures. To assess the amount of a possible systematic error, a reference data set of 61 points was extracted from the d-GPS elevation measurements arranged in a 20 m by 20 m grid. The points that were not affected by linear erosion processes were selected by analysis of aerial photographs and field observations. For these locations, the elevation was assumed to be relatively constant in time, and differences to the corresponding reference data were calculated. In absence of systematic and random errors, the mean and variance of these deviations would be negligible (Derose et al., 1998; Martinez-Casasnovas et al., 2003).

As statistical quality criteria, the Root Mean Square Error (RMSE), the Mean Error (ME) and the error standard deviation (SDME) were computed from the deviations between each set of elevation data and the reference data set (Fisher and Tate, 2006):

$$RMSE = \sqrt{\frac{\sum (Z_{DEM} - Z_{REF})^2}{n}}$$

$$ME = \frac{\sum (Z_{DEM} - Z_{REF})}{n}$$

$$SD_{ME} = \sqrt{\frac{\sum [(Z_{DEM} - Z_{REF}) - ME]^2}{n - 1}}$$

where Z_{DEM} is the elevation in the digital elevation data set, Z_{REF} is the elevation of the corresponding point in the reference data set, and n is the number of elevation points. The 2D spatial distribution of deviations from the reference data was depicted in 'error maps'. In order to account for the spatial variability in elevation errors, the elevation data were locally adjusted to the reference data set in a fitting procedure using GOCAD. The procedure, similar to a geocoding, shifted elevation data to the position of the reference data points and iteratively computed the new position of data points in areas where no reference data were available.

4.3.3 Surface digital elevation models

The DEMs were constructed from the filtered and adjusted topographic point elevation data. TIN elevation models of the surface were created by Delauny Triangulation in GOCAD. The surface elevation models were delimited to the catchment area using a polygon constructed from the point coordinates representing the catchment's border. In case of those elevation models that were recorded after the construction of the delineating rampart, elevation information on the topography of the catchment's boundary was included: a curve was constructed from the 81 GPS points marking the topography of the rampart. This

curve was split into segments of 1 m in length and the resulting nodes were added to the elevation dataset before triangulation. The areal extent of the elevation models was calculated in GOCAD. No elevation data were available for the pond area because photogrammetric measurements could not deal with the water surface. This area was excluded from the interpretation. For delineating the contours of the lake, monitoring data of the water level were used to virtually flood the pond area (i.e., all elevation data at the time of data acquisition were shifted to the water level).

4.3.4 Construction of a 3D grid model of the catchment

A 3D grid model defining the spatial delineation of the catchment was constructed using both the elevation model of the subsurface catchment area and that of the surface representing the initial situation (November 2005). The TIN elevation model of the catchment's subsurface delineation (the surface of the clay liner) was constructed in GOCAD. The irregular spacing of data points required further enhancement of the TIN by adjustment of the triangle sizes in GOCAD. The subsurface catchment area was then extracted from the DEM by a manual digitalization of local watersheds. The areal extent of the subsurface catchment delineation was computed in GOCAD.

Because the lateral boundaries of surface and subsurface catchment areas do not fully coincide, several steps were necessary to construct the 3D model (see Fig. 4.2): First, the surface DEM was laterally extended to match the boundary coordinates of the subsurface DEM. A 3D block model was then constructed, based on the laterally extended DEM and the distances between the extended and the subsurface DEM. Subsequently, a surface representing the lateral boundary of the catchment was created from the borderlines of the two elevation models and split into parts inclined inwards or outwards in vertical direction. These surface parts were then used to define the model's lateral boundary by using an option in GOCAD that fits 3D volume models to surfaces, which is basically done by 'squeezing' the size of 'excess cells' (i.e., cells that are overlapping the lateral boundary) up to zero volumes. The grid model was subdivided into cells 1 m by 1 m by 0.2 m in size, to which sediment properties were attributed. Physical and chemical parameters of the sediment were assigned to the cells by Ordinary Kriging, following a 3D analysis of spatial variation. Bulk density data (only available for 0 - 3 cm) were interpolated onto a separate submodel representing the topmost 3 cm of sediment, which was constructed using the DEM of the initial surface. To include information about potentially differing sediment properties (resulting from the dumping of slightly differing basic materials in construction) to the model, areas in which material has been deposited in different phases of construction were digitized from aerial photographs.

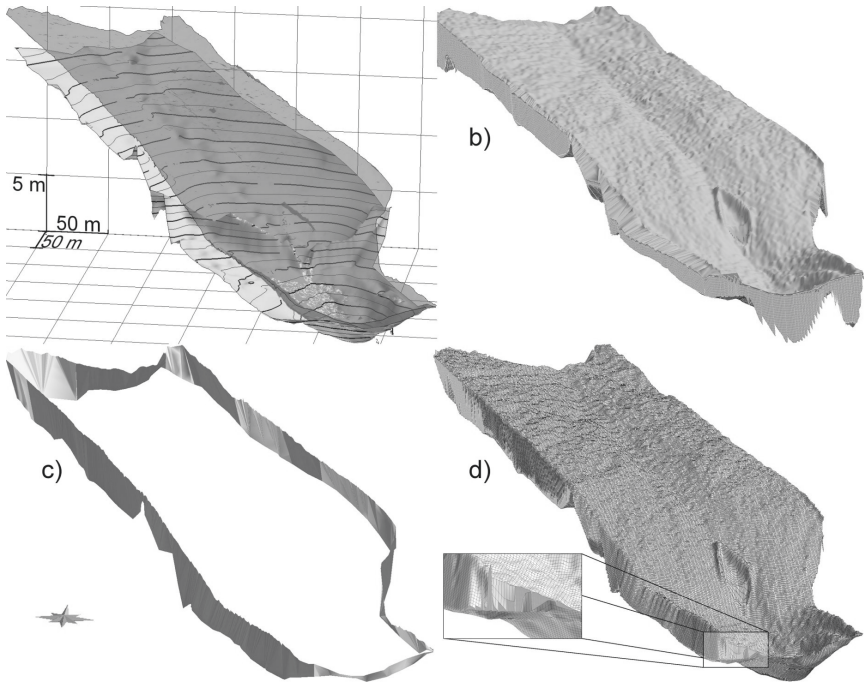

Figure 4.2: Construction of the 3D volume model: (a) The two confining digital elevation models. Topography of the clay liner DEM is indicated by contour lines. (b) The laterally extended surface DEM and the 3D block model. (c) Lateral bounding surface, split into parts inclined inwards and outwards. (d) 3D-grid model. The enlarged detail exemplarily shows a segment where the lateral boundary is not clearly defined. All images are displayed with 10 *superelevation.

4.3.5 3D models of volume and mass change

The change in sediment volumes and the mass balances were analysed using the TIN elevation models representing the successive stages of surface evolution as follows:

First, we constructed 3D models of volume change for each time interval confined by one pair of elevation models. The elevation distances between each node of one DEM and the vertically corresponding point on the other DEM were computed. Based on these differences, 3D volume bodies enclosing the volume of change were constructed. The volume bodies were divided into cells 1 m by 1 m in size to allow a spatially distributed analysis of volume change. Cell volumes were computed and information about the direction of change was added from the calculated elevation differences. To derive mass change from volume change, we assigned the spatially interpolated distribution of bulk density to the cells and multiplied cell volumes and bulk densities. Bulk density in depths below 3 cm was assumed to equal the values of the topmost 3 cm. In the outermost eastern and northern areas of the catchment (outside of the fence around the monitoring area, see Fig. 3.1), sur-

face development unaffected by disturbances by human visitors or game animals cannot be ensured. These areas thus were not considered when interpreting mass changes. Moreover, the pond area, where the water table rather than the sediments represent the surface, was separated from the models of change and also not included in the interpretation.

In order to detect volume and mass differences in the 3D models caused by propagated errors of the 2D elevation data, regions of significant elevation change were separated after converting elevation differences to a *t* statistic (Brasington et al., 2003), following Lane et al. (2003), and Taylor (1997). For this, it was assumed that elevation data Z are normally distributed and independently measured at each date of recording (1, 2) and that there is no spatial variation in accuracy of the raw data. From the standard deviations in elevation (σ_1, σ_2 = 0.147 m) of each pair of elevation models used to construct the model of change, the standard deviation in elevation change, σ_c, is obtained by:

$$\sigma_c = \sqrt{\sigma_1^2 + \sigma_2^2} = 0.2079 \text{ m}$$

The standard deviation in volume change, σ_v, was calculated as:

$$\sigma_v = d^2\sqrt{\sigma_1^2 + \sigma_2^2}$$

In case of a spatial resolution of volume change in cell sizes d = 1 m, the values of the standard deviation in volume σ_v equal that of σ_c, the standard deviation in elevation differences. A *t* statistic T is calculated for each grid cell by:

$$T = \frac{Z_1 - Z_2}{\sqrt{\sigma_1^2 + \sigma_2^2}}$$

with $Z_1 - Z_2$ = the elevation difference between the pair of DEMs.

Threshold values of T were used to determine areas where significant change occurs. Under the *t* distribution, a threshold value of T = 1.96 was used to extract areas where a significant change occurs with a confidence of 95 % or greater. As another threshold value, T = 1 was used to extract areas with a confidence limit of 68 %. Regions of significant mass change have not been determined because the accuracy of mass change is strongly influenced by the interpolated values of bulk density.

Mass changes were analysed separately in areas of potentially differing sediments by visual interpretation of maps and descriptive statistics (minimum and maximum values, mean, median and variance) using SPSS Statistics 17.0.0. The models of change were divided into subregions based on the digitized areas of potentially differing sediment properties, and

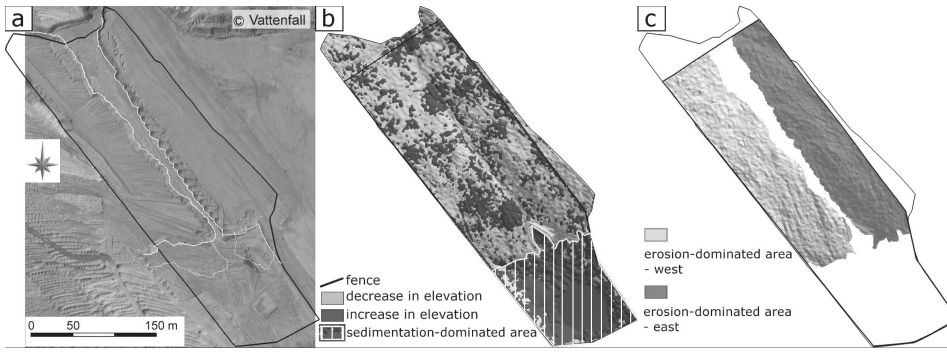

Figure 4.3: Reconstruction of areas of differing source sediments. The catchments boundary is marked by solid lines. The aerial photograph recorded in April 2005 (a) shows the dumping of material in two sections on the western and eastern part of the artificial catchment. White lines show the digitized areas. Based on the observed changes in elevation, the model is divided in erosion- and sedimentation-dominated areas (b). By combining (a) and (b), the regions used for separate analysis of mass changes are defined (c). adapted from Schneider et al. 2011.

mass balances were analysed separately in the eastern and western part of the hillslope. In order to better distinguish between processes of erosion and sedimentation in the statistical analysis, a boundary between the erosion-dominated area and the sedimentation-dominated area was manually defined, based on the visual assessment of the fractions of recorded elevation increase and decrease (see Fig. 4.3).

4.3.6 Characterization of surface structures

Topographic attributes were computed from the elevation data to characterize surface structures. The TIN elevation models were transformed to gridded elevation models to enable the computation of the specific catchment area (CA) for each cell using the Deterministic Infinity Algorithm (Tarboton, 1997) implemented in the module 'parallel processing' in SAGA. Local slope β [rad] for each node of the TIN surface models was computed in GOCAD. To analyse surface structures, we calculated for each grid cell the Stream Power Index (SPI), defined as (Moore et al., 1991)

$$SPI = CA \cdot tan\beta$$

to reflect the erodibility due to surface topographic conditions (high values of the SPI reflect high erodibility), and the Topographic Wetness Index (TWI), defined as (Beven and Kirkby, 1979)

$$TWI = ln\frac{CA}{tan\beta}$$

to indicate areas of flow accumulation and potentially high soil moisture contents (high values of the TWI indicate areas of flow accumulation (Florinsky, 1998)).

4.4 Results

4.4.1 Mass and 3D-spatial distribution of sediment components

A 3D model of the catchment's storage layer (Fig. 4.2) was constructed from the DEM of the clay liner's surface and the DEM of the surface's state on November 26, 2005. After excluding the pond area from the model, a sediment volume of 122608 m^3 was computed. Based on an accuracy of ± 0.147 m for both the delineating soil and clay surface elevation models, the accuracy of the calculated volume is about ± 12300 m^3, i.e., about ± 10%. Computation of the areal extent of the clay liner and surface DEM shows that the subsurface catchment area is larger than the surface catchment area (Table 4.1). From the areal extension of the 3D model and the total sediment volume, a mean sediment thickness of 1.93 m was calculated.

The spatial interpolation of the sediment samples' physical and chemical properties onto the 3D grid model reveals that sediment properties are not homogeneously-distributed throughout the catchment. The spatial distribution of both physical and chemical properties shows a difference between the western and eastern part of the sediment body. Sand content, for example, roughly ranges between 77 % and 86 % in the western and between 80 % and 95 % in the eastern part (Fig. 4.4). Correspondingly, silt content is higher (up to 20 %) in the western than in the eastern part. Organic carbon content ranges between 0 % and 0.15 % in the eastern part while in the western part organic carbon contents of up to 0.7 % occur (not shown).

Table 4.1: Quantitative results obtained with DEM's and the 3D model on the catchment's areal extension, volume, and sediment thickness. DEM_surft0 is the DEM of the surface at starting time of system development (t0: November 26, 2005); DEM_clay is the DEM of the clay liner's surface.

Areal extension [m^2] of				Computed total sediment volume [m^2][c]		Computed mean sediment thickness [m]	
Surface (DEM_surf_t0)	Subsurface delineation (Dem_clay)	3D model[a]	initial pond region[b]	mean	standard deviation	mean	standard deviation
59210	62296	63375	1993	122608	±12300	1.93	± 0.19

[a] including the pond region. Areal extension is larger than that of the confining DEMs because DEMs do not coincide.

[b] the pond region was digitized by visual interpretation of the 3D model

[c] to calculate the total sediment volume and mean sediment thickness, the pond area was excluded from the 3D model

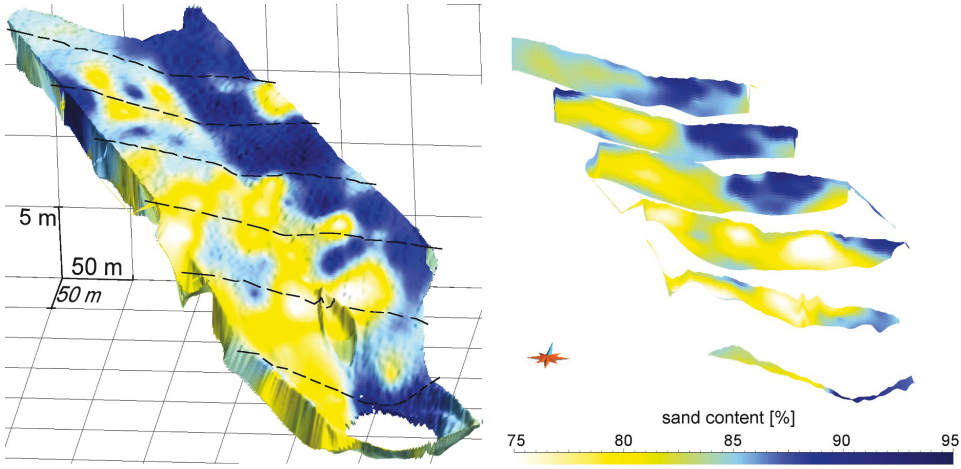

Figure 4.4: 3D-spatial distribution of the sand fraction (left) in an overall view of the grid model (displayed with 10 *superelevation) and (right) in six vertical cross-sections through the sediments (marked by dashed lines in the left image). Sand content was interpolated from sampling points onto the 3D-grid by Ordinary Kriging, using a spherical variogram model.

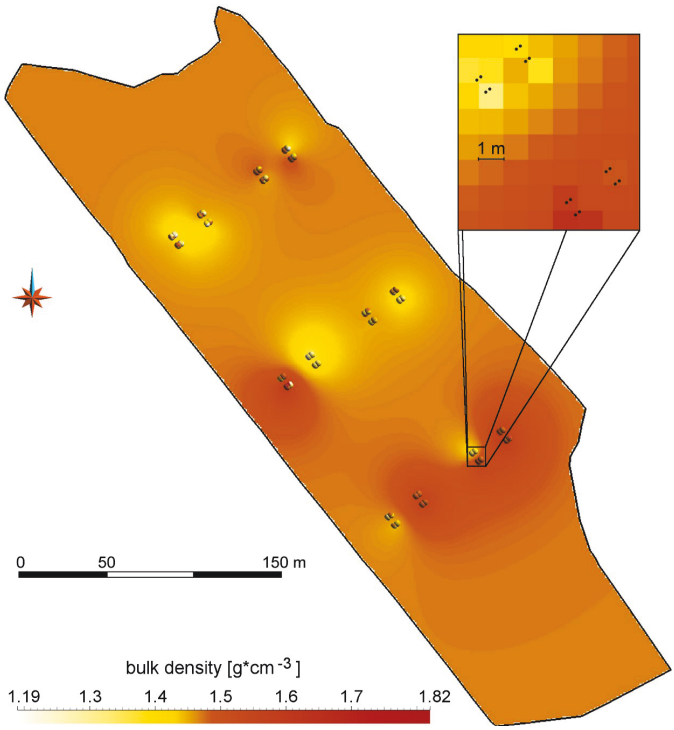

Figure 4.5: Two-dimensional map of the spatial distribution of the soil bulk density near the surface (0-3 cm depth). The spatial interpolation was carried out by Ordinary Kriging. Data points are indicated by circles on the map and by black dots on the enlarged detail.

From analysis of spatial variance in the bulk density data, an exponential variogram model with nugget = 0.0052, sill = 0.00952 and range = 17 m was derived. Spatial interpolation by Ordinary Kriging, based on this model, results in a 2D map of bulk density values (Fig. 4.5) ranging from 1.19 $t \cdot m^{-3}$ to 1.82 $t \cdot m^{-3}$. However, the range of the variogram model is limited to a lag distance of 17 m (i.e., no spatial autocorrelation at larger distances between sampling points). The Ordinary Kriging procedure estimates global mean bulk densities of 1.47 $t \cdot m^{-3}$ (Fig. 4.5) for the larger distances.

Areas of potentially differing parent material can be distinguished by analysis of aerial photographs: The aerial photograph taken in April 2005 (Fig. 4.3) shows that storage layer material had been dumped by the spreader in two sections on the western and the eastern part of the catchment, whereas in an elongated region in the centre of the hillslope, the clay liner was still exposed to the surface at that time. Later photographs show that the material was spread out by caterpillars to the areas further downslope from each of the heaps of sediment. To fill the central area of the backslope, material from both sides was spread out and therefore the sediments in this region must have been mixed somehow. The footslope area surrounding the lake could not further be subdivided with respect to the construction procedures.

4.4.2 Quantification of mass balances from multi-date DEMs

The quality assessment of the raw elevation data for the four DEMs yields criteria (Table 4.2) that prove the presence of errors in the elevation data. The mean error in elevation data varies between -0.128 and 0.123 m. No temporal trend in the sequence of errors can be observed, but error maps reveal a spatial concentration of higher erroneous values in some parts of the recorded area. For example, the error map computed for the elevation data set of November 2007 (Fig. 4.6) suggests a steplike increase in error in the backslope region. This structure may result from the linkage of two aerial photographs prior to the automated photogrammetric data acquisition or from a 'firth effect' (a characteristic pattern of misestimation of elevation in automated digital photogrammetry) as it is described by Hunter and Goodchild (1995).

Table 4.2: Statistical quality criteria of elevation data

Photographs recorded in	RMSE	ME	SD_{ME}
	———[m]———		
November 2005	0.116	-0.100	0.058
May 2006	0.148	0.123	0.083
November 2007	0.141	-0.128	0.058
August 2008	0.073	-0.048	0.055

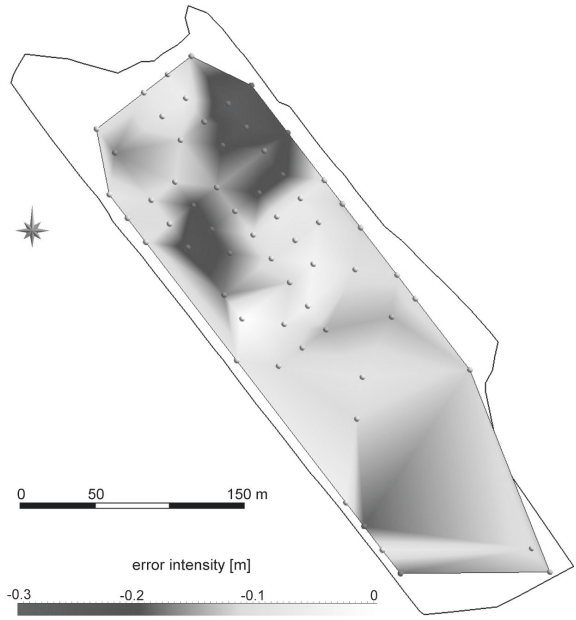

Figure 4.6: Error map for the digital elevation model of November 21, 2007, derived from the differences between the elevation data and the reference data set. Location of the reference data points is indicated by circles.

Errors were reduced based on these data as described above, however, visual analysis of the resulting DEMs shows that the corrected models are seemingly still of differing quality regarding the surface structure (Fig.4.7). We assume that the differing patterns are a result of differing quality of aerial photographs and of seasonally differing development of vegetation cover. The elevation model from data recorded in November 2005 depicts the initial condition as a quite even and regular surface. The elevation data recorded in May 2006, however, seem to be more irregular and the overall surface appears rough. In the DEM of November 2007, major erosion rills are observable, while the surface between the rills appears smooth and regular. Deeply incised erosion rills are again clearly observable in the DEM of August 2008, yet the surface between the rills here seems slightly more irregular. Overall, the DEMs reflect the diversification of surface structures through the development of a network of erosion rills on the catchment's surface from November 2005 to August 2008.

Rates of mass changes in the three time intervals defined by the four processed elevation models have been computed (Table 4.3) and their spatial distribution has been depicted in maps. A comparison of the spatially distributed erosion and sedimentation dynamics in the three time intervals (Fig. 4.8) reveals that mass changes are rather uniformly dis-

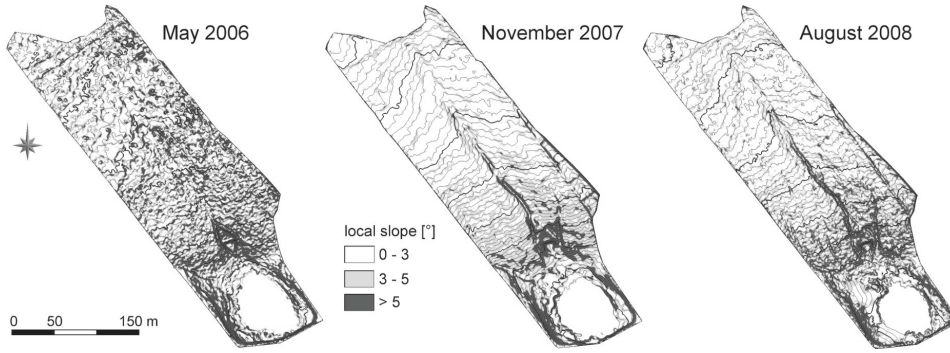

Figure 4.7: Digital elevation models of the surface for different stages of development. Topography is depicted by contour lines and local slope distribution. Local slope resolution is 1 m.

tributed throughout the catchment in the first interval of development. In the time span from May 2006 to November 2007, distinctive formation of linear erosion structures and alluvial fans took place. Between November 2007 and August 2008, development of the existing erosion and sedimentation structures continued. The numerical results (Table 4.3) suggest that there is no clear and constant disparity in the spatial extension of areas affected by mass increase and decrease. The maps of calculated mass changes (Fig. 4.8) show that in large areas of the hillslope, low amounts of positive as well as negative changes have been recorded. Comparatively low amounts of negative change are recorded on major parts of the hillslope, whereas relatively high amounts of surface heightening are observed in spatial concentration in the area of alluvial fan formation. The higher spatial concentration of elevation and mass increase is recorded in the constantly higher values of spatial variance (Table 4.3). The different characteristics of recorded positive and negative change are also reflected in the identification of regions of significant volume change (Table 4.4): Significant negative volume change with a confidence level of 68 % is detected in an area of 1342 m^2 (i.e., on about 3.4 % of the backslope area). Mainly the six most distinct erosion rills are depicted in this region of significant erosion. Contrarily, 68 % significant sedimentation is recorded in an area of 4144 m^2, i.e. on about 40 % of the footslope area.

A first total mass balance for the time span from November 2005 to August 2008 (Table 4.3) indicates the erosion of 2870 tons of sediment and the resedimentation of 5066 tons of material. The maps of mass changes (Fig. 4.8) depict differing erosion dynamics in the western and eastern part of the catchment. Erosion seems to be more intense in the eastern part. Furthermore, few but relatively pronounced erosion rills are clearly recognizable on the eastern part, whereas on the western part the spatial concentration of erosion is less distinct. Separate statistical analysis (Table 4.5) of the rate of mass change in the areas of

Table 4.3: Rates of mass change for the entire interpreted area, separated into increase and decrease of sediment mass, in three single time intervals and the whole observed time interval.

Time interval		Area affected [m^2]	Rate of sediment mass change [$tons \cdot m^{-2} \cdot year^{-1}$]				Total mass change [t]
			Min.	Max.	Mean	Variance	
26.11.2005 -	Increase	25816	0.0061	2.7872	0.3140	0.0635	3464.38
01.05.2006	Decrease	23199	-2.4342	-0.0061	-0.2604	0.0366	-2581.77
01.05.2006 -	Increase	22358	0.0022	0.7662	0.1043	0.0091	3623.05
21.11.2007	Decrease	26208	-0.7378	-0.0024	-0.0959	0.0058	-3903.68
21.11.2007 -	Increase	26158	0.0009	1.5298	0.1367	0.0172	2635.16
18.08.2008	Decrease	22827	-05704	-0.0027	-0.1056	0.0065	-1776.10
26.11.2005 -	Increase	25349	0.0006	0.7414	0.0735	0.0103	5065.92
18.08.2008	Decrease	24340	-0.4729	-0.0010	-0.0434	0.0020	-2870.03

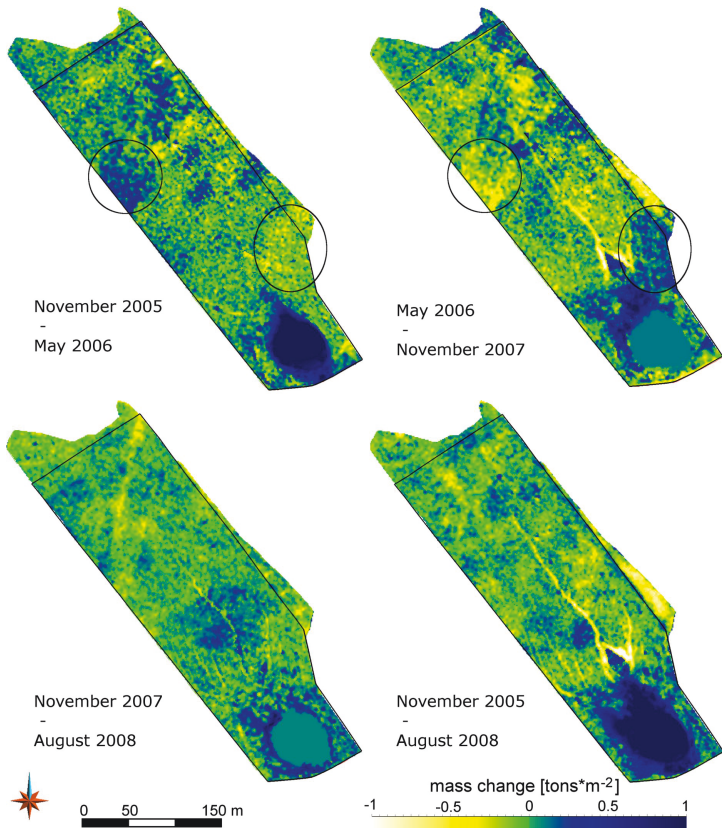

Figure 4.8: Spatial distribution of calculated mass changes for three individual time intervals and for the time interval between November 2005 and August 2008. Areas outside the fencing (marked by solid line) are affected by anthropogenic influence and thus excluded from interpretation. Negative mass changes indicate linear erosion features; positive values reflect the formation of alluvial fans in the lake area. Areas marked by circles are further discussed in the text.

Table 4.4: Increase and decrease of surface elevation and changes of sediment volume in the entire model and in regions of significant change.

	Area affected [m^2]		Sediment volume change [m^3]		
	Decrease of elevation	Increase of elevation	Decrease	Increase	Volume Balance
Entire model	24340	25349	-1946.051	3442.369	+1496.318
68 % siginificance	1342	4378	-440.707	2078.863	+1638.155
95 % siginificance	383	2238	-199.485	1475.988	+1276.503

Table 4.5: Sediment mass change in subregions of the 3D model for the time period between November 2005 and August 2008 (Var. =Variance).

		Area affected [m^2]	Rate of sediment mass change [tons·m^{-2}·$year^{-1}$]					
			Min.	Max.	Mean	Median	Var.	Total
Total mass change	West[a]	17762	-0.371	0.159	-0.0097	-0.0124	0.002	-172.72
	East[a]	16561	-0.473	0.216	-0.0180	-0.0153	0.003	-298.86
Decrease	West[a]	10372	-0.371	-0.001	-0.0382	-0.0296	0.001	-396.47
	East[a]	10113	-0.473	-0.001	-0.0486	-0.0345	0.003	-491.59
Increase	West[a]	7390	0.001	0.159	0.0303	0.0235	0.001	223.76
	East[a]	6448	0.001	0.216	0.0299	0.0240	0.000	192.73

[a] Subregions "West" and "East" are derived from analysis of aerial photographs as illustrated in Fig. 4.3

material dumped on the western and, respectively, the eastern part of the catchment (defined as shown in Fig. 4.3) confirms the observed differences. Deep incision of channels, marked by highly negative rates of mass change, predominantly occurs in the eastern part. The variance of erosion rate cell values is higher in the eastern part, i.e., there is a more pronounced spatial separation between few deeply incised erosion rills and areas of relatively stable terrain.

4.4.3 Surface structural development

Local slope was computed for each of the processed elevation models. Statistical analysis (Table 4.6) shows no temporal trend in the development of the mean local slope. However, the increasing variance of the derived values over time indicates a stronger fragmentation of the surface into flat and steep terrain areas and thus a diversification of surface structures.

The Topographic Wetness Index TWI and the Stream Power Index SPI, derived for each of the DEMs representing different stages of surface development, (e.g., Fig. 4.9) trace the evolution of surface structures: Structures that are apparent on DEMs of the initial surface continue to exist on DEMs of the further developed surface. Patterns in the spatial distribution of TWI and SPI index values appear more continuous and more contrasting with time,

which reflects the enhancement of structures due to erosion processes. A comparison of initial structures reflected in the terrain attributes (Fig. 4.9) and spatial structures of mass change (Fig. 4.8) reveals that initial structures are clearly correlated to erosion and sedimentation processes in the first years of surface evolution. Erosion seems to have taken place mainly in those areas where the SPI of the initial surface DEM predicts a higher erodibility.

Table 4.6: Mean and variance of local slope in the processed surface models

DEM	Local slope [°]	
	Mean	Variance
November 2005	3.35	5.67
May 2006	4.22	7.47
November 2007	3.31	8.36
August 2008	3.78	13.98

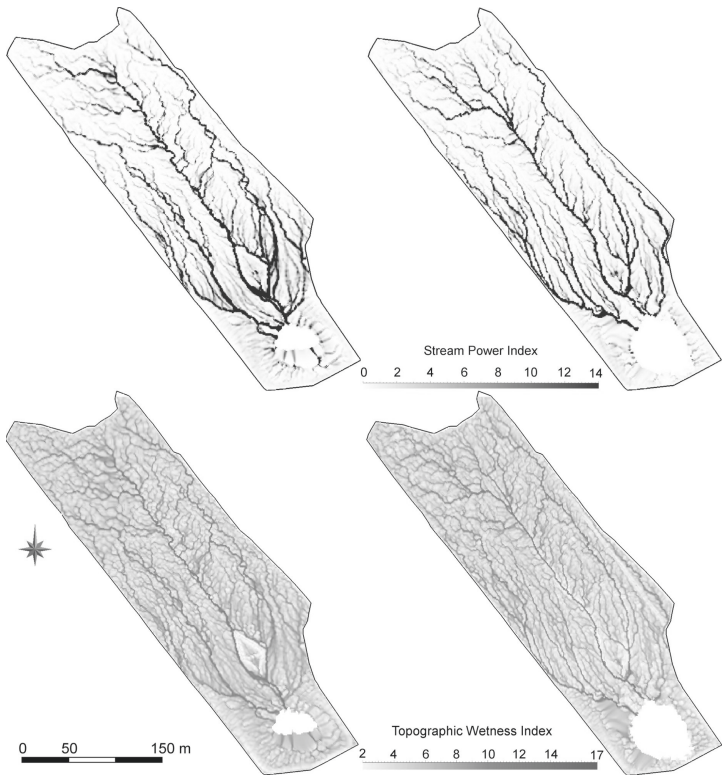

Figure 4.9: Spatial distribution of the Stream Power Index (SPI) and the Topographic Wetness Index (TWI), computed on cells of 1 m2 size, for the elevation models of November 2005 (left) and August 2008 (right). Indices are not calculated for locations in the lake area. High values of the indices trace the surface structures.

4.5 Discussion

4.5.1 3D-spatial distribution of sediment components

A 3D model of the catchment's storage layer was constructed that computed a sediment volume of 122608 m^3 with an accuracy of about ± 10%, based on the accuracy of the delineating elevation models. The uncertainty in the subsurface elevation model might be higher compared to that of the surface DEM, because of the lower spatial density in input data. The accuracy of the calculated volume is further limited because of the complex geometry of the catchment's lateral boundaries (see Fig. 4.2d). Nevertheless, the sediment volume obtained with the 3D model roughly corresponds with the volume (117500 m^3) estimated in the catchment's construction plans (Kendzia et al., 2008).

Sediment physical and chemical parameters were assigned to the 3D-grid model by interpolating sampling data obtained in a 20 m by 20 m grid. As the spatial variability of most physical and chemical sediment properties in mine spoils can be structured, mainly as a result of sediment segregation and compaction during the dumping process (Buczko et al., 2001), the actual heterogeneity most probably cannot be captured by this approach. However, results of the interpolation depict the most distinct differences in sediment properties. Material properties vary between the western and eastern parts of the catchment. Considering the successive dumping of material in several phases of construction, this spatial heterogeneity in sediment properties most probably results from the application of slightly differing source materials. This interpretation is supported by the analysis of aerial photographs of the catchment's construction, which reveals the dumping of material in two sections in the western and eastern area.

The spatial distribution of soil bulk density based on Kriging interpolation is still relatively limited by lack of data and bulk density below a depth of 3 cm could only be assumed at the moment. Because of the large heterogeneity of the material in the artificially constructed sediment layer, predictions about how bulk density changes with depth are uncertain. As for most sediment properties, spatial variability of bulk density can be high in mine spoils (Buczko and Gerke, 2005; Buczko et al., 2001), and bulk density does not vary regularly with depth (Armstrong and Bragg, 1984; Chong and Cowsert, 1997). The spatial variability of bulk density may not sufficiently be captured by sampling and interpolation of sampling data. Results could possibly be improved by simulation of the internal structure based on imitating technogenic processes of catchment construction including sediment transport and dumping (Maurer et al., 2009).

4.5.2 Quantification of mass balances from multi-date DEMs

Before constructing the DEMs of the surface, it was attempted to remove outliers and spatially varying systematic errors from the elevation data. However, visual interpretation of the DEMs showed that the models are of different quality. This may, on the one hand, be caused by artefacts that could not be successfully removed by the applied filter. On the other hand, it might result from different quality of the orthophotographs or from photogrammetric processing. However, as we are working with pre-processed elevation data, we can only assess such effects from analysing the elevation models. Effects of varying DEM quality on calculated mass changes should be considered when interpreting the results of the 3D-models. For example, when a 3D model of change is constructed from the 'rough' DEM of May 2006 and another,'smoother' DEM, both positive and negative differences in elevation are most probably overestimated. This assumption is affirmed by the results of the analysis of change in the discrete time intervals (Table 4.3): Relatively high rates of change are observed between November 2005 and May 2006. Minimal and maximal observed rates of change are comparatively high between May 2006 and November 2007 as well.

Regions of significant volume change have been delimited. These regions largely coincide with the areas where major sediment redistribution is expected, comparing the results with field observations and structures observable in aerial photographs (Gerwin et al., 2009b). However, it needs to be kept in mind that the statistically-based approach can only account for the expected random error of the DEMs. Artefacts in the elevation data can lead to the determination of high changes in elevation and volume which are unintendedly identified as significant. Further limitations of the approach mainly result from the underlying assumptions (Lane et al., 2003), which presume that there is no spatial variation in precision. However, precision might be spatially varying in connection with different surface textures in photogrammetrically derived data. In contrast to the assumed error independence, errors might be spatially clustered in areas of complex topography (Lane et al., 2000).

The establishment of a total mass balance from a comparison of DEMs revealed a considerable imbalance in the amounts of recorded erosion and sedimentation. This is particularly the case considering that material deposited inside the pond (i.e., below the water table) is not yet accounted for. Accounting for these deposits would further increase the imbalance. The values are still highly uncertain because of the summation of partly small alterations over a large area (see also the analysis of uncertainty in the Materials and Methods chapter). An underestimation of erosion as well as an overestimation of sedimentation needs to be considered when examining possible reasons for this imbalance. Consideration of the several factors that might influence the quality of observed mass balances suggests that the approach probably underestimates the total amount of soil erosion, namely because:

(i) Mass change was calculated by multiplying observed volume change and an interpolated spatial distribution of highly uncertain bulk density values, which is the main factor of uncertainty in the calculated mass changes. However, it might be expected that the errors resulting from interpolation of bulk density do not falsely cause spatial differences in the calculated mass changes, as the interpolation results in similar bulk density values of around 1.47 $t \cdot m^{-3}$ in the areas distant to the sampling points.

(ii) Quality of elevation data was assessed and corrections were made based on a comparison with a selection of reference point coordinates which had been recorded at a later date than that of the acquisition of elevation data sets. A similar approach has been applied by Betts and DeRose (1999). The deviations between DEMs and the reference data set can result from systematic as well as random errors. However, it cannot be excluded that the reference points have experienced lowering in elevation caused by diffusive erosion processes or subsidence of sediment. Therefore, it is to be presumed that the corrected elevation data misestimate the real elevations. As a consequence, surface lowering and erosion determined by combining the corrected elevation data might be underestimated.

(iii) TIN elevation models with a node spacing of 1 m have been used to analyse the sediment redistribution. Many of the small erosion rills that have developed on the catchment's surface might not be recorded in these elevation data (Fig. 4.10). In case of larger erosion rills, not the whole extent of the actually canyon- or U-shaped rills is recorded, but rills are depicted in a V-shaped form. Rill volume and with it erosion could thus be underestimated. Further problems for the estimation of changes in volume might result from inaccurately recorded elevations inside of erosion rills due to complex rill topography, overhanging edges or shadowed areas (Marzolff and Poesen, 2009).

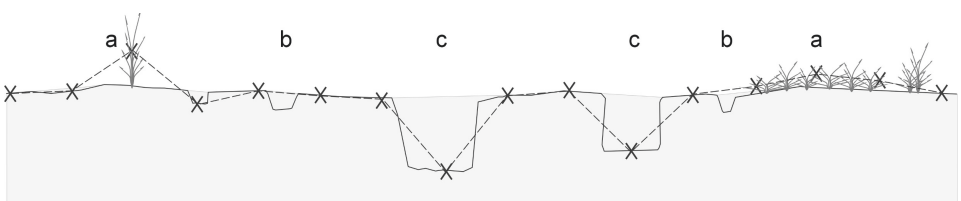

Figure 4.10: Schematic illustration (not to scale) of potential errors in models of change, caused by inaccurate representation of the soil surface in DEMs. An initial surface is shown in grey; the solid line represents a fictitious shape of a soil surface at later development stages. The dashed line marks the developed surface as depicted in a DEM interpolated from recorded elevation data, marked by crosses. (a) Increasing vegetation cover causes overestimation of elevation, (b) smaller rills are not captured in the DEM, and (c) larger rills are not depicted in their actual shape.

(iv) Attempts to remove vegetation depicted in the elevation data were made by applying a threshold filter to the raw data. However, a few single artefacts remained in the DEMs. The results of the approach should be satisfactory as long as the surface is poorly vegetated, but it may not be suitable when the vegetation cover is further developed. Accounting for seasonal variation of vegetation cover, it can be assumed that especially the DEMs of May 2006 and August 2008 are affected by these errors. A widespread but low canopy cover cannot be removed by the procedure and would result in an erroneous detection of surface heightening (Fig. 4.10), as it is also described by Betts et al. (2003). In particular, vegetation growing in the alluvial area around the lake could lead to the false detection of large amounts of sedimentation. Because this vegetation cover is comparably dense and high, its recording might not only result in single outliers but in a cluster of falsely recorded elevation data that is not removed by the threshold filter. Sedimentation erroneously detected by this effect is difficult to reveal by spatially distributed analysis of maps of change, as it is computed in an area where we actually expect sedimentation.

(v) Erosion might be underestimated because of the higher spatial distribution of erosion in comparison to deposition. Lane et al. (2003) examine the effect of noise in DEMs of difference on the level of detection of erosion and deposition and conclude that a bias is introduced to the DEMs of difference in direction to the spatially less distributed process.

(vi) Since the artificial catchment is located on top of an incompletely consolidated mine spoil massive, changes in elevation may also result from subsidence of the underlying spoil, which can affect the catchment as a whole or regions inside the catchment. Surface lowering due to subsidence would affect the calculated mass balances.

(vii) In the very beginning of catchment development, on unvegetated, bare soil surfaces, wind erosion and sedimentation processes could have been of importance (Maurer and Gerke, 2008). Wind erosion and sedimentation may contribute to decrease or increase the total sediment volume and cause disparities in the balance.

A comparison of the maps of mass change in the four presented time intervals (Fig. 4.8) helps to observe errors in the detected mass change which can be assumed to be caused by errors in the elevation models. For example, in the 3D-model of change representing the time interval November 2005 - May 2006, implausibly high positive change is observed in an area at the western side of the backslope (marked in Fig. 4.8). In the time interval from May 2006 to November 2007, however, high negative change is modelled in this area. This suggests that elevations are inaccurately represented in the DEM of May 2006. The same phenomenon can be observed when comparing the detected change in the easternmost part of the catchment (as marked in Fig. 4.8) in the same time intervals. The conclusion of inaccurately represented elevations in these areas is affirmed by the fact that few reference data for reducing the systematic error are available in these regions (see Fig. 4.6).

A boundary between erosion- and sedimentation-dominated areas was set. The so - delimited sedimentation - dominated area overlaps with the basal region of the steep foot-slope (see Fig. 4.3). The area of overlapping is covered by comparably dense vegetation, which might have favoured sediment trapping despite the larger slopes. Nevertheless, calculated sedimentation may slightly be overestimated in this area.

Mass changes have been analysed separately in the western and eastern part of the hillslope and differences have been observed. A large possible error is inherent in these data, but we assume that this error, which results primarily from random errors and vegetation artefacts, is spatially uniformly distributed over the elevation models. It is therefore possible to qualitatively interpret the spatial differences. A uniform distribution of the error moreover allows for deducing higher intensity of erosion in the eastern part of the catchment. Our interpretations of patterns and qualitative characteristics of erosion behaviour are supported by field observations. The description of rill network development given by Gerwin et al. (2009b), based on the analysis of aerial photographs, supports the results of the approach regarding the spatial as well as the temporal evolution of sediment redistribution patterns.

4.5.3 Surface structural development

Terrain parameters characterizing surface structures were computed from the same elevation models that were used to construct the models of change. The potential errors in these DEMs therefore also influence the computed terrain attributes. It is assumed that initial surface structures are the most important factor influencing the spatial distribution of erosion. Therefore, a direct correlation of sediment redistribution and sediment properties is not possible, even though differences between eastern and western part have been observed regarding sediment properties as well as erosion patterns and intensities. Influence of parent material properties and initial surface structures could not be separated.

4.6 Summary and Conclusions

This study aimed at the quantification of 3D sediment mass balances in the initial phases of ecosystem development and the spatially distributed detection and analysis of sediment redistribution processes. A 3D volume model was constructed based on elevation data of the catchment's surface and subsurface delineation; the model was used to quantify the sediment volumes extending between the impermeable clay liner at the bottom and the soil surface. Results of modelling the 3D initial sediment distribution suggest that there are larger-scale differences in sediment properties between the eastern and western part of the catchment, most probably resulting from the dumping of sediment masses in two separate

deliveries. However, also smaller-scale variations in textural properties, resulting from construction processes, are to be presumed. These variations are not detected by the sampling approach and cannot be included in the model by interpolation of sample data. Here, other modelling approaches will be required, which take into account the technical processes during construction. The 3D models of volume change could be constructed based on elevation data from multi-date aerial photographs after analysis and correction of errors in elevation data. Testing the significance of volume changes showed a relatively high uncertainty, due to limited accuracy in elevation data. The calculated mass balances showed an imbalance between erosion and sedimentation, which might be the result of several factors of inaccuracy in the models. Nevertheless, correlations between surface structures reflected in terrain attributes and spatial distribution of erosion processes could be observed and it was possible to detect differences in erosion processes in areas of differing sediments. Interpretations of maps of sediment redistribution could be substantiated by basic statistical analysis. The models of volume change suggest that spatially-resolved erosion and sedimentation in the catchment are highly dependent on initial surface structures. The initial surface structures do not essentially change in the first phases of surface evolution but only evolve to more connected and clearer structures. Spatial distribution of surface structures and erosion processes thus might remain relatively stable during the first years of evolution.

The potential of models of change for quantifying mass balances is mainly limited by the accuracy and resolution of the DEMs representing subsequent stages of surface evolution. It can reasonably be assumed that an improvement in DEM quality would enable a further differentiation of surface structural development. Constructing models of change from a temporal sequence of four elevation models and comparing the results of the individual time slices allowed a critical assessment of the suitability of the elevation models for quantification of mass balances. Because mass balances were computed for the whole time interval from November 2005 to August 2008 and for three sub-intervals, errors in single DEMs became more obvious. A comparison with even more time slices or with elevation data acquired by other methods could further substantiate these results.

A first approximation of erosion-affected surface structural dynamics in the artificial catchment was achieved, and interdependencies of initial surface structures and mass changes were shown. Verification of the results and an improved quantification can be attempted by accounting for material deposited in the pond, by improving data on bulk density and internal structure, and by the use of DEMs with higher resolution from terrestrial or air-borne laser-scanning.

5 A 3D volume model of sediment structures based on a DEM time series and landscape evolution model simulations

Parts of the material of this chapter were presented in a summarized form in Schneider, A., Maurer, T., Gerke, H.H., 2011. 3D-räumliche Beschreibung initialer Sedimentumverteilung in einem künstlichen Einzugsgebiet. In: Böden verstehen - Böden nutzen - Böden fit machen, 3. - 9. September 2011, Berlin. available online at http://eprints.dbges.de/546/. (in german).

5.1 Abstract

Sediment internal structures and mechanical and hydraulic properties can differ significantly between sediment layers deposited by natural processes and layers that are affected by technogenic processes. Therefore, a 3D volume model of an artificially constructed catchment needs to allow for a differentiation of the sediment body into layers with specific sediment properties. The aim of this study was to develop methods for the integration of such a representation of different sediment layers in a 3D volume model of the sediment body of the Hühnerwasser catchment. Two approaches were combined for constructing a volume model of the sediment body after five years of development: 1) The geometry of the sediment body and specific layers was defined from a time series of DEMs, from which sediment layer boundary surfaces were constructed; and 2) a representation of the internal structure of newly deposited sediment layers was generated using the CAESAR landscape evolution model and transferred to the 3D volume model. The resulting multi-layer volume model allowed for a realistic depiction of stratigraphy, depending on the dates of recording and the uncertainty of the input DEMs. Simulations of sediment redistribution resulted in modified particle size distribution for the highest-intensity erosion and sedimentation areas. Simulation results could be transferred to the 3D volume model in the alluvial fan area, but not in areas of lower-intensity deposition. Results show that the internal structure

of a catchment affected by erosion and deposition can be represented in a multi-layered 3D volume model based on a time series of surface DEMs. Results further suggest that the transfer of simulation results to such a 3D volume model is possible for specific areas of sediment deposition; but that methods for an integration of 3D volume model construction and process-based modeling for the total area of a catchment still need to be developed.

5.2 Introduction

Sediment bodies that are artificially constructed or considerably affected by technogenic modification, e.g., in mining reclamation areas, show characteristic internal sediment structures (Maurer et al., 2011b). Sediment redistribution by natural processes on the surface of such sediment bodies results in the deposition of sediment layers that can considerably differ from the underlying technogenic substrate in their internal structures. While technogenic construction mainly results in homogenization and compaction, sediment redistribution by water or wind erosion can result in the deposition of well-sorted and stratified sediment layers. Sediment hydraulic properties can differ considerably between technogenic and naturally deposited sediment layers, and characteristic internal structures can affect runoff and soil moisture patterns (Hölzel et al., 2013). A 3D model of such a sediment body therefore needs to represent different sediment layers and spatially varying sediment properties within these sediment layers in order to allow for further analyses of ecosystem development, e.g., for the derivation of substrate hydraulic properties by pedotransfer functions or for the use as a database for hydrologic modeling. Integrated surface-subsurface hydrological models are commonly applied and can make use of 3D spatially-distributed information on substrate hydraulic properties (Gascuel-Odoux et al., 2010; Sciuto and Diekkrueger, 2010).

In most studies that attempt a 3D spatial mapping of soils or substrates, the model representation of soil horizons or sediment layers is based on point information gathered from drillings or outcrops. Boundary surfaces between horizons or layers and sediment properties within the horizons or layers are obtained by spatial interpolation between these point data (Cosandey et al., 2003; Delarue et al., 2009; Mendonca Santos et al., 2000). While the 3D spatial description of soil horizon geometry requires a mapping of horizon depths from drillings or outcrops, the geometry of sediment layers deposited in time intervals can generally be described without a destructive sampling by deriving information on erosion and deposition depths from time series of DEMs. However, the use of DEM time series data in 3D soil mapping and soil landscape modeling has hardly been approached. Instead of describing the 3D spatial distribution of sediment properties based on destructive sampling and spatial interpolation, process-based models could be employed to simulate char-

acteristic sediment internal structures. 3D models of stratigraphy and sediment properties have been employed as input data for process-based hydrological modeling in a number of studies (Gauthier et al., 2009; Sciuto and Diekkrueger, 2010). However, the integration of process-based models to supplement 3D stratigraphic models has hardly been evaluated. Michael et al. (2010) describe the integration of process-based modeling and object based geostatistics for the 3D spatial simulation of subsurface heterogeneity for simulating the sedimentary development of a turbidite system.

The aim of this study was to construct a 3D volume model representing different layers of sediment for a development state of the Hühnerwasser catchment's sediment body. Therefore, the 3D volume model for the sediment body at the initial state of surface development (*t0*) needed to be supplemented to obtain a 3D volume model for a later development state (*tz*), which includes a representation of the 3D geometry of the initial sediment body as affected by sediment erosion, of newly deposited sediment layers and of the 3D spatial distribution of the properties of the sediments solid phase within these layers.

The objectives of the study were:

- to describe a method for the construction of a 3D volume model of the sediment body at a development state *tz*,
- to describe and evaluate methods for the integration of sediment redistribution simulation with a landscape evolution model to the 3D volume model, and
- to evaluate the possibilities and limitations for the description of 3D spatial sediment distribution for a development state *tz* with the available data and developed methods.

5.3 Material and Methods

Two approaches were combined to derive a representation of the sediment body after five years of development: In a first step, a time series of DEMs was used to describe the geometry of the part of the initial sediment body that was not eroded after five years of development, and the geometry of the newly deposited sediment layers. In a second step, a representation of the spatial distribution of sediment properties in newly deposited sediment layers in the alluvial fan area was generated by transferring data from the 3D volume model to the CAESAR landscape evolution model and transferring data simulation results back to the 3D volume model.

5.3.1 Construction of a multi-layered 3D volume model

For the construction of the 3D volume model, the clay liner model and the photogrammetry-based DEMs of the catchment surface, as described in Chapter 4, were used. The DEM for the initial development state (November 2005) and DEMs for eight other states of surface development (May 1, 2006; November 3, 2006; November 21, 2007, April 24, 2008; August 18, 2008; June 13, 2009; December 5, 2009, and March 4, 2010) were included in the construction. For November 3, 2006, about 9500 m^2 in the northernmost part of the catchment were not covered by the DEM. The elevation models were processed in order to reduce systematic errors, imprecise representation of elevations in rill and alluvial fan areas, and artefacts resulting from the recording of vegetation cover. For this purpose, DEMs were referenced to d-GPS data recorded in a 20 m by 20 m grid. Within rill and alluvial fan areas, DEMs were modified based on hydro-geomorphic principles, i.e., by removing increases of elevation along rills in downslope direction. In interrill areas, elevation values were modified based on logical comparison by replacing elevation values in areas that showed an implausible development of elevation over time by elevation values from other DEMs of the time series. Detailed descriptions of these modifications are given in Appendix A.

The states of surface development represented in the DEMs define the boundaries of the newly deposited sediment layers integrated in the volume model, and the volume model describes the state of sediment body development for the end of this DEM time series. To derive a 3D representation of a sediment layer that was deposited in each development period *tx* until the development state *tz*, it was necessary to define the upper and lower boundaries of the volume of sediment that was deposited between *t0* and *tx* and not eroded between *tx* and *tz* (Fig. 5.1). To derive these sediment layer boundaries, the elevation models were processed by decreasing elevations of models representing older development states *tx* to the minimum elevations of the series of all models representing younger development states *txn*, $n = x+1, \ldots, z$ in erosion-affected areas, i.e., in areas where elevation for any of the younger models was lower than elevations for the older model (if $Ztxn, n = x+1, \ldots, z < Ztx$). The processing was carried out using the option 'Edit Remove Crossings' in GOCAD, which can be used to move nodes of a surface below or above a reference surface.

Based on the processed elevation models, the stratigraphy of the sediment body was defined as a *'Stratigraphic column'* in GOCAD, in which the DEM of March 2010 was the top surface, the clay layer model was the bottom surface, and the other DEMs of the time series represented boundaries between stratigraphic units which were ordered from top to bottom based on the age, defined in months before April 2010, of the respective top surface. A new volume model was then constructed as described for the initial sediment body model (Schneider et al., 2011), using the DEM of March 2010 as the top surface and integrating the

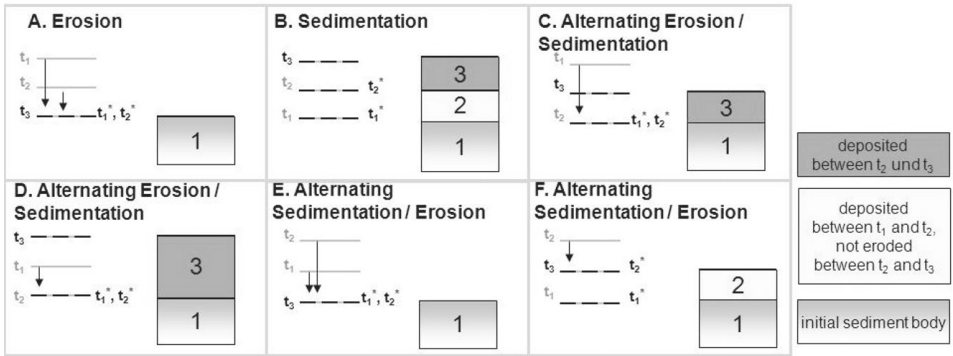

Figure 5.1: Schematic diagram of the processing of DEMs and construction of the 3D volume models representing different sediment layers, exemplarily for three states of surface development t1, t2, and t3.

stratigraphic column model in the *'3D Reservoir Grid builder'* workflow in GOCAD. Cell sizes of 1 m by 1 m in horizontal direction were specified. Cell size in vertical direction was defined to correspond to the total thickness of the respective layer, i.e., to the elevation difference between the two DEMs defining the layer for each cell.

To evaluate this method for volume model construction, a volume model was constructed from three elevation models (i.e., the DEMs for November 2005, May 2006 and November 2006), so that six scenarios of elevation development and up to two deposition layers, as shown in Fig. 5.1., can occur. Areas for that elevation developed according to one of the six scenarios were then identified and cell layering and computed cell volumes were visually evaluated in GOCAD.

5.3.2 Simulation of sediment redistribution

The CAESAR landscape evolution model (Coulthard et al., 2002) was chosen for the simulations in this study because it allows for simulating sediment erosion and deposition in a considerably high temporal resolution, as compared with other landscape evolution models (Coulthard, 2001); because its application for relatively small simulation areas has been previously described (Coulthard et al., 2012; Hancock et al., 2011); and because it provides the possibility to generate 3D spatial output information on particle size distribution for multiple sediment layers (Van De Wiel et al., 2007). A more detailed description and evaluation of the model is given in Chapter 8.

The simulation of sediment redistribution using the CAESAR model was carried out for the period from November 26, 2005 (i.e., the recording date of the DEM representing the surface at t0) and December 31, 2009 (i.e., the end of the precipitation record available at

the time of processing). The DEM of November 26, 2005 was processed in several steps in SAGA to be used as the input surface elevation model. To allow for outflow at the right edge of the simulation area and for a main flow direction from left to right, as required by CAESAR, the DEM was rotated by -52.5°. The southernmost part of the pond area was not included in the simulation to omit long simulation times due to ponding of water and re-distribution of sediment within the pond. To omit outflow from the catchment, elevations along the catchment border were increased by a constant value of 1 m. Surface irregularities resulting from the construction works were digitized from the aerial photograph for November 26, 2005; and elevations along these irregularities were reduced by a constant value of 0.1 m to form initial flow paths and to enforce rill incision. Local sinks in the elevation model were filled using the Planchon and Darboux (2002) algorithm in SAGA. Around the western branch of the central erosion rill next to the trapezoidal spring area, elevations were increased by values of up to 0.2 m (Fig. 5.2) to enforce flow routing to the alluvial fan area. The clay layer model was used as the 'bedrock' elevation model, i.e., the DEM representing the non-erodible lower boundary of the sediment body.

A data file representing the initial particle size distribution for model cells of 1 m by 1 m size in up to eleven layers of 0.2 m vertical thickness was generated based on the initial sediment body volume model and was used to define the initial sediment distribution for the simulations. For each layer, point datasets that represent the location of the centers of the volume model cells and the grain size information assigned to the volume model cells were generated in GOCAD. Datasets giving the x- and y- coordinates of these points, the layer number, and the particle size proportion were then exported from GOCAD for each of the seven sub-fractions of the fine grain fraction and for the fraction > 2 mm; and were combined to generate the data file required to represent grain size distribution in CAESAR.

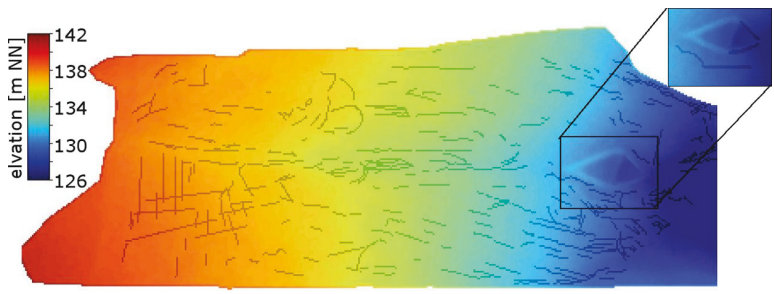

Figure 5.2: The DEM of November 26, 2005 as used as the input surface DEM in the simulation. Grey shading in the main image shows DEM cells were elevations were decreased by 0.1 m, and grey shading in the detail shows DEM cells were elevations were increased by up to 0.2 m.

Table 5.1: Model parameters and settings (* default settings)

Active layer thickness	Maximum erode limit	Flow distribution width	Method for calculating shear stress	Sediment transport rule	Soil creep exponent	Slope failure threshold
0.2*	0.05	5	Velocity	Wilcock and Crowe*	0.0025*	60
Minimum discharge for depth calculation	Water depth threshold above which erosion will happen		TOP - MODEL m value	Lateral erosion rate	Vegetation maturity and critical shear stress	Soil erosion rate
0.0001	0.0001		0.002	0.0000001	0, 180*	0.03

Table 5.2: Partitioning of hourly rainfall values into 10 min values

hourly precipitation [mm]	generated 10 min precipitation [mm]					
0.1	0	0	0.1	0	0	0
0.2	0	0.1	0.1	0	0	0
0.3	0	0	0	0.1	0.1	0.1
0.4	0.1	0.1	0.1	0.1	0	0
0.5	0	0.1	0.1	0.1	0.1	0.1
0.6	0.1	0.2	0.1	0.1	0.1	0
	generated 10 min precipitation [% of hourly value]					
> 0.6 and ≤ 4	35	20	15	15	10	5
> 4 and <10	0	60	30	10	0	0
≥ 10	0	0	50	30	20	0

The option for transport in suspension was chosen for the clay, fine silt and medium silt fractions, and sinking velocities were calculated according to Stokes' law. Other model parameters were specified as listed in Table 5.1. The TOPMODEL m value was calibrated by comparing simulated water discharge to data for the fast inflow to the pond calculated by Biemelt et al. (2011) from pond storage change, precipitation on the pond surface and pond outflow. The months from March to December 2007 were chosen as the calibration period because dry periods, low and high intensity precipitation events occurred in this period. Precipitation data recorded in the catchment (Biemelt et al., 2011) were used as the input precipitation dataset. Simulations with hourly and 10 min sums of precipitation were carried out to evaluate effects of the resolution of the precipitation input data. Because precipitation data in 10 min resolution were not available for the period from November 2005 to February 2008, an approximation of 10 min intensities for this time period was generated from hourly data. Based on an analysis of the distribution of measured 10 min and hourly

precipitation intensities for 40 hours of the precipitation records (representing eight precipitation events in April, May, July and September 2010), hourly precipitation intensities were partitioned into 10 min intensities following different rules (Table 5.2). Based on the hydrological model calibration, 10 min precipitation data were used as input data for the total simulation period, and the TOPMODEL m value was set to 0.002.

5.3.3 Transfer of particle size distribution data to the volume model

Particle size information was assigned to the cells of the updated volume model in GOCAD specifically for different regions of the model. In model cells representing parts of the initial sediment layer not affected by erosion, grain size information was transferred from cells of the initial sediment body model. In the cells representing newly deposited sediment layers, grain size information was transferred from processed CAESAR output datasets. Therefore, the columns representing the x- and y- coordinates and the grain size proportion for the data points of each layer were extracted from the file generated by CAESAR and imported to GOCAD. Elevation information based on the last DEM of the time series and the sediment layer thickness was then assigned to the output coordinates, so that the elevation for the coordinate representing the top sediment layer 0 was the surface elevation *Ztz* - 0.1 m and the elevation of each of the coordinates representing one of the lower sediment layers 1 to x was $Ztz - 0.1 + 0.2n$ for $n = 1, \ldots, x$. Data points were then transferred to a volume model with a regular layer thickness of 0.2 m, and information was assigned to the irregular layers of the updated volume model using the option '*transfer property from nearby grid node or cell*' in GOCAD, which, for each cell central point of the updated grid, copies the value from the nearest cell of the regular layer grid.

5.4 Results

5.4.1 Geometry of the 3D volume model

The model constructed from the three elevation models for November 2005, May 2006, and November 2006 reflects a stratification that corresponds to the logically derived stratification for the six possible scenarios of elevation development (Fig. 5.3). Areas without deposited sediment for one or both periods are represented by model cells with negligible cell volumes. For scenarios A (erosion during both periods) and E (deposition during the first and higher erosion during the second period), both layers of the model are represented by cells with zero volumes. For scenario B (sedimentation during both periods), two layers of cells with volumes > 0 are represented. For scenarios C and D, only the cells in layers representing deposition during the second period have volumes > 0; and for scenario F, only cells deposited during the first period, i.e., the cells in the lower layer, have volumes > 0.

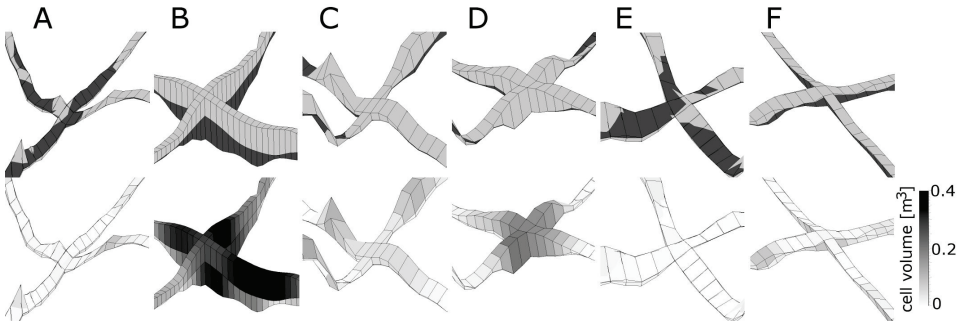

Figure 5.3: Stratification (top) and cell volumes (bottom) for regions of a 3D volume model constructed from three DEMs that represent six possible scenarios of elevation development (see Figure 5.1); shown in vertical cross sections through the volume model. Elevation development scenarios apply for the cells in the centers of the cross-sections. The figures are not to scale; cell size is 1 m by 1 m in horizontal direction.

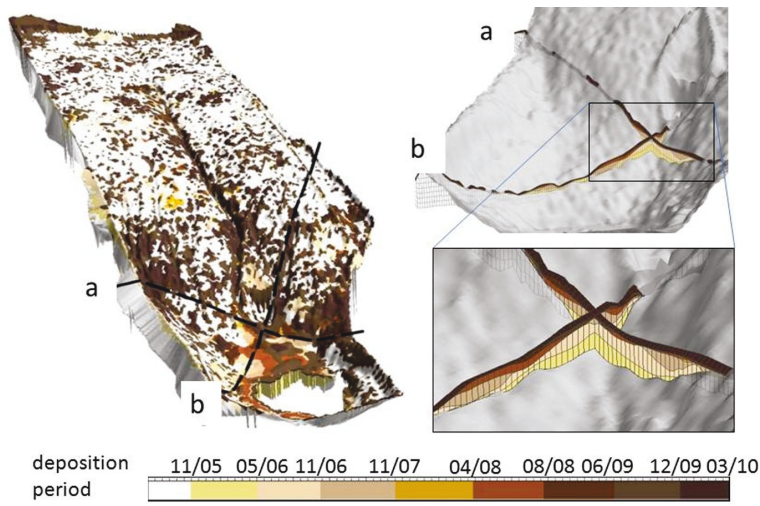

Figure 5.4: Total view of the 3D volume model (left) and sections crossing the alluvial fan area (right). In the total view, the pond area and cells with a volume below 0.01 m^3 are not shown.

The 3D volume model representing the sediment body on March 2010 (Fig. 5.4) shows the deposition of sediment in several layers, especially in the alluvial fan area. Deposition of sediment is also shown for other areas of the catchment. The total volumes of the newly deposited layers (Table 5.3) are considerably high for those layers deposited in the first periods of development, i.e., until November 2007. High volumes were also derived for those sediment layers deposited in the last development periods represented in the model, while volumes for intermediate development periods were lower.

Table 5.3: Volume of the sediment layers representing deposition periods in the 3D volume model

Deposition period	until 11/05 (technogenic)	11/05 - 05/06	05/06 - 11/06	11/06 - 11/07	11/07 - 04/08	04/08 - 08/08	08/08 - 06/09	06/09 - 12/09	12/09 - 03/10
Number of model cells within a volume > 0.01 m^3	1199260	4141	5092	3501	1180	2327	4270	18074	8581
sediment volume [m^3]	113443	285	314*	228*	51	143	208	719**	347**

* about. 9500 m^2 in the northernmost part are not included due to missing elevation data for 11/06
** about 1700 m^2 in the northernmost part are not included due to the catchment boundary modification

5.4.2 Landscape evolution model simulations

A comparison of results of the analysis of 10 min rainfall intensities for 40 hourly records (Fig. 5.5a) with the generated distribution for the same hourly intensities (Fig. 5.5b) suggested that for the measured and the generated datasets, hourly values are relatively equally partitioned into 10 min values for relatively small hourly intensities; 10 min values show a high variation for relatively high hourly intensities, and again show lower variation for exceptionally high hourly intensities.

Simulated water discharge for the calibration period from March to December 2007 was in relatively good agreement to the pond inflow data calculated by Biemelt et al. (2011) for simulations using precipitation input data in 10 min resolution and a TOPMODEL m value of 0.002 (Fig. 5.6), although both an over- and an underestimation of highest-intensity runoff events were observed. Lower m values resulted in an overestimation of runoff intensities, while higher values resulted in an underestimation for the high-intensity runoff events. For hourly precipitation data, similar intensities were simulated for lower and medium intensity runoff events, but intensities were underestimated for the highest-intensity runoff event.

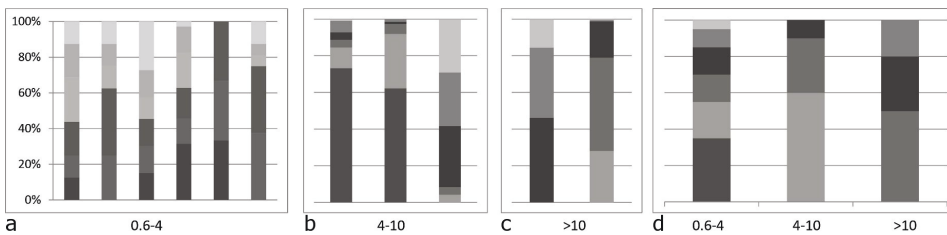

Figure 5.5: Proportions of 10 min precipitation intensity on hourly rainfall intensities for relatively low, high, and very high hourly intensities based on the analysis of meteorological monitoring data (a-c) and on the partitioning of hourly sums according to Table 5.2.

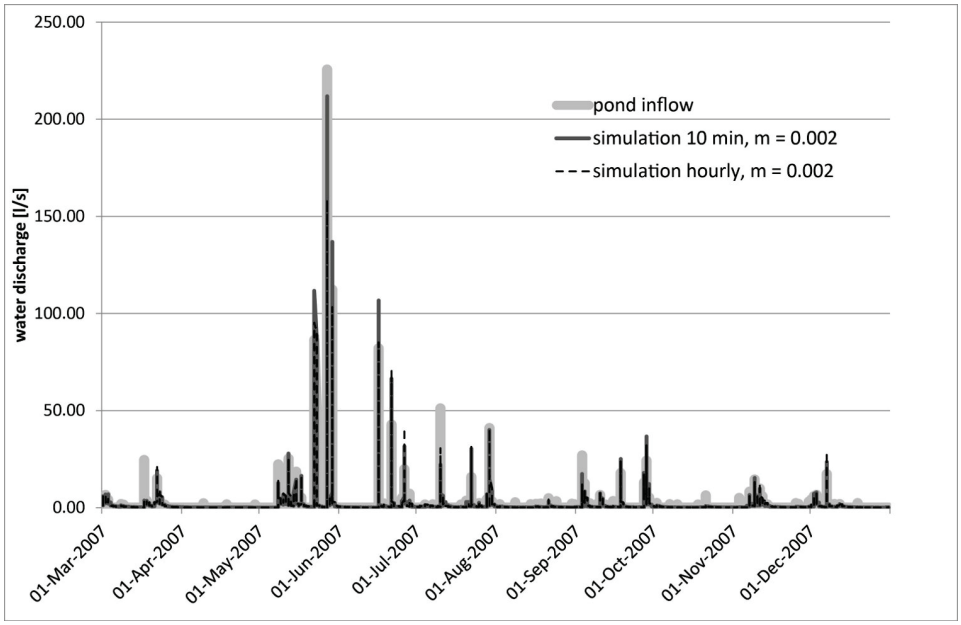

Figure 5.6: Pond inflow, as calculated from monitoring data (Biemelt et al., 2011), compared to simulated discharge for the calibrated hydrological model using hourly precipitation data and 10 min data generated from hourly data.

A comparison of elevation changes resulting from the CAESAR simulation (Fig. 5.7 b) with elevation change derived from calculating elevation differences between the DEMs for December 2009 and November 2005 (Fig. 5.7 c) shows that simulated erosion intensity was considerably lower as compared with erosion intensity suggested by the elevation model differences. However, characteristic patterns of elevation change were represented by the simulations. Simulations of sediment redistribution resulted in considerably modified grain size distributions in the topmost sediment layer (0 - 0.3 m, Fig. 5.8). For the areas affected by linear erosion, simulation results show a depletion of sand and an enrichment of clay, silt and particles > 2 mm. In the area of highest simulated sedimentation, results show increased proportions of sand, very low proportions of clay and relatively low proportions of particles > 2 mm. In the resulting multi-layer volume model (Fig. 5.9), the newly deposited sediment layers are clearly discernible from the remaining volume of the initial sediment layer by the differing spatial structure and higher variation in the spatial distribution of sediment properties.

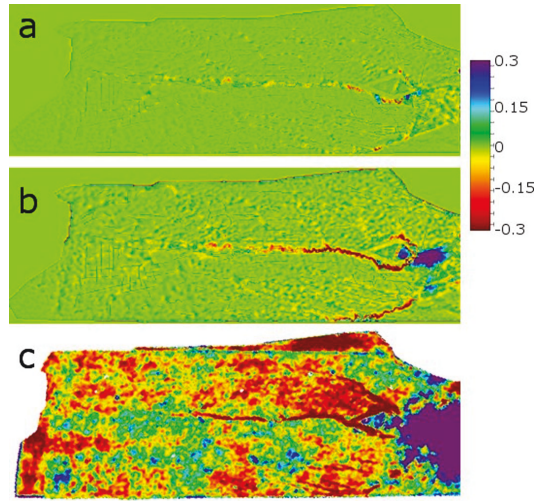

Figure 5.7: Elevation differences resulting a) from the simulation after 150 days, b) from the simulation at the end of the simulation period, and c) from the difference between the DEMs for November 2005 and December 2009. Negative values show erosion, positive values show deposition.

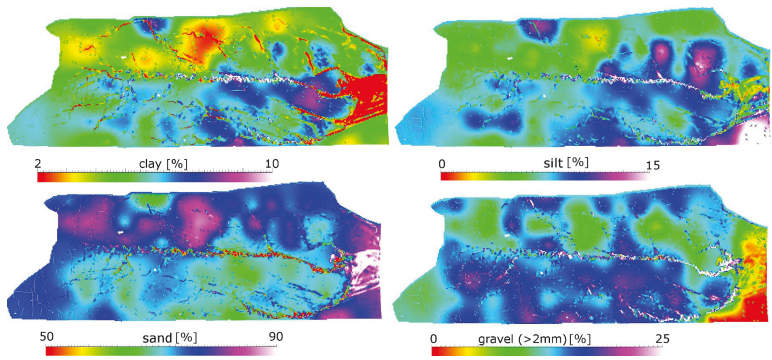

Figure 5.8: Proportions of clay, silt, sand, and gravel in the top sediment layer resulting from CAESAR simulations.

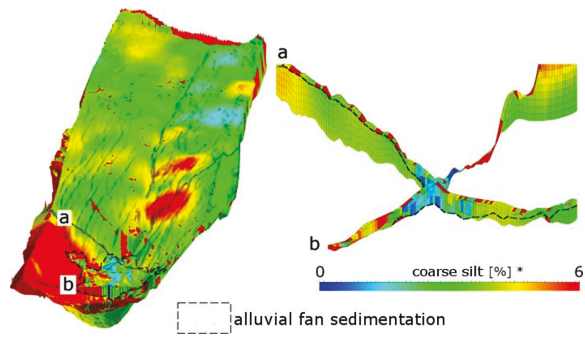

Figure 5.9: Spatial distribution of grain sizes for the example of the coarse silt content for different layers of the updated 3D volume model in the top layer (left) and along to sections (right). For the sections, the dotted line delineates the boundary between model cells representing the initial sediment body and cells representing newly deposited layers.

5.5 Discussion

5.6 Construction of the 3D volume model

The evaluation of the method for constructing the 3D volume model for specific scenarios of elevation development in a model constructed from three DEMs (Fig. 5.3) showed that stratification for all scenarios was represented correctly in the model. However, each of the layers of the model covers the total model area. In areas where, according to the elevation models, no sediment layers exist; model cells with a minimum volume result from the construction. The geometry of these cells was irregular and cell volumes were close, but not equal to zero, in erosion-dominated areas (e.g., Fig. 5.3e); which limits the quantification of deposition volumes based on the model layers. The irregular cell geometry results from the construction because the corners of the 3D volume model cells do not coincide with the nodes of the DEMs used for construction, but boundary surfaces of the model are interpolated from the DEMs in the *'3D Reservoir Grid builder'* workflow in GOCAD. The fact that the total model area is covered by cells for all layers also limits the visual interpretation of the model, so that for visualization of deposition patterns (Fig. 5.4) it is necessary to only depict model cells with a volume higher than a defined threshold value.

Quantification of deposition volume is limited by the inaccuracy of the DEMs used to construct the model. For volume quantification in 3D models of elevation difference for specific time intervals, an uncertainty of 0.21 m^3m^{-2} was derived from general DEM uncertainty (Schneider et al., 2011), which also applies for volume quantification in the multi-layer 3D model. Because the mean volume of model cells is considerably smaller than this uncertainty for all deposition layers of the model (Table 5.3), the 3D volume model does not allow for a significant quantification of volume change. However, a qualitative interpretation of the considerably differing total volumes of the model layers for the eight time intervals (Table 5.3) can be attempted. The higher volumes for the model layers representing deposition in the earliest development periods can be interpreted as the representation of a generally decreasing intensity of sediment erosion and deposition during the time period depicted in the model. The higher volumes of layers representing the latest development periods can be interpreted as a result of alternating deposition and erosion, which reduces the volumes of deposited layers over time.

5.6.1 Landscape evolution model simulations

The comparison of calculated pond inflow and simulated water discharge for CAESAR simulations over the hydrological model calibration period showed a relatively good agreement of both hydrographs. For the first 27 months of the total simulation period, precipitation in-

put data in 10 min resolution were generated from measured precipitation records in hourly resolution based on very basic rules for three classes of hourly precipitation intensity. Generated 10 min data were employed for the simulation in this study because hydrological model calibration showed that peak discharge intensities were better represented using 10 min data. Higher peak discharge intensities were assumed to be associated with higher depths of surface runoff for individual time steps of simulated runoff events and therefore with higher erosion intensity, which was affirmed by a visual evaluation of erosion patterns in the CAESAR user surface in pre-calibration simulations (not shown here). The central objective of the simulation carried out here was to enforce the simulation of deposition in the alluvial fan area to generate output data that can be used to test methods for the integration of model outputs in the 3D volume model. The method to generate 10 min precipitation data can be considered appropriate for meeting this objective. However, for a study aiming at a realistic simulation of spatio-temporal patterns of deposition and sediment discharge intensities, more sophisticated methods need to be applied for the temporal downscaling of precipitation intensities. As summarized by Foufoula-Georgiou and Vuruputur (2000), the recognition of effects of small-scale precipitation variability on runoff production has induced considerable research efforts on methods for statistical precipitation downscaling. Foufoula-Georgiou and Vuruputur (2000) demonstrate that the description and modeling of underlying statistical structures in rainfall patterns is possible but requires detailed analysis and sophisticated transformation methodologies.

Hydrological model calibration was carried out by modifying the TOPMODEL m parameter. The parameter value of 0.002 is relatively low in comparison to the range of values used in most TOPMODEL applications, however, similarly low values have been applied in applications for small catchments (Beven, 1997). For other parameters and settings, the default values were used (Table 5.1), or parameter values were chosen based on a visual interpretation of surface runoff and erosion intensity and spatial distribution in pre-calibration runs in the graphic user surface of the CAESAR model. A detailed calibration and sensitivity analysis for the CAESAR model was not the aim of this study; however, effects of other model settings on the simulation of runoff and sediment redistribution can be assumed and were shown by the results of a more detailed evaluation of the model (Chapter 8). A horizontal resolution of 1 m by 1 m was chosen for the input DEM and grain size dataset in this study, based on the resolution of the available elevation data and the 3D volume model for the initial state. It can be assumed that the underestimation of erosion intensity by the simulations is to some extent due to this resolution, which is relatively coarse in relation to the widths of the erosion rills in the Hühnerwasser catchment. Simulated sediment redistribution might also be affected by the surface flow routing simulation in CAESAR. This simulation did not result in surface runoff along straight flow paths, but in a dominance

of flow in diagonal directions and in a 'zigzag' pattern of flow along the main flow paths; which was reflected in runoff patterns observable during simulations in the graphical surface of the model (not shown here) and in the corresponding erosion pattern in the major erosion rills (Fig. 5.7a and b). A similar dominance of diagonal runoff and erosion patterns was observed in other CAESAR simulations (reported in the CAESAR discussion board (Coulthard, 2005; Coulthard, 2010; Schwanghart and Coulthard, 2007)) and could result from the flow routing algorithm of the model or from DEM inaccuracy resulting from rotating the model by a value that is not a multiple of 90°.

Differences in the hydrological and mechanical properties of different sediment layers in a catchment can considerably be affected by the distribution of bulk density in these deposits. The simulation of bulk density distribution was not included in this study, since sediment transport simulation in CAESAR was based on volumetric sediment load, and the sediment data file generated by the simulation gives information on particle size distribution in volumetric proportions of the model cell size, not including information on bulk density or porosity.

5.6.2 Transfer of simulation results to the 3D volume model

Transferring the grain size information resulting from the simulations to the multi-layer volume model based on the x- and y- coordinates in the output grain size file was only possible in the area of highest sedimentation, i.e., in the alluvial fan area. In the slope areas and in erosion rill beds, however, patterns of sedimentation resulting from the simulation were not concordant with sedimentation patterns depicted in the 3D volume model, so that it was not possible to assign simulated sediment structures to the volume model. Generally, the transfer of simulation results to the 3D volume model based on the x- and y- coordinates would require an exact agreement of simulated deposition patterns to those depicted in the volume model, which can hardly be achieved. Alternatively, simulation results could be assigned to the geometry model by statistically describing the sediment structures within characteristic regions of the output dataset, similar to the approach described by Michael et al. (2010), and by generating internal structure for corresponding regions of the volume model using this characterization. As pointed out by Michael et al. (2010), high-resolution simulations of the depositional process that result in a distinct heterogeneity of internal structures are necessary to allow for the identification and parameterization of such characteristic regions. The representation of stratigraphy in the alluvial fan in the simulation results and the 3D volume model was further limited by the resolution of the CAESAR simulations, and by the resolution of the cells of the 3D volume model. Information on grain size distribution generated by CAESAR was averaged in cells with a horizontal resolution of 1 m by 1 m, defined by the horizontal resolution of the input DEM and sediment file, and with a vertical

resolution of 0.2 m, defined by the parameter 'active layer thickness'. The resulting spatial distribution of the grain size information assigned to the cells suggests that this resolution allows for depicting larger-scale horizontal variations in the grain size distribution in deposition areas, e.g., an increasing content of coarse silt towards the lower end of the alluvial fan area (Fig. 5.8). However, vertical variations due to the deposition of sediment in fine strata cannot be depicted using this method. Information was further averaged as a result of the transfer from the cells of the auxiliary regular layer grid to the cells of the 3D volume model with irregular layer thickness in GOCAD. An analysis of the effects of this method of data transfer to 3D volume model cells for a larger dataset by Maurer et al. (2011b) suggests that the data transfer can result in slight distortions of the value distribution. In this study, a higher spatial resolution of the 3D volume model and of the LEM simulations was not possible since computational limitations did not allow for increasing the number of model cells. Because a LEM simulating both erosion and deposition was employed, the simulation area needs to cover the total catchment area. A higher-resolution simulation of deposition patterns could be approached with a process-based model that only simulates the deposition of sediment based on sediment input from one or several source points, as described by Michael et al. (2010).

5.7 Conclusions

Results show that the geometry and internal properties of sediment layers resulting from different processes, i.e., technogenic and natural deposition, can be represented in a multilayer 3D volume model. The evaluation of an exemplary volume model with two sediment layers showed that the described method of processing DEMs to obtain boundary surfaces between sediment layers allows for constructing model layers that realistically depict sediment layers with an accuracy that depends on the accuracy of the available elevation data. The spatial concordance of sediment deposition depicted in the volume model and simulated with the LEM only allowed for a transfer of simulation results to the volume model based on the spatial position of the data points in areas of considerably high deposition (i.e., the alluvial fan area). The discrepancies between simulated erosion intensities and erosion intensities derived from DEM analyses suggest that 1) a more detailed calibration and evaluation of model set-up and parameterization and 2) a general assessment of the applicability of the CAESAR landscape evolution model for simulating initial phases of landform evolution on a small scale are necessary. For the alluvial fan area, the updated 3D volume model shows different patterns of spatial sediment properties in areas of technogenic and natural deposition; which suggests that the volume model could be used as a basis to, e.g., derive characteristic hydraulic properties for specific morphologic units of a catchment by pedotransfer functions.

6 Evaluation of remotely-sensed DEMs and modification based on plausibility rules and initial sediment budgets of an artificially-created catchment

The material presented in this Chapter was published as Schneider, A., Gerke, H.H., Maurer, T., Seifert, S., Nenov, R., Hüttl, R.F., 2012: Evaluation of remotely-sensed DEMs and modification based on plausibility rules and initial sediment budgets of an artificially-created catchment. Earth Surface Processes and Landforms, 37 (7): 708-725. doi: 10.1002/esp.2274.

6.1 Abstract

To quantify landscape change resulting from processes of erosion and deposition and to establish spatially distributed sediment budgets, 'models of change' can be established from a time series of digital elevation models. However, resolution effects and measurement errors in DEMs may propagate to these models. This study aimed to evaluate and to modify remotely-sensed DEMs for an improved quantification of initial sediment mass changes in an artificially-created catchment. DEMs were constructed from photogrammetry-based, airborne (ALS) and ground-based laser scanning (TLS) data. Regions of differing morphological characteristics and vegetation cover were delineated. Three-dimensional (3D) models of volume change were established and mass change was derived from these models. DEMs were modified region-by-region for rill, interrill and alluvial areas, based on logical and hydro-geomorphological principles. Additional DEMs were constructed by combining multi-source, modified data. Models were evaluated by comparison with d-GPS reference data and by considering sediment budget plausibility. Comprehensive evaluation showed that DEM usability depends on a relation between the technique used to obtain elevation data, surface morphology and vegetation cover characteristics. Photogrammetry-

based DEMs were suited for quantification of change in interrill areas but strongly underestimated surface lowering in erosion rills. TLS DEMs were best suited in rill areas, while ALS DEMs performed best in vegetation-covered alluvial areas. Agreement with reference data and budget plausibility were improved by modifications to photogrammetry- and TLS-based DEMs. Results suggest that artefacts in DEMs can be reduced and hydro-geomorphic surface structures can be better represented by applying region-specific modifications. Photogrammetry-based DEMs can be improved by combining higher and lower resolution data in defined structural units and applying modifications based on principles given by characteristic hydro-geomorphic evolution. Results of the critical comparative evaluation of remotely-sensed elevation data can help to better interpret DEM-based quantifications of earth-surface processes.

6.2 Introduction

Rill and gully erosion are formative processes in landscape development (Horton, 1945; Schumm, 1998). The incision of small rills can start rapidly on sediments newly exposed to surface conditions, and once rill erosion occurs, sediment transport rates can increase considerably (Brunton and Bryan, 2000). The quantification of small changes in surface morphology resulting from erosion and deposition is therefore an important basis for studies of landscape evolution. The soil surface morphology can be described and quantitatively studied in DEMs obtained by remote-sensing methods. Changes in surface elevation with time are indicative of changes in sediment mass balance (Church and Ashmore, 1998). To assess the full range of sediment redistribution processes in a catchment, spatially distributed sediment budgets (Brown et al., 2009; Dietrich and Dunne, 1978) can be established which identify and quantify sources, sinks, and intermediate storages of sediment as well as fluxes of material based on the principle of conservation of mass. One viable method for the spatially and temporally resolved reconstruction of sediment redistribution on catchment scale is the construction of difference models or models of change from a time series of DEMs (Brasington and Smart, 2003; Lane et al., 1994). The approach of using DEM difference models has been applied to reconstruct morphological change in a variety of environments and at different spatial and temporal scales, using GPS (Global Positioning System) data (Wu et al., 2008), terrestrial laser scanning (TLS) (Milan et al., 2007; Perroy et al., 2010), photogrammetry (Betts et al., 2003; Bird et al., 2010; Brasington and Smart, 2003; Marzolff and Poesen, 2009), or a combination of photogrammetric and field-survey data (Lane et al., 1996; Lane et al., 2003).

Methods of DEM acquisition are limited in resolution and prone to measurement errors (e.g., Fisher and Tate, 2006). Chandler (1999) and Robinson (1994), among others, point

out the importance of thoroughly understanding the quality of elevation data in analyses of morphological change. As models of change are constructed from two or more DEMs, errors in input data might multiply, and absolute in addition to relative accuracy is crucial for model quality. In addition to general inaccuracy, systematic errors or artefacts in DEMs can propagate to difference models. Depending on the method of elevation data acquisition and processing (Milledge et al., 2009), these types of error are, to varying degrees, influenced by morphology (Hancock, 2005; Lane et al., 2000; Thompson et al., 2001) or vegetation cover (Chandler, 1999) and therefore introduce spatially auto-correlated uncertainty to the models. The problem of uncertainty in DEM difference models has often been approached by defining minimum levels of detection (Fuller et al., 2003; Lane et al., 2003) based on the general accuracy of elevation data. Milan et al. (2010) and Wheaton et al. (2010) developed methods for the propagation of uncertainty in DEMs from ground-based surveys which include the consideration of spatially varying errors in relation to local topography. Especially for remotely-sensed DEMs, attempts to propagate DEM uncertainty require a thorough understanding of model quality and the characterization of the spatial nature of elevation uncertainty in relation to topography and vegetation cover characteristics. This can be approached by comparing DEMs to additional, more accurate elevation information. Several studies have compared remotely-sensed DEMs with point data gathered by total stations or GPS (Baily et al., 2003; Collins et al., 2008; Evans and Lindsay, 2010; Fuller et al., 2003). Fewer studies have carried out a spatially distributed comparison of several DEMs from different remote-sensing techniques: Adams and Chandler (2002) compared a DEM based on airborne laser scanning (ALS), a DEM generated by automated digital photogrammetry and a third DEM from total station surveys. Milledge et al. (2009) evaluated DEMs based on radar remote sensing and digital photogrammetry as well as the effects of different processing filters by comparison with GPS reference data. Perroy et al. (2010) compared DEMs generated from ALS and TLS with ground-based survey data and state that, building on the results of such quality assessment, corrections can be applied to LIDAR-based estimates of erosion volume. Nachtergaele and Poesen (1999) determined a correction factor for gully volumes estimated from photogrammetry. Chandler et al. (2002) developed a method to improve photogrammetry-based DEMs by merging overlapping elevation models. The detailed evaluation of DEM quality in areas of differing surface and vegetation cover characteristics and the modification of DEMs based on the results of quality assessment, however, have hardly been attempted.

In this study, changes in the three-dimensional (3D) sediment mass balance of the artificially-created catchment 'Hühnerwasser' ('Chicken Creek') during its first years of development are quantified. For one time frame in catchment development (i.e., spring 2009), three elevation datasets from photogrammetry, ALS, and TLS are available. Elevation data based

on photogrammetry and ALS were provided as parts of datasets from regular mine surveying of Vattenfall Europe Mining (VEM) AG (Cottbus), while TLS and GPS elevation data were recorded by the authors of this study. A combined analysis of these data can help to evaluate different types of remotely-sensed DEMs regarding their suitability for the quantification of sediment budgets. In addition to evaluation using reference data, the plausibility of sediment budgets derived from models of change can be used to evaluate DEMs of the artificially-created catchment, as it is intensively monitored and its area is consistently defined. The objectives of this study were: (1) to explore the spatial nature of uncertainty in different types of remotely-sensed DEMs; especially for photogrammetric and ALS datasets, for which no full insight in processing is possible; (2) to evaluate whether DEM uncertainty can be reduced by modifying DEMs, and (3) to establish improved sediment budget quantifications for the catchment from multi-source, modified elevation data and from modified photogrammetry-based data.

Three tasks had to be completed to achieve these objectives: (i) the assessment of the suitability of DEMs for the quantification of mass change and its dependence on morphology and vegetation cover; (ii) the development of plausible rules for the modification of DEMs, considering the hydro-geomorphic evolution of different landscape units, and the combination of multi-source, modified data in order to accomplish an improved budget quantification, and (iii) the modification of DEMs based on photogrammetry in order to accomplish an improved budget quantification from these datasets only. These tasks were carried out stepwise (cf. Fig. 6.1 and explanations below in Material & Methods): (a) DEMs were constructed from photogrammetry-based, TLS, and ALS data to obtain 3D-volume models, in which units of differing morphological and vegetation cover characteristics were defined. DEMs were evaluated unit-specific by comparison with reference data and consideration of sediment budget plausibility; (b) for units of different morphological and vegetation cover characteristics, data were extracted from the DEMs and modified based on logical and hydro-geomorphological principles. Surface and 3D model construction and evaluation as in step 1 was repeated to test the method; and (c) modified photogrammetry-based DEMs were additionally evaluated by unit-specific comparison to those models found to give the best representation of the surface in step 1.

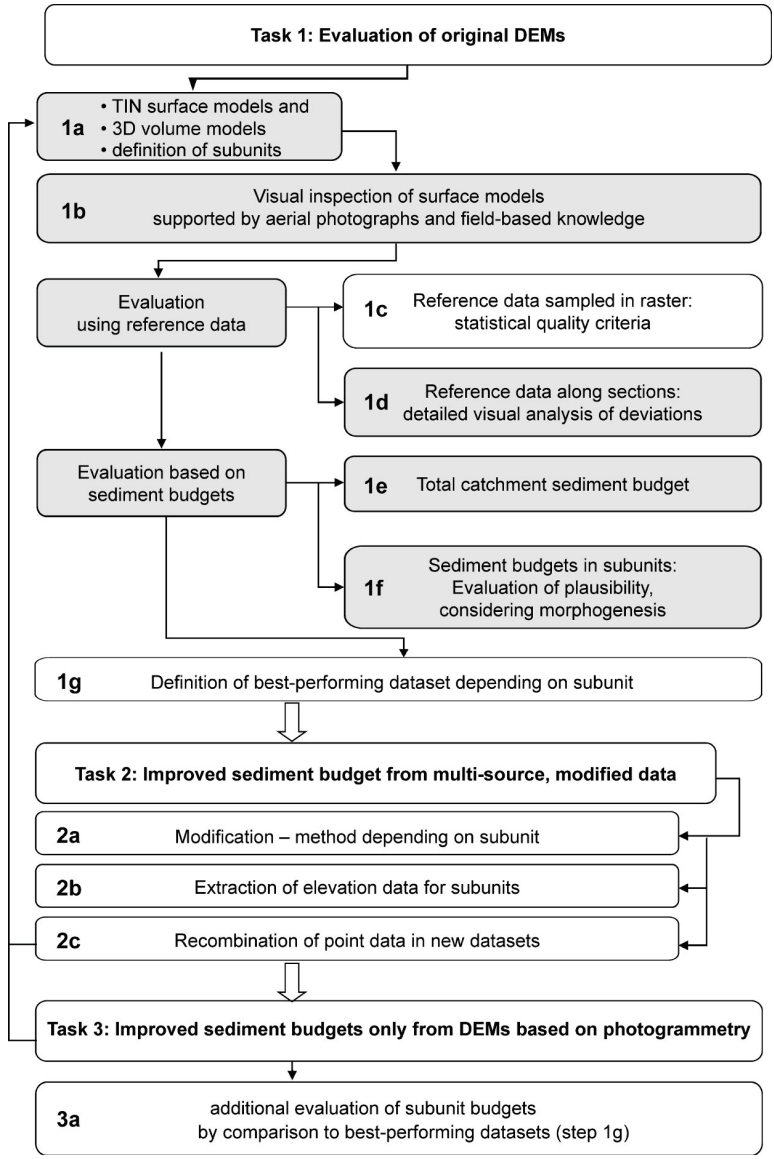

Figure 6.1: Schematic diagram of central tasks and working steps. Working steps shown in grey boxes are repeated for Tasks 2 and 3.

6.3 Material and Methods

6.3.1 Database

The evolution of the artificial catchment was continuously monitored in time intervals from the initial point in time of ecosystem development (i.e., the completion of the construction). The monitoring data that were utilized in this study (Table 6.1) were obtained by different methods of remote sensing or field surveys.

In the mine surveying department of Vattenfall Europe Mining (VEM) AG, Cottbus, surface elevation data for several specific days between Nov 26, 2005 and Mar 4, 2010 were obtained from aerial photographs by automated digital photogrammetry, using the software packages Match-T and DTMaster (inpho GmbH). Aerial photographs had been recorded by a digital Camera (DMC01-997 Z/I Imaging Intergraph) at a flight altitude of about 1250 m. Dominik (2007) determined a ground resolution of about 0.16 m from the photographs and a vertical accuracy of about ± 0.147 m, based on flight altitude and camera parameters. Elevation data arranged in 1 m by 1 m and 0.5 m by 0.5 m grids were derived from the photographs in two repetitions of the automated routine for elevation generation. Data providers pointed out that the 0.5 m by 0.5 m resolution exceeded the data spacing that is conventionally achieved from the aerial photographs, i.e. the default resolution that is suggested in the DEM generation software (Petra Zeumer, VEM AG Cottbus, personal communication, July 2009). In consequence, the general inaccuracy of the higher-resolution dataset might be substantially increased as compared with the 1 m by 1 m resolution. The data provided were the 3D-coordinates and elevations were given in m a.s.l., rounded to a precision of three positions after the decimal point. The mine surveying department of VEM AG furthermore recorded the surface by ALS on April 06, 2009 (Table 6.1); grid point spacing was 1 m by 1 m, and vertical accuracy was about ± 0.15 m (Hagen Röder, VEM AG Cottbus, personal communication, July 2009). The data provided were the 3D-coordinates. Elevations were given in m a.s.l., rounded to a precision of one position after the decimal point.

In May 2009, we scanned the catchment with a Terrestrial Laser Scanner (TLS, LMS-Z420i, Riegl Laser Measurement Systems GmbH, Horn, Austria). The angular resolution of this scanner is 0.0025° and the distance measurement accuracy is 10 mm. The scanner was mounted on a 6 m portable tower and positioned at 13 locations in the catchment (Fig. 6.2) to ensure almost complete coverage of the surface area. All scans were conducted with a maximum horizontal ground point spacing of 0.1 m from each setup position. The raw point clouds were aligned to the Gauss-Krüger coordinate system by scanning 30 reference reflectors. The coordinates of the reflectors were recorded by d-GPS in 2008. The overall standard deviation of the registered scanner positions according to the reflector positions is

Table 6.1: Overview of monitoring data and data sources

Dataset/source	recorded by	data spacing/ resolution	number of data points	date recorded
gridded elevation data/©Vattenfall Europe Mining AG	automated digital photogrammetry	1 m x 1 m	61296 61936 61704 61746 60351 61158	Nov 26, 2005 Apr 24, 2008 Aug 18, 2008 Jun 13, 2009 Dec 05, 2009 Mar 4, 2010
		0.5 m x 0.5 m	239770	Jun 13, 2009
gridded elevation data	ground based laser scanning	0.5 m x 0.5 m	228645	May 12-15, 2009
gridded elevation data/©Vattenfall Europe Mining AG	airborne based laser scanning	1 m x 1 m	62482	Apr 6, 2009
elevations of catchments' border	d-GPS	irregulary spaced, recorded following topographic variation	81	Jul 22,2008
reference raster elevation data	d-GPS	20 m x 20 m	121 123 123	Aug 20, 2008 Nov 10, 2009 Apr 22, 2010
hillslope cross section elevation data	d-GPS	irregularly spaced, recorded following breaks in topography	165, 152, and 77 data points in three sections	Jul 2, 2009
rill longitudinal profile elevation data	d-GPS	irregularly spaced, recorded following rill topography	333, 158, and 130 data points along three erosion rills. 89, 41, and 45 points extracted for longitudinal profiles	Jul 7, 2009, Jul 30, 2009
high resolution aerial photograph mosaic	digital camera Pentax Optio A40, mounted on microdrone, altitude ~80 m	ground resolution ~0.02 m		Jul 10, 2008 Jul 1, 2009
aerial photo-graph/©Vattenfall Europe Mining AG	digital camera DMC01-997 Z/I imaging Intergraph, altitude ~1250 m	ground resolution ~0.16 m		Aug 18, 2008
2D model of bulk density distribution	Interpolated by Kriging from 192 sampling points, 0-3 cm depth	1 m x 1 m		Aug 2008
pond level	1-3 sensors at different positions in the pond			continuously recorded

commonly about 0.025 m. It was attempted to remove noise and potential vegetation effects by applying a two-stage filtering process: First, all points representing erroneous measurements (i.e., points below 125 m a.s.l. and above 142 m a.s.l.) were removed. All points were sorted in a 0.5 m by 0.5 m grid, and values higher than a tolerable threshold value above the median of each grid cell, which mostly represent towers and ropes or measurement devices in the catchment area, were removed. Few erroneous points above the pond water surface, which is not recorded in the LIDAR signal, were manually removed. The coordinates of the x-y-position of the centre of the grid cells and the minimum elevation measured in each of the cells were then used for the creation of the soil surface DEM used in this study.

Additional topographic data were recorded using Trimble R8 d-GPS: The rampart delineating the catchment area was recorded in July 2008 to be able to integrate the rampart to DEMs of the catchment surface. We further recorded d-GPS reference data for the evaluation of remotely-sensed DEMs: 121 points arranged in a 20 m by 20 m grid across the hillslope were repeatedly recorded (Table 6.1). Along three transects across the hillslope (Fig. 6.2), surface morphology was measured in detail by d-GPS. Furthermore, the geometry of three erosion rills was recorded (Table 6.1). High-resolution aerial photographs of the catchment's surface were taken on July 10, 2008 and July 01, 2009; using a digital Camera (Pentax Optio A40, 12 MPixels) mounted on a GPS-controlled microdrone (MD 4-200, Microdrones, Siegen) from an altitude of about 80 m. Aerial image mosaics of the catchment area were then composed from 132 rectified and georeferenced photograph clippings, each covering an area of about 20 m by 20 m.

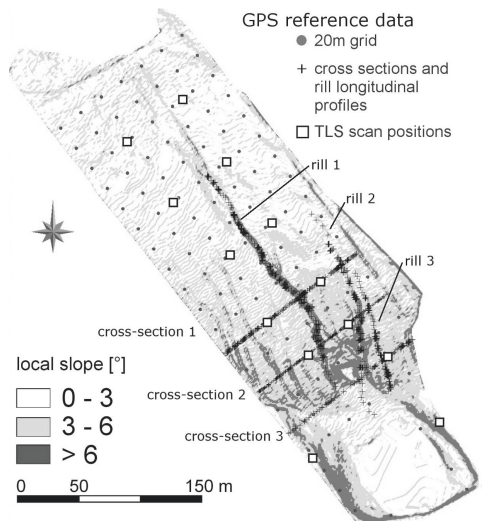

Figure 6.2: Locations of GPS reference data and TLS scan positions, shown on a map of morphology (depicted by local slopes in a 1m by 1m grid) in April 2009, based on elevation data from airborne laser scanning (ALS). The dotted line in the map and the black line in the photo mark the location of a fence delineating the monitoring area. Adapted from Schneider et al., 2012.

6.3.2 Construction of surface DEMs

The GPS-coordinates of the rampart delineating the surface catchment area were added to each of the elevation datasets recorded after September 2006. To remove single outliers from the photogrammetry-based datasets, a threshold filter was applied that replaced elevation values that differ more than 0.3 m from the average of surrounding elevations in a 5m by 5m window with this average elevation. The parameters were iteratively adjusted to ensure that only individual outliers are affected. TIN elevation models (Table 6.2) were constructed (step 1a, Fig. 6.1) from the source elevation datasets to enable the combination of elevation data and the construction of 3Dmodels in the 3D-modelling software GOCAD Suite 2.5.2. The pond water surface in the TIN models was represented by water level monitoring data that were used to virtually flood the pond region (unit pond in each DEM) by replacing all the elevations with the water level at that time.

The areal extent (2D or map area) and the 3D area (which includes the total surface by integrating the areas of all elements of the TIN model) of each TIN DEM were calculated and the 3D/2D-area-ratio was computed to obtain an indicator of surface roughness. Datasets were visually inspected (step 1b in Fig. 6.1) and deviations to the d-GPS reference data sets arranged in a 20 m by 20 m grid were analysed (step 1c in Fig. 6.1): Each DEM was compared with the reference data set that was recorded with the smallest time-lag to the original data set, and the DEMs recorded in spring 2009 were compared with both the reference data sets measured before and after the date of DEM recording (Table 6.2). To account for the time differences between original and reference datasets, all points located in areas of morphodynamic activity (as further described in Appendix A.1) were excluded from the datasets.

Table 6.2: Assignment of reference data sets to elevation models and statistical quality criteria. Denominations of surface models referred to in the text are given in the left column.

method of recording	recorded on	data spacing [m]	reference data recorded on	number of reference data points	RMSE [m]	ME [m]	SD_{ME} [m]
photogrammetry	Nov 26, 2005	1	Aug 20, 2008[a]	61	0.116	-0.100	0.058
photogrammetry	Apr 24, 2008	1	Aug 20, 2008[a]	61	0.145	-0.138	0.047
photogrammetry	Aug 18, 2008	1	Aug 20, 2008[a]	61	0.073	-0.048	0.055
photogrammetry *model photo_raw_1*	Jun 13, 2009	1	Aug 20, 2008	61	0.100	0.086	0.050
			Nov 10, 2009[a]	74	0.054	0.019	0.051
photogrammetry *model photo_raw_05*	Jun 13, 2009	0.5	Aug 20, 2008	61	0.099	0.081	0.059
			Nov 10, 2009[a]	74	0.060	0.014	0.059
photogrammetry	Dec 5, 2009	1	Nov 10, 2009[a]	114	0.089	-0.035	0.084
photogrammetry	Mar 4, 2010	1	Apr 22, 2010[a]	114	0.206	-0.199	0.053
ALS model *ALS*	Mar 6, 2009	1	Aug 20, 2008	61	0.047	0.031	0.036
			Nov 10, 2009	74	0.048	-0.037	0.030
TLS model *TLS*	Mar 12-15 2009	0.5	Aug 20, 2008	61	0.035	0.017	0.031
			Nov 10, 2009	74	0.058	-0.049	0.032

[a] reference data used for referencing of photogrammetry-based elevation data

The vertical distance between reference data and the TIN DEMs was computed, and statistical criteria (Fisher and Tate, 2006) were determined: Root Mean Square Error (RMSE), Mean Error (ME) and Error standard deviation (SDME), as follows

$$RMSE = \sqrt{\frac{\sum d_z^{\,2}}{n}}$$

$$ME = \frac{\sum d_z}{n}$$

$$SD_{ME} = \sqrt{\frac{\sum \left[d_z - ME\right]^2}{n-1}}$$

where d_Z (i.e., $d_z = Z_R - Z_T$) is distance in vertical direction (L) between the reference point, Z_R, and a corresponding value, Z_T, of the TIN model, n is number of data points, and subscript z denotes the vertical axis.

6.3.2.1 Fitting photogrammetry-based DEMs to reference elevations

As statistical criteria (Table 6.2) indicated the presence of a considerable systematic elevation error in the photogrammetry-based DEMs, the models were adjusted to the corresponding reference data set in a fitting procedure which shifted elevation data to the reference and iteratively adapted elevations of surface nodes between reference points. Further information on the referencing is provided in Appendix A.1. As a result, rectified photogrammetry - based DEMs with 1 m data spacing for June 2009 (surface model *photo_1*) and 5 other times were derived, as well as a rectified DEM with 0.5 m data spacing for June 2009 (surface model *photo_05*).

6.3.2.2 Definition of surface subunits

To delineate units of differing morphological and vegetation cover characteristics, the geometry of the rill network, the alluvial fans and the very densely vegetated area around the pond (Fig. 6.3) were digitized from the aerial photograph mosaic of July 01, 2009 in ArcGIS 9.3 (ESRI Inc., Redlands). Densely vegetated rills and rill segments were assumed to be 'surface-inactive' and therefore not included. The main flow paths in the rills and along the alluvial fans were digitized to a *polyline* shapefile, and the areal extent of the rill network was digitized to a polygon shapefile following the rills' upper edges. As the alluvial fan surface was not clearly observable (see Fig. 6.3) because of the relatively denser vegetation cover, the aerial photograph recorded by VEM AG in August 2008 (Fig. 6.3) and the photograph mosaic of July 10, 2008 were additionally used for digitization. Length of each segment of the polyline as well as the area of each polygon were computed, and mean widths of rills and alluvial fan segments were calculated from areas divided by the length of the segments.

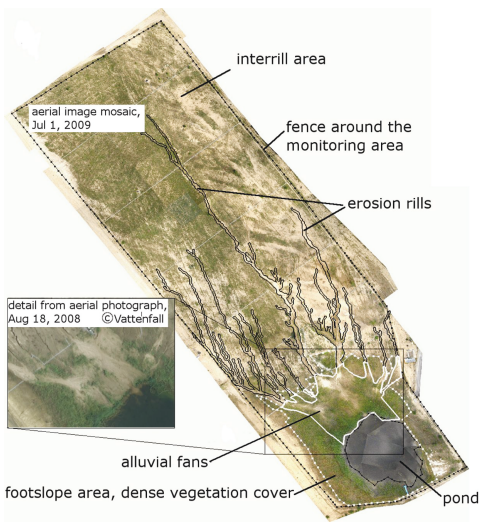

Figure 6.3: The surface of the 'Hühnerwasser' in aerial photographs and units of differing morphological and vegetation cover characteristics. The outline boundary of the pond was extracted from the elevation models of spring 2009, and location of the fence around the monitoring area was recorded by d-GPS.

Characteristic units of differing morphometry and vegetation cover were then delineated in the models. The digitized outlines of the rill, alluvial, and the more densely vegetated area around the pond were used to spatially define the structural units *rillbed*, *alluvial*, and *footslope_veg*, respectively. To define the erosion rill unit (*rill*), we extended the outline of the rill network by a constant distance of 0.5 m by applying a buffer function in SAGA, so that the rill's upper edges are also included in the unit. The *interrill* unit was then defined as the remaining area not included in one of the other units. Furthermore, the sparsely vegetated interrill areas (unit *interrill-veg*) were defined by subtracting unit *footslope_veg* from the *interrill* unit. The monitoring area was defined in the DEMs as the area inside the fence (see Fig. 6.3). The pond area was defined in each DEM by intersecting the DEMs with a plane representing the water table at the time of DEM recording.

6.3.2.3 Region-specific modification of DEMs

Modifications were applied to the DEMs in the *rillbed, interrill* and *alluvial* units (step 2a, Fig. 6.1). Modifications were carried out region-specific because the underlying principles and plausibility rules apply differently for the structural units, considering their specific morphological and vegetation cover characteristics.

Modifications in interrill areas, based on logical comparison

A logical comparison of several DEMs of the time series was carried out to reveal areas of inaccurately represented elevations, which cause inconsistent changes over time (i.e., elevations in one DEM are higher than in the models before and afterwards). Alternating elevation changes were assumed to be plausible only in dynamically evolving rill and alluvial areas but not in interrill areas. Data points showing inconsistent elevation development over time were identified in the DEM based on photogrammetric data (*photo_1*): Elevation differences between the DEM of June 2009 (06/09) and two DEMs previous and next to it (04/08, 08/08, 12/09, and 03/10) were determined for each node of the DEM. When all the differences were either positive or negative as compared with each of the four other DEMs, this was assumed as indicative for inconsistencies caused by errors in the DEMs. For DEM nodes in the interrill areas that met the inconsistency criteria, elevations were replaced by elevations of the next following DEM (i.e., 12/09) of the time series.

Modifications in rill and alluvial areas

In rill and alluvial fan areas, the drainage network's longitudinal profiles were extracted from the surface models by projecting the digitized drainage network *polyline* onto each of the DEMs. Before projection, the density of the *polyline* nodes was increased to obtain maximum segment lengths of 0.25 m in rill areas to capture the complex morphology. Elevation

values of the resulting polyline nodes were then modified to account for a hydraulically reasonable representation of the rill network: If the elevation value of a data point was higher than that of any of the upslope data points in the same segment, it was replaced by the elevation value of the upslope data point. To approximate the rill network's and alluvial fans' lateral extension, two additional coordinates were generated along the network, left and right from each grid point perpendicular to the polyline in distances of 0.75 · rill width. The value of 0.75 was optimized iteratively such that the whole rill floor was represented but high overlaps at rill confluences were avoided. From the resulting data points, an 'auxiliary' surface was created by triangulation, representing the modified rill floor and alluvial fan geometry. Elevations of this surface were used to replace the original elevations inside the *rill* and *alluvial* model units. Finally, triangulation between the modified data points was optimized without modifying the positions of the TIN nodes.

The vertical distance, $d_z{}^i$, between the modified, Z_m, and the original, Z_o, surface elevation

$$d_z{}^i = Z_m{}^i - Z_o{}^i,\ \mathrm{i} = 1, \ldots, \mathrm{n}$$

was computed for each of the n nodes to assess the effect of the modifications.

6.3.2.4 Construction of surface models from multi-source data

Elevation data in the structural units *rill, interrill-veg, alluvial* and *footslope_veg*, extracted from the original and modified datasets, were used to construct additional surface models (Table 6.3), which combine data from different sources (steps 2b and 2c in Fig. 6.1). In surface 1 (Table 6.3), we combined those unmodified datasets that we found to give the best representation of specific units. Surface 2 was constructed to evaluate the effects of modification in the interrill areas. To evaluate the effects of modifications in the rill areas for TLS, *photo_1* and *photo_05* datasets, we constructed surfaces 3a to 3d, and to evaluate the effect of modifications in the alluvial fan area for the *photo_1* and *TLS* data, surfaces 4a and b were constructed. Finally, surface 5 was constructed by replacing unmodified data as combined in surface 1 by modified datasets that were found to give improved surface representation.

Table 6.3: Data basis for surface models constructed by combining multi-source data for surface structural units.

surface model	rill area, buffered (*rill*)	interill aera		alluvial area (*alluvial*)
		backslope, sparse vegetation cover (*interrill-veg*)	footslope, dense vegetation cover (*footslope_veg*)	
1	TLS	photo_1	ALS	ALS
2	TLS	photo_1, modified	ALS	ALS
3a	TLS, modified	photo_1	ALS	ALS
3b	photo_1, modified	photo_1	ALS	ALS
3c	photo_05	photo_1	ALS	ALS
3d	photo_0.5, modified	photo_1	ALS	ALS
4a	TLS, modified	photo_1	photo_1	photo_1, modified
4b	TLS, modified	photo_1	photo_1	TLS, modified
5	TLS, modified	photo_1, modified	ALS	ALS

6.3.3 Construction of 3D grid models of change

Gridded 3D models of sediment mass change were constructed from each of the spring 2009 DEMs in combination with the photogrammetry-based DEM representing the initial catchment surface (11/05) as follows: The vertical distance, $d_{zt}{}^{i}$, between the surface elevations with time in each of the DEMs ($Z_t{}^{i}$) and that in the 11/05 DEM ($Z_{to}{}^{i}$)

$$d_{zt}{}^{i} = Z_t{}^{i} - Z_{to}{}^{i},\ \mathrm{i} = 1, \ldots, \mathrm{n}$$

was computed for all *n* nodes of the surface models of times *t*. For 3D grid models based the unmodified photogrammetric, ALS, and TLS DEMs, the standard deviation in elevation change, σ_c, was obtained by (Lane et al., 2003)

$$\sigma_c = \sqrt{\sigma_t{}^2 + \sigma_{to}{}^2}$$

based on the general accuracy of the input elevation models (σ = 0.147 m, σ = 0.15 m, and σ = 0.02 m for photogrammetry-, ALS, and TLS-based data, respectively). To give an approximation of the propagated error, statistical significance of change in elevation for these models was then assessed following Lane et al. (2003) and Brasington and Smart (2003) by computing

$$T^i = \frac{Z_t{}^{i} - Z_{to}{}^{i}}{\sqrt{\sigma_t{}^2 + \sigma_{to}{}^2}}$$

and, using a threshold value of T > 1, delineating areas where elevation change is above a minimum level of detection with a confidence limit of 68 %.

Based on elevations of the 11/05 DEM and the distances $d_{zt}{}^{i}$, 3D volume bodies with 0.5

m by 0.5 m wide cells were constructed and the spatially distributed difference volume was calculated. Direction of change was obtained by vertical projection of $d_{zt}{}^{i}$ from the surface models. To derive sediment mass change, spatially distributed values of soil bulk density were assigned to the model cells and volume of change was multiplied with bulk density in each cell. Near-surface (0-3 cm) bulk density distribution had been obtained by spatial interpolation using Ordinary Kriging from 192 sampling points (Papritz et al., 2011) in the catchment by Schneider et al. (2011). Bulk density below 3 cm soil depth was assumed to be equal to the values of the topmost 3 cm. Only grid cells in the area inside the fence and outside of the pond were included in the interpretation of mass change. For separate interpretation, cells of the 3D grid models were spatially assigned to structural units (*rill, alluvial, interrill-veg, footslope_veg*). Additionally, the erosion-dominated interrill area (*interrill_slope*) was delineated by subtracting *rill* cells from the area upslope of the alluvial fans (see Fig. 6.3).

6.3.4 Evaluation of surface models

The generated models were evaluated in two approaches. First, the elevations of DEMs and reference d-GPS points were compared along vertical cross-sections and rill longitudinal profiles (step 1d in Fig. 6.1). Cross section elevation data were extracted from the DEMs by intersection of the TIN models with a vertical extension of the d-GPS transect line. RMSE, ME and SDME were computed from the vertical distances in elevation between reference data points and corresponding points in surface models. Model rill longitudinal profiles were extracted by projecting the digitized rill network *polyline* onto the DEMs. Second, catchment sediment budgets and their spatially distributed negative and positive components were compared. When assuming that no sediment enters or leaves the catchment's outer boundaries, the net sediment budget including sediments accumulated in the pond should be balanced. Thus, our criterion for surface model quality was to most closely approximate the closed sediment balance (step 1e, Fig. 6.1). Additionally, sediment budgets were separately computed and analysed in the model subunits. Model quality was evaluated considering geomorphological principles (step 1f, Fig. 6.1), e.g., for the transition from the initial and unrilled surface to the eroded landscape, only a decrease in elevation and thus sediment mass is plausible in areas where rills have developed.

6.4 Results

6.4.1 2D DEMs

Statistical quality criteria computed from elevation datasets and d-GPS reference data (Table 6.2) reflect errors in the elevation data. For the photogrammetry-based datasets of 06/09, positive mean errors reflect lower elevation values as compared with reference data sets acquired before and after DEM recording, which indicates a systematic error in elevation (see Appendix A.1). Referencing the photogrammetry-based DEMs to d-GPS elevation points resulted in surface models *photo_1* and *photo_05*, in which deviations from d-GPS reference data are set to zero. Visual inspection reveals that the DEM surface is comparably smooth in the ALS model(Fig. 6.4 a), while in the referenced photogrammetry-based DEMs (*photo_1*, Fig. 6.4b, and *photo_05*, Fig. 6. 4c), especially in the *photo_05* DEM, more irregular peaks occur, in particular, in the area near the pond (Fig. 6.4b, 6.4c details ii, iii). In the TLS DEM, erosion rills in the lower slope area are most clearly observable (Fig. 6. 4d), while peaks resulting from erroneous recording of vegetation are obvious in areas distant to measurement locations, especially near the catchment's borders and in the area around the pond (Fig. 6.4d, details iv, v). Low surface roughness in the ALS model and higher roughness in the higher-resolution models is reflected in the 3D/2D area ratios, which are 1.0110 and 1.0057 for the 1 m-resolution *photo_1* and ALS models and 1.0210 and 1.0159 for the 0.5 m-resolution TLS and *photo_05* models.

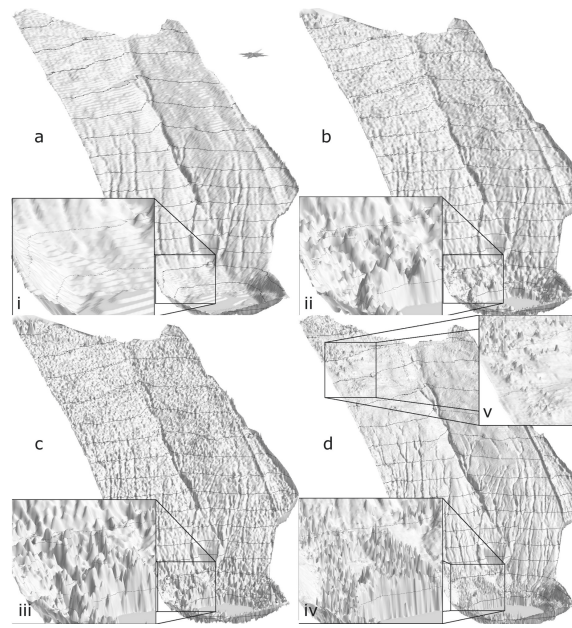

Figure 6.4: 3D-views of TIN DEMs for comparing effects of data source and grid spacing. (a) DEM based on airborne laser scanning, April 2009, data spacing 1 m. (b), (c) DEMs based on automated digital photogrammetry; (b) data spacing 1 m; (c) data spacing 0.5 m, both June 2009. (d) DEM based on ground based laser scanning, May 2009, data spacing 0.5 m. Spacing of elevation contour lines is 1 m, 3D views are depicted with 10*superelevation. Enlarged details show critical surface structures in the areas near the pond (i-iv) and in the upslope area (v).

6.4.2 Effects of DEM modification

6.4.2.1 Modification in interrill areas

The definition of DEM nodes with inconsistent change based on comparison of the *photo_1* DEM with other DEMs of the time series reveals that in the interrill area, a high amount of DEM nodes were lower as compared to all the other four surfaces (Table 6.4). By replacing elevation values with data from the 12/09 model, nodes were shifted by, in the mean, about 0.1 m (Table 6.4).

Table 6.4: Effects of modification of elevations in the interrill, rill and alluvial fan areas on the elevation of TIN nodes

	modification to lower elevations		modification to higher elevations	
	number of nodes shifted / % of nodes in unit	mean amount of elevation change as a result of modification [m]	number of nodes shifted / % of nodes in unit	mean amount of elevation change as a result of modification [m]
unit *interrill* photo_1	4565 / 10.3%	-0.118	13272 / 29.9%	0.107
unit *rillbed*				
photo_1	1125 / 52.2%	-0.075	1026 / 47.6%	0.032
photo_05	5613 / 65.1%	-0.089	2996 / 34.8%	0.031
TLS	5193 / 60.7%	-0.086	3339 / 39.0%	0.028
unit *alluvial*				
photo_1	1519 / 55.4%	-0.275	1053 / 38.4%	0.121
photo_05	5392 / 49.7%	-0.280	4894 / 45.1%	0.135
TLS	7350 / 67.9%	-0.187	3480 / 32.1%	0.056

6.4.2.2 Modification in rill and alluvial areas

For the example of erosion rill 3 (location see Fig. 6.2), Fig. 6.5 shows that as an effect of modifications in rill areas, high increase of elevation was removed at the downslope end of the profiles (e.g., ii in Fig. 6.5). The numbers of shifted nodes and the mean amounts of change (Table 6.4) reveal that elevation was reduced in higher extents than it was increased throughout the datasets. Modification was more distinct in the *alluvial* as compared to the *rillbed* areas. Visual inspection of the DEMs after applying the modification confirms the expected effects of the modification: rill floors are represented with uniform elevations, rill walls appear steeper, and surface geometry in the alluvial fan area is flattened (Fig. 6.6).

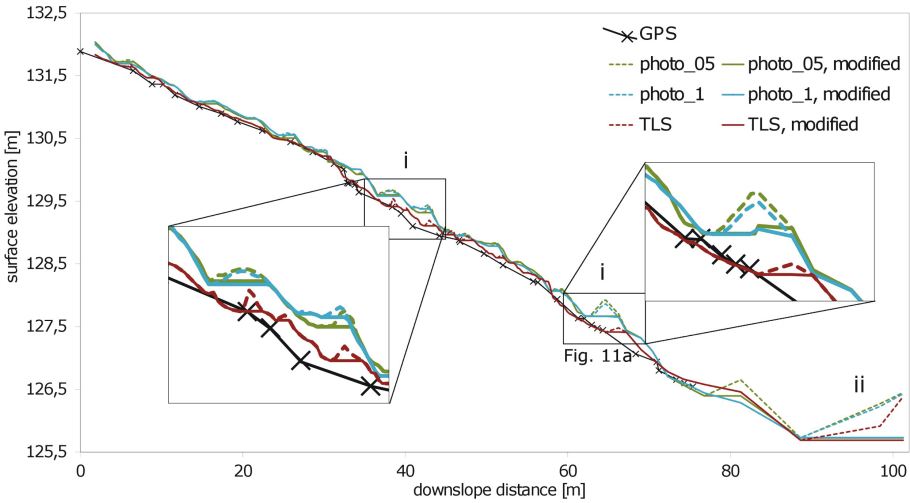

Figure 6.5: Longitudinal elevation profile of rill 3 (for location see Fig. 6.2) obtained from DEMs, comparing the effects of DEM modification in the rill areas for datasets recorded by different techniques in spring 2009. Roman numerals mark segments where elevations were modified along the slope (i) and at the downslope end of the profile (ii). The marked segment is shown in 3D view for discussion in 6.11(a).

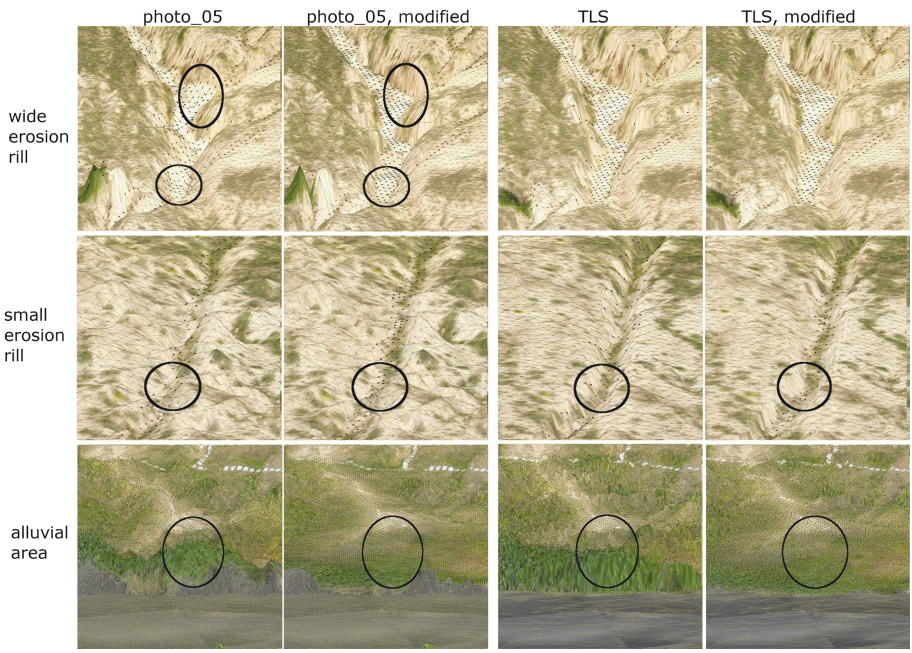

Figure 6.6: Comparison of unmodified and modified DEMs from photogrammetry and TLS, .details for characteristic surface structures. DEMs are overlaid with drone-based aerial photographs and 3*superelevated for visualization. Nodes and triangles of the TIN are visualized by grey lines; node spacing is 0.5 m. TIN nodes inside the model regions affected by the modification are visualized by black dots. Areas of noticeable effect of the modification are encircled.

6.4.3 Evaluation of surface model cross sections

6.4.3.1 Original surface models

The comparison of cross sections through the unmodified DEMs and d-GPS reference data (Fig. 6.7, Table 6.5) shows that ALS data seem to be slightly shifted upwards compared to d-GPS topography and considerably underestimate widths of rill floors and depths of smaller rills (e.g., i in Fig. 6.7). TLS data best represent rill geometry for most of the rills along the cross-sections. Especially in the alluvial area (western part of section 3), the TLS DEM shows few, but high deviations from the reference data (e.g., ii in Fig. 6.7). Photogrammetry-based elevation data show relatively small deviations from reference data in the interrill areas (e.g., iii in Fig. 6.7). These variations are, however, considerably higher in the *photo_05* as compared with the *photo_1* model. Depth of almost all the rills in the cross-sections is considerably underestimated by the *photo_1* model. The *photo_05* model gives a better representation of rill depths (e.g., iv in Fig. 6.7).

Table 6.5: Quality criteria for unmodified and modified DEMs as computed from deviations to reference data along transects 1-3.

surface model	RMSE	ME	SD_{ME}
unit *interrill* (n = 234)[a]			
photo_1	0.076	0.007	0.076
photo_1, modified	0.069	-0.006	0.069
photo_05	0.078	0.013	0.077
ALS	0.079	-0.037	0.070
TLS	0.074	-0.019	0.071
unit *rillbed* (n= 100)[a]			
photo_1	0.212	-0.127	0.170
photo_1, modified	0.200	-0.122	0.159
photo_05	0.182	-0.099	0.153
photo_05, modified	0.175	-0.053	0.168
ALS	0.148	-0.086	0.121
TLS	0.135	-0.045	0.128
TLS, modified	0.142	-0.040	0.137
total transects (n=394)[a]			
photo_1	0.131	0.026	0.129
photo_05	0.118	0.017	0.117
ALS	0.108	0.041	0.100
TLS	0.097	0.021	0.095
5	0.102	0.009	0.101

[a] n: number of points compared

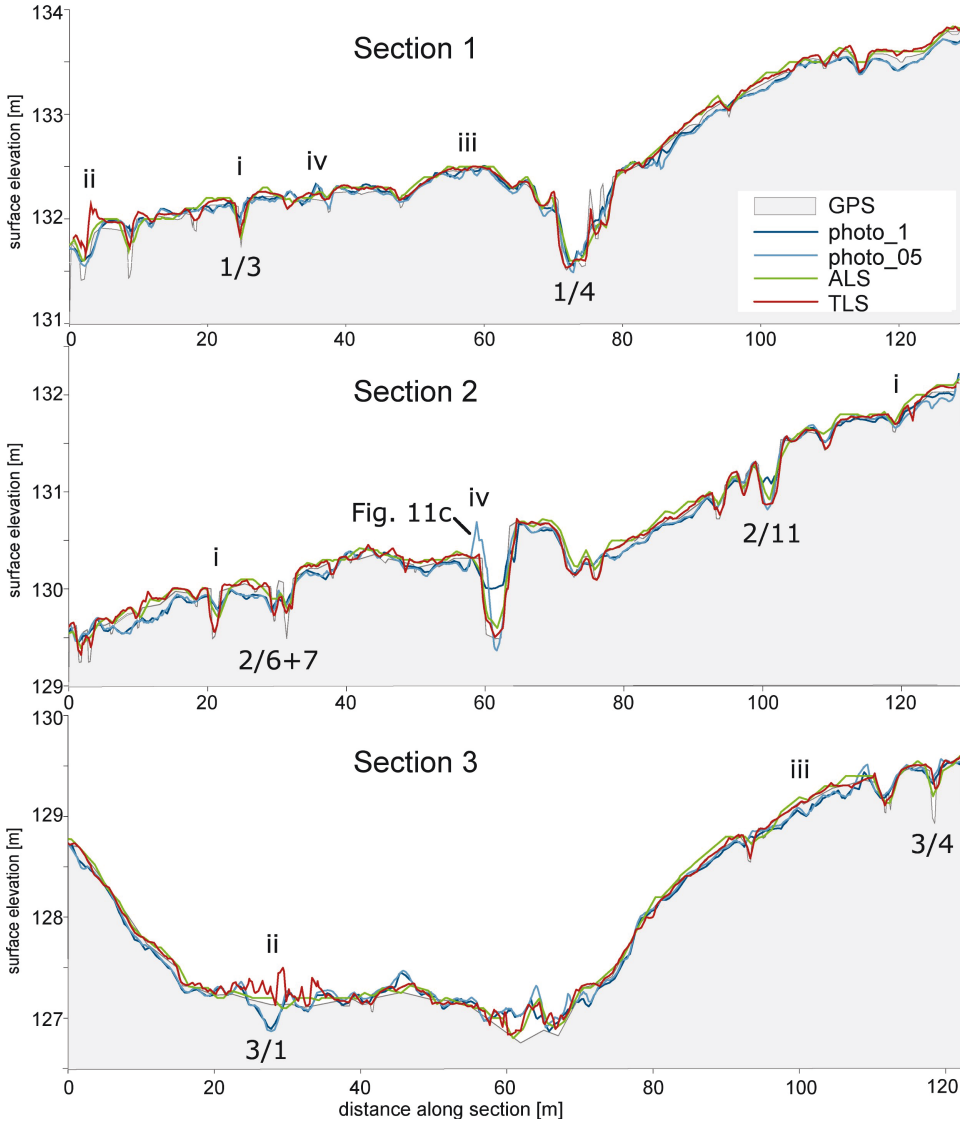

Figure 6.7: Vertical elevation cross-sections (location see Figure 6.2) extracted from original DEMs comparing remotely-sensed DEMs with d-GPS reference data. Roman numerals mark areas of characteristic surface representation in DEMs: underestimation of rill width and depth, especially in photogrammetry-based and ALS models (i), single, high deviations from reference data in the TLS model (ii), typical deviation of photogrammetry based DEMs from reference data in interrill areas (iii), and better representation of rill geometry in the photogrammetry-based model with 0.5 m data spacing as compared to models with 1 m data spacing (iv). The numbers refer to the enlargements in Figure 6.9 or to locations of details shown in Figure 6.11.

6.4.3.2 Modified surface models

Fig. 6.8 shows that agreement of the *photo_1* surface model to reference data was improved by the modifications in the interrill unit for most parts of the cross-sections, especially in small depressions (i in Fig. 6.8), where local outliers appeared in the original data (ii in Fig. 6.8), and in long segments of smooth morphology (iii in Fig. 6.8). Statistical quality criteria (Table 6.5) affirm a slight improvement, as the RMSE for the modified DEM is about 9.2 % smaller as compared with the unmodified DEM. However, in some areas of the modified DEMs, deviations from the reference data were found to be increased (iv in Fig. 6.8). Results of the modification in the units *rillbed* and *alluvial* are illustrated for some rills of different width and depth in Fig. 6.9 and quality criteria are given in Table 6.5. RMSE for transect areas in the *rillbed* region is reduced by 5.7 % and 3.8 % for photogrammetry-based models with 1 m and 0.5 m data spacing, respectively, while RMSE for TLS data is increased by 5.2 %. The mean error (ME) is reduced for all models. For the *photo_1* surface model, the representation of rill geometry was improved in broader (e.g., Fig. 6.9e) and some small rills (e.g., Figs. 6.9a, 6.9b); however, rill depth remained mostly underestimated. Agreement with reference data was slightly improved in the modified *photo_05* surface model. In some of the narrow, V-shaped rills, agreement with reference data was reduced (section 1/ rill3 and section 2/ rills 6+7 in Fig. 6.9). In the alluvial fan area, deviations in TLS and photogrammetry-based data were reduced (e.g., section 3/ rill 1 in Fig. 6.9). Quality criteria for all areas of the reference data transects show that in surface model 5, RMSE is smaller as compared with the photogrammetric and ALS models, and ME is smaller as compared with all the unmodified models.

6.4.4 Evaluation of sediment budgets

Fig. 6.10 gives the spatial distribution of mass change as computed from 3D models and shows areas where elevation change above the minimum level of detection defined with a confidence limit of 68 % is indicated. Maps show that highest decrease in elevation in rill areas is indicated in the model using TLS data (Fig. 6.10b); and that especially photogrammetry- and TLS based models indicate high elevation increase distributed over the backslope and around the pond area. Total sediment budgets for the monitoring area (excluding the pond) are given for models based on original DEMs and the multi-source surface models *1* and *5* in Table 6.6, and budgets for individual units of interest (in which input data differ between the models being compared) are given in Table 6.7. The value of net change is negative in all the models, as an amount between 2445 t and 3103 t of sediments deposited in the pond is not considered here. The deposition of 2445 t was determined by Kleeberg et al. (2010) in August 2008, and the value of 3103 t was estimated for the time until May 2009 by extrapolation assuming sedimentation continued at a constant average rate.

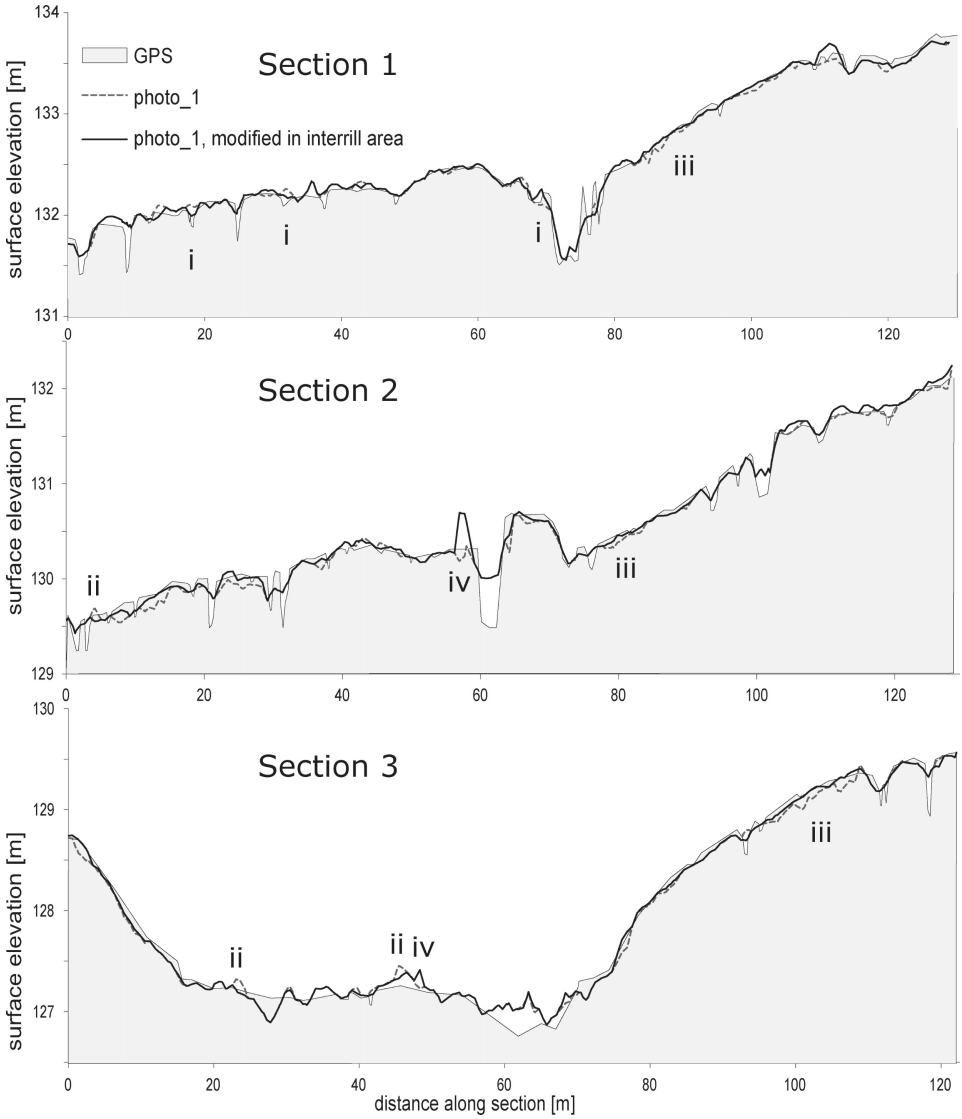

Figure 6.8: Vertical elevation cross-sections (location see Figure 6.2) extracted from original and modified photogrammetry-based DEMs, compared with d-GPS reference data. Roman numerals mark segments of improved agreement to reference data in small depressions (i), where local outliers appeared (ii), and in long segments of smooth morphology (iii) and segments of increased deviation from reference data (iv).

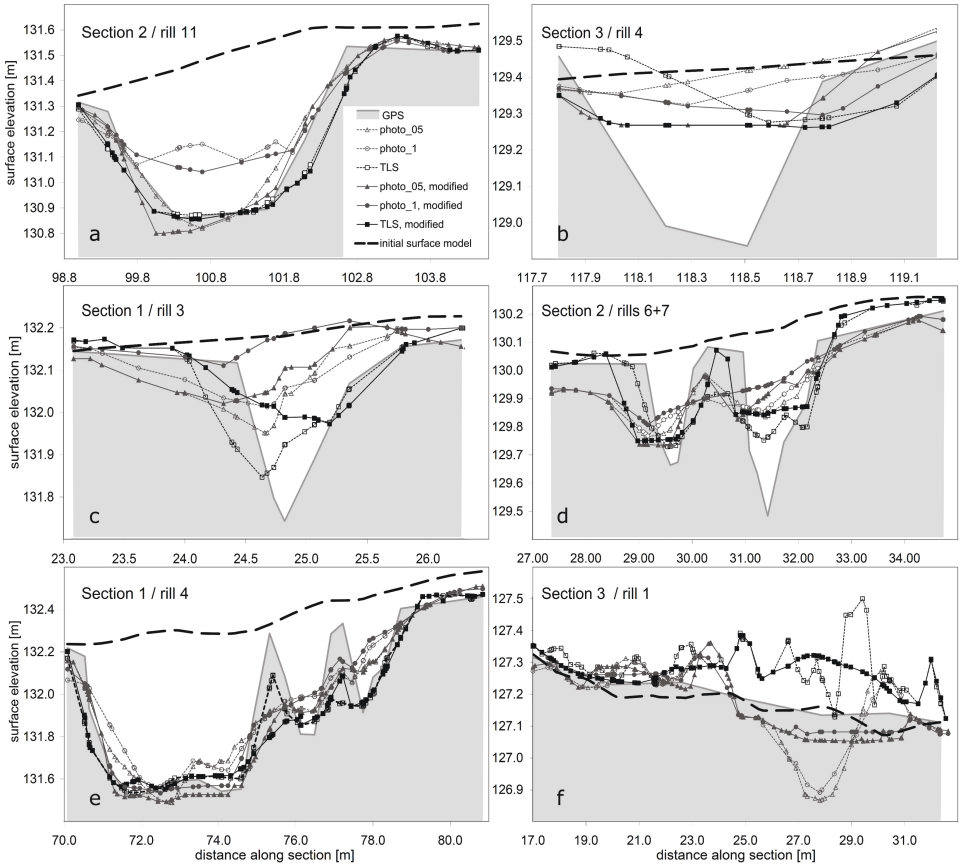

Figure 6.9: Comparison of rill cross section geometry as depicted in original and modified DEMs from spring 2009 to d-GPS reference data and the initial soil surface elevation in a DEM of November 2005. Position of the cross-sections is given in Figure 6.7. (a), (b) Relatively small rills; (c), (d) narrow and steepwalled rills; (e) the large central rill; and (f) western part of the alluvial area.

Table 6.6: Change of sediment volume and mass for the monitoring area (not including the pond) for November 2005 to April/May/June 2009, calculated from different 3D grid models. Region-specific sediment budgets for models photo_1, ALS, TLS are given in Table 6.7.

	decrease in sediment volume / mass				increase in sediment volume / mass				
budget model	area [grid cells]	area [m²]	mean [m³/m²]	total change [t]	area [grid cells]	area [m²]	area [m³/m²]	total change [t]	net change [t]
photo_raw	177174	44293.50	-0.207	-13482	17811	4452.75	0.234	1534	-11948
photo_1	141701	35425.25	-0.124	-6451	53284	13321.00	0.140	2755	-3698
ALS	120554	30138.50	-0.095	-4207	74431	18607.75	0.088	2421	-1786
TLS	113701	28425.25	-0.098	-4116	81270	20317.50	0.111	3316	-801
1	140861	35215.25	-0.126	-6518	54124	13531.00	0.111	2204	-4313
5	134198	33549.50	-0.113	-5576	60787	15196.75	0.100	2234	-3343

photo_raw: model from original, not georeferenced photogrammetry data, data spacing 1 m; *photo_1*: model from original, georeferenced photogrammetry data, data spacing 1 m; *ALS*: model from airborne laser scanning; *TLS*: model from ground based laser scanning, *1* and *5*: models from multi-source DEMs, see Table 6.3.

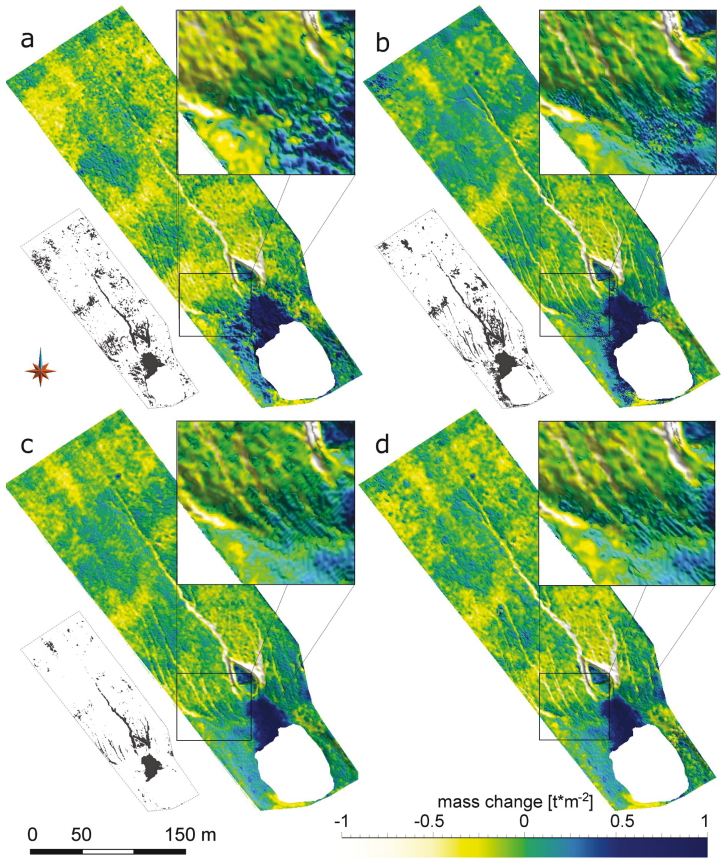

Figure 6.10: Comparison of the spatial distribution of sediment mass change as quantified from different 3D models of change. Models were constructed from the photogrammetry-based DEM of November 2005 and (a) DEM photo_1 (06/09), (b) DEM TLS (05/09), (c) DEM ALS (04/09), (d) surface model 5, combining modified, multi-source data. The area outside the fence and the pond area are excluded. Enlarged details show mass change in the transitional area between erosion rills and alluvial fans. Small maps show areas of change in elevation above a minimum level of detection determined with a confidence limit of 68 % for unmodified input DEMs.

6.4.4.1 Sediment budgets from original surface models

A large negative value of net change is found for 3D grid model *photo_raw*, which was constructed using photogrammetry-based datasets not fitted to reference elevation data. A smaller negative value of net change results from budget *photo_1*, calculated from the DEMs after fitting to reference data. In the total budgets derived from the ALS and TLS DEMs, the negative component of the budget is considerably smaller as compared to the photogrammetry - based model (Table 6.6). Table 6.7 gives region-specific change in volume and sediment

Table 6.7: Region-specific sediment budgets, determined for model subunits from different 3D grid models of change. Overall sediment budgets for the monitoring area of models *photo_1*, *ALS*, and *TLS* are given in Table 6.6. Subunit budgets for models *2-4* (see Table 6.3) were determined for region-specific evaluation of DEM modifications. Region-specific budgets for models *1* and *5* correspond to subunit budgets of models *photo_1*, *ALS*, and *TLS* (Table 6.3).

budget model	data used in unit	unit	decrease volume / sediment mass			increase volume / sediment mass			net budget [t]
			number of cells	mean [m³/m²]	total [t]	number of cells	mean [m³/m²]	total [t]	
	photo_1	*Rill*	13147	-0.231	-1130	842	0.046	14	-1115
photo_1	*photo_1*	*interrill_slope*	120252	-0.114	-5039	32269	0.059	704	-4335
	photo_1	*Alluvial*	1173	-0.109	-47	8168	0.472	1421	1374
	ALS	*Rill*	12907	-0.218	-1048	1082	0.043	17	-1031
ALS	*ALS*	*interrill_slope*	100032	-0.081	-2977	52489	0.052	1004	-1973
	ALS	*Alluvial*	870	-0.044	-14	8471	0.345	1075	1061
	TLS	*Rill*	12777	-0.264	-1253	1209	0.060	27	-1227
TLS	*TLS*	*interrill_slope*	90741	-0.077	-2557	61779	0.059	1337	-1220
	TLS	*Alluvial*	768	-0.073	-21	8572	0.450	1421	1401
2	*photo_1, mod*	*interrill_slope*	111367	-0.095	-3867	41154	0.055	831	-3036
3a	*TLS, mod*	*Rill*	13211	-0.282	-1384	778	0.049	14	-1370
3b	*photo_1, mod*	*Rill*	13292	-0.241	-1190	697	0.045	11	-1179
3c	*photo_05*	*Rill*	13020	-0.251	-1213	969	0.059	21	-1192
3d	*photo_05, mod*	*Rill*	13260	-0.274	-1348	729	0.052	14	-1333
4a	*photo_1, mod*	*Alluvial*	1021	-0.114	-43	8320	0.404	1239	1196
4b	*TLS, mod*	*Alluvial*	751	-0.057	-16	8590	0.346	1094	1078

photo_1: model from original, georeferenced photogrammetry data, data spacing 1 m; *ALS*: model from airborne laser scanning; *TLS*: model from ground based laser scanning, *2 - 4*: models from multi-source DEMs, cf. Table 3; *mod*: datasets after region-specific modification

budgets: In model *ALS*, less erosion is recorded in the rills as compared to models *photo_1* and *TLS*. The highest amount of erosion in rills was derived from the *TLS* model. Higher amounts of sedimentation in the alluvial unit are indicated in the photogrammetry-based and *TLS* models, as compared with the *ALS* model.

6.4.4.2 Sediment budgets from modified surface models

Comparison of the interrill region (unit *interrill_slope*) in the models of change from photogrammetry-based (*photo_1*) and modified photogrammetry-based (model *2*) data shows that as a result of the modifications in this area, less volume and mass decrease and slightly more increase is indicated. Comparison of the rill area budget in model *1* (based on unmodified TLS data) and model *3a* (based on modified TLS data) indicates more erosion and less sedimentation as a result of the modification. Similarly, replacing unmodified by modified photogrammetry-based data for calculation of budgets *3b* (from modified *photo_1* data) and *3c* and *3d* (from DEM *photo_05*, *original and modified DEM*) causes higher volume and mass decrease and slightly lower increase (Table 6.7). In the models based on unmod-

ified photogrammetric and TLS data (*photo_1* and *TLS*), increase in the alluvial fan area is considerably higher, while it is lower in the models based on the modified datasets (*4a* and *4b*). In the model based on multi-source, modified data (model 5), lower amounts of volume and mass change are indicated as compared to most of the other models (Table 6.7).

6.5 Discussion

6.5.1 Combined assessment of surface models

Based on these results, a 'best performing' dataset can be defined by evaluating surface models and modifications in an iterative analysis of the models, considering several criteria of surface model quality.

For the original surface models, rill areas are best represented by TLS data (Fig. 6.4d). This is confirmed by comparison with reference data (Fig. 6.7) and region-specific evaluation of mass change in rill areas (Table 6.7). The ALS DEM is most suitable for quantification of mass change in the alluvial areas, as concluded from visual analysis of DEMs and from comparison with reference data. For quantification of change in interrill areas the photogrammetry-based DEM with 1 m data spacing was found to be most suitable because of its better agreement with reference data as compared to the other models. Thus, budget model *1*, combining the so-defined best-performing input datasets for specific regions, allows an improved quantification of sediment budgets for November 2005 to spring 2009 as compared to the single-source photogrammetry-, ALS-, and TLS-based DEMs. However, the budget derived from model *1* is still distinctly imbalanced in direction of negative values, which is mainly caused by the high mass decrease indicated in the interrill area (Table 6.7).

A slight improvement of surface representation in the *photo_1* model was achieved by modifications in interrill areas, as suggested by comparison to reference data (Fig. 6.8) and the smaller negative component in the sediment budget of unit i*nterrill_slope* (Table 6.7). Representation of rill geometry in TLS data is slightly improved by modifications (Fig. 6.9, Table 6.7). Surface model 5 thus allows further improved budget quantification, confirmed by the more balanced net budget of budget model 5 and reduced errors along reference data transects (Table 6.5).

Modification of DEMs also aimed at evaluating possibilities to improve surface representation in photogrammetry-based data (step 3 in Fig. 6.1) in order to establish improved sediment budget models from this type of data only. Improved agreement with reference data and reduced deviations between the *alluvial* unit budgets of photogrammetry-based and ALS-based models show that photogrammetry-based budget quantification was improved

by modifications in this area. Similarly, the comparison of *rill* unit budgets in the modified photogrammetry-based models with the budgets from TLS data indicates improved budget quantification in rill areas, especially for photogrammetry-based models with 0.5 m data spacing.

Although budget model 5 allowed an improved sediment budget for the 'Hühnerwasser' catchment for November 2005 to spring 2009, the model still includes uncertainty and errors indicated by implausible budget quantification: Mass increase is simulated in the rill areas, and mass decrease is indicated in the alluvial area. It cannot be determined if mass decrease in the models alluvial area is due to inaccuracy in surface elevations or to the limited delineation of the area.

Additional factors might influence the quality of the budget quantification. First, photogrammetry - based DEMs were referenced using d-GPS data recorded at dates different to those of DEM acquisition. Reference points considered as unstable were eliminated; however, it cannot be excluded that the remaining points have been lowered by diffusive erosion processes or subsidence. This is of special importance for the photogrammetry-based model for 11/05, which might influence all the sediment budgets evaluated in this study. Maps of shifts in elevation resulting from the referencing of the 11/05 DEM (see Appendix A.1) show that large areas of the DEM were shifted towards lower elevations. Assuming that elevations are underestimated as a result of referencing, the amount of surface lowering and thus the negative component of the sediment budgets for the overall study period would be underestimated in the models of change. Second, sedimentation in the pond was extrapolated from measurements in summer 2008 (Kleeberg et al., 2010), so that only a range for pond sedimentation until spring 2009 can be included in sediment budgeting. Sediment budgets were determined for the fenced monitoring area (90 % of the total surface area), for which undisturbed surface development is ensured. Although areas outside of the fence have shown to be relatively stable, the transport of material into the monitoring area needs to be considered. Multi-source surface models were constructed from datasets recorded at differing dates between April and June 2009. Although no considerable erosion events were noticed in field observations, it cannot be excluded that surface morphology had slightly changed during this period. It further is to be considered that vegetation cover characteristics can differ between the dates of DEM recording. Visual assessment of surface models constructed by combining different datasets did not show any remarkable 'steps' or breaks in elevation as a result of the merging of datasets. Third, the catchment is not a closed system regarding sediment balance as assumed. Wind erosion or aeolian deposition are likely to have occurred during the very early phases of development (Maurer and Gerke, 2008). Furthermore, the catchment is located on top of a not fully consolidated mine spoil massive, so that surface lowering resulting from subsidence of the underlying material cannot

be excluded. Fourth, for sediment budgets in this study, mass change was calculated from models of change because the 3D-models aim at the quantification of overall catchment sediment budgets, which integrate artificially and naturally deposited sediments of considerably differing bulk density. Deriving mass change from volume change allowed to add the amount of sediment deposited in the pond to the overall budget, for which Kleeberg et al. (2010) determined a mean bulk density of 1.91 t m^{-3}. Uncertainty in the spatially interpolated distribution of soil bulk density used to calculate mass change is another source of error in the quantification of sediment budgets, especially in areas distant to the bulk density sampling points where interpolated values are highly uncertain. As interpolation of bulk densities resulted in similar values of around the mean of sampled values (1.47 t m^{-3}) in the areas distant to the sampling point, we do not expect that interpolating bulk densities falsely causes spatial differences in calculated mass change when change for larger areas is summed up.

Some aspects in the evaluation of surface model modification can be further explained by overlaying DEMs with aerial photographs (Fig. 6.11): (1) in segments of rill longitudinal profiles where a noticeable downslope increase in elevation appears throughout all the original datasets (Fig. 6.5), particularly narrow rills or dense vegetation cover (Fig. 6.11 a) most probably hindered the recording of the rill floor surface; (2) modifications lead to worse representation of narrow rills where the digitized stream pathway is very close to the edge of a rill in the DEM and is therefore not projected to the rill floor (Fig. 6.11 b); and (3) erroneous increase of deviations from reference data caused by modifications in the interrill area (Fig. 6.8) occurred because of dense vegetation cover (Fig. 6.11 c) recorded in all the DEMs of the time series.

Figure 6.11: Illustration of characteristic problems in DEM modification. Details are from the original TLS DEM with 0.5 m data spacing (3*superelevation), overlaid with drone-based aerial image mosaic. Locations are given in Figures 6.5 and 6.7. Black lines show original rill longitudinal profiles and cross-sections extracted from the DEM, white lines show results of modification. (a) Downslope increase of elevation in the unmodified longitudinal profile of rill 3, caused by vegetation cover around the rill area (area of detail about 40 m by 30 m); (b) reduced agreement with reference data after modification of the DEM in the rill area, resulting from the projection of the rill network polyline onto the rill wall in narrow rills (area of detail about 15 m by 20 m); (c) reduced agreement with reference data after modification of the DEM in the interrill area, caused by exceptional vegetation cover (area of detail about 20 m by 30 m).

6.5.2 Budget quantification from remotely-sensed DEMs in relation to morphology and vegetation cover

Evaluation of DEMs in this study showed that rill depth is, with few exceptions, underestimated by all methods of DEM acquisition, whereas rill width is both over- or underestimated. Our data (Fig. 6.9) show that rill depth is underestimated by up to 75 % in narrow rills in the *photo_1* surface models. In surface models from higher-resolution photogrammetry - based and TLS data, rill depth is underestimated by up to 60 % in those rills which have been closely examined. Rill width cannot satisfactorily be determined from the cross sections; however, it mainly seems to be overestimated. Similar misestimation of rill geometry in remotely-sensed DEMs has frequently been described: Evans and Lindsay (2010) determined underestimations of depths of small gullies an ALS-based DEM by up to 75 % and overestimations of width by up to 90 %. Gimenez et al. (2009) determined misestimation of gully cross section area in high-resolution photogrammetric data by up to 53 % and demonstrated that this misestimation is strongly affected by the width/depth-ratio of gullies. In photogrammetry-based DEMs, according to Gimenez et al. (2009), gullies with a width/depth ratio < 0.5 generally suffer from high inaccuracy because of shadowing effects.

In alluvial fan areas, morphology is less complex and thus more likely to be accurately depicted in DEMs. However, evaluation of DEMs in this study showed that recording of the ground surface by remote sensing methods may be severely limited by a characteristic dense cover of riparian vegetation. Further difficulties in quantification of change arise from alternating erosion-sedimentation dynamics occurring in areas of transition between rills and alluvial fans. Fewer sources of error occur in morphologically less complex, sparsely vegetated areas between rills. However, these areas account for a major fraction of the hillslope and large errors in total budgets may be caused by the summation of relatively small inaccuracies. DEMs evaluated in this study do not allow the detection of spatially continuous surface denudation in the unit *interrill_slope*, but indicate positive as well as negative values of mass change in this unit (Fig. 6.10).

Comprehensive evaluation shows that DEM quality depends on a relation between the technique of elevation data recording and morphology and vegetation cover: TLS, in our study, produced best surface models in areas with complex morphology (rill network) but quality was limited in vegetation-covered areas distant to locations of measurement or areas where vegetation is particularly dense. Although it was attempted to remove erroneous high points from TLS data, ground surface could not be well represented in these areas. Digital photogrammetry produced comparably good models for sparsely vegetation-covered areas, but did not succeed in capturing ground surface in areas with dense vegetation cover and complex morphology. Higher-resolution photogrammetry-based datasets gave better esti-

mates of rill depths for single points, however, were particularly 'noisy', i.e., general inaccuracy was very high. ALS models represented the ground surface well in vegetation-covered areas, but did not capture complex topography. Similar results are described in the study by Perroy et al. (2010), where TLS largely outperformed ALS data, but ALS performed better in deeply incised channels. Similar to our results for the interrill areas, Adams and Chandler (2002) describe stronger variations of photogrammetry-based DEMs around reference topography compared to ALS data. Results also show that, while uncertainty is only associated with morphology and vegetation cover for photogrammetry and ALS DEMs; it is furthermore dependent on the distance to the measurement points in TLS DEMs. With further evolution of a newly developing surface, as described in this study, both effects of vegetation cover and complex morphology become more important for DEM quality and thus, the possibilities of recording elevation data by photogrammetry or TLS become more limited.

DEM grid size is known to have a major influence on the registration of surface topography (Ramos et al., 2008; Thompson et al., 2001), as morphologic variation smaller than spacing of data points might not be captured in a DEM. Hancock et al. (2008) showed that even a TLS-based DEM with 0.2 m data spacing did not fully represent erosion rill morphology on a densely rilled hillslope. While some overall geomorphic descriptors were found to be relatively insensitive to DEM grid size, especially the representation of drainage networks becomes more incorrect with increasing DEM grid size (Hancock et al., 2006a; Martinez et al., 2010). Resolution of DEMs based on ALS or aerial photographs is dependent on the flying height from which data are recorded (Baltsavias, 1999; Chandler, 1999). Data spacing of the ALS and photogrammetry-based DEMs in this study was determined because ALS data and aerial photographs had originally been recorded for mine surveying purposes.

6.5.3 Region-specific modification of DEMs

In rill and alluvial fan areas, downstream increase in elevation was depressed. Generally, downstream elevation gain in rills might occur as a result of overdeepenings or bank collapse, however, it was not observed in field inspections in the study site and the analysis of d-GPS rill longitudinal profiles (e.g., Fig. 6.5). Depressing downstream elevation gain in rills causes only slight modifications in surface geometry and does not affect morphology in interrill areas, so that effects on subsequent terrain analysis are smaller as compared to other methods of modifying DEMs to represent known hydrology (Callow et al., 2007). Evaluation of modified datasets showed that enhanced use can be made of photogrammetry datasets by using lower- and higher-resolution elevation information from stereo photographs, applying the modifications in rill areas to the higher-resolution but less accurate dataset, and subsequently combining the two datasets in a single DEM.

In alluvial fan areas, a substantial modification of surface geometry was observed to result from the processing (Fig. 6.6). Evaluation of one modified DEM in this study showed improved agreement to reference data, however, it cannot be excluded that false elevation values might be introduced to the DEM by the method. Modification might thus be too extreme to allow an interpretation of absolute elevations; however, modified DEMs are improved for hydrological modelling, as 'topographic obstacles' on vegetation-covered alluvial fans are removed. In the interrill areas, a multitemporal analysis was applied to identify and replace erroneous elevation data. As we compared each processed DEM to four other elevation models, it can reasonably be assumed that errors can well be identified. However, the method requires a high amount of input data, and the modification procedure cannot be applied for DEMs recorded at both ends of a time series without additional assumptions. For the DEM analysed in this study, errors which most probably resulted from the capturing of vegetation were reduced by applying the modifications. It can be assumed that the method will reduce this type of error whenever a DEM recorded during the vegetation period can be combined with other DEMs recorded at times of less dense vegetation cover.

6.5.4 Interpretation of rates of change from the improved budget model

For the period between 11/2005 and 05/2009, an erosion rate of 1370 t of sediment in rills that are covering an area of 3497 m^2 was calculated using modified TLS-based data (Table 6.7, budget model 3a). This corresponds to an erosion rate of 392 kg per m^2 rill area in 3 ½ years. Sedimentation of 1061 t of material in alluvial fans from 11/2005 to 04/2009 was derived using ALS based data (Table 6.7, model *ALS*). Adding an estimated minimum of 2445 t of pond sediments (cf., Kleeberg et al. (2010)), and assuming that all the material eroded in the catchment area was transported to either the alluvial fans or the pond, an erosion rate of 21.8 kg per year and m^2 related to the monitoring area (46536 m^2, excluding the pond and alluvial areas) can be obtained. This rate derived from the 3D-budget model is considerably higher than the erosion rate of 13.9 kg m^{-2} a^{-1} derived by Kleeberg et al. (2010) based on sediment deposited in the pond. Although budget quantification from 3D models is uncertain, this considerable difference demonstrates the importance of including intermediate storage of sediments, e.g., in alluvial fans, to sediment budgets, as it has also been concluded in studies for larger catchments (Notebaert et al., 2009; Otto et al., 2009).

6.6 Conclusions

Based on the comprehensive evaluation of DEMs and budget models, it can be concluded that the quality of different types of remotely-sensed DEMs strongly depends on morphological characteristics and vegetation cover. For the comparably large and complex-structured study area, this implies that no method of remote sensing is best suited to obtain DEMs for the quantification of sediment budgets, but a hybrid DEM combining information extracted from best-performing datasets in defined landscape units can allow an improved depiction of erosion-sedimentation dynamics. For other areas, the evaluation shows the importance to choose the method of DEM recording in accordance with characteristic surface structures. The results and evaluation of DEM modification suggest that an improved understanding of specific errors in DEMs allows applying region-specific modifications to (i) diminish outliers and artefacts by logical comparison of a DEM time series and (ii) to improve surface representation in defined structural units based on basic principles of hydro-geomorphic evolution. Applying this method for DEM modification, time series of DEMs generated by automated digital photogrammetry can be improved by combining modified lower- and higher-resolution data in areas of differing morphology. Results suggest that 'noise' in DEMs created by falsely recorded elevations can be diminished and hydro-geomorphic structures of the surface can be better represented. It can therefore be assumed that also an improved suitability of the DEMs for the derivation of topographic indices or for hydrological modelling applications can be achieved. Results of the critical comparative evaluation of elevation data recorded by different methods can help to better interpret quantifications of earth surface processes using a single source of remotely sensed-data.

7 Initial hydro-geomorphic development and rill network evolution in an artificial catchment

The material presented in this Chapter is currently in press and was published online as Schneider, A., Gerke, H.H., Maurer, T., Nenov, R., (2013). Initial hydro-geomorphic development and rill network evolution in an artificial catchment. Earth Surface Processes and Landforms 38 (13), 1496-1512. doi: 10.1002/esp.3384.

Additions were made in Chapters 7.3.4, 7.4.2, 7.4.3, and 7.5.2, partly based on Schneider, A., Maurer, T. and Gerke, H.H., 2011. Aspects of initial surface development. In: M. Elmer, W. Schaaf, D. Biemelt, W. Gerwin and R.F. Hüttl (Editors), The artificial catchment 'Chicken Creek' - initial ecosystem development 2005-2010. Ecosystem Development 3, pp. 11-32. urn:nbn:de:kobv:co1-opus-23730.

7.1 Abstract

The formation of erosion rills and gullies is a critical step in land surface development, but possibilities to study initial unaffected surface development under natural conditions and with well-defined initial and boundary conditions are rare. The objective of this study was to characterize rill network development from 'point zero' in the artificially-created catchment 'Hühnerwasser'. To ensure unaffected development, the study was largely restricted to the analysis of remotely-sensed data. We analysed a series of photogrammetry-based digital elevation models for ten points in time, over a period of five years and beginning with the initial state. The evolving erosion rill network was quantitatively described based on mapping from aerial photographs. DEMs and rill network maps were combined to specifically analyze the development of morphometry for different parts of the network and to characterize energy dissipation and connectivity. The restriction to remote-sensing data did not allow for analyzing specific processes governing rill network development, nevertheless, two major development phases could be characterized. We observed a phase of growth of the rill network along with variations in drainage patterns during the first two

years of development and a subsequent phase of reduction of its area along with comparably stable patterns. Region-specific analysis of morphometry indicates that, besides effects of changing sediment characteristics and vegetation cover development, locally evolving hydro-geomorphic feedback cycles influenced this development. Results show an increasing similarity of overall statistical characteristics (e.g., drainage density) for two parts of the catchment, but a persistent influence of initial conditions on specific rill geometry. The observed development towards higher orderliness and increased connectivity is consistent with experiments and concepts on drainage network evolution across scales; however, we did not observe major influences of rill piracy and cross grading or a reduction of energy dissipation with network development.

7.2 Introduction

The formation of erosion rill or channel networks is a critical threshold in initial landform development. The regularity of drainage networks and their similarity across scales have been subject to many geomorphological studies (Horton, 1945; Schumm, 1956). Although the comparability of erosion rill and river channel evolution is limited because of differences in hydraulic characteristics (cf. Rieke-Zapp and Nearing, 2005), several studies have documented similarity between drainage networks from plot to basin and catchment scale (cf. Gómez et al., 2003). The hypothesis that drainage network formation across scales is governed by similar mechanisms is thus frequently followed (Pelletier, 2003; Raff et al., 2004). Conceptual models of drainage network evolution have been formulated, mainly inferred from mature networks based on the assumption of ergodicity. Studies of badland landscape development have contributed to this research (Faulkner, 2008; Gallart et al., 2013). Glock (1931) postulated a model of several stages of drainage network growth and subsequent contraction. Horton (1945) focused on the mechanisms of micropiracy and cross-grading modifying an initial network of parallel rills. Several models postulate headward growth of the networks, along with bifurcation at channel heads (Howard, 1971) or tributary production by lateral branching (Willgoose et al., 1991). Dunne (1980) describes network growth and addition of tributaries as a result of seepage erosion and piping. Alternative theories explain the regularity of drainage network patterns. On the one hand, there is the idea that landform development is governed by certain underlying principles. This idea is central in the concept of entropy in landscape evolution introduced by Leopold and Langbein (1962), that states that drainage networks evolve towards the most efficient structures. Rodríguez-Iturbe et al. (1992) concretized the optimality concept in global and local principles of optimal energy expenditure. On the other hand, there is the viewpoint that regularity emerges from local interactions of system components (Paik and Kumar, 2010) and that drainage

surfaces are self-forming by basic mechanisms of sediment relocation (Smith and Bretherton, 1972). The theory of self-organizing dynamic systems, which connects both ideas in stating that systems move towards greater orderliness and locally decreasing entropy as a result of interactions between components, was related to rill network formation by Favis-Mortlock (1998). As pointed out by Rodríguez-Iturbe et al. (1992), evolution of drainage networks' energy expenditure towards 'optimal conditions' is controlled by the need for effective connectivity, which relates to the coupling of runoff or sediment source areas and the corresponding sinks (Croke et al., 2005). Faulkner (2008) described a mesocale model for badland evolution, according to which changes in drainage network connectivity during different stages of development are crucial for badland drainage development. It has been demonstrated that the principles of optimal drainage networks, as well as metrics for their quantification, can be applied to natural river networks (Rinaldo et al., 1992; Rodríguez-Iturbe et al., 1992) as well as to rill networks for plot-scale experiments (Berger et al., 2010; Gómez et al., 2003; Rieke-Zapp and Nearing, 2005).

Several studies have attempted to predict the location of erosion rills or gullies based on topographic attributes, assuming constant rainfall and runoff conditions (cf. Nouwakpo and Huang, 2012). Concepts for critical lengths of overland flow have been introduced by Horton (1945) and extended to thresholds of contributing area (Desmet and Govers, 1997). Thresholds of inverse slope-area relationships have been developed mainly for assessing gully erosion in agricultural areas, but have been applied for characterizing areas of linear erosion under various conditions (Montgomery, 1994; Montgomery and Dietrich, 1989; Willgoose et al., 1991). However, spatial patterns of drainage networks are also influenced by soil properties that affect erodibility, infiltration, and flow behavior (Auzet et al., 2004; Bryan, 2000; Grayson and Blöschl, 2000). These characteristics can be highly heterogeneous in space and time, especially on surfaces that are not subject to tillage. The spatial variability of infiltration characteristics was found to be high and to affect sediment redistribution patterns especially for badlands (Yair et al., 2013). Temporal changes of infiltration characteristics affecting drainage network development were shown for post-mining landscapes by Ritter and Gardner (1993).

Research on the initiation and development of hydro-geomorphic surface structures has concentrated on conceptual approaches on the scale of river networks, one the one hand, and on experimental studies on the plot scale, on the other hand. Surface development has been studied in experimental drainage basins under laboratory conditions (Berger et al., 2010; Brunton and Bryan, 2000; Gordon et al., 2012; Pelletier, 2003) , and in reclaimed mining areas (Haigh, 1980; Nicolau, 2002; Nyssen and Vermeersch, 2010; Ritter and Gardner, 1993). Studying unaffected drainage network and ecosystem co-evolution from an initial state under natural conditions was only possible in exceptional cases of land surface devel-

opment (Bowman et al., 2011; Morisawa, 1964). Laboratory experiments can hardly simulate the complex interacting development of geomorphology, hydrology and biota (Hopp et al., 2009), while field 'experiments' can hardly reconstruct the initial state and allow only little control on boundary conditions (Kleinhans et al., 2010). The artificial hydrologic catchment 'Hühnerwasser' (or 'Chicken Creek') was created as a real world laboratory (Gerwin et al., 2009b) to close the gap between laboratory and natural-systems studies on initial ecosystem development. Here, erosion-affected development could be studied on the scale of a relatively small hydrologic catchment with well-known geometry, initial and boundary conditions; beginning with the very initial state and over a timespan of several years. The general concept of the site required avoiding any disturbance to its development, which restricted the methodological design of this study to the use of remotely-sensed data, complemented by a few ground-based measurements and field observations.

The aim of this study was to characterize and to identify characteristic phases of rill network development in the artificially-created catchment as an example for initial hydro-geomorphic landform development in temperate climate. To achieve this aim within the possibilities of the study site it was necessary

- to assess the possibilities and limitations of analyzing hydro-geomorphic development from remotely-sensed data,
- to describe erosion rill network initiation and evolution based on a time-series analyses of available aerial photographs and photogrammetry-based DEMs, and
- to examine the applicability of methods and concepts of drainage network evolution analysis on rill network evolution in the artificial catchment.

The erosion-affected development is analysed for a period of 5 years. Ten states of surface and four states of rill network development are characterized based on DEMs and aerial photographs.

7.3 Material and Methods

7.3.1 Basic elevation data and aerial photographs

The mine surveying department of Vattenfall Europe Mining (VEM) AG took aerial photographs of the catchment's surface in irregular time intervals during routine mine survey flights. Photographs were recorded at a flight altitude of about 1250 m AGL and ground resolution was about 0.16 m. VEM AG provided elevation data arranged in a 1 m by 1 m grid derived from the photographs by automated digital photogrammetry. Vertical accuracy of elevation data, determined based on flight altitude and camera parameters, was about

0.147 m. Elevation data were provided for ten specific days between November 26, 2005 and March 04, 2010 (Table 7.1). The datasets recorded in 11/2006 and 12/2008 covered only parts of the catchment. As no full insight into data processing and accuracy could be provided, example datasets were evaluated in comparison to airborne and ground-based laser scanning data (Schneider et al., 2012). On September 8, 2010, the elevation of the ground surface was recorded using ALS by MILAN Geoservice GmbH, Spremberg. Data spacing of the DEM derived from this survey was 0.25 m, and a vertical accuracy of 0.05 to 0.07 m was reported by the data providers.

For a detailed monitoring of surface structures, high resolution aerial photographs were taken from a helicopter on September 22, 2006 and June 14, 2007 and from a microdrone on July 10, 2008 and July 1, 2009. Ground resolution of the photographs was between 0.01 m and 0.03 m. Aerial image mosaics covering the monitoring area were composed after photo rectification (Veste et al., 2010). Additional point elevation data for 121 points arranged in a 20 m by 20 m grid were recorded using d-GPS on August 20, 2008, November 10, 2009, and October 28, 2010. The elevation of the rampart delineating the surface catchment area was recorded in 81 points in July 2008 and in 15 additional points along the modified part in November 2009. To assess further initial and boundary conditions, we used aerial photographs of the catchment's construction provided by VEM AG, and meteorological and hydrological monitoring data (Biemelt et al., 2011).

Table 7.1: Statistical quality criteria of elevation datasets and assignment of GPS reference data.

elevation data based on aerial photograph recorded on	d-GPS reference data recorded on	number of reference data points	RMSE [m]	ME [m]	SD_{ME} [m]
November 26, 2005	August 20, 2008	61	0.116	-0.100	0.058
May 1, 2006	August 20, 2008	61	0.148	0.123	0.083
November 3, 2006	August 20, 2008	50	0.211	-0.188	0.094
November 21, 2007	August 20, 2008	61	0.141	-0.128	0.058
April 24, 2008	August 20, 2008	61	0.145	-0.138	0.047
August 18, 2008	August 20, 2008	61	0.073	-0.048	0.055
December 4, 2008	August 20, 2008	55	0.087	-0.008	0.087
June 13, 2009	November 10, 2009	74	0.054	0.019	0.051
December 5, 2009	November 10, 2009	114	0.089	-0.035	0.084
March 4, 2010	April 22, 2010	114	0.206	-0.199	0.053
ALS DEM, September 8, 2010	October 28, 2010	123	0.040	0.035	0.020

7.3.2 Characterization of the erosion rill network

The geometry of the developing erosion rill network was digitized from the aerial photograph mosaics in ArcGIS 9.3 (ESRI Inc., Redlands, California). The main flow paths observable in rills and along alluvial fans were digitized as *polylines* and the areal extent of the rill network (along the rills' upper edges) and alluvial fans were digitized as *polygons*. We intended to only capture those rills that were subject to active erosion around each time of digitization. Densely vegetated rill segments, in which no recently exposed or deposited sediment was observable, were assumed to be 'surface-inactive' and not digitized. The boundary between erosion rills and alluvial fans was drawn along identifiable transitions, i.e., changes in geometry and sediment colour. Alluvial fans could not be digitized for 2009 because of particularly dense vegetation cover. Geometry of the rill network and alluvial fans was determined by fist calculating length L of the *polyline* segments and area of the *polygons*. The mean widths of rill and alluvial fan segments were then calculated from *polygon* areas divided by the length of *polyline* segments, assuming a rectangular shape. Values of Stream Order according to Strahler (1957) were manually assigned. Sinuosity S (Leopold et al., 1964) of the channels was determined as:

$$S = \frac{L}{\sqrt{(x_2 - x_1)^2 + (y_2 - y_1)^2}}$$

where x_1, y_1 and x_2, y_2 are the coordinates of the upstream and downstream end points of the channel, respectively. Drainage density DD (Horton, 1945) was calculated for the total catchment and defined subunits as

$$DD = \frac{\sum L_i}{A}$$

where L_i is the length of the i-th rill segment, and A is the area of the catchment or subunit.

To approximate rill depth, a differential elevation model was constructed by determining for each node i of the ALS DEM of 09/2010 the vertical difference, D_i, to the photogrammetry-based DEM of the unrilled surface in 11/2005. Using the polygon dataset of the rill network area for 2009, the minimum value inside each of the rill segment polygons was then extracted from the differential elevation model to determine the maximum depth. The accuracy of the elevation differences, σ_{diff}, was determined from the general accuracies of the photogrammetric (σ_p = 0.147 m) and ALS (σ_l = 0.07 m) input DEM following Lane et al. (2003) as:

$$\sigma_{diff} = \sqrt{{\sigma_p}^2 + {\sigma_l}^2}$$

7.3.3 DEM processing and analysis

TIN (Triangulated Irregular Network) DEMs were constructed from the point elevation data arranged in a 1 m by 1 m grid to enable DEM processing and analysis using the 3D-modelling software GOCAD Suite 2.5.2. The TIN models were confined to the surface catchment area. To evaluate the datasets, each DEM was compared with a d-GPS reference dataset recorded with a small time-lag to the elevation data. As deviations to the reference data indicated the presence of systematic errors in the photogrammetry-based elevation data (Table 7.1), the DEMs were adjusted to the corresponding reference dataset (see online supplementary material). GPS-based elevations of the rampart around the catchment area were added to those DEMs recorded after the rampart's construction. As the pond surface was not captured in the DEMs, all elevations inside the pond as delineated from aerial photographs were replaced by pond level monitoring data. To allow unobstructed flow into the pond for the application of flow-routing algorithms, rill floors and alluvial fan surfaces in the DEMs were smoothed by depressing increasing elevations along flow paths. Therefore, the digitized flow path polylines were vertically projected onto the DEMs. Elevations along the erosion rills were then extracted from the DEMs, and whenever increasing elevation in downslope directions was observed, the elevation value was replaced by the lower upslope elevation value (cf. Schneider et al., 2012).

As a measure of overall terrain roughness, the ratio R was calculated for each DEM as

$$R = \frac{A_{3D}}{A_{2D}}$$

where A_{3D} area is the total surface area integrating the areas of all elements of the TIN model, and A_{2D} is the area of the DEM. Further morphometric parameters were computed in SAGA after transferring the TIN models to gridded DEMs. Local slope, β, was calculated using the method of Zevenbergen and Thorne (1987). To describe local variation in topography, β– values were calculated from the gridded DEMs with 1 m by 1 m grid cell size; and to depict the overall slope topography, slopes were determined from gridded DEMs aggregated to a cell size of 5 m by 5 m by calculating the cell area weighted mean elevation value of the 1 m grids. To compensate for a possibly incomplete representation of the rampart delineating the catchment, a constant value of 1 m was added to the grid cells along the catchment's borderline. Depressions in the DEMs were filled using the algorithm of Wang and Liu (2006). For the derivation of surface flow paths, the contributing area (CA) of each grid cell was determined using the Multiple Flow Direction algorithm (Freeman, 1991). The Stream Power Index (SPI), which is used as a measure of the erosive power of flowing water

as determined by morphology, was calculated according to Moore et al. (1991) as

$$SPI = CA \cdot \tan\beta$$

7.3.4 Combined analysis of morphometry and rill network maps

Morphometric parameters were analysed separately for several areal units in the DEMs: Units of differing parent material (*mat_SW, mat_NE*) were defined by digitizing the areal extent of sediment dumped on the SW and NE part of the catchment from aerial photographs of the construction phase, recorded on April 23, 2005 and August 12, 2005 (Fig. 7.1a). The rill areas for each date of network mapping (*rill06-09*) were delineated based on the *polygon* sets digitized from the photographs recorded with the smallest time lag to DEM acquisition. To include the rills' upper edges, the area of the *polygons* was increased by applying a 0.5 m buffer function. The erosion- and sedimentation-dominated parts of the hillslope were delineated by connecting the starting points of the alluvial fan polygons for each date of digitization, and by merging all fan polygons and connecting the starting points for the entire study period (Fig. 7.1b). Model cells containing starting points of the actively eroding rills (*rillheads06-09*) were defined using the digitized rill network polyline. Interrill areas (*interrill06-09*) were defined by subtracting the rill units from the erosion-dominated unit. After combining the units in one gridded model in GOCAD, further subunits were delineated using Boolean Combinations. By combining the erosion rill units (*rill06-09*), we defined

- rill areas that became surface-active (*act07-09*), compared with all previous mapping dates, e.g., $act09 = rill09 \neg (rill08 \cup rill07 \cup rill06)$,
- rill areas that became inactive (*inact07-09*) compared with the previous mapping dates e.g., $inact07 = rill06 \neg (rill07 \cup rill08 \cup rill09)$, and
- rill areas that were actively eroding for one date and had been actively eroding at the previous dates (i.e., the 'core areas' of the rill network, *actall07-09*), e.g., $actall09 = rill09 \cap rill08 \cap rill07 \cap rill06$.

For analyses within rills developed in different parent material, rills on the SW and NE part were defined by intersecting units *rill06-09* and units *mat_SW* and *mat_NE* and subtracting the central erosion rill and the two branches it splits into around the trapezoidal spring area from the resulting units. Areas outside of the monitoring area were excluded from all the units. To allow the region-specific analysis in GOCAD, all parameters were transferred to the same gridded elevation model by spatially interpolating parameter values and then vertically projecting values to the grid model cells.

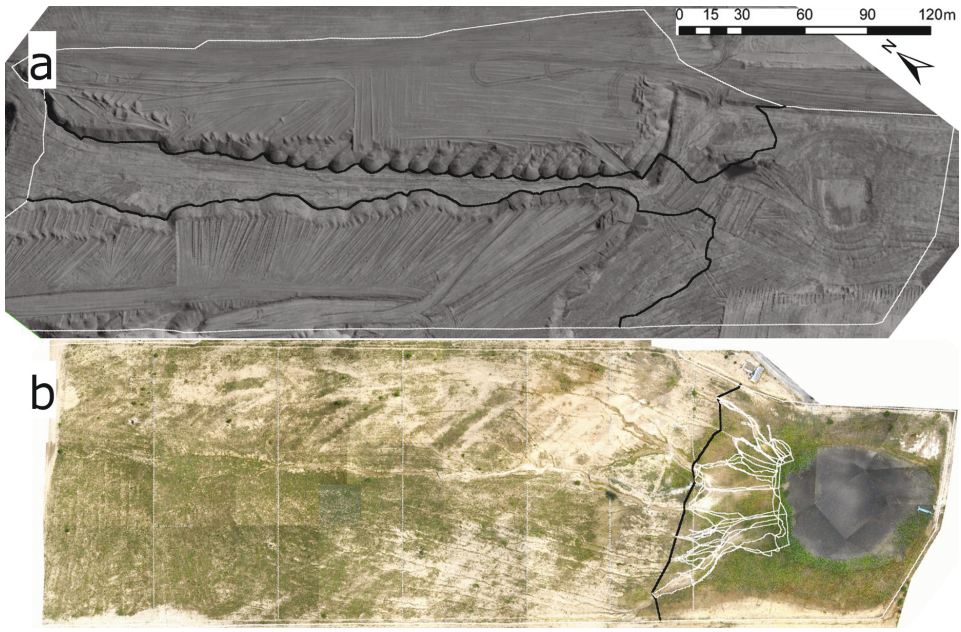

Figure 7.1: a) Delineation of model regions of differing parent material (black lines). Sediment dumped on the SW and NE part of the catchment is depicted in the aerial photograph of April 23, 2005 (© VEM AG); subsequent spreading of the sediment was digitized from other aerial photographs from the construction phase. b) boundary between erosion- and sedimentation-dominated parts of the hillslope (black line), defined based on alluvial fan areas (white lines), depicted on the aerial photograph mosaic recorded on July 1, 2009.

Energy expenditure E of the total erosion rill network and the rate of energy expenditure P_i for each rill segment, $i = 1, \ldots, n$, were calculated following Ijjász-Vásquez et al. (1993) in substituting the flow discharge in the formulation of Rodríguez-Iturbe et al. (1992) by CA and assuming a constant flow discharge as

$$E = \sum_{i=1}^{n} P_i = \sum_{i=1}^{n} {CA_{max_i}}^{0.5} \cdot L_i$$

where L is the length of segments, CA_{max} is the segments' contributing area, and n is the number of segments. To extract the parameters, the DEMs representing the surfaces in 05/2006, 11/2007, 08/2008, and 06/2009 were combined with rill network polygons digitized for 09/2006, 06/2007, 07/2008, and 07/2009, respectively. The maximum value of CA for each rill polygon (CA_{max}) was extracted from the corresponding DEM in ArcGIS to obtain and assigned to the flow paths polyline dataset to be combined with rill segment length.

The subcatchments of major erosion rills were extracted from the DEMs by determining the upslope areas of the rills' terminating points using the D8 flow routing algorithm

(O'Callaghan and Mark, 1984) in SAGA. DEMs and rill network polygons were combined as listed for the determination of energy expenditure. As a prerequisite, the elevation of DEM cells inside the mapped erosion rills needed to be lowered by 0.1 m so that DEM-based flow paths conformed to rill areas.

The GIS-based index of connectivity (*IC*) formulated by Borselli et al. (2008) to describe catchment connectivity determined by general topographic properties was computed for each DEM cell *i* as

$$IC_i = \log_{10}\left(\frac{\beta_i \sqrt{CA_i}}{\sum_{k=1}^{n_i} \frac{L_k}{\beta_k}}\right)$$

where β_i is the average slope gradient of the upslope contributing area, CA_i is the upslope contributing area, L_k is the length of the downslope flow path, and β_k is the slope gradient. The computation of *IC* values and components was restricted to the erosion-dominated area of the slope as defined in Fig. 7.1b.

To analyze the relations between initial surface morphology and the geometry of the developed rill network, parameters derived from DEMs were assigned to the rill network map of 2009. For each of the mapped rill segments, the maximum values of Contributing Area CA and the mean values of slopes determined in a 5 m grid based on the DEM of November 2005 were extracted from the grid models. The maximum elevation decrease was assigned to the rill segments based on the differential model of the DEMs for November 2005 and September 2010. Relations of initial morphology and rill geometry were analysed 1) for all the segments of the rill network, distinguishing their Stream Order, and 2) for the segments of six specific streams of the network, not including small tributaries of these streams.

7.4 Results

7.4.1 Analysis of the DEM and aerial photograph time series

Digitized flow paths and areal extent of erosion rills (Fig. 7.2) and network parameters (Table 7.2) show that in 09/2006, more rills were present on the SW part of the catchment as compared with the NE part. Erosion features not connected to the network were observed on both parts. Rill networks expanded and became denser until 2007 (Fig. 7.2b). Network development on the SW part was characterized by headward growth, by the connection of isolated segments, and by the formation of additional rills parallel to existing incisions, joining higher order segments at low angles (Fig. 7.2). On the NE part, development was predominantly characterized by the formation of additional short rill segments with higher junction angles and by increasing bifurcation, reflected in the decrease of mean segment

Table 7.2: Characteristics of the erosion rill network for four states of digitization. For the computation of sinuosity, rill segments of the same Stream Order and forming one stream were merged.

aerial photographs recorded on		rill segments (polyline dataset)			rill networt polygons		
		number (+isolated/parallel segments[a])	cumulative length [m]	mean length [m]	drainage density [km km^{-2}][c]	cumulative area [m^2]	mean width [m]
September 22, 2006	monitoring area	92(+26)	1640(+403)	17.83	38.68	2174	0.93
	SW part	58(+20)	937(+239)	16.15	62.88	622	0.69
	NE part	18(+3)	340(+91)	18.87	24.02	306	0.78
June 14, 2007	monitoring area	228(+14)	3610(+239)	15.84	72.88	2370	0.65
	SW part	118(+5)	2054(+44)	17.41	112.19	745	0.45
	NE part	94(+8)	1116(+184)	11.87	72.46	809	0.63
June 10, 2008	monitoring area	114(+24)	2172(+331)	19.05	47.39	1478	0.61
	SW part	67(+14)	1268(+142)	18.93	75.40	497	0.41
	NE part	41(+8)	655(+159)	15.98	45.37	409	0.56
July 1, 2009	monitoring area	94(+2)	1772(+31)	18.85	34.14	1232	0.71
	SW part	52(+1)	957(+4)	18.41	51.39	392	0.45
	NE part	36(+1)	574(+27)	15.93	33.50	352	0.58

aerial photographs recorded on	Stream Order	number of streams	mean sinuosity of streams	cumulative area of alluvial fan polygons [m^2]
September 22, 2006	1	44	1.047	1670
	2	11	1.023	
	3	3	1.027	
June 14, 2007	1	118	1.042	1963
	2	35	1.041	
	3	11	1.041	
	4	3	1.031	
July 10, 2008	1	61	1.047	1979
	2	15	1.042	
	3	4	1.030	
	4	1	1.021	
July 1, 2009[b]	1	52	1.054	not digitized
	2	14	1.040	
	3	3	1.054	

[a] erosion rill segments not connected to the network or parallel stream paths along network, not included in calculation of drainage density and sinuosity

[b] without alluvial fan area

[c] related to the monitoring area (52815 m^2) and its SW (18701 m^2) and NE (17941 m^2) part as defined in Fig. 7.1

length (Table 7.2). In the subsequent years, the length, number and area of actively eroding rills decreased (Table 7.2). The decrease was strongest for 1^{st} order rill segments. While branching of rills was observed in 2006, flow became more restricted to single flow paths until 2009. Rills were widest in 2006 and became narrower until 2008, while from 2008 to 2009 a slight increase in mean width was observed (Table 7.2). Generally, mean rill width was higher on the NE part. Sinuosity of higher order segments increased over time. A development towards more similarity for the two parts was observed regarding rill network total length and area, but not regarding mean length and width of rill segments. Depth of rill incision between 11/2005 and 09/2010 could be approximated from the photogrammetry- and ALS-based DEMs with an accuracy of σ_{diff} = 0.163 m (Fig. 7.3), as comparing the ALS DEM to GPS reference data affirmed the accuracy given by the data provider (Table 7.1). For the overall catchment, the mean and standard deviation of maximum rill segment depths were 0.53 m ± 0.26 m. Mean values and standard deviations for the SW and NE part (0.39 m ± 0.13 m and 0.52 m ± 0.25 m, respectively) indicate greater depths and higher variability for the NE part.

Slope maps (Fig. 7.4) and values of the 3D/2D-area-relationship *R* (Table 7.3) reflect the morphologic diversification. Maps of contributing areas *CA* and the Stream Power Index *SPI* (Fig. 7.5) show comparably strong variations in drainage patterns for the DEMs of 11/2005 to 11/2007 and indicate that drainage paths became straighter and more equally spaced across the hillslope cross-section during this phase. From November 2007 to March 2010, the patterns appear comparably stable.

Table 7.3: Development of surface roughness R for the total erosion-dominated area and for its SW and NE part.

DEM	erosion-dominated area	SW part	NE part
November 26, 2005	1.0025	1.0018	1.0024
May 1, 2006	1.0055	1.0036	1.0068
November 21, 2007	1.0022	1.0016	1.0023
April 24, 2008	1.0025	1.0019	1.0025
August 18, 2008	1.0038	1.0028	1.0038
June 13, 2009	1.0085	1.0076	1.0079
December 5, 2009	1.0044	1.0035	1.0042
March 4, 2010	1.0039	1.0029	1.0039

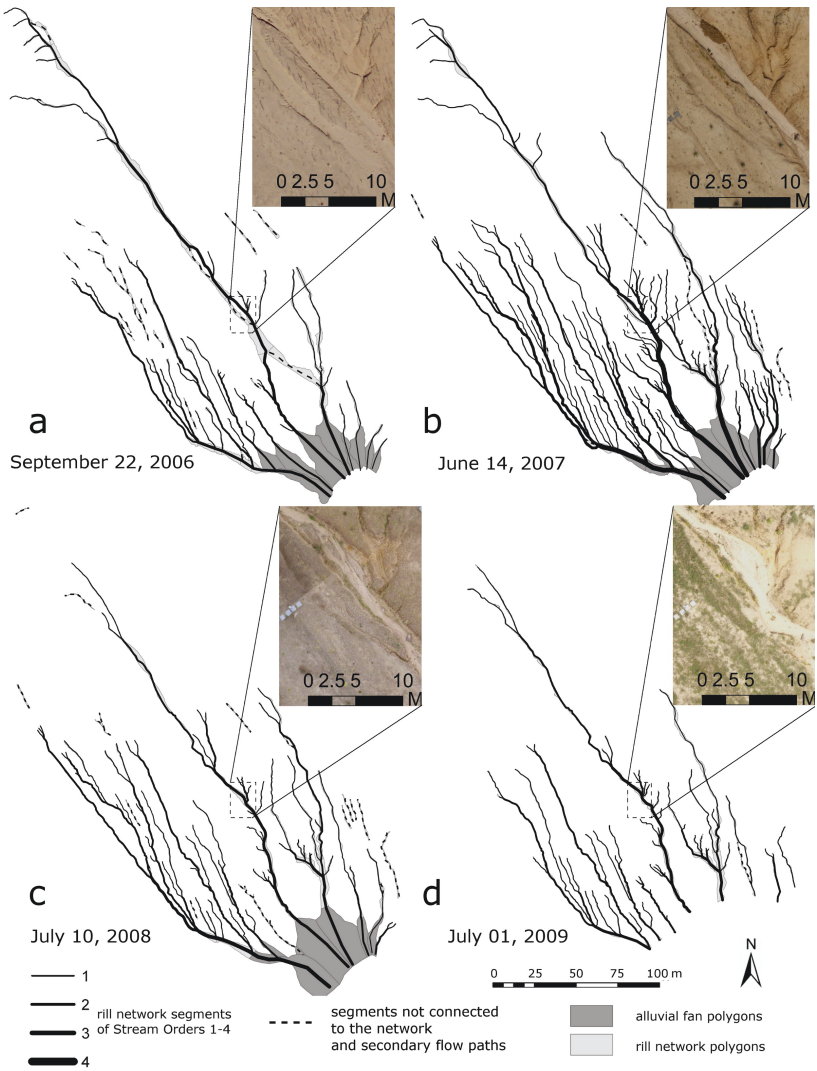

Figure 7.2: Surface flow paths (black lines) and areal extent of erosion rills and alluvial fans (grey areas) digitized from aerial photograph mosaics for a) September 2006, b) June 2007, and c) July 2008; and d) July 2009 (without alluvial fans). Enlarged details of aerial photograph mosaics show a segment of the major erosion rill.

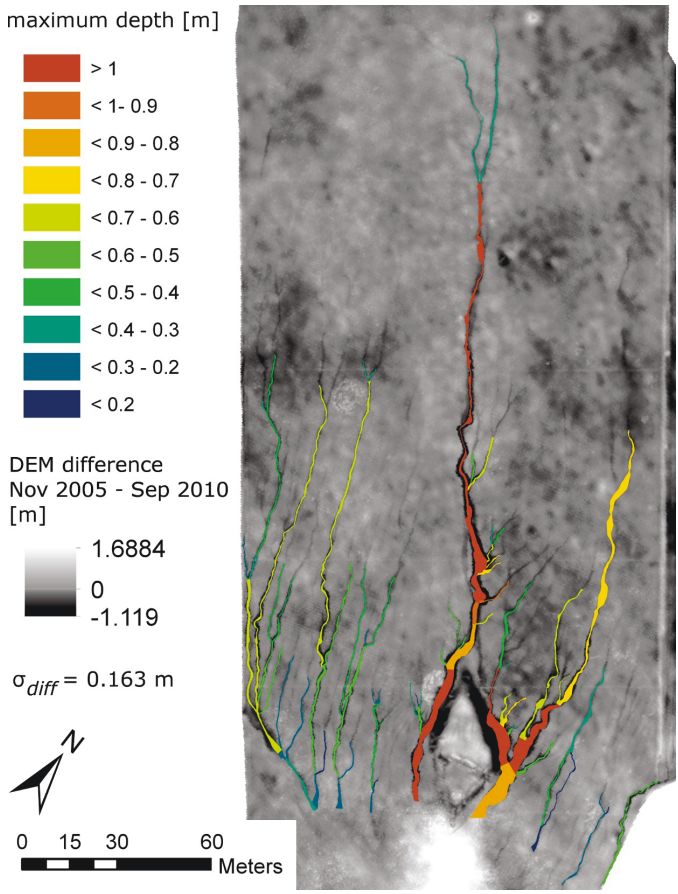

Figure 7.3: Elevation differences between a photogrammetric DEM of November 2005 and an ALS DEM of September 2010 (background), and maximum values of elevation difference inside of rill segments assigned to the rill network map of July 2009 to approximate rill depth.

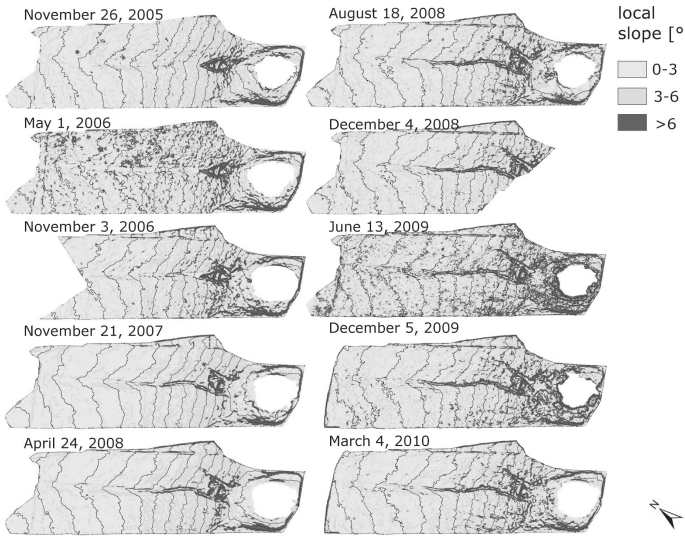

Figure 7.4: Maps of local slopes in a 1 m by 1 m grid, derived from the processed time series of ten DEMs. Overall topography is indicated by contour lines with a spacing of 1 m. Pond areas were excluded from the maps.

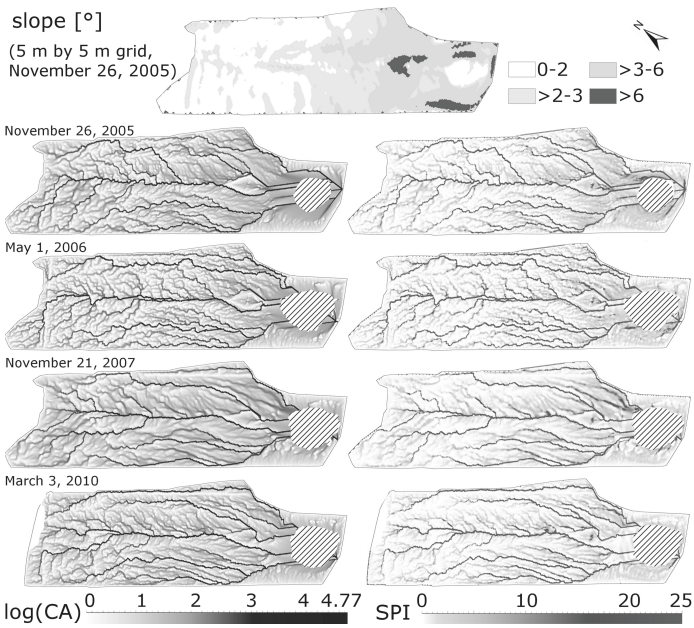

Figure 7.5: Initial overall slope, calculated from a 5 m by 5 m gridded DEM, and development of the spatial distribution of DEM cells' CA (left) and SPI (right) values for four characteristic states, based on 1 m by 1 m gridded DEMs. Dark colors indicate areas of high flow accumulation or values of the Stream Power Index. Pond surfaces indicated by the hatched areas were excluded from the maps.

Inside the actively eroding rills (units *rill06-09*, Fig. 7.6a), median values of both *CA* and *SPI* increased from 2005 to 2009, while the rill network area concurrently increased until 2007 but decreased from 2007 to 2009. Lower values of *CA* and *SPI* for 12/2009 and 03/2010 correspond to the reduction in total catchment area. A separate analysis of *CA* (Fig. 7.6b) in the SW, NE, and central part of the slope shows that rills were initiated in regions of lower *CA* in the SW as compared with the NE part. These differences became less pronounced with time. Median *CA* and *SPI* until 2009 increased in the 'core areas' of the rill network (Fig. 7.7a). This increase was highest in those areas that were actively eroding at all mapped states (*actall09*, Fig. 7.7a). Median values of *CA* in interrill areas decreased after 2008 (Fig. 7.7b). Median *SPI* values in rill areas that became 'surface-inactive' and areas that became 'active' from one to the next date of mapping (Fig. 7.7c) show that Stream Power slightly decreased in 'inactive' rills and increased before the 'activation' of rills.

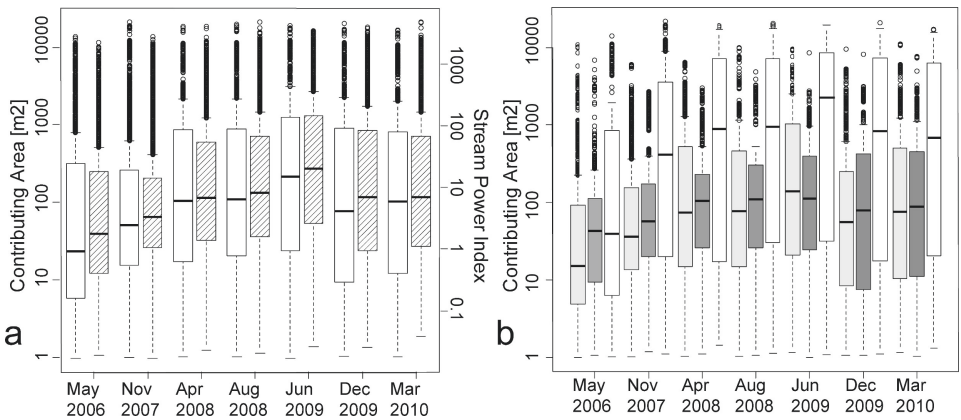

Figure 7.6: Box-Whisker plots of a) values of Contributing Area (white) and Stream Power Index (hatched) inside of actively eroding rills and b) values of Contributing Area inside of actively eroding rills in the SW (light grey), NE (dark grey) and central (white) part of the catchment.

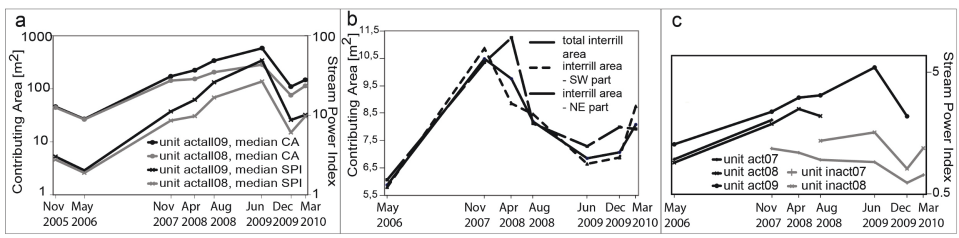

Figure 7.7: Median of values of a) Contributing Area and Stream Power Index in areas that were actively eroding at three subsequent/ four dates of rill network digitization ('core areas' of erosion rills) from November 2005 to March 2010; b) Contributing Area in interrill areas from May 2006 to March 2010; and c) Stream Power Index in rills that became 'surface-active' or 'surface-inactive' before and around the time of activation and around and after the time of deactivation, respectively.

Changes in the size and shape of rills' subcatchments were observed until 2007 (Fig. 7.8) and patterns remained comparably stable afterwards. Changes are noticeable for subcatchment 8 (Fig. 7.8), in which several rill segments were newly formed in 2007 and became inactive in the subsequent years. An analysis of *CA* (Fig. 7.9) suggests that surface flow paths from the adjacent subcatchment on the western side were redirected to subcatchment 8 between 2006 and 2007. From 2007 to 2009, high values of *CA* became increasingly concentrated in areas further downslope (Fig. 7.9).

The development of energy expenditure *E* is largely governed by rill length, both for the total network (Table 7.4) and for single segments (Fig. 7.10). A spatial organization of energy dissipation through the network is indicated in the maps of rill segments' rates of energy expenditure, *P*: especially in 2007, low rates occurred over all parts of the hillslope and rill network (Fig. 7.10b), while in 2009, low rates were concentrated to tributaries of the main erosion rills (Fig. 7.10d). The maps of *IC* values for 11/2005 and 06/2009 (Fig. 7.11) indicate increased connectivity in the lower parts of the slope for the 2009 DEM. Connectivity increased from 2005 to 2007 and only slightly varied with further development (Fig. 7.12). Smaller means of *IC* values for 12/2009 and 03/2010 might result from the reduction of the catchment area in autumn 2009. Variability of *IC* values decreased over time (Fig. 7.12), indicating a decreasing spatial differentiation.

Table 7.4: Development of relative energy expenditure and drainage density of the rill network. Values of the first stage of development are set to 1.

CA values extracted from DEM of	rill network digitized from aerial photograph of	relative energy expenditure	relative drainage density
May 1, 2006	Sep 22, 2006	1	1
November 21, 2007	Jun 14, 2007	1.36	1.88
August 18, 2008	Jul 10, 2008	1.19	1.23
June 13, 2009	Jul 1, 2009	1.02	0.88

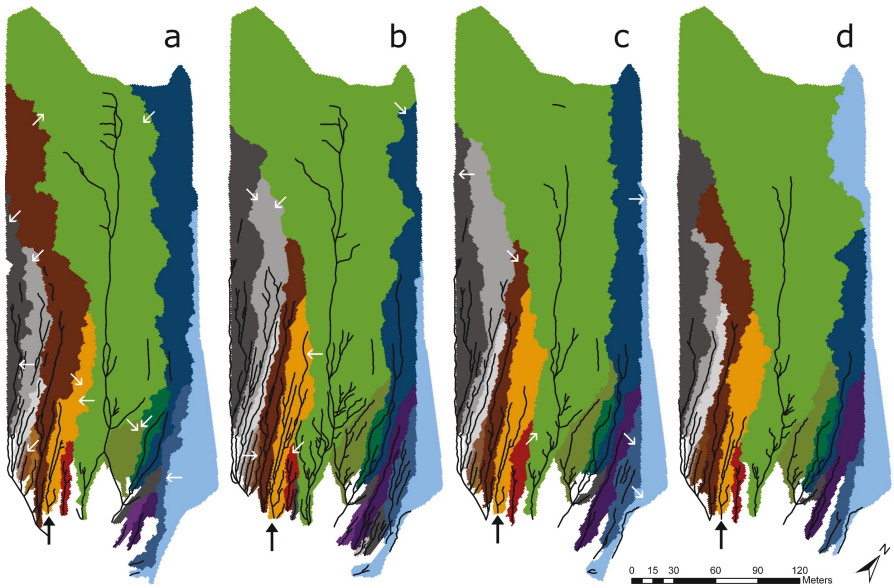

Figure 7.8: Delineation of subcatchments of major erosion rills over time, based on rill network maps and DEMs for a) Sep 06 and May 06, b) Jun 07 and Nov 07, c) Jul 08 and Aug 08, and d) Jul 09 and Jun 09, respectively. White arrows mark areas where piracy, as compared with the next stage of development, is indicated. The black arrow marks subcatchment 8, which is shown in more detail in Figure 7.9.

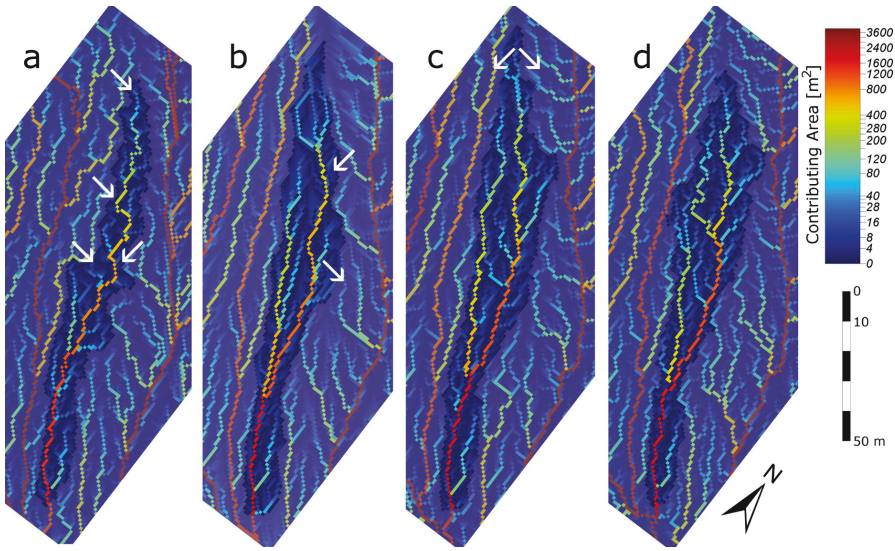

Figure 7.9: Distribution of DEM cell values of Contributing Area inside of subcatchment 8 (Figure 7.8) over time. Grid cell size is 1 m by 1 m, delineation and CA values are based on rill network maps and DEMs for a) Sep 06 and May 06, b) Jun 07 and Nov 07, c) Jul 08 and Aug 08, and d) Jul 09 and Jun 09, respectively. Areas outside of the subcatchment are faded, white arrows mark areas where piracy, as compared with the next stage of development, was observed.

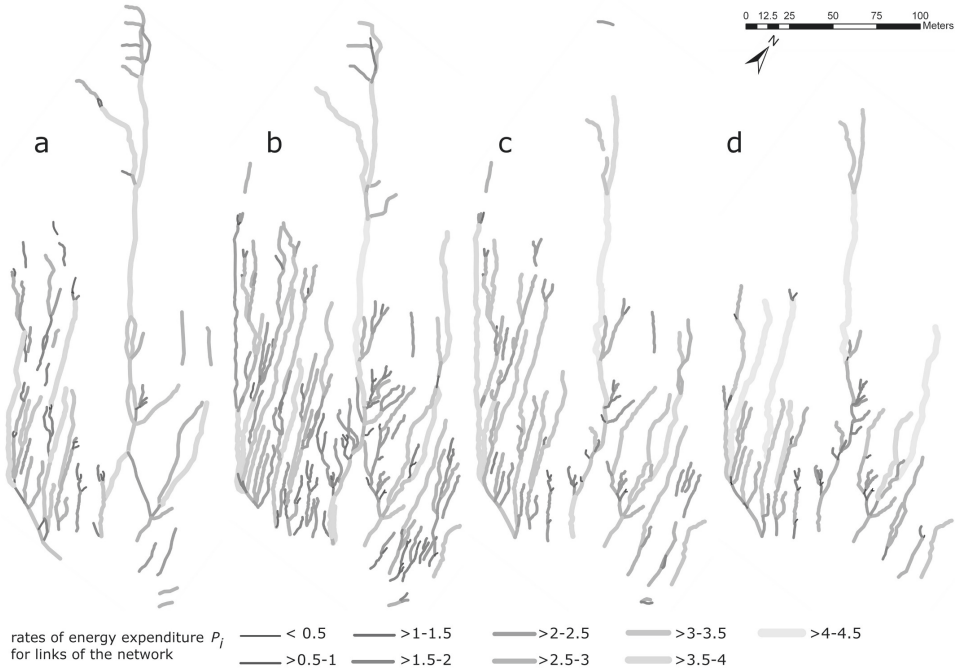

Figure 7.10: Rates of energy expenditure P_i for links of the rill network over time, computed based on rill network maps and flow accumulation from DEMs for a) Sep 06 and May 06, b) Jun 07 and Nov 07, c) Jul 08 and Aug 08, and d) Jul 09 and Jun 09, respectively.

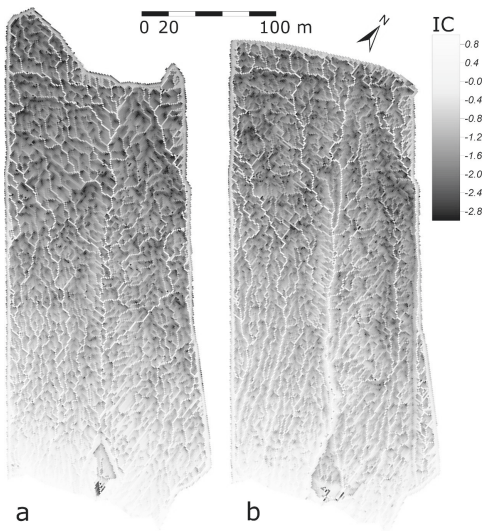

Figure 7.11: Spatial distribution of DEM cell values of the Connectivity Index IC in the erosion-dominated area (as defined in Figure 7.1b), based on DEMs for a) November 2005, and b) March 2010. Grid cell size is 1 m by 1 m. Modification of the surface catchment area in autumn 2009 results in lower IC values in b).

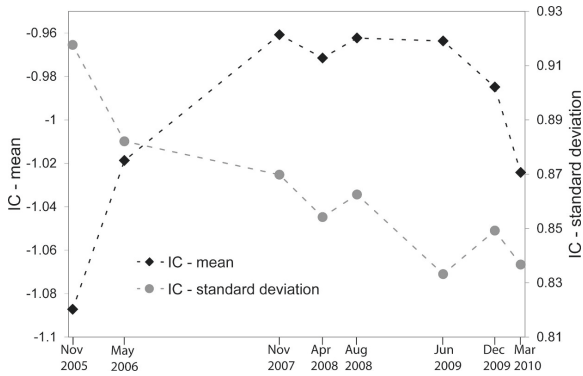

Figure 7.12: Means and standard deviations of values of the Connectivity Index IC for the erosion-dominated part of the monitoring area (as defined in Figure 7.1b) over time. Delineation of the upper catchment boundary was modified in autumn 2009, probably resulting in lower IC values in December 09 and March 10.

7.4.2 Spatially distributed elevation change from November 2005 to September 2010

The differential elevation model from the DEMs of November 2005 and September 2010 (Fig. 7.13) shows a clear concentration of high intensity erosion to the central erosion rill and its main tributaries on the NE part of the catchment. For the SW part, the model reflects high erosion in more, narrow-spaced rills. The highest amounts of alluvial sedimentation are clearly concentrated below the trapezoidal spring area. High decrease in elevation in the area outside of the monitoring area in the eastern part of the catchment, resulting from further construction works, is also observable in the model. Results of the delineation of areas with elevation change above a minimum level of detection defined with a confidence limit of 68 % show that the inaccuracy of the input DEMs limits the significant detection of change to the major erosion rills and the alluvial fan below the trapezoidal spring area.

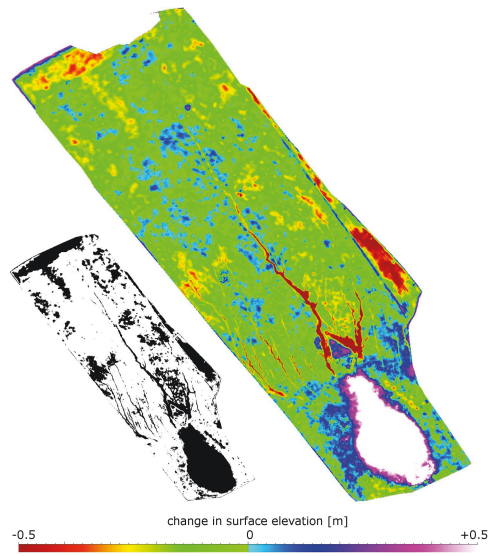

Figure 7.13: Differences in surface elevation between the DEMs of September 8, 2010 and November 26, 2005. Negative indicate erosion, positive values show deposition. The small map shows areas of elevation change above the minimum level of detection. The pond area needs to be excluded from interpretation.

7.4.3 Relations of initial morphometry and rill geometry

Fig. 7.14 shows plots of contributing area versus local slope angle for three stages of rill network development, distinguishing DEM cells in rills, interrill areas and at rill heads in the erosion-dominated area and its SW and NE part. For the newly developed rill network (May 2006, Fig. 7.8a) no difference in the area/slope-relationships of rill and interrill cells is observable, while in the plots for later stages of development (November 2007, Fig. 7.8a b, and June 2009, Fig. 7.8a c) model cells of the unit rill form a group with higher slope angles and/or higher values of flow accumulation. In the earlier stage of rill network evolution (November 2007), rills cells show higher values of CA and more distinct differences in the slope-area relationships to interrill cells in the NE compared with the SW part of the catchment. For the later stage of surface evolution (June 2009), differences between the SW and NE part are less clear. Weak inverse relationships of area and slope are observable for rill head cells in the eastern part of the catchment in the models for November 2007 and June 2009.

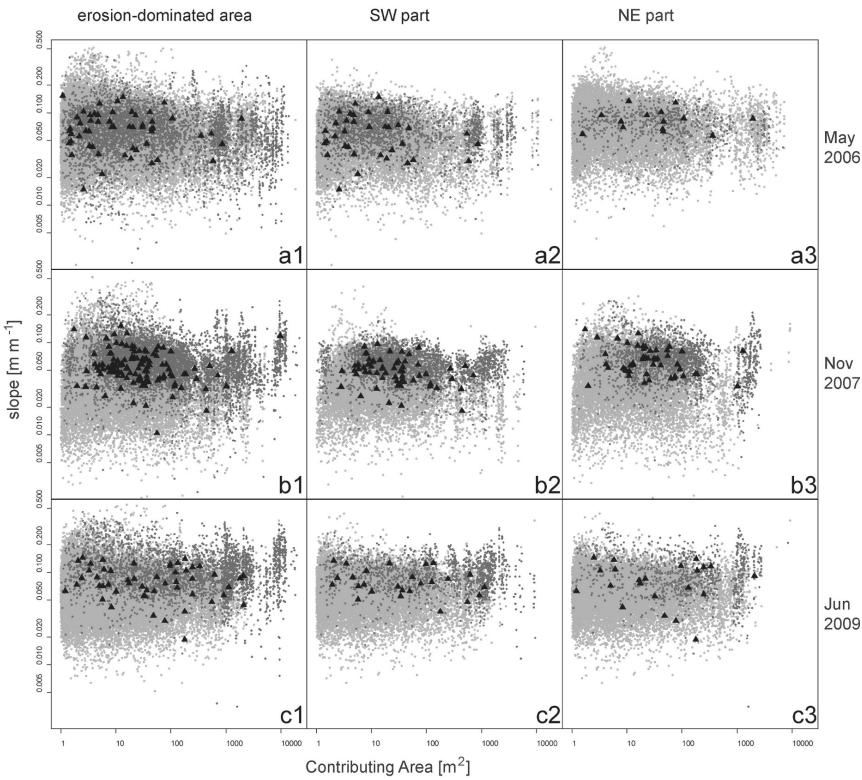

Figure 7.14: Plots of local contributing area and slopes in model cells (1 m² in size) classified as interrill areas (light grey dots), actively eroding rills (dark grey dots), and rill heads (black triangles). Model cells were analysed separately for 1) the overall erosion-dominated area, 2) the SW, and 3) the NE part of the catchment. Plots are depicted for states of surface development in a) May 2006, b) November 2007, and c) June 2009.

Maps of the mean slopes of the initial surface and the highest values of elevation decrease in the period between 2005 and 2010 within the segments of the rill network as mapped for 2009 (Fig. 7.15) indicate that highest-intensity erosion occurred in the steeper footslope area, but also in the upslope parts of the central erosion rill. For rill segments of higher stream orders, higher rill widths for areas of higher initial slope are suggested (Fig. 7.16 a1). However, no increase in rill depth with increasing initial slope was observed (Fig. 7.16 a3). For the central erosion rill and the major erosion rill on the northeastern part of the catchment, rill depth and width are higher for segments with steeper initial slopes, however this relationship is not observable for the rills on the southwestern part of the catchment (Fig. 7.16 b1 and b3). Similarly, rill width is higher with increasing contributing area for rill segments of second and third order streams (Fig. 7.16 a2). There is a distinct increase of rill width with contributing area for the major erosion rill on the northwestern part of the catchment, while the other rills analysed here do not show clear tends in the relation between contributing area and rill width (Fig. 7.16 b2). No clear increase of rill segments' depth with increasing contributing area could be shown (Fig. 7.16 a4 and b4).

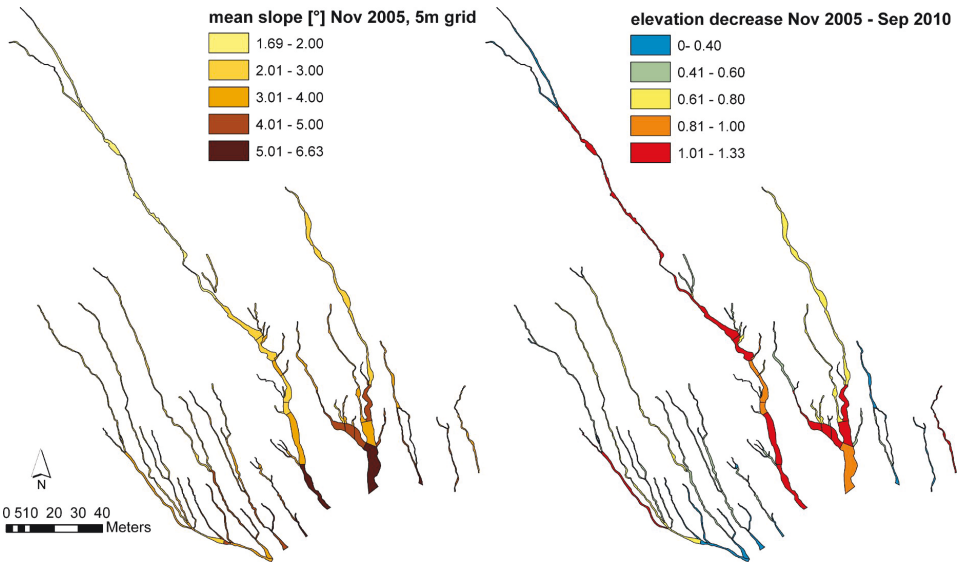

Figure 7.15: Mean values of slope angles calculated of a 5 m grid DEM for November 2005 and maximum values of elevation decrease between the DEMs of November 2005 and September 2010 for 89 segments of the rill network as mapped for July 2009.

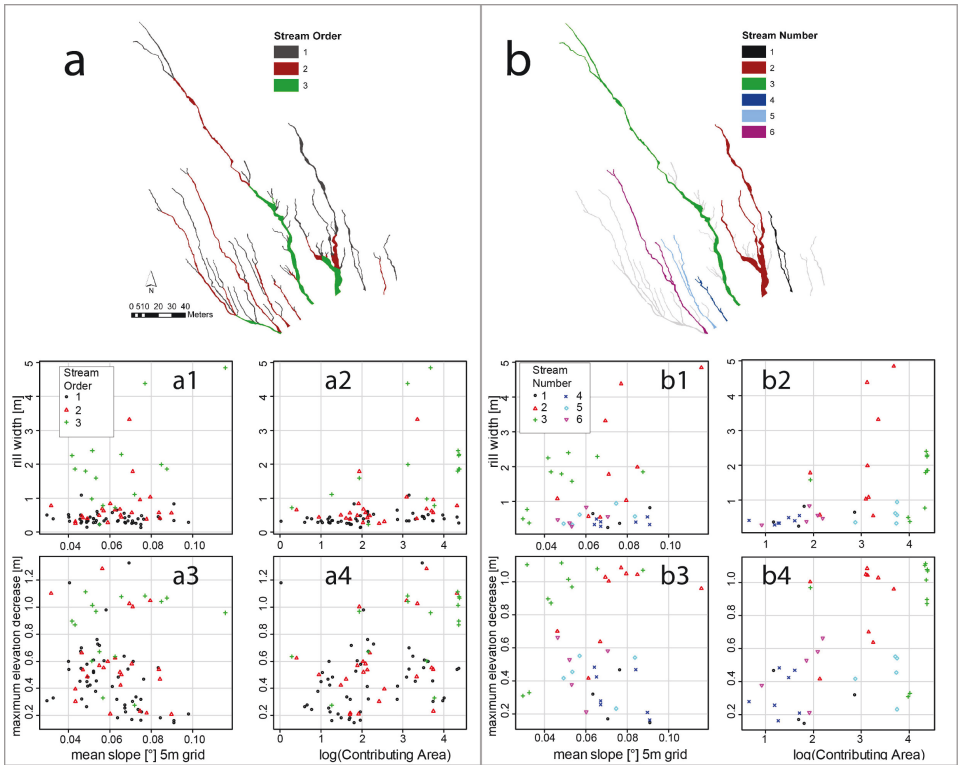

Figure 7.16: Relations of initial surface morphology and rill segment geometry in 2009 for a) stream segments of different stream order and b) stream segments of specific erosion rills: Relations of rill width to initial mean slope, calculated from the 5m grid DEM for November 2005 (a1, b1), and to initial contributing areas, calculated from the 1m grid DEM for November 2005 (a2, b2); relations of rill depth to initial mean slope (a3, b3) and initial contributing areas (a4, b4).

7.5 Discussion

7.5.1 Limitations due to database uncertainty and the artificial catchment study concept

Limitations arising from database uncertainty need to be considered in the interpretation of the results. The aerial photograph mosaics used for mapping the rill network were rectified using ground control points arranged in a 40 m grid (2006-2007) or in a 20 m grid (2008-2009), but were not differentially rectified for topography, i.e., they are no orthophotographs. Maximal offsets of 0.5 m between digitized structures, comparing photographs of the four dates, were observed. Mapping those rills for which evidence of active erosion was confirmed in aerial photographs might limit comparability to studies that assess rill net-

works based on morphology only; however, it allows a characterization of the dynamics of network development. Vertical accuracy and horizontal resolution of the DEMs is comparably low in relation to the dimensions of the morphologic structures, so that smaller features (e.g., erosion rills of less than 1 m width) are not fully represented. Systematic elevation errors and artifacts might propagate to morphometric parameters. Generally, surface recording is more likely to be imprecise in areas of dense vegetation cover or complex topography (Lane et al., 2000), which was confirmed for DEMs of the artificial catchment (Schneider et al., 2012). Local slope is highly sensitive to DEM artifacts (Wise, 1998). Topographic indices based on flow routing algorithms (i.e., in this study, *CA*, distances of overland flow, and *SPI*) can be expected to be sensitive to artifacts for areas of few pixels, but less sensitive for larger areas (Wise, 2000). Similar data spacing and uncertainty (Table 7.1) for the DEMs allowed for comparing morphometric parameters over time. The vertical accuracy of the photogrammetry-based elevation data did not allow a quantification of elevation changes for short time intervals (Schneider et al., 2012), so that the development of rill depth was approximated for 09/2010 only, using the additional ALS-based DEM. The analyses of network development were therefore based on the rill network planform geometry. Uncertainty in the results of region-specific analyses of morphometric parameters, the delineation of subcatchments, and the calculation of energy expenditure emerges from the time-lag between data acquisition for DEMs and photographs (see Table 7.1) and from the combination of all morphometric parameters in one grid model by projection. Furthermore, the study was limited by the temporal resolution of DEM and photograph time series, which did not allow considering specific runoff events, the magnitude of rainfall events, or seasonal dynamics of geomorphic processes. Seasonal dynamics were described as relevant for badland drainage network development in semi-arid climate by Desir and Marin (2007).

This study attempted to characterize surface development based on available monitoring data, which had been recorded by remote-sensing methods to avoid any disturbance to ecosystem development. This concept allows for analyzing unaffected drainage network development, which otherwise can hardly be ensured because erosion processes and rill network dynamics can be considerably influenced by interferences of humans or large animals (Bryan, 2000; Marzolff et al., 2011). However, specific processes that govern the evolution of the rill system such as infiltration patterns and runoff generation could not adequately be considered because ground-based information on spatially distributed substrate hydraulic and mechanical characteristics was limited. An initial grid-based sampling provided information on the overall spatial distribution of substrate characteristics (Fig. 3.1d). However, detailed studies on specific sampling points in the catchment showed higher substrate heterogeneity that affected hydraulic behavior at a smaller scale (Badorreck et al., 2012), and it is to be expected that substrate hydraulic behavior changed over time with developing

soil crust cover (Biemelt et al., 2011; Spröte et al., 2010). The fact that the study site was constructed as a closed catchment draining into a pond allowed for spatial interaction effects between erosion and deposition, which can be relevant for rill network development (Stroosnijder, 2005). However, it implied that water and sediment discharge could not be quantified at one single outlet and related to flow hydraulics or sediment transport in rills. Govers et al. (2007) and Wirtz et al. (2010) stress interactions of flow hydraulics and sediment transport in rills that limited the description of rill erosion by basic morphometric parameters. Aerial photographs and field observations of the Hühnerwasser catchment did not show any visible indication of subsurface erosion; however, this process might be important for drainage network development for other sites (Bryan and Jones, 1997).

7.5.2 Relations between initial morphology and rill network development

A comparison of aerial photographs and DEMs of the construction phase and initial surface with the DEM time series and rill network maps suggests major influences of initial topography on rill network development. The intended concentration of flow in the center of the catchment and the dams constructed around the trapezoidal spring area (Fig. 7.5) caused the rapid incision of the central erosion rill and its splitting into two branches. Major rills are oriented along the main slope direction, and drainage density was highest in the steepest slope area for all stages of network evolution. A comparison of *SPI* maps and the rill networks (Figs 7.5 and 7.2) shows that the *SPI* is a relatively good predictor of areas susceptible to rill formation in areas with an overall slope of > 2°. This aligns with the statement that persistent rilling requires slopes >2 - 3° (Savat and De Ploey, 1982). The relatively good agreement of rill network maps with *CA* and *SPI* patterns in the NE part of the catchment can be interpreted as an indication of a dominant influence of initial surface morphology on rill formation. In the SW part of the slope, rill spacing is closer and rills are straighter than suggested by the *SPI* patterns. These discrepancies and the differences in drainage density between the SW and the NE part (Table 7.2) show that the location of rills cannot fully be explained by the initial overall topography depicted in the DEMs. The comparison of rill network maps with the aerial photograph of the initial surface (Figs. 7.17, 7.2 and 3.2b) suggests that smaller-scale surface irregularities remaining after construction might have affected rill initiation. Especially in the SW part, machinery-created surface structures parallel to the main slope direction (see Fig. 3.2b) are similar to the pattern of the developed rill network (see Fig. 7.2) . Here, comparable to tillage patterns that have been shown to influence runoff and erosion (Takken et al., 2001), the structures might have acted as preferential flow paths, concentrating surface runoff along parallel drainage lines and thus increasing flow concentration per cross-sectional length as compared with the less-structured surface on the NE part.

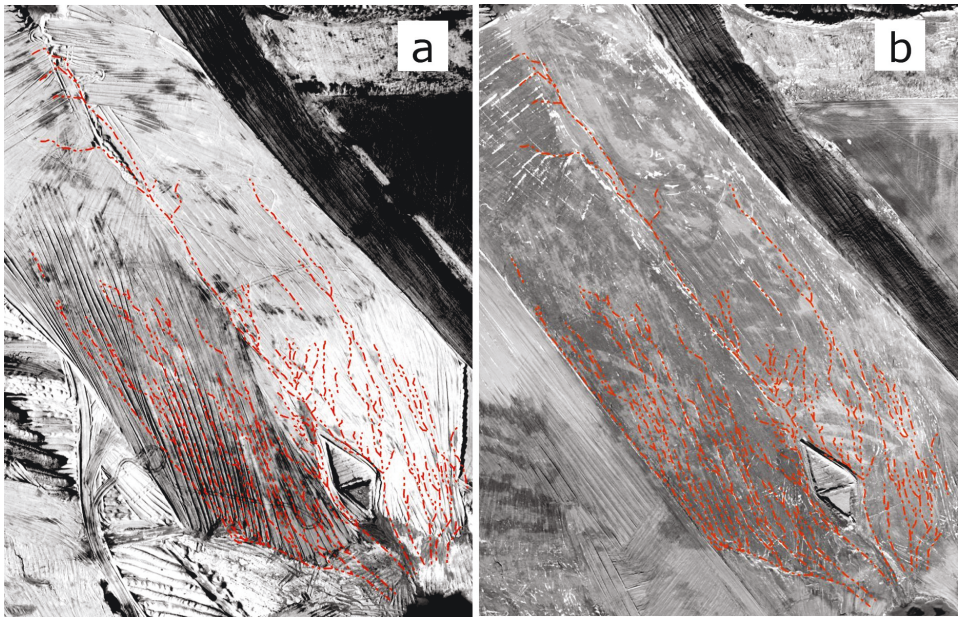

Figure 7.17: The rill network as mapped from aerial photographs of June 14th, 2007 (orange) in comparison to aerial photographs of the construction phase. a) aerial photograph taken on August 12th, 2005, before final flattening shows bulldozer tracks on the surface b) aerial photograph taken on November 26th, 2005 after final leveling of surface shows remaining small-scale structures (e.g., tracks from tractor wheels).

No differences in area-slope relationships of rill and interrill cells and no inverse relationships between CA and slope for initiation points of rills were found for the first stage of surface evolution (Fig. 7.14). In later stages of development, an increasing differentiation of area-slope-relationships of rill and interrill cells was observable. Correlations of local slope and CA for the initial surface to erosion intensity and rill width (Fig. 7.16) were only suggested for central rill and the major rill on the NE part, and no clear relations of initial slope or CA to rill depth were found. Correlations of initial morphometry and rill geometry were not analysed statistically because of the different statistical distributions of the variables. The fact that the erosion rills could not be delineated based on threshold values of morphometric indices suggests that rill incision to a high extent is influenced by other factors that overall morphology. Results also show that a differentiation of area-slope relationships increases as a result of slope-forming processes and rill incision. These interpretations area similarly described by Hancock and Evans (2006), who state that plotting gully position and measuring its features is indicative of the gully status at the time of measurement and not of conditions for the time when gully development started; and that the absence of a critical slope or drainage area for the commencement of gullies demonstrates that other factors than slope and area influence gully development. The fact that relations between morphom-

etry of the initial surface and the width and depth of erosion rills was only observed for the major rills, but not for smaller incisions further affirms that development of the geometry was not exclusively controlled by initial morphology.

7.5.3 Rill network development in relation to sediment characteristics, precipitation and vegetation cover

Further observations on rill network development are discussed by inferring to hydro-geomorphic processes from characteristic patterns in the aerial photographs, supplemented by field observations and by a comparison with results from other studies. Several observations suggest an influence of spatially and temporally varying infiltration characteristics and dominant runoff processes: Results show that on the SW part, rill incision commenced in areas with lower flow accumulation and progressed more rapidly (Fig. 7.6) and that isolated segments became connected to the network earlier (Fig. 7.2) as compared with the NE part. This might be due to differing sediment properties, e.g. to higher infiltration on the sandier substrates (Fig. 3.2a and 3.2d, Gerwin et al., 2009b) or to higher spatial variability of sediment properties. For the NE part, vegetation and moisture patterns in aerial photographs (e.g. Fig. 7.1b) and local patterns of soil crust development (Biemelt et al., 2011) indicate structures of heterogeneity arranged perpendicular to the main slope direction. These patterns are most likely related to the dumping of material in spoil ridges which causes sediment sorting and spatially varying compaction (Maurer et al., 2011b). The structures may have caused alternating flow generation and infiltration and have reduced the continuity of surface flow and rill incision, as described for badland slopes (Kuhn and Yair, 2004; Yair et al., 2013). Furthermore, the comparably high variations in the widths of single rills observed for the first two years of development (Fig. 7.2) might be related to spatially varying infiltration characteristics or sediment erodibility. The formation of narrower rills on the SW part could be influenced by the higher silt and clay content, as described by Bryan (2000).

Erosion rills were initiated both at the lower slope area and as isolated rill segments in areas further upslope (Fig. 7.2a). Aerial photographs show fan-like structures at the segments' downslope ends, indicating that termination of linear incision resulted from the diverging of runoff after short distances of local flow concentration, as described by Dunne (1980). Isolated rill segments could also have resulted from the infiltration of runoff in areas of differing sediment properties. Rill initiation along isolated segments and a subsequent connection (Fig. 7.2a, b) have also been described for a flume experiment with cohesive substrate by Berger et al. (2010) and for early phases of evolution of badland gullies or streams in semiarid systems (Bull, 1997; Faulkner, 2008; Leopold et al., 1964). In contrast, most laboratory experiments describe a clear dominance of headward rill growth, which can be

related to the external forcing of rill growth by base level lowering (Gordon et al., 2012). The continuity of the erosion rills in the Hühnerwasser catchment clearly increased over time, differing from observations in badland systems where increasing flow discontinuity due to feedbacks between infiltration and erosion was described (Yair et al., 2013). Increasing rill continuity could be related to progressing erosion, as described by Faulkner (2008), or to an increase in the role of saturation-excess overland flow, as suggested by Grayson and Blöschl (2000). Increases in infiltration capacity over time might also have contributed to the termination of rill network growth, as described for post-mining landscapes by Ritter and Gardner (1993). Effects of increasing groundwater levels on the surface morphology are possible in the lower-slope parts of the central erosion rill. In this area, groundwater seepage could have contributed to the development of small tributary rills and to widening of the rill during the period from 2008 to 2009. Annual precipitation was similar for 2007, 2008 and 2009, however, precipitation temporal variability differed between the years (Biemelt et al., 2011). A comparison of precipitation and runoff monitoring data with mapped rill network area (Fig. 7.18) suggests that the progress of rill formation from 2006 to 2007 could be related to meteorological conditions in autumn 2006 and in spring 2007, when high-intensity storms followed dry periods and resulted in high discharge from the pond outlet. The stabilization of lower-order channels with decreasing storminess with no change in annual rainfall was also observed in landscape evolution model simulations by Tucker and Slingerland (1997) and ascribed to reduced effective shear stress. Although a detailed mapping of vegetation cover was not attempted in this study, the distribution of vegetation cover could be visually analysed in the high-resolution aerial photographs. A distinct concentration of vegetation in the surface-inactive rills could be observed (e.g., Fig. 7.1b). Vegetation most probably contributed to the stabilization of such areas, as described by Gallart et al. (2013) and Molina et al. (2009). Stabilization of these 'deactivated' rill areas is expected to continue under the present climatic conditions.

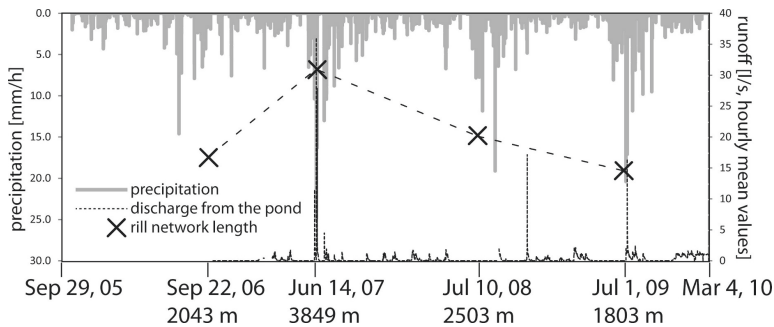

Figure 7.18: Precipitation rate (mm/h) as recorded in the catchment (Biemelt and Nenov, 2010) and the total length of the actively eroding rills (grey) as digitized from aerial photographs for four states of development.

7.5.4 Drainage network internal dynamics

From 2006 to 2008, we observed a decreasing width of most erosion rills (Table 7.2, Fig. 7.2). This can be interpreted as a result of increasing concentration of flow after the onset of rill incision, as similarly described for unvegetated bare mine spoils by Haigh (1980). For 2009, a slightly higher rill width, along with higher sinuosity of higher-order rill segments, was observed (Table 7.2), and aerial photographs indicate increased sidewall erosion and evolution towards a meandering shape of the rills. Lateral erosion was largely concentrated to those areas were tributaries are joining with the major erosion rills at relatively high angles (Figs 7.2 and 7.13), which most probably favored lateral erosion due to locally modified flow structures and kinetic energy of the flowing water. Aerial photographs (Fig. 7.2) and field observations affirmed lateral erosion along the tributary mouth and at the opposite side of the rill. Patterns seem to be consistent with the observations that morphologic effects of stream confluences increase with junction angles (Benda, 2008) and that junction angles increase with the order of the receiving stream (Lubowe, 1964). Development of rill geometry is consistent with Sidorchuk (1999), who states that depths and lengths of gullies develop more rapidly than its volume and thus width.

The separate analysis of morphometry in different parts of the rill network (Figs 7.6 and 7.7) indicates an effect of feedback cycles between runoff concentration and rill incision on rill network development. The fact that active rill erosion became concentrated to areas of higher *CA* over time (Fig. 7.6) might be a consequence of a reduced total amount of surface flow due to lower precipitation or increased infiltration. But moreover, results show that higher proportions of surface flow became accumulated in the 'core areas' of the rill network (the areas that were actively eroding at all four dates) (Fig. 7.7a), indicating that rill network development resulted in runoff concentration in these areas. *SPI* values show a higher increase as compared with *CA* values (Fig. 7.7a) because the steepening rill walls are included in the calculation of the *SPI*. Concurrently with the increasing runoff concentration in the central (Fig. 7.7a) and newly activated (Fig. 7.7c) parts of the network, we observed a decrease of flow accumulation and *SPI* in the interrill (Fig. 7.8b) and deactivated (Fig. 7.7c) parts. This runoff concentration might have contributed to the termination of network growth. The observations show the importance of integrating a dynamic representation of topography in drainage network evolution models, as suggested by Hofer et al. (2012) for the Hühnerwasser catchment. Runoff concentration in central parts of stream networks is mainly described as a consequence of rill micropiracy (Favis-Mortlock, 1998; Horton, 1945). However, we observed only slight changes in rills' subcatchments (Figs. 7.8 and 7.9). Note that changes in the easternmost areas resulted from construction works in 2006 and 2008. Mostly equally-shaped, elongated subcatchments developed (Fig. 7.8). Elongated subcatch-

ments have been related to predominant headward rill growth by Schumm (1956), but also resulted from rill initiation within the slope in experiments by Berger et al. (2010). The detailed analysis of flow accumulation in subcatchments (e.g., Fig. 7.9) indicates a slight reorganization of the subcatchments by rill piracy during the first phases of development and a subsequent concentration of overland flow to existing rills inside the subcatchments. This limited effect of piracy and cross grading might be due to the a priori concentration of flow towards the central slope area, as observed in other studies: While rill piracy and cross grading where found to considerably affect drainage network development on slopes of uniform cross-sectional profiles by Pelletier (2003), Hancock and Willgoose (2001) did not describe these mechanisms for an open-book shaped experimental slope.

We did not observe a consistent trend in the development of the rill networks energy expenditure (Fig. 7.10, Table 7.4). Contrarily, in the majority of experimental studies, decreasing values of *E* were observed (Berger et al., 2010; Rieke-Zapp and Nearing, 2005), except for a rough and moderately inclined slope described by Gómez et al. (2003), who related the increase of *E* to the dominance of diffusive sediment redistribution. The deviation between results from the artificial catchment and laboratory studies might indicate differing dynamics of network evolution under naturally varying rainfall characteristics as compared with constant rainfall as applied by Berger et al. (2010) and Rieke-Zapp and Nearing (2005). It might also be due to neglecting the rills' cross-sectional geometry and slope, since the concept of minimization of E is based on the assumption of constant flow velocity (Rodríguez-Iturbe et al., 1992). However, we observed a concentration of lower *E* rates in steeper slope areas (Fig. 7.10), along with an increasing spatial organization of rill segments' geometry towards increasing widths in downslope direction (Fig. 7.2). This evolution towards a more orderly state is consistent with the concept of evolution towards an uniform energy distribution of Leopold and Langbein (1962). The increase of mean *IC* values (Fig. 7.12) indicates that this organization involved an increase in connectivity of the flow paths at the surface. For subsurface drainage pathways, Hofer et al. (2011) inferred to a threshold-like behaviour of connectivity from a percolation theory model.

The basic hydro-geomorphic patterns of the catchment were established during the period of rill network growth until 2007 and remained comparably stable for the next years until March 2010. Such temporal stability could be observed in the development of overall rill network geometry (Fig. 7.2), flow accumulation patterns (Fig. 7.6) and the spatial distribution of rills' subcatchments (Fig. 7.8). These results confirm the importance of the very first stages of drainage network evolution as pointed out by Morisawa (1964) and Sidorchuk (1999). Regarding the parameters describing the overall rill network (e.g., cumulative length and area, drainage density, Table 7.2), the network evolution led to an increased similarity between the SW and NE part. However, differences in specific parameters (e.g., in segment

lengths and widths, Table 7.2) remained until 2009. Increasing similarity of drainage density, along with differing rates of rill incision and depth of developing rills, was also reported for experimental drainage basins with differing initial microrelief (Gómez et al., 2003) and slopes (Rieke-Zapp and Nearing, 2005). The observations also align with the common assumption that initial topographic conditions influence the exact arrangement of landform components, but have less influence on the general statistic characteristics of a landscape (Perron and Fagherazzi, 2012).

7.6 Conclusion

This study aimed at characterizing hydro-geomorphic development during the very initial ecosystem development stages based on remotely-sensed data exemplified for the 'Hühnerwasser' catchment. Based on the available DEM and aerial photograph time series, two major development phases could be reconstructed: (i) a growth of the rill network with relatively high variation in spatial patterns and (ii) a subsequent reduction of the area of actively eroding rills along with more stable spatial patterns. Agreement between flow accumulation patterns derived from DEMs, structures observable in aerial photographs of the initial surface and maps of the actually developed rill network suggests that overall initial surface morphometry and small initial surface irregularities affected for morphologic development. The combination of aerial photographs and DEMs in region-specific analyses of morphometric parameters was found useful for identifying hydro-geomorphic feedbacks during the hydro-geomorphic development.The relative stability of rill network geometry, morphologic patterns, and the spatial arrangement of sub catchments after the first phase of development suggests that dynamics during the very initial phase of surface development deserve closer attention. Despite the increasing similarity in drainage density over the catchment, the initial conditions seem to have a relative persistent influence on spatial surface morphological patterns and rill network geometry. The development of the rill network geometry and the energy dissipation suggests a spatial organization of the system towards 'greater orderliness'. The spatial patterns are accompanied by an increase in morphological connectivity, which is consistent with most studies and concepts on initial surface development across scales. However, the results do not show effects of rill piracy on network development or a reduction of total energy dissipation in the network, which might not have been captured in the spatial and temporal scale of our analysis or might be due to the specific initial morphometry of the artificial catchment.

The identification of processes and thresholds of rill evolution was limited by the relatively low resolution of the datasets in relation to the dimensions of surface structures and by a lack of ground based information. As a consequence, it was not possible to describe spa-

tial patterns of infiltration rates, runoff generating processes or sediment erodibility. Such limitations to ground-based measurements, however, are an inevitable counterpart to the advantages of the site on which unaffected initial development could be studied. To compensate for such limitations would require a more detailed characterization of sediment properties during construction and an intensive monitoring by instrumentation adapted to heterogeneity structures or by novel applications of minimal invasive techniques.

8 Simulation of sediment redistribution with the landscape evolution model CAESAR

8.1 Abstract

Because high rates of sediment redistribution and the diversification of geomorphic structures are characteristic for initial phases of landform development, the simulation of sediment redistribution for this phase requires a spatially distributed and temporally dynamic soil erosion or landscape evolution model. In this study, the application of the landscape evolution model CAESAR for simulating sediment redistribution during the initial five years of development in the Hühnerwasser catchment was assessed. The study further aimed at evaluating effects of input data resolution, initial topographic conditions and precipitation characteristics on surface development in the catchment using CAESAR simulations. The DEM of the catchment surface at the initial state of development and hourly precipitation data recorded in the catchment were used for the simulations. Maps of the developing erosion rill network, DEMs for several states of surface development, and discharge data were used for parameter calibration and validation. The effects of DEM resolution, roughness of the input DEM, and precipitation characteristics on model outputs were evaluated. Results showed that characteristic patterns of sediment redistribution could be simulated with the landscape evolution model; however, sediment discharge could not be adequately quantified. Resolution of the input DEM was found to affect the density of the simulated erosion rill network. Results affirm that initial surface roughness and technogenic irregularities have affected drainage network geometry in the catchment. Results of simulations using modified precipitation input data suggest that the low precipitation intensities during the first year and the considerably high intensities during the second year have contributed to the concentration of erosion rills in the lower slope areas and to the high density of the rill network observed in the Hühnerwasser catchment.

8.2 Introduction

A spatially distributed and temporally dynamic model with high spatial and temporal resolution is necessary to simulate sediment redistribution in the initial phase of landform development because of the high rates of sediment redistribution and the differentiation of geomorphic structures which characteristically occur in this phase. Local feedbacks between erosion and flow accumulation, in addition to initial and boundary conditions, can considerably affect drainage network development during the initial phase. A dynamical adaptation of topography during the simulation of surface development is necessary for modeling these structure-process interactions. While soil erosion models have mainly been developed for the simulation of sediment redistribution over comparably short temporal and small spatial scales, most geomorphic landform evolution models focus on longer temporal and larger spatial scales. However, most models that were developed for simulating soil erosion determine erosion rates based on one state of surface development, represented by the input datasets, and integrate erosion and discharge rates over the simulation area or over elements of the simulation area (e.g., the WEPP model (Laflen et al., 1997)). Models that simulate sediment redistribution by slope and fluvial processes often require an ex-ante specification of process domains, i.e., unchanneled areas and channels (e.g., the KINEROS2 and EUROSEM erosion models, (Smith et al., 1995)), which does not allow for the simulation of surface evolution from an initial state for that drainage structures are not yet developed. The LISEM soil erosion model (DeRoo et al., 1996) has been adapted to allow for the incision of gullies into an initial elevation model using empirical algorithms (Jetten et al., 2006). The EROSION3D model allows for a physically-based simulation of spatially and temporally resolved soil erosion and deposition and has been applied for simulation periods from single rainfall events to decades (Schob et al., 2006) and for simulation areas from experimental flumes to small watersheds (Schindewolf and Schmidt, 2012; Schmidt et al., 1999), however, dynamic adaptation of morphology for single erosion events has not been discussed for this model. Geomorphic landscape evolution models (LEMs), in contrast, use a spatially distributed representation of topography in gridded elevation models (e.g., LAPSUS (Schoorl et al., 2002), SIBERIA (Willgoose et al., 1991)) or TIN models (CHILD, (Tucker et al., 2001), CASCADE (Braun and Sambridge, 1997)) that is dynamically adapted for repeated computation cycles. LEMs are therefore able to simulate local feedbacks between runoff distribution and elevation change. However, most LEMs do not compute sediment redistribution for single rainfall and runoff events, but determine time-averaged rates of erosion and deposition (see Coulthard, 2001).

For some numerical models, applications with an emphasis on the initial phase of surface development have been described. The RillGrow model (Favis-Mortlock, 1998; Favis-

Mortlock et al., 2000) explicitly focuses on the initiation and evolution of erosion rills and the self-organized evolution of geomorphic drainage patterns, based on elevation and precipitation data. Applications have so far only been described for synthetic and experimental plot DEMs and simulation times of a few hours (Favis-Mortlock et al., 2000). The SIBERIA slope evolution model (Willgoose et al., 1991) couples models for hillslope evolution by diffusive and mass transport processes and for the development of channel networks by fluvial processes. It operates based on an input DEM, and discharge is computed for DEM cells as a function of the drainage area and several constants that need to be calibrated to conditions of the study site. Therefore, the model does not simulate specific rainfall and runoff events but longer-term landform evolution for uniform rainfall conditions (Hancock et al., 2011; Tucker and Hancock, 2010). SIBERIA has been applied in several studies on erosion-affected evolution of post-mining areas (Evans and Willgoose, 2000; Hancock et al., 2008; Willgoose and Riley, 1998), undisturbed natural catchments (Hancock et al., 2002), and an experimental catchment model (Hancock et al., 2006b), but studies have mainly focused on landform development over several thousands of years. The CAESAR landscape evolution model was developed for simulating geomorphic development of river catchments or reaches over the Holocene (Coulthard et al., 2002). It allows for simulating sediment redistribution by fluvial processes in high temporal resolution, resolving individual runoff and flood events. Applications have been described for a comparably wide range of spatial and temporal scales. Coulthard et al. (2012) describe the application of the model for the simulation of soil erosion on 30 m by 30 m experimental plots.

In this study, the application of the CAESAR model for simulating sediment redistribution and rill network formation during the initial five years of development in the artificially created catchment 'Hühnerwasser' is tested. The monitoring program and the previous analyses of hydro-geomorphic development provide a data base for model calibration and evaluation. Analyses of geomorphic development showed that drainage network development in the catchment was influenced by initial surface topography, initial sediment properties, the developing vegetation cover, precipitation characteristics, and evolving structure-process interactions within the network. These analyses gave reason to the formulation of several hypotheses to be tested using LEM simulations:

- **Small technogenic irregularities in initial topography affected the development of rill network geometry**
  The small-scale surface irregularities that remained from the construction works in the catchment acted as preferential paths for surface flow, so that convergent runoff and therefore a higher concentration of runoff to cross-sectional areas resulted for areas in that these structures occurred. The irregularities can also have affected flow routing because of a generally increased surface roughness. For a lower roughness of

the initial surface, it can be expected that unconcentrated flow dominates in larger parts of the slope, so that flow concentration thresholds for rill incision are not exceeded in these areas, resulting in a lower drainage density.

- **Erosion and sedimentation patterns established during the very initial phase of development remain through further surface development**
  The main patterns in surface runoff have developed during the first two years in the Hühnerwasser catchment and have remained relatively stable afterwards. It is hypothesized that this initiation of surface structures during the earliest development periods and the subsequent stability are not a result of the specific effects of initial and boundary conditions during these years, but that patterns formed during the initial phase persist for different initial surface structures and different meteorological influences.

- **Precipitation characteristics during the very initial phase of development affect rill network geometry**
  A considerably high temporal variability of precipitation was observed for the year 2007, i.e., in spring and summer of this year an alternation of dry periods and high-intensity precipitation events occurred. For the years 2008 and 2009, annual precipitation was similar as for 2007, but peak precipitation intensities and the variance of hourly values were lower. It is hypothesized that the intensity of those surface runoff events that occur during the initial phase of surface flow path organization is formative for the developing network of erosion rills, so that rill incision is limited to smaller areas when precipitation intensities are moderate during the first years, but a higher rill density develops when very high-intensity events occur during these first years.

The CAESAR model was chosen to approach these hypotheses because it includes a representation of dynamically evolving topography and a coupled simulation of erosion and sedimentation, which allows for simulating the effect of structure-process feedbacks; because it allows for simulations and provides output data in the appropriate spatial and temporal resolution; and because it implements the most relevant processes for the development of drainage networks on hillslopes.

The objectives of the study were

- to evaluate the suitability of the CAESAR model for the simulation of the initial phase of hydro-geomorphic development at the scale of a small hydrologic catchment;

- to assess the influence of initial surface irregularities on geomorphic development and the possibilities to integrate such structures into DEMs; and

- to assess the effects of differing precipitation characteristics during the initial development phase.

8.3 Material and Methods

8.3.1 Overview on the structure of the CAESAR model

The CAESAR landscape evolution model (Coulthard et al., 2002) simulates morphological change, flow and sediment transport for gridded elevation models. Simulations are carried out by the repeated application of local rules for hydrological, fluvial and slope processes in time steps that are adapted to the volume of sediment erosion and deposition and thus to the amount of surface runoff (Fig. 8.1.).

In this study, version 6.2m of the CAESAR model was used. An overview of the model structure and the most relevant computation steps and parameters is given in the following paragraph. Descriptions of the model are provided by Coulthard et al. (2002) and Van de Wiel et al. (2007).

In this study, the CAESAR model was used in the catchment mode, in which surface runoff is computed based on input precipitation information. Total water discharge Q_{tot} in this mode is calculated using an adaptation of TOPMODEL (Beven and Kirkby, 1979) as

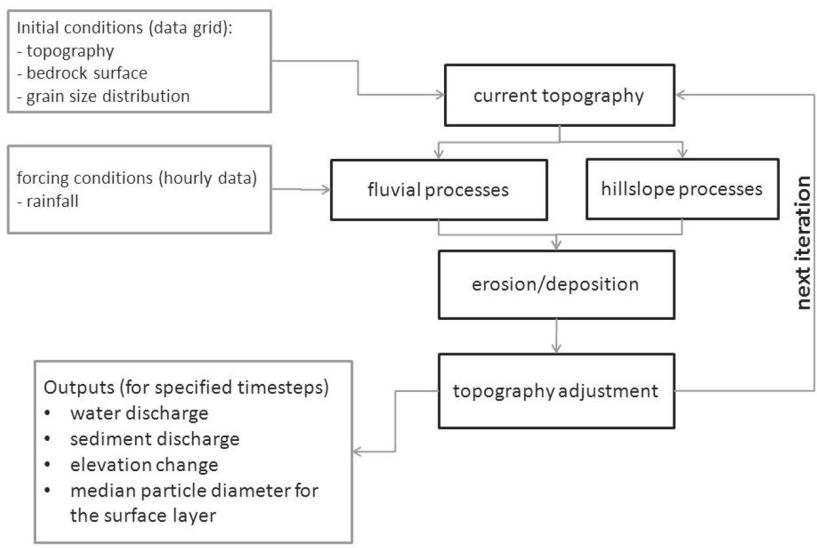

Figure 8.1: Conceptual structure of the CAESAR model and output data generated in this study. Adapted from van die Wiel et al. (2007).

$$Q_{tot} = \frac{m}{t} \log \left(\frac{(r - j_t) + j_t \exp\left(\frac{rt}{m}\right)}{r} \right)$$

where t is the time step in seconds, r is the rainfall rate in $m^{-1}\ h^{-1}$, and m is the TOPMODEL parameter that controls the rise and the fall of soil moisture store j_t. Soil moisture store for each iteration (j_t) is calculated based on the value of j_t for the previous iteration and the time step, the rainfall rate and the m parameter. A threshold value is then calculated as

$$Treshold = K \text{ß} D x$$

from substrate hydraulic conductivity K, slope $ß$, and the grid size Dx; and runoff below and above this threshold value is routed as subsurface and surface flow, respectively. A minimum discharge (*MinQ*) for the calculation of runoff depth can be specified to omit computation for very low amounts of discharge. This value is also used as a minimum value for the infiltration threshold in the CAESAR model. For this study, the *MinQ* value was not used as the minimum threshold value, but all discharge was treated as surface runoff for infiltration threshold values smaller than the *MinQ* value. The flow is then distributed over a specified range of cells in a 'scanning' algorithm, as described in Coulthard et al. (2002). Flow depths d_w are calculated based on a the surface fraction of the discharge Q, the local slope $ß$ and a Manning's coefficient n of 0.03 as

$$d_w = \left(\frac{Q\, n}{\text{ß}^{0.5}} \right)^{3/5}$$

Flow velocities U are determined from flow depth and the slope to the lower neighboring cell. The option to calculate shear stress from flow velocity was chosen in this study. Based on the source code of CAESAR version 6.2.m, shear stress τ was calculated as

$$\tau = 1000 \cdot 9.81\, n^2\, {d_w}^{-1/3}\, U^2$$

A threshold value of water depth in a cell (*wdet*) can be specified, below that the computation steps for sediment erosion and deposition are not carried out. Sediment entrainment and transport is simulated for nine specified particle size classes. In this study, the sediment transport simulation based on the Einstein-Brown equation (Einstein, 1950) was used. For this method, according to Coulthard et al. (2002), a balance between the forces moving and restraining the particles ψ is calculated in the form

$$\psi = \frac{(\rho_s - \rho)^D}{\rho\, d_w \text{ß}}$$

where ρ_s and ρ are the densities of water and the sediment (a value of 2250 kg m^{-3} is used for ρ), D is the particle size diameter in meters, and d_w is the flow depth. The dimensionless bedload transport rate ϕ is defined as

$$\phi = Qs\sqrt{\frac{\rho}{(\rho_s - \rho)gD^3}}$$

where Qs is the volumetric sediment transport rate for the time step in m^3 s^{-1}, and g is gravitational acceleration. The transport rate ϕ is related to ψ by

$$\phi = 40\left(\frac{1}{\psi}\right)^3$$

, and the equations are solved for sediment transport rates Qs. In the source code of CAESAR version 6.2m, the sediment transport rate Qs was calculated in the form of

$$Q_s = \frac{40\left(\frac{\tau/g}{(\rho_s - \rho)D}\right)^3}{\sqrt{\frac{\rho}{(\rho_s - \rho)g\,D^3}}}$$

The sediment transport rate is converted to a volume by a multiplication with the length of the time step (in seconds) and elevation decrease in a model cell affected by erosion is calculated based on this volume and on cell size (Coulthard et al., 2002). Based on a user-defined specification, particle size classes are transported either as bedload or suspended load. Bedload is deposited and re-entrained in every simulation step and distributed according to local slope by

$$V_{i,k} = \frac{ß_k}{\sum ß} V_i$$

where i and k denote the sediment fraction and the direction of the neighboring cell, respectively, and V is the sediment volume. Suspended load is distributed according to flow velocity U (Van De Wiel et al., 2007) as

$$V_{i,k} = \frac{U_k}{\sum U} V_i$$

and is deposited according to its concentration, a specified settling velocity v_i and the length of the simulation time step dt. A system of multiple active layers is used that changes the thickness of an active surface layer when sediment is eroded or deposited and incorporates subsurface sediment layers when the thickness of this surface is below or above defined

thresholds (Coulthard et al., 2002; Van De Wiel et al., 2007). Soil erosion *SE* is represented as a continuous process and controlled by the slope *ß*, cells' drainage area *CA*, and a user-specified rate

$$SE(year^{-1}) = \frac{ß\, rate_{SE} \sqrt{CA}\, dt}{D\, x}$$

Vegetation growth is represented by a linear growth model. The parameter 'vegetation maturity' specifies a time period (in years) after that 100 % vegetation cover develops, given the absence of disturbance by erosion or sedimentation. For a development stage of > 50 %, sediment erosion is prevented ($Q_s = 0$). Vegetation cover decreases with the doubled increase rate when areas are under water, and is reset to zero when shear stress exceeds a user-defined threshold.

8.3.2 Workflow overview

Calibration and evaluation of the CAESAR model was carried out in several steps (Fig. 8.2): First, the required input datasets were compiled from catchment monitoring data. In pre-calibration runs, appropriate parameter ranges for a more detailed evaluation in later steps were determined. Therefore, the information available in the graphic user interface (i.e., surface runoff patterns, erosion and deposition patterns, and discharge) was compared with knowledge from field observations and previous geomorphic analyses. The hydrological model was then calibrated by comparison with runoff data; and soil erosion and vegetation parameters were calibrated by comparison with results of geomorphic analyses. In the next steps, input DEMs were modified to assess effects of DEM resolution and surface roughness. A 'best scenario simulation' was determined from the stepwise evaluation and analysed in detail. Finally, modified precipitation input data were used to assess the effects of differing meteorologic characteristics on simulated surface development.

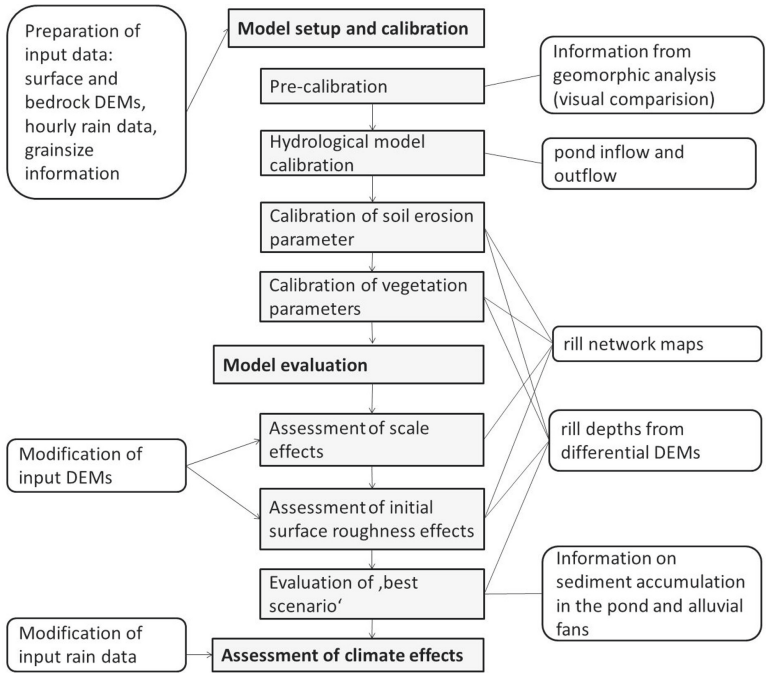

Figure 8.2: Schematic diagram of the main working steps, input data for simulations (left) and reference data and information used for specific working steps(right).

8.3.3 Input data compilation and basic model setup

The photogrammetry-based DEM of the catchment's surface recorded at November 26, 2005 was used as the input surface elevation dataset. For the elevation dataset representing the bedrock surface, we used the elevation model of the clay liner surface, which represents the lower boundary of the erodible sediment. Both elevation models were rotated by 270° in ArcGIS so that the outlet of the catchment was at the right border of the model and that the main flow direction was from left to right, as required by CAESAR. The DEMs were then resampled to a grid size of 0.5 by 0.5 m using a B-Spline Interpolation in SAGA. To omit any outflow from the catchment, a constant value of 1 m was added to elevations along the catchment boundary, except for the outflow area at the right border of the model. Sinks in the surface DEM were filled using the method of Planchon and Darboux (2002) in SAGA. Elevations were increased by up to 0.36 m by sink filling mainly in the lower part of the trapezoidal spring area and in small depressions in the backslope area. As the areal extent of the clay base liner model did not exactly match the extent of the surface DEM, the clay DEM was clipped or extended to fit the outline of the surface DEM. No information for the clay liner elevation was available for the northernmost part of the catchment, therefore a

constant depth of 2 m below the surface was assumed for this area. The lowest part of the slope was clipped from both DEMs to 1) omit long simulation times due to the simulation of water and sediment redistribution in the pond area and 2) because of limitations to the size of the DEMs that could be loaded into the model.

Hourly rainfall data recorded in the catchment (Biemelt et al., 2011) since September 29, 2005, were used as precipitation input data. March 31, 2010 was chosen for the end of the simulation period. Sediment particle size distribution (Table 8.1) was defined from the mean values of 125 samples taken in a depth of 0 - 30 cm in the initial raster sampling in the catchment (Gerwin et al., 2009b), assuming a homogeneous spatial distribution. The arithmetic means of the size classes were used to specify the particle size in CAESAR. For the clay and silt fraction, the option for suspended transport was chosen, and fall velocities were calculated using Stokes' law for a temperature of 10 °C. Parameters used for all simulations are listed in Table 8.2. Water and sediment discharge data were saved hourly, and spatially distributed simulation results giving the elevation difference and the median particle diameter (D50) were saved in time steps of 30 days. Output data for simulation times of 360 days, 630 days, 1020 days, and 1380 days were assigned to reference rill network maps for September 22, 2006, June 14, 2007, July 10, 2008, and July 01, 2009, respectively, for evaluation and interpretation.

Table 8.1: Grain size distribution and settling velocity used for simulations.

Grain size [mm]	0.001	0.00415	0.01315	0.0415	0.1315	0.415	1.315	25
Proportion [%]	5.33	1.67	2.61	3.63	23.39	40.20	10.50	12.67
Fall velocity [mm s^{-1}]	0.00069	0.01186	0.11907	1.18586	No suspended transport			

Table 8.2: Model parameters and settings used without previous calibration.

Active layer thickness [m]	Maximum erode limit [m][a]	Flow distribution width [cells]	Method for calculating shear stress	Sediment transport rule	Soil creep exponent	Slope failure threshold [°]
0.2	0.03	3	Velocity	Einstein	0.0025	60

[a] - the computation time step is decreased when erosion exceeds this limit

8.3.4 Hydrological model calibration

As reference data for hydrological model calibration, data for the fast inflow to the pond calculated by Biemelt et al. (2011) from pond storage change, precipitation on the pond surface and pond outflow, were used. Discharge from the pond measured at the weir at the single outlet of the catchment was used for additional interpretation, however was not used for calibration because it is considerably affected by the buffer function of the pond. The period from February 24, 2007 December 31, 2007 was chosen for calibration of the hydrological model in order to reduce computation time and to include dry periods, low and high intensity rainfall events. Pre-evaluation runs were carried out to assess which parameters influence the simulated discharge. Parameter ranges used for calibration of the minimum discharge for the calculation of water depth at the surface (*MinQ*), the minimum water depth for the calculation of erosion (*wdet*), and the TOPMODEL 'm' value (*m*) were derived from the pre-calibration runs (Table 8.3).

Table 8.3: Model parameters and settings used without previous calibration.

Model parameters	minimum discharge for depth calculation (MinQ)	water depth erosion threshold	TOPMODEL m value	vegetation maturity [years][a]	vegetation critical shear stress	Soil erosion rate
Calibration parameter range	0.00005 - 0.001	0.001 - 0.004	0.001 - 0.02	0/4/10	1/50/180	0/0.02/0.05
Parameters used	0.0003	0.003	0.001	10	50	0.02
Reference data for calibration	pond inflow data			rill network maps and DEM time series analysis		
Output data used for calibration	water discharge			elevation difference maps		

[a] no vegetation effects are computed for a vegetation maturity value of 0

8.3.5 Evaluation methods for the calibration of soil erosion and vegetation parameters and the assessment of effects of input data modification

A basic calibration of the soil erosion and vegetation parameters was carried out by comparing the water and sediment discharge data and maps of elevation differences resulting for different parameter combinations with reference data and field observations. The same evaluation steps were carried out to assess the effects of differing resolution and roughness of the input DEM. Reference information used for evaluation were the rill network maps from aerial photographs for September 2006, June 2007, July 2008 and July 2009 (Schneider et al. 2013), rill depths approximated from a differential elevation model for the period from November 2005 to September 2010 (Schneider et al. 2013), and approximations of sediment output from the erosion-dominated area of the catchment (Kleeberg et al., 2010; Schneider et al., 2012).

Spatial patterns of erosion were compared with rill network maps from aerial photographs for the end of simulation period. Therefore, the rill maps were transferred to grid models with a constant value of 1 within the rills and a cell size corresponding to that used in the simulation. A 0.1 m buffer function was applied to the rills' outlines to allow for the representation of narrow rills in the gridded models. A grid model representation of all the areas that had been subject to rill erosion for one of the mapping states was produced by merging the models for the four specific states, and subtracting the area of the alluvial fan (Fig. 8.3). The elevation difference maps produced by the model were classified into areas with a decrease in elevation of more than 5 cm ('rill areas') and areas of no or positive elevation change ('unrilled areas'). By combining the classified simulation and reference grids, a grid representing classes of cells with an accordance of simulated elevation difference and mapping results; 'false negatives', (i.e., grid cells for which no incision > 5 cm was simulated but which were mapped as rills); and 'false positives' (i.e., grid cells for which incision was simulated but which were not mapped as rills), was obtained. To assess the overall density of erosion features, the proportion of cells with a simulated incision of > 5 cm in relation to the total number of cells in the simulation area was compared to the proportion of mapped rill cells. To assess drainage density distribution over the slope, the number of linear erosion features along eight profiles across the slope (Fig. 8.3) was determined based on maps of the classified elevation differences. Small and local erosion scars were not counted as rills. Simulated erosion rill depth was assessed by comparing the mean, standard deviation and maximum of elevation differences for the cells with an elevation decrease of > 5 cm with reference data from the differential elevation model. Spatial distribution of rill depths was further assessed by visual interpretation of elevation change maps.

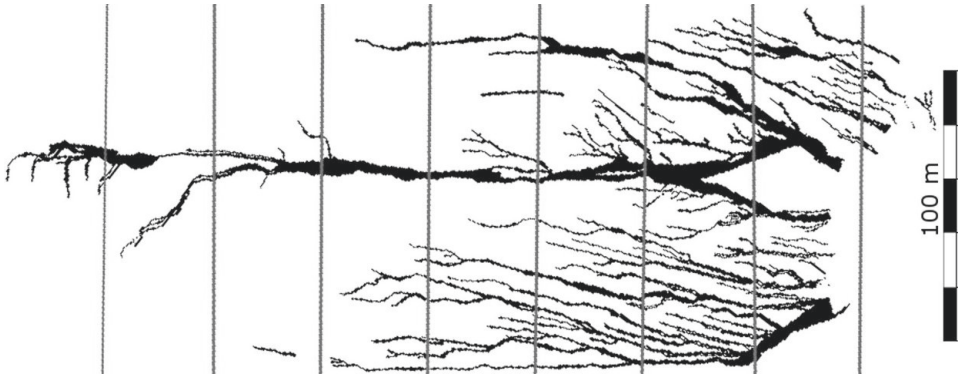

Figure 8.3: The reference rill network for the end of the simulation period, resulting from merging rill network maps for four states of development, and the location of the slope cross-profiles used for the evaluation of drainage density.

8.3.6 Modification of input DEM resolution, roughness and precipitation characteristics

To assess the effect of an increased input DEM resolution, simulations for a subcatchment in the SW part of the catchment were carried out. The subcatchment DEM was extracted from the original DEM by determining the upslope area of the lowest model cell of the subcatchment using the D8 flow routing algorithm (Freeman, 1991). The subcatchment DEM was then resampled to grid cell sizes of 0.3 m by 0.3 m and 0.25 m by 0.25 m using B-Spline interpolation in SAGA. Lower values for the *MinQ* threshold (Table 8.4) were used to account for the reduced cell size.

To evaluate the effects of differing initial surface roughness, modifications were applied to the input DEM. A Gaussian Filter (standard deviation 1, search square 4 by 4 cells) was applied to create a surface with reduced roughness. To assess the effect of initial surface irregularities that are not captured in the elevation data, surface structures observable in an aerial photograph of November 2005 were digitized (see Fig. 5.2) and transferred to a grid dataset. DEM elevations were lowered along the digitized structures by 2 cm, 3 cm, and 5 cm to create different modified elevation models. Resulting sinks at the downslope ends of the digitized structures were then filled using the Planchon and Darboux (2002) algorithm in SAGA.

Table 8.4: Parameters used and elevation differences along erosion rills for the end of the simulation period for simulations in higher resolution. Number of rill cells in the subcatchment n = 107440 for 25 cm by 25 cm cell size, n = 71656 for 30 cm by 30 cm cell size and n =25088 for 50 cm by 50 cm cell size.

Simulation	30 cm - 1	30 cm - 2	25 cm - 2	30 cm - 2smooth	30 cm - 2struct5	50 cm
DEM	unmodified	unmodified	unmodified	Gaussian filter	Irregularities deepened 5 cm	unmodified
MinQ	0.00003	0.00001	0.00001	0.00001	0.00001	0.0003
proportion of rill cells	2.55	3.51	2.16	3.00	3.48	3.99
rill cells not mapped as rills	1448	1972	1608	1861	1611	711
rill cells mapped as rills	377	546	706	542	630	291
Mean and standard deviation of depth	0.09 ± 0.04	0.11 ± 0.05	0.09 ± 0.04	0.1 ± 0.04	0.11 ± 0.06	0.14 ± 0.08
Maximum elevation difference / rill depth	0.24	0.31	0.24	0.27	0.43	0.42

Table 8.5: Annual precipitation and variance of hourly values (data from Biemelt et al. 2011).

	Annual precipitation [mm]	Variance of hourly values
2006	403	0.10
2007	667	0.27
2008	660	0.18
2009	665	0.22

For assessing the effect of differing precipitation characteristics, precipitation input data were modified. To maintain the characteristic seasonal dynamics, the rainfall record was partitioned into records for the single years. The period from September to December 2005 was placed at the beginning and the period from January to March 2010 was placed at the end of the rain input data file for each of the simulations. The variance of hourly precipitation was determined for each of the years 2006 to 2009 (Table 8.5), and the yearly records for these years were rearranged 1) in reverse order, as compared with the rainfall record (*rain_rev*); 2) by decreasing (*rain_dec*) and increasing (*rain_inc*) variability of hourly values, and 3) by repeating records for one year for four times (*rain_2006, rain_2007, rain_2008, rain_2009*) to simulate the effects of an increase or decrease in precipitation variability during the initial phase of landform development or of a generally decreased or increased variability as compared to the recorded data.

8.4 Results

8.4.1 Hydrological model calibration

Discharge volumes and water depths at the catchment surface observable in the CAESAR user interface during pre-calibration runs suggested that simulated water discharge was sensitive to changes in the values of *MinQ* (the minimum discharge for that water depth at the surface is calculated), *wdet* (the minimum water depth at the surface for that sediment erosion is calculated), and the TOPMODEL m parameter. Sensitivity analysis for the *MinQ* value (Fig. 8.4 a and b) showed that a lower value results in a higher intensity of most simulated runoff events, but in reduced intensity for the highest peaks of the discharge curve, and therefore in less variation in the simulated discharge intensities as compared with the pond inflow reference data. Increasing the value of *MinQ* resulted in considerably decreased intensity for most runoff events, and no simulated discharge for low-intensity precipitation. Computation time varied between 8 and 45 hours for the calibration period for different *MinQ* values. A reduction of the TOPMODEL *m* parameter (Fig. 8.4 c and d) similarly resulted in an increased intensity for the majority of runoff events, but in a decrease in water discharge for the highest-intensity events, and thus underestimated the variability of pond inflow data. For a higher value of 0.02, no discharge was simulated for most events, discharge intensity for high-intensity events was considerably reduced, and a longer duration of runoff events was observed. Computation time was 45 minutes for a value of 0.02, and 37 hours for a value of 0.0008. Reducing the *wdet* value to 0.001 (Fig. 8.4 e and f) resulted in reduced variability of simulated discharge, similar to the effects of the reduction in the *MinQ* and TOPMODEL *m* values. Increasing the *wdet* value to 0.01 resulted in an overall decrease of discharge intensities, but also in reduced variability of intensities as compared with a *wdet* value of 0.003. Computation time for the calibration period varied between 8 and 31 hours for different *wdet* values.

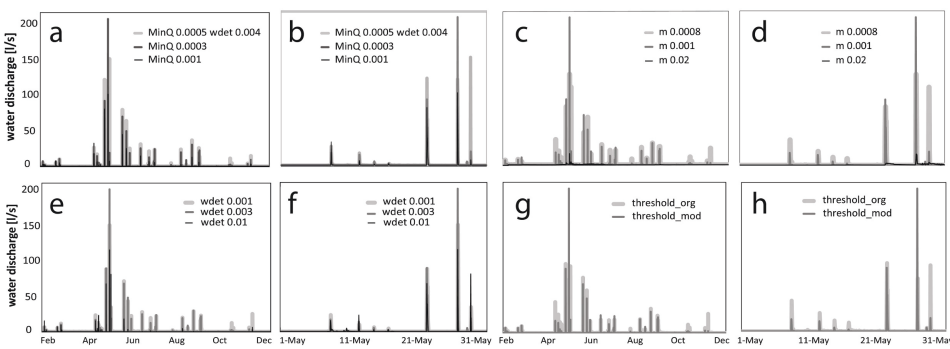

Figure 8.4: Simulated water discharge resulting from modifications in the parameters a,b) MinQ; c,d) m; and e,f) wdet; and g,h) for a simulations with the calibrated parameters with the original and modified calculation of the infiltration threshold; for the total calibration period (left) and for May 2007 (right).

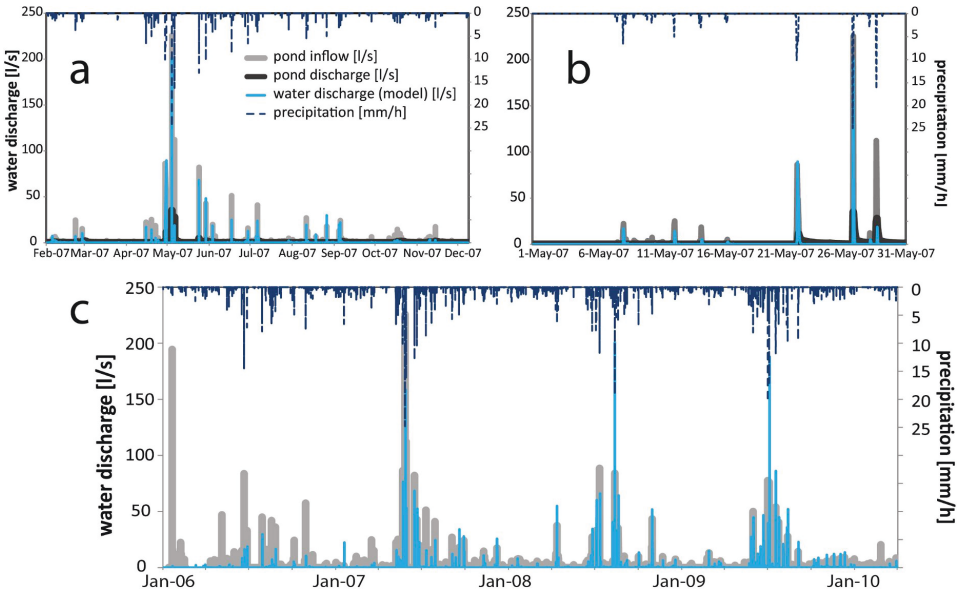

Figure 8.5: Rainfall, runoff into the pond and discharge from the pond (measured) compared to simulated discharge for the calibrated hydrological model (MinQ = 0.0003, wdet = 0.003, m = 0.001) for a) the total calibration period, b) one month of the calibration period, and c) the total simulation period (pond discharge is not shown for c).

Closest similarity to pond inflow data was observed for using *MinQ* = 0.0003, *wdet* = 0.003, and *m* = 0.001 (Fig. 8.5 a and b). Simulated discharge was lower as compared with the pond inflow data especially for medium-intensity runoff events (10 - 50 l s^{-1}); however, variability of peak intensities and duration of events was similar to reference data. Computation time using these settings was about 30 hours for the calibration period. Using the modified computation of the infiltration threshold value, for that all runoff is treated as surface runoff in case of very low infiltration thresholds, discharge was higher for high intensity events and slightly lower for moderate intensity events, and similarity to the reference pond inflow data was higher as compared with the original computation method (Fig. 8.4 g, h). A comparison of simulated water discharge with pond inflow data for the total simulation period (Fig. 8.5 c) suggests that the intensities of runoff events in the first year of the simulation period were mainly underestimated, while intensities for the latest periods were mainly overestimated.

8.4.2 Calibration of the soil erosion and vegetation parameters

Considerable differences in simulated elevation change and in the geometry of the resulting linear incisions resulted from varying the soil erosion parameter between values of 0 and 0.02. For a soil erosion rate of 0, very few linear incisions deeper than 5 cm were simulated. These simulated rills were considerably narrow and deeply incised (Tables 8.6 and 8.7).

Table 8.6: Visual assessment of erosion patterns as compared with reference data for the end of the simulation period for different soil erosion and vegetation parameters and roughness of the initial DEM.

Simulation	SE 0	SE 0.02	SE 0.05	V 4/50	V 10/50	V10/180	smooth	struct2	struct5	nosusp	
Input DEM	unmodified						Gaussian Filter	Irregularities deepened 2cm	Irregularities deepened 5cm	Irregularities deepened 5cm	reference rill network maps
Soil erosion setting	0	0.02	0.05	0.02	0.02	0.02	0.02	0.02	0.02	0.02	
vegetation critical shear stress	1	1	1	50	50	180	50	50	50	5	
Rill width	-	0	+	0	0	-	+	-	-	+	-
Rill Continuity	+	0	-	-	0	0	+	0	0	-	+
Rill Sinuosity	0	0	-	+	0	+	-	0	-	+	-
Sedimentation along rills		+		+	0	+	+	-	-	+	-
Braiding	-	0	-	0	-	+	+	-	0	0	0
Bifurcation	+	0	-	-	0	0	-	0	+	+	+

+ high, 0 moderate, -low

Table 8.7: Elevation differences along erosion rills as compared with reference data for the end of the simulation period for different soil erosion and vegetation parameters and roughness of the initial DEM.

Simulation	SE 0	SE 0.02	SE 0.05	V 4/50	V 10/50	V10/180	smooth	struct2	struct5	nosusp	
Input DEM	unmodified						Gaussian Filter	Irregularities deepened 2cm	Irregularities deepened 5cm	Irregularities deepened 5cm	reference data
Soil erosion setting	0	0.02	0.05	0.02	0.02	0.02	0.02	0.02	0.02	0.02	
vegetation maturity	0	0	0	4	10	10	10	10	10	10	
vegetation critical shear stress	1	1	1	50	50	180	50	50	50	50	
proportion of rill cells	4.06	6.68	9.77	3.43	5.34	4.83	5.70	4.99	5.66	8.34	9.66
Rill cells not mapped as rills	5991	10153	15506	4954	8304	7550	9131	7229	8650	13251	
rill cells mapped as rills	2462	3772	4866	2205	2825	2526	2744	3179	3140	4122	
Mean and standard deviation of depth	0.27 ± 0.23	0.19 ± 0.16	0.17 ± 0.13	0.15 ± 0.11	0.16 ± 0.12	0.15 ± 0.11	0.17 ± 0.13	0.17 ± 0.14	0.16 ± 0.13	0.22 ± 0.19	0.5 ± 0.3
Maximum elevation difference / rill depth	1.31	1.27	1.11	1.01	1.28	0.84	1.11	1.10	1.08	1.07	1.1

For a soil erosion rate of 0.05, simulated incisions were very broad and shallow, highly overestimating the width of the mapped erosion rills. Furthermore, the high soil erosion rate resulted in a low continuity of the linear incisions. With increasing soil erosion rate, the rill density, according to the proportion of cells with an elevation decrease of more than 5 cm increased. However, also the number of 'false positive' rill cells resulting from the simulation increased (Table 8.7). Simulated rill depths (Table 8.7) and drainage density along slope profiles (Fig. 8.6 a) were smaller as compared with the mapped networks for all settings.

Simulated drainage density along slope profiles was lowest for most profiles without soil erosion effects, and was higher in the central and lower parts of the slope for an erosion rate of 0.02 and higher in the backslope area for an erosion rate of 0.05. Overall, the best approximation of mapped rill network geometry, according to visual comparison of rill geometry to mapped networks (Table 8.6), to the analysis of elevation difference maps (Table 8.7) and to the distribution of linear incisions across the slope profile (Fig. 8.6 a) resulted from simulations with a soil erosion rate of 0.02.

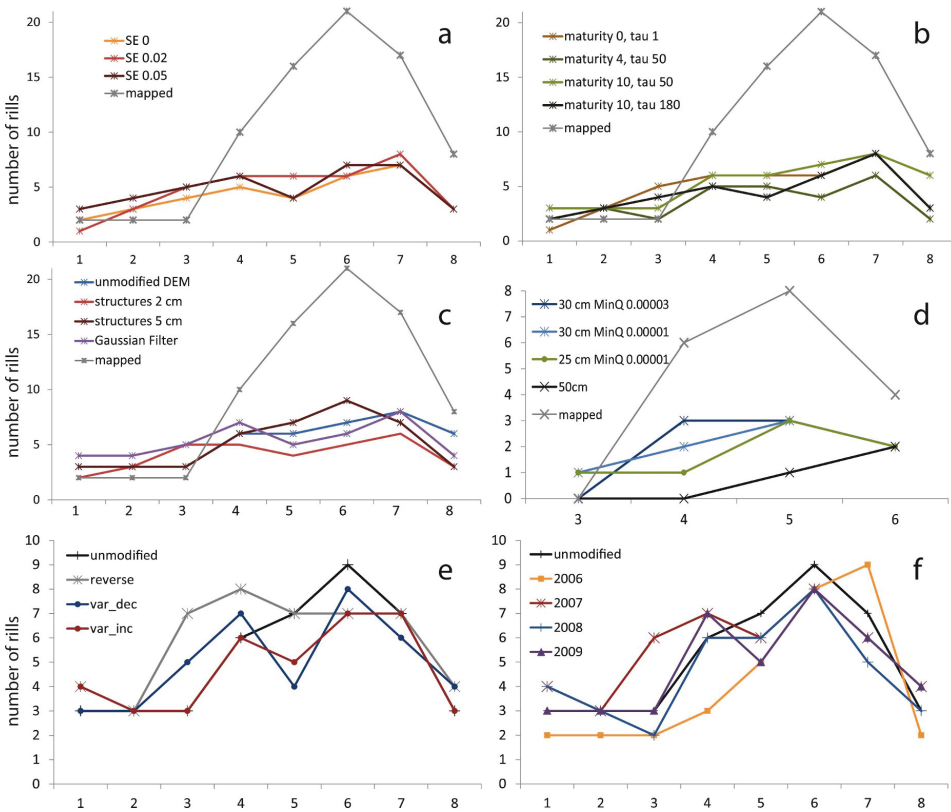

Figure 8.6: Number of erosion rills along profiles across the slope for a) different soil erosion rates, b) different vegetation parameter settings, c) modified initial surface structures, d) different DEM resolutions for a subcatchment, e and f) modified precipitation data. The x-axes denote the slope profiles, as given in Figure 8.3, in downslope order.

Modifications to the parameters controlling the vegetation growth rate and the critical shear stress for vegetation disturbance resulted in slight differences in the patterns of elevation change (Tables 8.6 and 8.7) and in density of linear incisions across the slope (Fig. 8.6 b) for the final simulation state. Differences were also observed in the development of rill density for slope profiles over the simulation period (Fig. 8.7 a - d), in the temporal development of the simulated sediment discharge (Fig. 8.8 a) and in ratios of sediment to water discharge (Fig. 8.9 a-c). After the total simulation period, fewest linear incisions were observed for a vegetation maturity value of four years. The densest network of erosion rills was simulated for a vegetation maturity of 10 years and a critical shear stress of 50. Relatively narrow rills, local braiding of incisions into two or more channels and a pattern of parallel rills were observed for these settings. Increasing the critical shear stress resulted in a decrease of rill width and in high simulated sedimentation along the erosion rills, especially along the central erosion rill that split into two channels over most of the slope area. Mean depths of the rills were similar for all settings. The number of rills along slope cross-sections for the end of the simulation period was lowest for the low vegetation maturity value (Fig. 8.6 b). In the simulations with a vegetation maturity value of 10, as compared with a simulation without vegetation effects, final drainage density was lower in the backslope area but higher in the lower slope areas. Sediment discharge for the simulation period was considerably lower for all vegetation parameter combinations as compared with the simulation without vegetation effects (Fig. 8.8 a). Lowest sediment discharge was observed throughout the simulation period for the lower maturity parameter. The ratios of sediment to water discharge were smaller for all simulations with vegetation influence as compared without the simulations with a vegetation maturity value of 0, for that no vegetation effects were simulated (Fig. 8.9 a-d).

8.4.3 Effects of differing roughness of the input DEM

Smoothing the input DEM or adding irregularities to the surface resulted in slight differences in the overall parameters characterizing the incisions (Table 8.7), and in different patterns of the simulated elevation change (Table 8.6). For the DEM smoothed by a Gaussian Filter, higher intensity erosion along the central erosion rill and two incisions in the SW part was observed during the first year of the simulation period. During the second year, higher intensity incision took place in the backslope area, and during the later development phases, no further addition of tributaries but an increase in drainage density by a splitting of the major incisions into two channels was observed. For the final state, the rill density was similar to the original DEM, but the rills were distributed more equally over the slope longitudinal profile (Fig. 8.6 c). For the DEMs that were modified by 2 and 3 cm deepening along surface irregularities, only slight differences to simulations using the original DEM were observed.

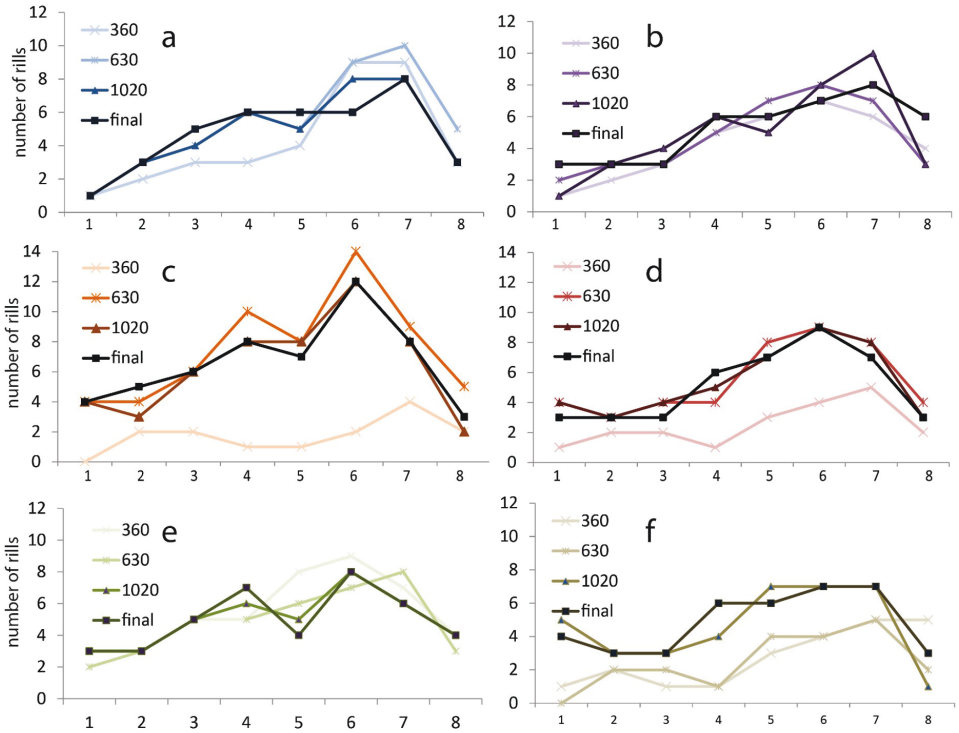

Figure 8.7: Number of erosion rills along profiles across the slope for simulation times of 360, 630, and 1020 days and the final state for a) the unmodified DEM without vegetation effects, b) the unmodified DEM with vegetation effects, c) the DEM with added initial structures without vegetation effects, d) the DEM with added initial structures with vegetation effects, e) the simulation with decreasing and f) the simulation with increasing variance of precipitation events. The x-axes denote the slope profiles, as given in Figure 8.3, in downslope order.

Differences in the development and the final pattern of the rill network were observed in simulations using the DEM with 5 cm deepening of surface irregularities. Sedimentation in the central part of the deepened areas and erosion at their edges and upslope ends was observed during the first development phases. Isolated incisions formed along the deepened areas during the first phase and became connected to continuous erosion rills during the second phase. Drainage density for slope cross-profiles was therefore considerably lower after the first development phase, but rapidly increased during the second phase, both for simulations without and with vegetation effects (Fig. 8.7 c and d). Development of elevation differences in the fourth phase was characterized by higher headward growth and less braiding and tributary addition, as compared with the original DEM simulation. For the final state, an increased drainage density for slope profiles was observed for the DEM with 5 cm deep irregularities. Elevation difference maps suggested that the increased density resulted from higher braiding of rills into several channels and from increased bifurcation at

rill heads; and that rills in the SW part were more parallel and oriented in a direction similar to that of the mapped rills for this simulation. Sediment discharge for the total simulation period was highest for the smoothed surface and lowest for the unmodified DEM (Fig. 8.8 b).

8.4.4 Scaling effects

In the subcatchment simulations with increased DEM resolution, the proportion of cells with an elevation decrease > 5 cm and the mean depth of these rill areas were lower as compared with the original resolution (Table 8.4), and more alternation of erosion and sedimentation along the drainage lines in the subcatchment was observed. However, drainage density along cross-profiles increased with increasing resolution (Fig. 8.6 d). Simulated rills were longer and had more bifurcation points and tributaries for higher DEM resolution. No considerable further increase in drainage density, but a different distribution of cross-section drainage density along the subcatchment and higher simulated rill depths were observed for a reduced *MinQ* value in higher-resolution simulations (Fig. 8.6 d). Smoothing the subcatchment DEM with 0.3 m by 0.3 m resolution resulted in slightly reduced rill density across slope profiles and reduced depth, while adding irregularities did not cause considerable differences in rill density distribution.

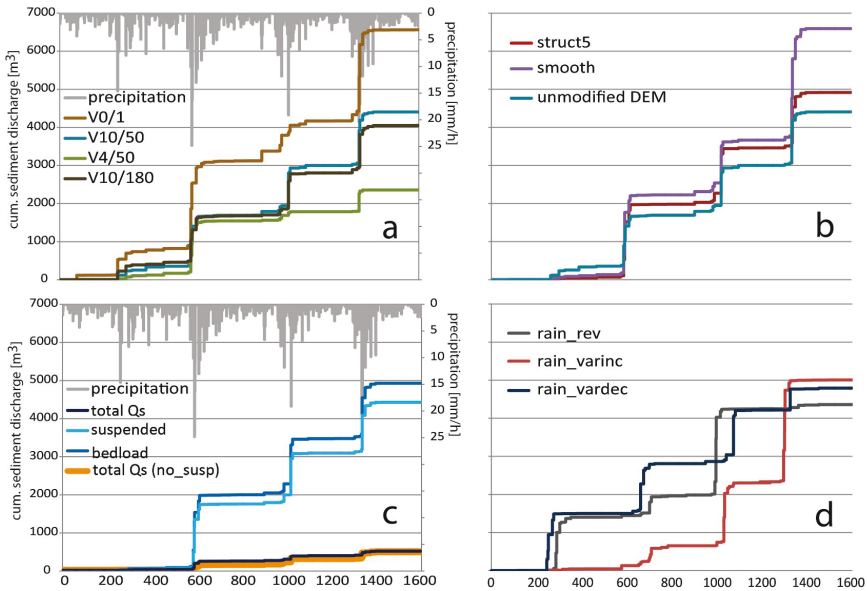

Figure 8.8: Cumulative sediment discharge simulated for a) the unmodified DEM and differing vegetation parameter combinations, b) DEMs with differing initial roughness, c) the best scenario simulation (total, suspended load, and bedload discharge) and the best scenario simulation without simulation of sediment transport in suspension, and d) precipitation input data modified by sorting yearly records in reverse order and by variance of hourly sums.

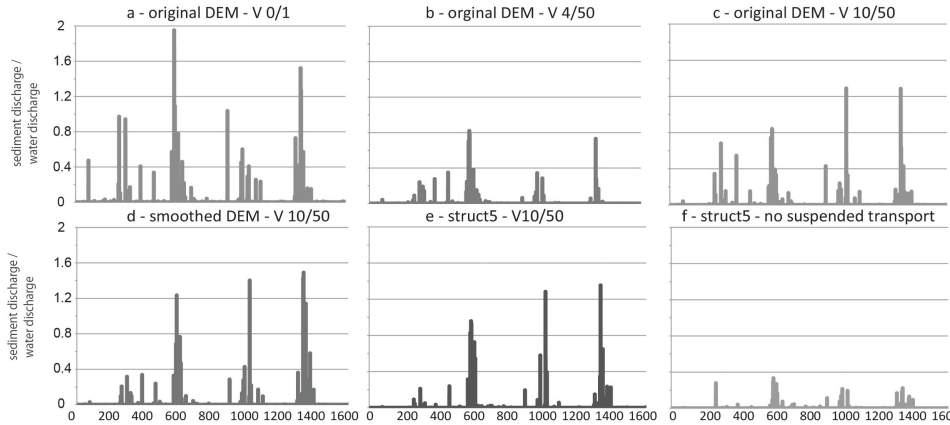

Figure 8.9: Development of the sediment discharge to water discharge ratio for differing vegetation parameters (a, b, c) and roughness of input DEMs (c, d, e) and for the simulation without suspended sediment transport (f). The x-axes denote the simulation time in days.

8.4.5 Surface development in the best scenario simulation

From an integration of results of visual erosion pattern evaluation and the characterization of elevation differences, the simulation with a soil erosion rate of 0.02, vegetation maturity and critical shear stress values of 10 and 50, and the input DEM with surface irregularity deepening of 5 cm was identified as the best approximation of hydro-geomorphic development that was possible for a DEM cell size of 50 cm by 50 cm. The progress of elevation change (Fig. 8.10) and the development of the particle size distribution, based on maps of the median particle diameter (D50) for DEM cells (Fig. 8.11), are described in more detail in the following.

The majority of changes in surface elevation and particle size distribution in the surface sediment layer was observed during phases of high-intensity surface runoff in the periods between day 600 and 630, between day 990 and 1080, and between day 1350 to day 1410 of the simulation period, which correspond to the precipitation events in May / June 2007, July /August 2008, and June / July 2009. Until the 150th day of the simulation, elevation decrease was only dominant along the central erosion rill, and alternating patterns of erosion and deposition were simulated for further linear structures especially in the SW part. Incision along the central rill was limited to narrow cross-sections, while sedimentation was simulated for broader cross-sections, especially above the trapezoidal spring area. After 600 days (May 2007), higher incision for a slightly broader cross-section along the central rill and incision along two major lines on the SW and one major line on the NE part of the lower slope area were simulated.

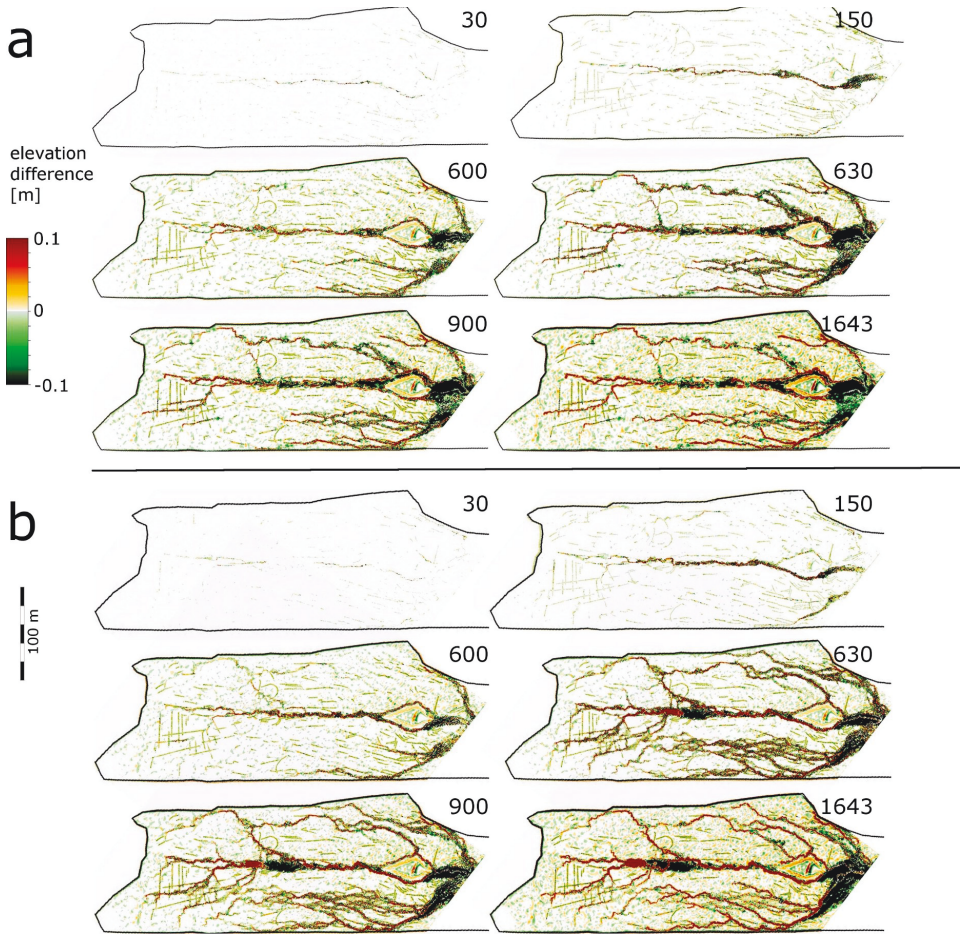

Figure 8.10: Spatial distribution of elevation differences for six simulation steps, resulting from the best scenario simulation using the DEM with added initial structures a) with and b) without simulation of sediment transport in suspension. Positive values denote erosion, negative values denote sedimentation.

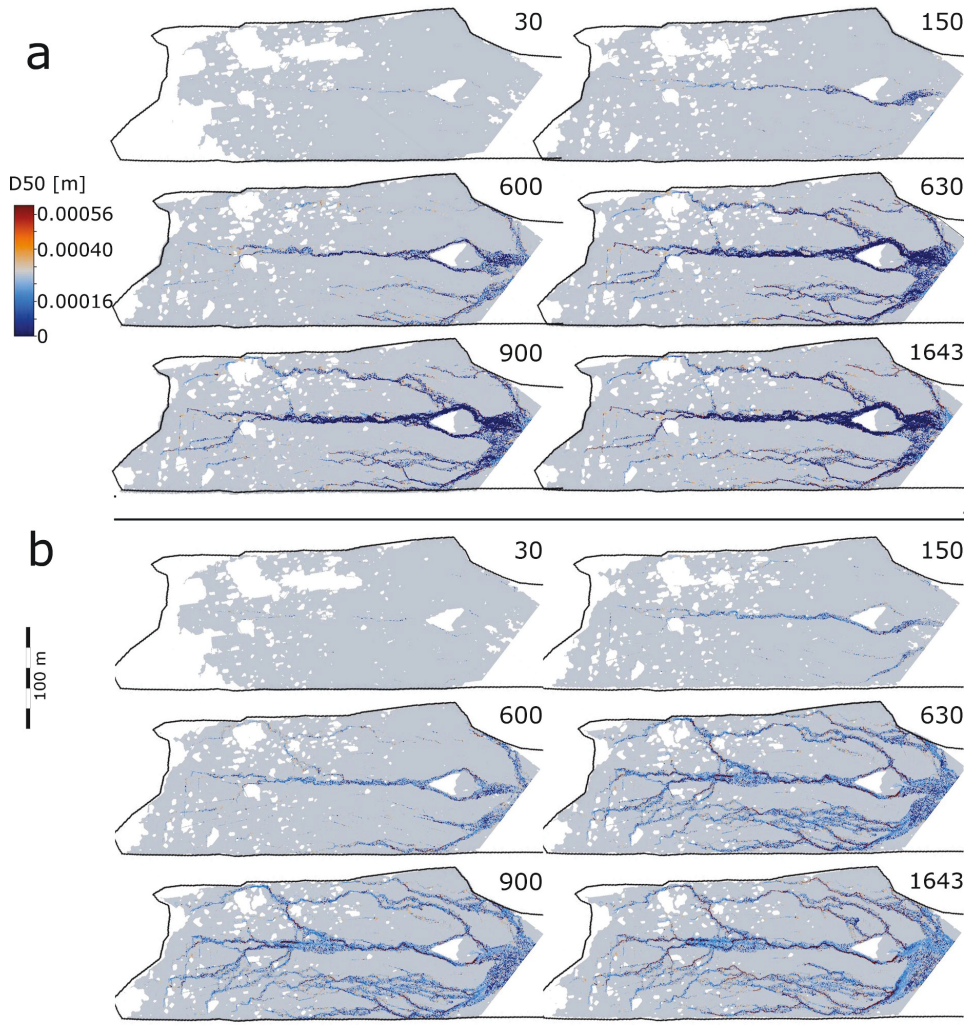

Figure 8.11: Spatial distribution of the median particle size diameter in the surface sediment layer for six simulation steps, resulting from the best scenario simulation using the DEM with added initial structures a) with and b) without simulation of sediment transport in suspension. Blue colors denote a fining and red colors denote a coarsening of the sediment as compared with the initial median diameter of 0.00028 m.

The high-intensity runoff events during the next month of the simulation resulted in headward growth of all previously initiated rills, in increased sedimentation and the incision of alternative channels along the central rill, in the formation of additional tributaries and parallel channels to rills in the SW part, and in the formation of an additional major erosion rill in the NE part. Sedimentation in the lower slope area considerably increased during this period. No considerable changes to these patterns were observed after 900 days of the simulation, and simulated surface development proceeded by further incision, slight widening, and further headward growth along the established rills. Highest intensity erosion was concentrated to the major rills for the simulated period until September 2006 (Fig. 8.12 a), was distributed over all erosion rills and not considerably differing for upper, central and lower slope areas between September 2006 and June 2007 (Fig. 8.12 b), and was clearly concentrated to the lower slope areas for the simulated period from June 2007 to July 2009 (Fig. 8.12 c).

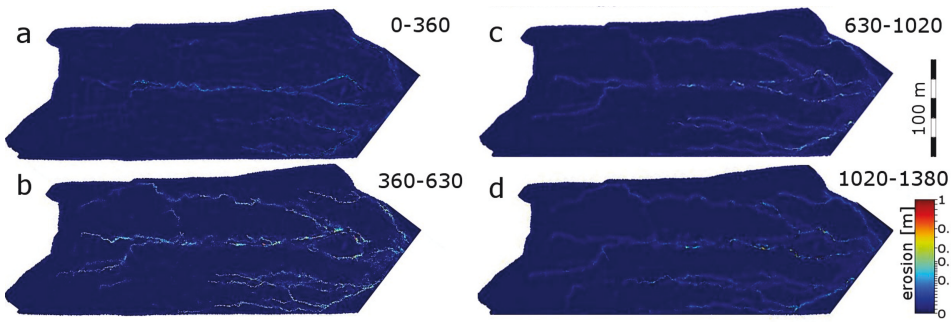

Figure 8.12: Spatial distribution of decrease in surface elevation for four development periods corresponding to the periods between rill network mapping, a) until day 360 of the simulation (September 2006), b) between day 360 and day 630 (June 2007), c) between day 630 and day 1020 (July 2008), and d) between day 1020 and day 1380 (July 2009).

Figure 8.13: Development of mean and standard deviation of D50 for the 'best scenario' simulation, with (a) and without (b) simulation of suspended sediment transport.

The mean value and standard deviation of the overall median particle diameter constantly increased over the simulation period (Fig. 8.13 a). Maps of the surface D50 spatial distribution (Fig. 8.11) suggest that high-intensity depletion of fine material, restricted to relatively few cells, and accumulation of fine material in relatively large areas along the flow paths were simulated. After the first month of the simulation period, alternating increase and decrease in D50, corresponding to the patterns observed in elevation change maps, were observed. Overall D50 (Fig. 8.13) increased slowly until 600 days, along with an increasing differentiation into areas of high increase in the backslope areas, high decrease in the areas of highest flow accumulation (i.e., at the downslope part of the central erosion rill), and moderate decrease in other parts of the major flow paths. A strong increase in overall D50, restricted to considerably small areas at the upslope ends and confluences of erosion rills was simulated for the period from 600 to 630 days. For the final development state, a clear concentration of intensive coarsening to areas of high flow accumulation and rill heads was observable. Strong fining was observed along the central areas of rills, especially along the major erosion rill. The maps reflect a clear dominance of fining in the sedimentation areas, but both coarsening and fining in the erosion areas. A classification for areas with moderate and high erosion and sedimentation (Table 8.8) shows considerable fining in areas of high sedimentation and slight fining in areas of moderate sedimentation and moderate erosion. Very high coarsening and high variability are shown for areas of high erosion.

The best scenario simulation was repeated without using the option to simulate suspended sediment transport, so that particles of all size classes were transported by the rules for bedload transport. For this simulation (*no_susp*), lower sediment redistribution in the interrill areas and a clearer incision of erosion rills were observed (Fig. 8.10b). The drainage density and the location and geometry of simulated rills were similar to the simulation including sediment transport in suspension. Similar to simulations including suspended transport, the simulation resulted in a coarsening of the median particle size diameter the surface sediment layer at rill heads and at a fining along major rills, however, fining along the rills (Fig. 8.11 b) and in the sedimentation areas (Table 8.8) was lower and the overall increase of D50 was higher (Fig. 8.11 b, 8.13b).

Table 8.8: Final mean [mm] and standard deviation (σ) of D50 for areas of erosion and sedimentation for original and modified rainfall input data. D50 for the initial state is 0.28 mm.

Simulation	unmodified precipitation data, no suspended transport		unmodified precipitation data		decreasing variability		increasing variability	
Elevation change	n data cells	Mean, σ	n data cells	Mean, σ	n data cells	Mean, σ	n data cells	Mean, σ
> + 10 cm	9170	0.24 ± 0.26	8096	0.17 ± 0.47	8942	0.15 ± 0.36	9772	0.1 ± 0.55
+ 1 cm - + 10 cm	29715	0.27 ± 0.18	31374	0.27 ± 0.31	29893	0.27 ± 0.22	30031	0.27 ± 0.43
+ 1 cm - − 1 cm	99028	0.28 ± 0.02	103689	0.28 ± 0.13	102804	0.28 ± 0.17	101875	0.28 ± 0.14
− 1 cm - − 10 cm	38964	0.27 ± 0.29	36814	0.29 ± 0.55	37989	0.29 ± 0.55	37867	0.28 ± 0.48
> − 10 cm	11982	2.81 ± 5.46	7332	2.15 ± 5.13	6975	2.03 ± 5.09	8135	2.03 ± 5.05

8.4.6 Effects of modified precipitation characteristics

Modifications in the input precipitation data resulted in differing patterns of incision, drainage density and particle size distribution for the final state of the simulation period. The percentage of cells classified as rills (Table 8.9) was slightly higher for the simulation with decreasing precipitation variability and slightly lower for increasing variability as compared with the unmodified precipitation simulation. Drainage density for slope profiles was higher in the backslope area and lower in the lower slope area for reverse ordering, and lower in the backslope and central slope area for both decreasing and increasing variability, as compared with the unmodified precipitation simulation (Fig. 8.6 e). For the simulation with reduced precipitation amounts and reduced variability (*rain_2006*), considerably lower density in the backslope and central slope area, but similar and higher density in the lower slope area was observed, while the simulation with higher variability (*rain_2007*) resulted in higher density in the backslope and similar or lower density in the lower slope area, as compared with unmodified precipitation (Fig. 8.6 d).

The final D50 in erosion-affected model cells did not considerably differ for simulations with decreasing and increasing precipitation variability. Slightly higher fining was observed in sedimentation areas for the simulation with increasing variability. The development of sediment discharge and the ratio of sediment to water discharge, in relation to precipitation intensity, varied between the simulations with different modifications of the precipitation input data (Fig. 8.9 d).

Table 8.9: Elevation differences along erosion rills for the end of the simulation period for different precipitation characteristics.

Simulation	rain reverse	rain var_inc	rain var_dec	rain 2006	rain 2007	rain 2008	rain 2009
proportion of rill cells (to total number of cells)	5.66	5.12	5.78	3.30	6.41	5.75	5.28
mean and standard deviation of depth	0.15 ± 0.12	0.15 ± 0.11	0.14 ± 0.1	0.11 ± 0.06	0.16 ± 0.13	0.16 ± 0.12	0.13 ± 0.09
maximum elevation difference / rill depth	1.08	0.83	0.91	0.69	1.16	0.97	0.91

8.5 Discussion

Generally, the study in the Hühnerwasser catchment offered good possibilities for validation and evaluation, as compared with most other LEM applications for which initial conditions are often unknown and reference data are often sparse (Coulthard et al., 2007). However, a number of limitations to validation and evaluation of the simulation results of this study need to be considered: Calibration of the hydrological model was based water discharge calculated from climate and pond level data (Biemelt et al., 2011). Water discharge from the catchment was measured at the central outlet; however, these data are highly influenced by the buffer function of the pond. The calculation of fast pond inflow from other monitoring data, however, can be considered as a suitable representation of discharge for the high-intensity, erosive runoff events. The pond before the central outlet further acts as the sink for eroded sediment, so that sediment discharge could not be measured. Approximations of sediment accumulation were available for specific states of development, based on pond sediment surveys (Kleeberg, 2011; Kleeberg et al., 2010) and based on DEM analyses for the alluvial fan (Schneider et al., 2012). As noted by Coulthard et al. (2007), the validation of LEMs is generally limited because of internal dynamics and complexity in the model and modeled landscape. Although system complexity for the Hühnerwasser catchment is relatively low in relation to larger and more mature areas, intermediate storage of sediment in rill beds and alluvial fans can result in non-linear relations of precipitation and sediment discharge.

8.5.1 Model set-up and parameterization

A relatively good agreement of simulated water discharge and pond inflow data was observed for the period from March to December 2007 after parameter calibration. However,

for the total simulation period, an underestimation of intensities for the earliest and an overestimation of intensities for the later development phases were observed (Fig. 8.5 c). It can be assumed that vegetation and soil development in the catchment have resulted in increased infiltration and decreased relative amounts of fast surface runoff; and in increase buffering of subsurface discharge due to higher alternations in soil water contents induced by transpiration of the developing vegetation cover. Peak discharge intensities are therefore decreasing with the development, which could not be reflected by one set of parameter values for the total simulation period.

The hydrological model parameters used in this study are relatively low in comparison with most other applications of CAESAR; however, most of these applications simulated surface development for longer timespans and larger areas, and varying parameters were used, depending on the spatial and temporal scale of the application. In the study on downscaling the CAESAR model for the simulation of soil erosion on a 20 m by 20 m plot by Coulthard et al. (2012), lower values for the *MinQ* and *wdet* thresholds, but a higher value of the TOPMODEL *m* parameter was used, as compared with this study. TOPMODEL *m* parameter values in the range of 0.001, as used here, have been used in other TOPMODEL applications (Beven, 1997). In most studies, hourly precipitation data was used for CAESAR simulations. For the application on soil erosion plots, Coulthard et al. (2012) used precipitation data in 10 min resolution, but suggested that water and sediment discharge for low-intensity runoff events could have been more adequately simulated with even higher-resolution data. Calibration of the hydrological model in other CAESAR applications was mainly carried out by modifying the TOPMODEL *m* value, and effects of modifications in the *MinQ* and *wdet* values on simulated discharge have not been reported in other studies. Effects are, however, plausible, since both parameters are used in the routing of discharge in the model.

No lateral erosion was simulated in this study. Lateral erosion and an evolution towards meandering was not found to be of considerable importance for rill network development during the initial period in previous analyses in the catchment, however, effects of lateral erosion were observed in rill network maps for 2009 and in field observations for this phase of development. An integration of the lateral erosion simulation in CAESAR (Coulthard and Wiel, 2006) might improve the simulation of erosion rill geometry for those later development phases.

A vegetation growth rate of 10 years until the vegetation cover reaches its full maturity, as used after evaluation of differing growth rates in this study, was also generally suggested by Coulthard et al. (2002) for CAESAR applications. Modification of the critical shear stress for vegetation disturbance was hardly discussed in other CAESAR applications; however, results of this study showed that differing shear stress threshold values affected the amount

and pattern of sediment erosion and deposition. Effects of vegetation cover on the critical shear stress for rill or channel incision have been examined in many studies, which showed that vegetation can increase the critical shear stress threshold for channel incision from values of a few Pa on bare sediment surfaces to a few hundred Pa on vegetation-covered substrate (Prosser et al., 1995; Tucker et al., 2006). However, the effects of different vegetation parameter values observed in this study cannot fully be explained by the basic vegetation effects represented in the model: Generally, erosion is restrained in CAESAR when vegetation cover has reached a growth stage of 50 %, i.e., after two years for a growth rate parameter of 4 and after five years for a growth rate parameter of 10; in model cells not affected by erosion. For a growth rate parameter of 0, no vegetation growth is simulated. Because the simulation period of this study is less than five years, the threshold value of 50 % for vegetation stabilization is not reached in simulations using growth rate parameters of 0 and 10. However, different erosion patterns were observed for simulations using growth rates parameter values of 0 and 10, and for simulations using a growth rate parameter of 10 and different values for the vegetation shear resistance parameter. This suggests that additional effects of vegetation parameters are implemented in the model, which could, however, not be reconstructed from available documentation on the structure of the CAESAR model.

8.5.2 Model applicability for initial phases of landform development on the scale of a small catchment

All simulations described in this study show that the simulation of rill incision on an initially unrilled surface is possible with CAESAR. After parameter calibration; water discharge, the location of the major flow paths, and the distribution of drainage density over the slope were well reproduced. A concentration of erosion to the central and most deeply incised parts of the rill network for later phases of development as observed in the catchment was reflected by the simulations. This affirms that the repeated adaptation of topography during simulations needs to be implemented for the simulation of eroding landscapes and dynamically evolving drainage networks, as suggested before (Beven, 1996; Hasbargen and Paola, 2000; Hofer et al., 2012; Raff et al., 2003).

All simulations resulted in an underestimation of drainage density and erosion rill depth in comparison to rill network maps. On the other hand, a comparison of cumulative sediment discharge and approximations of sediment storage in the pond and alluvial fan suggests an overestimation of total sediment discharge: Kleeberg et al. (2010) estimated an accumulated sediment volume of 1280 m^3 until August 14, 2008, corresponding to a mean accumulation rate of 0.2 m a^{-1}. From another survey, Kleeberg (2011) determined that the accumulation rate decreased to about 0.1 m a^{-1} for the period from August 2008 to August 2010. Additional sediment was accumulated in the alluvial fans, which are not completely covered

by the simulation area of this study, so that part of the accumulation in the alluvial fans is part of the sediment discharge in simulation results. From differential elevation models, an accumulation of about 720 m^3 (1061 t) of sediment in alluvial fans until April 2009 was determined in Schneider et al. (2012). Compared with these estimates, simulated sediment discharge (Fig. 8.8) was clearly higher for all simulations. For most simulations, increasing sediment discharge was observed, which is in contrast to the reduction of pond sedimentation rates according to Kleeberg (2011). A comparison of volume change over the DEM and cumulative volumetric sediment discharge (Fig. 8.8 c) shows that the high simulated sediment discharge of 4900 m^3 is in a strong imbalance to the low net volume decrease over the catchment's surface of only 84 m^3. This strong imbalance suggests a misestimation of suspended sediment redistribution due to model errors. A high overestimation of sediment discharge is also suggested by the very high relations of sediment to water discharge (Fig. 8.8). High sediment discharge was mainly simulated for the particle size fractions for that suspended transport was simulated, while sediment discharge was considerably lower for the fractions transported as bedload (Fig. 8.8 c). Imbalances between volume change and volumetric sediment discharge were not observed for the simulation without transport in suspension. However, relations of simulated sediment to water discharge show a log-linear relation (Fig. 8.14), and relative temporal development of sediment discharge and sediment to water discharge relations seems to be plausible in relation to precipitation intensity and other boundary conditions.

The development of drainage density across the hillslope for different simulations (Fig. 8.6) and the development of elevation differences for the best scenario simulation (Fig. 8.10 a) show that the abstraction of the rill network observed in the Hühnerwasser catchment was underestimated by the simulations. While growth of the rill network was only observed un-

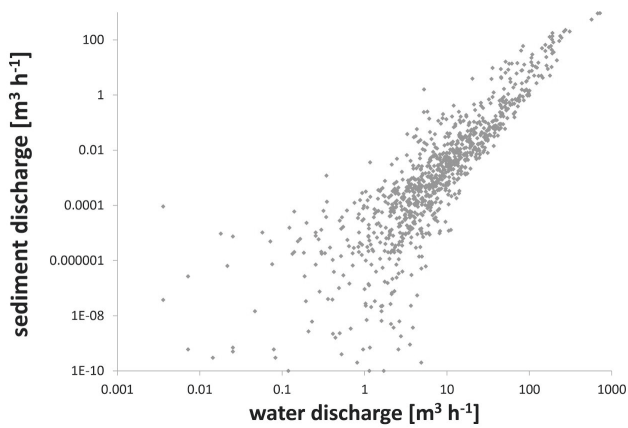

Figure 8.14: Relation of hourly values of simulated sediment discharge and simulated water discharge for the best scenario simulation with suspended sediment transport.

til 2007 in the catchment, proceeding headward growth of rills was simulated. Rill network abstraction in the catchment was suggested to be influenced by differing precipitation characteristics, internal network dynamics, and increasing vegetation influence (see Chapter 7). Effects of differing precipitation characteristic can be assumed to be sufficiently represented in the simulations, since the model time step is decreased to a very high resolution during precipitation events. Effects of network internal dynamics can be assumed to be generally represented; however might be underestimated because of the underestimation of rill depth in the simulations. Drainage density development along the slope for different vegetation parameter combinations (Fig. 8.6 b) shows that stabilization of erosion rills in the backslope area was also underestimated for the simulation with a higher vegetation shear resistance that resulted in high sedimentation in rills in the lower slope area. This discrepancy suggests that further mechanisms not represented in the CAESAR model are relevant for rill network contraction and stabilization in the backslope areas.

Scaling effects are a probable reason for the underestimation of drainage density. Results of the basic assessment of scaling effects show a higher simulated density of linear erosion features for increased resolution of the input DEM. Higher-resolution simulations for the subcatchment, especially using a 25 cm by 25 cm cell size, also resulted in high deposition at the subcatchment's downslope part, which counteracted the effect on drainage density because initial incisions were refilled in later phases of development. This observation suggests that the density of simulated rill networks could be increased by using an increased DEM resolution for the overall study area. However, increases to DEM resolution were not possible in this study because of computational limitations. The question if CAESAR is cell-size independent was raised by Coulthard et al. (2012), but scaling effects have rarely been approached in other studies. An effect of DEM resolution on the initiation of incisions can be assumed, as incisions with cross-sections below the grid cell size is not possible. For non-planar surfaces, increasing cell size implies that surface runoff is distributed over increasing cross-sections. Flow depth in areas of flow accumulation is therefore reduced, which in turn reduces sediment transport rates, flow velocity, and shear stress. DEM resolution could also affect soil erosion, which is affected by the cells' contributing area in CAESAR, since the spatial variability of contributing area values generally increases with increasing DEM resolution. These effects might, however, be only relevant for simulations in which the incision or stream cross-sections are smaller or only slightly exceeding DEM cell size, and might be of minor importance for simulations where flow channels are represented by more DEM cells.

Another probable reason for the underestimation of erosion rill depth and the overestimation of sediment discharge is an insufficient representation of sediment erosion, transport and deposition by the transport functions used in the model. Bed load sediment transport

equations that are based on excess shear stress are frequently used in rill and gully erosion models (Vanwalleghem et al., 2009). Istanbulluoglu et al. (2003) successfully applied sediment transport functions developed for rivers for gully erosion modeling, but showed that greater nonlinearities than represented in transport functions exist for fluvial erosion processes on steep slopes. Hillslope processes are represented by linear relations in CAESAR, but have been shown to be better represented by nonlinear transport relations (Martin, 2000). A correct representation of hillslope processes was not of central importance for the aims of this study, which focused on geomorphic development by fluvial erosion along rills and gullies; and on a very short period of development, during that mass movement processes do not considerably affect surface structures. However, results showed that different soil erosion rates considerably affected the density and geometry of erosion rills. Generally, process understanding and models of sediment redistribution are often regarded as insufficient, as sediment transport relations area mainly empirical or semi-empirical and not validated for differing site conditions and across scales (Gomez and Church, 1989). For the simulation in this study, sediment transport was calculated based on the Einstein equation, which was developed for sands and relatively low amounts of bed load, rather than based on the equation of Wilcock and Crowe (2003), which was developed for mixed sand and gravel sediments. However, both transport functions available in CAESAR were developed for coarser sediments than those of the Hühnerwasser catchment and for non-cohesive sediments. It needs to be considered that sediment redistribution is calculated based on the particle size distribution of the dried and sieved sediment; but that fine sediments in the Hühnerwasser catchment also occur aggregated to fragments of different sizes. From rill erosion experiments, Wirtz et al. (2013) concluded that most physically based models do not adequately represent rill erosion processes, as erosion rates in rills are affected by a combination and interaction of processes acting in different spatial and temporal resolution. Representation of erosion rill formation or fluvial channel initiation is also limited by the fact that transport functions were developed for equilibrium conditions and have not been evaluated for initial, non-equilibrium conditions. For the Hühnerwasser catchment, transport relations might furthermore be inadequate because of special technogenic mechanical characteristics of the initial sediment layer. Spatially varying sediment mechanical and hydraulic properties might have influenced the specific geometry of the erosion rill network (as discussed in Chapter 7).

Sediment mass balance development by sediment erosion and deposition is affected by the spatial distribution of bulk density. Effects of spatially varying bulk density could not be included in the simulations, as the CAESAR model does not allow for specifying bulk density values for DEM cells. The total volume of entrained sediment is computed in CAESAR based on a constant sediment density of 2250 kg m^{-3} and the reduction in elevation for

cells that are affected by erosion is calculated from this volume and from cell size. Elevation increase in cells affected by deposition is calculated based on the deposited volume and cell size. Therefore, porosity of the material is not considered in the model, which implies that the total eroded and deposited sediment volume is underestimated.

In most studies, an initial adjustment or 'spin-up' period was included in CAESAR simulations and was not included in the interpretation. The aims of including this adjustment period were to let particle size distribution and channel geometry develop to equilibrium conditions by removing initial roughness of the input DEM and sorting soil particle size distribution "across the catchment according to the topography and hydrology" (Hancock, 2009). This adjustment was mainly described to result from the removal of fine material from the simulation area and from the development of an armoring layer along the main flow paths (Hancock et al., 2011; Van De Wiel and Coulthard, 2010). For a simulation period of about 9000 years, Coulthard et al. (2002) used a spin-up period of 200 years, for which they observed an initial peak in sediment discharge. Hancock (2009) used a 44 year spin-up period for simulation period of 1000 years, but observed considerably high erosion rates during the first 20 - 30 years of this simulation period and concluded that a longer spin-up simulation should be carried out. For the Hühnerwasser catchment simulations, the model was applied without any adjustment period in order to deliberately include effects of initial, non-equilibrium conditions. Also Coulthard et al. (2012) do not describe a spin-up period for the simulation of soil erosion on experimental plots, and observed an initial peak in sediment discharge for the first year of development on these plots. In the simulations evaluated in the Hühnerwasser study, peak intensities of sediment discharge were increasing until the third year of the simulation period, and increasing fining rather than the development of a coarser sediment layer was observed along most parts of the flow paths. Similarly, Baetz (2010) observed considerably high volumes of sediment discharge, with daily sediment discharge exceeding daily water discharge by factors of up to 18, and a high fining of sediment in secondary flow channels for a simulation of braided river development over four years, although a spin-up simulation period was included in this study. In the study of Baetz (2010), this overestimation of sediment discharge was attributed to the an insufficient sorting of sediment during the adjustment period. Hancock (2009) pointed out that understanding of the adjustment period of LEMs is an area of ongoing research. Generally, a relative increase in peak intensities of sediment discharge in relation to water discharge could be interpreted as a result of an increasing continuity of surface flow resulting from the incision of linear flow paths, of the increasing concentration of surface flow in these flow paths, and of a step-wise transport of sediment from the lower slope areas to the alluvial fans and to discharge from the simulation area.

8.5.3 Effects of initial and boundary conditions

8.5.3.1 Roughness of the initial surface DEM

Results showed that the mapped rill network was best reproduced when an input DEM with a lowering of 5 cm along initial irregularities was used (Tables 8.3 and 8.4., Fig. 8.6 c). These simulations furthermore resulted in the simulation of relatively straight and parallel rills, as observed in the catchment, for the SW part of the slope. For the unmodified DEMs, relatively high drainage density had developed after the first 360 days of the simulation period, while for the DEM with initial structures, relatively low drainage density after this period and a rapid increase in the period between 360 and 630 days was observed. Simulations using the smoothed input DEM resulted in considerably low drainage densities for the first development period and in increasing drainage density along with the braiding of rills for later phases. Therefore, differences in surface structures decreased during later phases of the simulation period, although different development processes, i.e., a prevalent bifurcation at rill heads and tributary addition for higher initial roughness and a prevalent braiding along rills for lower roughness, dominated the evolution.

Effects of slightly different initial surface structures on developing drainage networks were also observed in simulations for soil erosion plots by Coulthard et al. (2012), who describes noticeable differences in sediment discharge between simulations for different plots with similar dimensions, and relate these differences to the unique drainage network patterns that developed for each plot. Several mechanisms causing nonlinear and complex behavior within a drainage network can influence the erosional response to precipitation influence, as described by Coulthard and Van die Wiel (2007) and Van die Wiel and Coulthard (2010). Clearly nonlinear relations of sediment discharge to water discharge were not observed in simulations for the Hühnerwasser catchment (see Fig. 8.14). The development of drainage density for the DEM with initial surface irregularities, however, indicates that these structures resulted in a decoupling of precipitation input and drainage density formation (Fig. 8.7 c and d): For these simulations, drainage density was very low after the first phase of development, during which isolated short incisions had formed, and highly increased in a next phase, in which these isolated incisions became connected to form rills. In contrast, drainage density was more constantly increasing in simulations using the unmodified and the smoothed DEM (Fig. 8.7 a, d). Although the drainage densities observed in the Hühnerwasser catchment considerably increased between the mapping dates in 2006 and 2007, the nonlinearity of this increase was less distinct than suggested by the simulations. This discrepancy most probably shows that the representation of the initial irregularities by reducing the elevations along the digitized irregularities does not sufficiently represent their actual structure and effects.

8.5.3.2 Precipitation characteristics

Results of the simulations using modifications of precipitation input data clearly show that differences in rainfall characteristics for specific years of development can result in different drainage network geometry. It was observed that higher drainage density resulted from a decreasing variability of hourly rainfall intensities within years, as compared with an increasing variability, i.e., the occurrence of high-intensity runoff events in the earliest development phase resulted in the formation of more erosion rills as compared with the occurrence of such events in later phases. This effect is consistent with the formulated hypothesis on precipitation variability effects and can, most probably, be attributed to the organization of flow paths as formulated in this hypothesis.

Furthermore, a considerably high drainage density in the lowest slope areas was observed for the unmodified precipitation record, which is not explained by the hypothesized effects. Higher drainage density in the lowest slope area, as compared with the unmodified precipitation simulation, was only observed for the simulation repeating the precipitation record with the lower annual precipitation (2006). Furthermore, all simulations for that the precipitation record of 2006 was placed at the beginning of the simulation period (i.e., the simulations with unmodified data, *var_inc* and 2006) resulted in relatively low drainage density in the backslope and relatively high density in the lowest slope areas. It can therefore, in addition to the initial hypothesis, be inferred that low precipitation during the very initial development phase supports a high concentration of drainage density to lower slope areas. This concentration most probably results from the restriction of incision to areas of highest relative flow accumulation during the phase with low precipitation, and from the addition of small tributaries to rills in these areas in later phases. In contrast, all simulations beginning with a year with higher total rainfall and high variance of hourly values (i.e., the years 2007 and 2009, and the simulations using reverse ordering, *var_inc*, 2007, and 2009) result in relatively high drainage density in the backslope areas, since rills are incised in areas of lower relative flow accumulation for the initial period and continue to function as preferential flow paths during later phases. According to these results, the actual distribution of drainage density in the Hühnerwasser catchment, as observed at the end of the study period considered in this work, can be related to the influence of relatively low precipitation in 2006, which favored the concentration of erosion rills to the lowest slope areas, and to the high-intensity events in 2007, which caused an increase in drainage density for all areas of the slope. All simulations with modified precipitation input data affirm that the main patterns of the rill network were formed in the first two years of development, while subsequent development periods were characterized by a further incision of existing rills or by the addition of tributaries in areas of highest drainage density. Considerable infilling

of existing rills was not observed, and existing rills were found to act as surface flow paths throughout the simulation period.

A sensitivity of channel network geometry to the peak hourly rainfall intensities was also shown in CAESAR simulations for a 200 year simulation period by Hancock and Coulthard (2012), who used rainfall data recorded in differing catchments in simulations for one DEM and showed channel stability for relatively high annual rainfall but low peak intensities and the formation of additional channels and higher erosion rates for lower annual rainfall with higher peak intensities. The results affirm temporal irregularity of precipitation and short-term peak intensities can have stronger effects on erosion rates and drainage network geometry than annual precipitation sums, as also suggested, e.g, by Wu et al. (2006).

8.6 Conclusions

Results affirm that the simulation of rill incision on an initially unrilled surface and the simulation of erosion patterns over a relatively short time period and for the scale of a small catchment with the CAESAR model are possible. The relatively good agreement between simulated and observed patterns of hydro-geomorphic development suggests that a fluvial erosion model with a basic representation of diffusive sediment erosion can allow for assessing the effects of specific boundary conditions on surface development. Limitations to the applicability of the CAESAR model for the initial phase of landform development on the scale of a small catchment are indicated by the underestimation of drainage density and the imbalance of sediment discharge and elevation change. Results of simulations with a higher-resolution DEM for a subcatchment suggest that the underestimation of drainage density is, at least to a certain extent, due to the limitations to resolution of the input elevation model. Reasons for the observed imbalances between sediment discharge and elevation change could not be revealed from the analysis of simulation results.

Simulation results affirm the hypotheses that initial morphologic irregularities and high-intensity precipitation events during the first two years of development have affected high drainage density in the Hühnerwasser catchment. Higher drainage density and therefore closer similarity to observed patterns was observed for a DEM including a representation of initial surface irregularities by reduced elevations along these structures. However, the slower rill formation for the first year of development observed for this DEM suggests that reducing elevations along the irregularities does not sufficiently represent their structure and effects on surface development. Results suggest that precipitation characteristics during the first years of development were formative for hydro-geomorphic structures in the catchment. Two effects of precipitation characteristics during the first years of development were observed:

1. High intensity runoff events that occured early in development resulted in higher drainage density as compared with high-intensity events later in development.

2. Low annual rainfall early in rainfall resulted in a clear differentiation into low drainage density in backslope and higher drainage density in lower slope areas.

Both effects can be attributed to an organization of surface flow towards those incisions that have once been formed, so that incisions emerged during the first precipitation events are maintained as flow paths during further development. Results furthermore affirmed that different hydro-geomorphic patterns established during the very initial development phase persist through surface development for differing initial and boundary conditions, although overall statistical characteristics of the drainage network become more similar.

Spatial variations of sediment properties were not considered in the simulations in this study, but could be integrated for further improved simulations. CAESAR allows for a specification of spatially varying particle size distributions, and spatially varying infiltration characteristics might possibly be integrated by implementing a grid representation of the spatial variation of sediment hydraulic conductivity, or by using spatially varying values for the TOPMODEL m parameter.

9 General Discussion

9.1 Methodological implications and limitations

9.1.1 Applications of a 3D model of catchment geometry and structure

The 3D volume model described in Chapter 4 has served as a basis for further work within the project on the development of a structure and process model for the Hühnerwasser catchment. The model had allowed for a quantification of the total initial sediment volume with an uncertainty of about 10 %; however, it did not describe the characteristic sediment heterogeneity of the catchment. The 3D spatial distribution of the sand fraction as shown in Chapter 4 was interpolated from sampling point data using Ordinary Kriging with a spherical variogram model (nugget = 0, sill =34.5 and range = 33 m, 33 m, and 1.9 m in x-, y-, and z-direction). However, the empirical variograms for the 3D-spatial variogram ellipsoids could hardly be described by variogram models, and a quantitative assessment of variogram model fit could not be carried out in the GOCAD environment. Papritz et al. (2011) showed that the identification of spatial auto-correlation patterns for sediment properties in the catchment is limited, most probably because of the characteristic technogenic structures. Therefore, a structure generator model was developed (Maurer et al. 2011b) that allows for the generation of spatially distributed sediment characteristics within spoil cones, based on mechanic rules of particle segregation during spoil dump transport and of dumping and compaction during dumping (Buczko et al., 2001). The geometry of the sediment body, as described in Chapter 4, was adopted for this study. The data generated for spoil cone cross sections were interpolated to the cells of the 3D volume model, and the volume model, in comparison to a quantification of the initially dumped sediment volume, was employed to assess the compaction of the sediment resulting from further steps of catchment construction. This model of 3D-spatially distributed sediment properties was used as a basis for the spatially-distributed description of substrate hydraulic properties based on pedotransfer functions (Maurer et al., 2011a).

Information combined in a 3D volume model can be used in integrated surface-subsurface hydrological models, which are commonly applied for the analysis of real catchments. A detailed representation of the lower boundary of the water storage layer can significantly improve hydrological modeling, since the geometry of this layer can significantly affect con-

nectivity of saturated zones and the generation of subsurface flow (Hofer et al., 2011; James et al., 2010). The representation of the clay layer representing the vertical boundary for seepage water in the Hühnerwasser catchment was used as an input dataset for hydrological modeling of the catchment (Hofer et al., 2011; Holländer et al., 2009; Hölzel et al., 2013). Spatially distributed information on substrate hydraulic properties can allow for describing relevant parameters for hydrological models, as demonstrated for the Hühnerwasser catchment by Hölzel et al. (2013). Vertical variations in sediment properties were shown to affect modeling results and were conceptualized in a number of approaches (Gascuel-Odoux et al., 2010; Zimmermann et al., 2013). The modeling of subsurface structures in GOCAD to generate spatially distributed input parameters that allowed for improved simulation results with a hydrologic model was also described by Gauthier et al. (2009). Parameters for surface and subsurface hydrological models are mainly discretized in orders of meters to hundreds of meters in the horizontal direction, while resolutions in the order of centimeters are commonly used in the vertical direction. Spatial discretization of information was shown to considerably affect model results (Sciuto and Diekkrueger, 2010). Furthermore, varying resolutions in the vertical direction can be employed to distinguish, e.g., higher variation of parameters in the unsaturated as compared with the saturated zone (Vogel and Ippisch, 2008). In relation to these approaches, horizontal resolution for the 3D model described in this work is relatively high, while vertical resolution is relatively low. A downscaling of cell sizes is generally allowed for in GOCAD, however, is limited by irregular cell geometry at the surface, subsurface and lateral boundaries of the model. A model consisting of regularly-shaped cells could allow for an adaptation of resolution for different purposes or for a stepwise analysis of hydrological model sensitivity to resolution, as suggested by Sciuto and Diekkrueger (2010); however, would imply losses in visualization quality. As an alternative to increasing the spatial resolution of 3D models, which is generally limited due to computational limitations, sub-grid scale parameterization methods have been suggested (Hutton et al., 2013).

The methods described for implementing a representation of sediment layers in a 3D volume model (Chapter 5) could be applied for soil landscape models that focus on dynamically evolving surfaces. Based on the different layers represented in the model, volumes of deposited sediment can be quantified with an accuracy that is determined by the accuracy of the input elevation models. Furthermore, information on the development of elevation over time for specific locations could be assigned to the model cells. This could, e.g., allow for the depiction of infilled drainage lines in a landscape, which can considerably affect drainage network formation although they are not reflected in surface morphology (Jones, 1987). Parameters assembled in a 3D model can be employed as covariates for the statistical prediction of other variables, e.g., soil properties or classes. The establishment of such

models can therefore contribute to an improved spatial prediction of soil characteristics by accumulating better and more soil data, as suggested by Minasny and McBratney (2007). Further differentiation into model regions or process domains, e.g., into the saturated and unsaturated zone or into areas of different root penetration depth can be made within the volume model, as suggested by Gerke et al. (2013). Analysis of information stored in the cells of the model can then be carried out layer- or region-specific. As described by Mendonca Santos et al. (2000) and Cosandey et al. (2003), 3D volume models could also be used for improved soil horizon modeling in areas of overlapping or heterogeneous horizon geometry, which cannot be sufficiently characterized by soil classification approaches, As described by Delarue et al. (2009), a 3D representation of soil horizons can allow for deducing conceptual models on pedogenic processes based on the improved visualization of horizon geometry.

9.1.2 Technical aspects of 3D catchment modeling with CAD and GIS

In order to assess the possibilities for employing 3D landscape models as constructed in this work in studies on geomorphologic or ecosystem development, technical aspects of model construction and applicability need to be considered.

Although attempts for the standardization of geo-data are made, there is still a high heterogeneity in data formats for geospatial volume and surface models (Breunig and Zlatanova, 2011). Different software applications requiring different data and file formats were necessary for the construction and analysis of 2D and 3D surface and sediment body models in this study. The major parts of the work were carried out with GOCAD (used for the construction of the 3D volume model), SAGA (employed for morphometric analyses) and ArcGIS (used for mapping and analysis of the rill network). Simulations in CAESAR were based on gridded elevation models processed in SAGA. While the standard representation of surface models in GOCAD was based on TIN models, gridded elevation models were required to carry out GIS-based morphometric analyses. The volume models constructed in GOCAD could not be viewed or processed in other programs. Therefore, the transfer of data between the applications frequently required transformations between point, TIN, and gridded data. Data processing and analyses using GOCAD in combination with GIS was approached in some studies (Bistacchi et al., 2011; Zanchi et al., 2009), however, GOCAD was mainly used for visualization in these studies. Applications of GOCAD in combination with geophysical software applications were described more frequently (Kostic et al., 2005; Lang et al., 2012; Schmidt and Götze, 1999), since similar data formats are supported by these applications and by GOCAD. GOCAD has also been used to construct elevation models directly from laser scanning- or photogrammetry-based point clouds (Bistacchi et al., 2011; Schober and Exner, 2011). In comparison to transferring gridded data to TIN

models, this approach allows for making better use from the possibility to adapt the node spacing of TIN models to the modeled morphology, i.e., to reduce node spacing in areas of little morphologic variation. The geometry of surfaces can be modified by a number of functions, e.g., using the Discrete Smooth Interpolation (Mallet, 1989), which were not employed in this work. The application of these functions in studies aiming at a quantitative analysis of datasets has not been described, but modifications were mainly applied for improved visualization of surface models (Bistacchi et al., 2011). Most studies using GOCAD aimed at the modeling of complex surface or subsurface geometry, making use of the possibility to depict multiple elevation values for one location, e.g., for fold surfaces (Bistacchi et al., 2008) or vertical outcrop surfaces (Schober and Exner, 2011). The possibilities for the modeling of complex geometry and overhanging structures is a clear advantage of 'true' 3D surface modeling in comparison to the representation of surfaces in gridded models, as implemented in most GIS systems. This possibility is rarely necessary for the modeling of surfaces of unconsolidated sediment bodies; however, overhanging structures can occur at the heads or walls of erosion rills and gullies.

Adaptations to the geometry of a 3D volume model constructed as described in this work are hardly possible, so that an own model for each specific stage of development needs to be constructed. Alms et al. (1998) describe an approach to the four-dimensional modeling of geologic objects, which allows to create models for any specified time step by interpolating between two models of a series of previously constructed 3D models. To implement such an approach for the representation of erosion-affected sediment surfaces would require the integration of a model of the spatial distribution of erosion and deposition intensity in the interpolation algorithm. GOCAD allows for calculations based on information stored in the cells of 3D models; however, the possibilities to implement more complex algorithms, e.g., for flow routing, are limited. In this work, mainly quantitative data were assigned to the cells of the 3D volume model. The database management functions in GOCAD are limited in comparison to most other GIS systems, e.g., it is not possible to assign qualitative information, as soil color or dating results, to model cells, which was pointed out as a disadvantage in comparison with other GIS systems by Losier et al. (2007). The modification of surface elevation models in order to obtain boundary surfaces between sediment layers was described using modules of the GOCAD Suite application in Chapter 5, but could also be implemented in other programs by modifying elevation values based on relational and logical operators. Information stored in the cells of the 3D volume model are assigned to the center coordinates of these cells in GOCAD, so that this information could also be represented in point cloud data or a series of gridded elevation models in other programs. Other common GIS programs, however, hardly allow for a volume quantification of irregularly shaped cells in volume models, and provide limited possibilities for 3D visualization, as compared with GOCAD.

9.1.3 Uncertainty, resolution and parameter selection in the analysis of initial landform development using remote-sensing data

DEM evaluation and analysis in this work was carried out for available datasets from airborne laser scanning and digital photogrammetry, which had been recorded for mine surveying. The parameters of the measurement campaigns were therefore not adapted to the requirements of the study on initial landform development. Several studies showed that more precise and higher resolution elevation data can be obtained by digital photogrammetry when measurement parameters, e.g., the altitude from that the datasets are recorded, are adapted (Bird et al., 2010; Lane et al., 2000; Marzolff and Poesen, 2009). However, adapting measurement campaigns for a higher resolution and accuracy of resulting DEMs results in higher measurement and processing times and higher amounts of data (Aber et al., 2010). Most studies using ALS data are based on datasets that are available from major measurement campaigns, which usually record datasets with a resolution and accuracy similar to that of the dataset described in this work (Cazorzi et al., 2013; James et al., 2007). Elevation data recording by ALS was specifically carried out for gully mapping by Baruch and Filin (2011), who recorded elevation data with a resolution of 4 data points per square meter and a vertical accuracy of ± 0.1 m. Similar or smaller vertical uncertainties were obtained in other studies that recorded ALS data for geomorphologic analyses (Joerg et al., 2012; Perroy et al., 2010). Terrestrial laser scanning allows for recording elevation data in high resolution and with high accuracy, depending on the area that is recorded from one measurement location. TLS data accuracy was shown to be mainly affected by data processing methods and spatial aggregation, with a decreasing accuracy for decreasing resolution of the generated datasets (Barneveld et al., 2013). The measurement campaigns for obtaining the TLS elevation data used in this study were designed in a way that allowed for a resolution of at least 0.1 m by 0.1 m for the original dataset (Biber et al., 2013), and were aggregated to the resolution of 0.5 m by 0.5 m during data processing. This aggregation allowed for filtering the measured data so that only the lowest elevation value, which most probably represents the ground surface, was maintained for each DEM cell. Furthermore, the horizontal DEM resolution was limited by computational capacity for the relatively large area of the Hühnerwasser catchment.

Uncertainty of the DEMs available for the first years of development for the Hühnerwasser catchment was high in relation to the changes in surface elevation that were analysed in this work. DEMs were processed by referencing to d-GPS data and by modifications based on hydro-geomorphic principles and plausibility rules in rill and interrill areas (see Appendix A). Evaluation of these modifications by comparison to reference data available for one of the DEMs (Chapter 6) suggested that DEM quality was improved by these modifications. However, since sufficient reference data were not available for all the DEMs, the effect on

DEM uncertainty could not be quantified. Therefore, the uncertainty in DEM difference models and sediment volume and mass balances was assessed using error propagation rules based on the uncertainty of the original photogrammetry-based elevation datasets (σ_z = 0.147), which was determined from camera parameters and flight height based on established rules (Luhmann, 2000) by Dominik (2007). More detailed evaluations of effects of DEM modifications were described for radar remote sensing elevation data filtered using noise removal filters by Stevenson et al. (2010) and Gaussian and threshold slope filters by Milledge et al. (2009), who showed that these processing steps could improve data precision by over 50 %. Based on general DEM uncertainty, an uncertainty for elevation differences computed from a pair of DEMs of σ_d = 0.21 m was calculated. This quantification and the delineation of areas with significant change as attempted in this work (see Chapters 6 and 7) could be improved by using methods of spatially distributed error and error propagation modeling, as described by Joerg et al. (2012), Erdoğan (2010), and Wheaton et al. (2010). Nevertheless, elevation change that occurred in the catchment exceeds DEM uncertainty only in the areas of high-intensity erosion and sedimentation, so that the change in elevation or sediment volume could not be quantified significantly for the overall catchment area. Most other studies that attempted sediment budgeting based on pairs of elevation models have recorded DEMs with a considerable high precision by d-GPS, close-range photogrammetry (Marzolff et al., 2011) or TLS for the quantification of relatively small elevation change (Brasington and Smart, 2003; Marzolff et al., 2011; Wheaton et al., 2010) or have aimed at the quantification of larger elevation changes (Day et al., 2012; James et al., 2012; Schiefer and Gilbert, 2007). Effects of DEM uncertainty on the computation of morphometric parameters were discussed in Chapter 7. Generally, the literature suggests that DEM errors have higher effects on local morphometric parameters (e.g., local slope), but smaller effects on parameters that are computed over larger areas (e.g., flow patterns), and that morphologically more complex areas require higher DEM resolution for a sufficient characterization of morphology (Cavazzi et al., 2013; Thompson et al., 2001).

Results of morphometric analyses presented in this work affirm that, besides elevation errors and uncertainty, the horizontal resolution of DEMs affects the suitability of morphometric parameters to describe landform patterns; and that higher resolution is not always better-suited but often provides too much detail, as stated by Cavazzi et al. (2013). The comparison of slope maps and rill network patterns (Chapter 7) illustrates this resolution dependence for the example of the suitability of local slopes to depict areas of rill formation: Because local slope maps based on DEMs with 1 m resolution capture small-scale variation, very high values occur at rill walls and very low values occur within rills for broader erosion rills. A combined analysis of local slope maps determined from DEMs with resolutions of 1 m by 1 m and 5 m by 5 m allowed for an improved estimation of areas dissected by rills, as

compared with slope maps from the higher-resolution DEMs only. Cavazzi et al. (2013) conclude that the best appropriate DEM resolution for specific parameters cannot be defined universally, but is dependent on terrain characteristics, so that parameters based on DEMs of differing resolutions should be computed and compared. In this work, DEMs were resampled from higher to lower resolution to derive the slope values for different resolution. Besides a resampling, different window sizes (e.g., a 3 cell by 3 cell window and a 7 cell by 7 cell window) could be used for the computation of morphometric parameters in different resolution. Possibilities to adapt cell size for parameter computation are limited in most GIS systems. However, adaptations of pixel size and window size cannot be used analogously, as pointed out by Cavazzi et al. (2013), who showed that variability of slope values decreases more rapidly with increasing pixel size as compared with increasing window size.

Morphometric analysis in this study was mainly based on the parameters slope and Contributing Area and the Stream Power Index, which is determined by combining both parameters. Further morphometric indices, e.g., the Connectivity Index of Borselli et al. (2008), were computed based on these basic measures. In addition to these parameters, slope curvature was frequently applied to depict patterns of relative flow acceleration or dissipation and moisture, vegetation or sediment concentration (see Florinsky, 1998). Curvature maps for the Hühnerwasser catchment were evaluated in the course of this study, but were not included in the analyses, because curvature as the second derivative of elevation shows relatively high spatial variations in the absence of clearly defined, continuous morphological structures. Furthermore, the relative elevation and the aspect as well as solar radiation indices derived from these parameters were often applied in soil-landscape analyses as surrogates for, e.g., plant productivity, rates of pedogenic processes or soil properties such as organic carbon content (see Thompson et al., 2012). These parameters were not analysed in this study because they mainly affect longer-term ecosystem and soil development and because they do not considerably vary over the slope of the Hühnerwasser catchment.

9.1.4 Implications for surface and drainage network analysis from remotely-sensed data

The evaluation of DEMs generated by different remote sensing methods (Chapter 6) allowed for a description of characteristic inaccuracy and artefacts in elevation data in relation to surface structures. The possibilities for this evaluation are hardly given in other studies, which are usually based on only one source of remote-sensing data and for which morphology and vegetation cover are hardly as well known. Methods and results are transferable to other studies that require to assess the quality of photogrammetry-, ALS-, or TLS-based DEMs for areas with relatively sparse vegetation cover and networks of erosion rills or relatively small gullies, i.e., for many agricultural areas or semi-arid environments.

Evaluation of photogrammetry-based datasets of different resolutions suggested that higher-resolution data better approximated depth of erosion rills but showed higher general inaccuracy or 'noise' in interrill areas, while lower-resolution data underestimated rill depths but better represented the relatively even interrill areas. Based on this evaluation, it was shown how improved DEMs could be generated by photogrammetry-based elevation data derived from one dataset of stereophotographs in two resolutions, based on the previously evaluated strengths and weaknesses of the different resolutions. This method is relatively labor-intensive, so that data acquisition with more suitable methods or photogrammetric survey flights from lower altitudes are most probably to be preferred when elevation data acquisition can still be planned. However, the described processing method could be applied for an improved use of available stereo-photograph pairs for past stages of surface development, e.g., for historical aerial photographs as used by Schiefer and Gilbert (2007) or Betts et al. (2003).

The combined analysis of time series of rill network maps derived from aerial photographs and morphometric parameters derived from DEMs is considered a viable method for drainage network evolution analysis, especially for smaller scale studies that focus on the dynamic development of drainage network structures. In most laboratory flume or plot studies, drainage networks are delimited and their evolution is analysed either based on qualitative descriptions or on mapping from photographs (Brunton and Bryan, 2000; Bryan and Rockwell, 1998; Pelletier, 2003) or on digital elevation data, using threshold values of morphometric parameters, mainly the contributing area (Berger et al., 2010; Gómez et al., 2003; Gordon et al., 2012; Rieke-Zapp and Nearing, 2005). Also studies for larger areas in natural systems have used a delineation of rill networks from threshold values of morphometric parameters or a combination of a definition of channel heads based on morphometric thresholds and a tracing of flow paths in downslope direction (Passalacqua et al., 2010; Pelletier, 2013). Drainage networks have also been delineated based on mapping from aerial photographs (Ritter and Gardner, 1993), often supplemented by field mapping (Bowman et al., 2011; Seeger et al., 2009). Raff et al. (2003) noted that drainage network extraction from DEMs often implies an a priori definition of drainage density, and found lower drainage densities than expected from morphology in a mapping of physically present erosion channels. Similarly, the results of this work (Chapter 7) show that areas delimited by threshold values of morphometric parameters do not necessarily correspond to those areas where rills or gullies as a morphological form are developed. Furthermore, those areas where rills or gullies are developed morphologically do not necessarily correspond to those areas where active erosion over a certain timespan takes place, but can also be remnants of previous phases of drainage network evolution. A critical comparison of 1) maps of drainage channels as morphological forms, 2) maps of drainage channels in which active redistribution of

sediment takes place, and 3) morphometric parameters derived from elevation data allows for a region-specific analysis of morphometry and for the detection of structure-process interactions in drainage network evolution.

9.2 Integrative interpretation and discussion of results

9.2.1 Questions of scaling and transferability

In this work, hydro-geomorphic surface development was analysed for a small, 6 ha hydrological catchment with a sediment thickness of up to about 4 m. Observations were thus made on a scale that is between the scale of studies on smaller experimental plots or in larger natural areas. A comparability of the results to those of other studies can not necessarily be assumed.

It was presumed in a number of studies that results from small-scale experiments on landscape development can be transferred to larger scales (see Paola et al., 2009). The assumption of similarity across scales was especially made and discussed for drainage network development. Jones (1987) emphasized that although the term 'drainage networks' is often used synonymously to 'river networks', drainage networks off all scales, i.e., from the scale of soil pores to that of river networks, are governed by the effects of a linear concentration of flow. Several studies have shown similarities of drainage networks of runoff on plots to river networks (Helming et al., 1999) and similarity of rill networks and river networks (see Gómez et al., 2003). Also Raff et al. (2003) stated "that micro-erosion channels, rills, gullies and rivers are functions of the same scale-invariant process of drainage network development", and showed that the geometry of natural erosion channel networks resembles that of larger river networks.

On the other hand, several differences between rill or gully and river networks need to be considered. As Lawrence (1996) notes in a discussion of the laboratory experiments of Schumm et al. (1987) and Parker (1977), the **relation of diffusive to advective** sediment transport processes is decreasing with scale, so that diffusive transport processes are usually dominant in experiments as compared with larger areas. **Flow hydraulic characteristics** can differ significantly for channels of different scales due to different effects of channel geometry and roughness. While some studies have suggested effects of local slope and sediment characteristics on flow hydraulics (e.g., Abrahams et al., 1996), other studies suggested that flow velocity in rills can be independent of the slope (Govers, 1992; Nearing et al., 1997). Wirtz et al. (2012) demonstrated that rill erosion processes are still poorly understood and are affected by complex interactions of substrate properties and rill geometry. Further differences in the hydraulic properties and development of erosion rill and river networks arise

from the fact that most rill or gully networks are dominated by **ephemeral flow**, while most river networks are characterized by continuous flow conditions. Gilley et al. (1990) showed that effects of hydraulic roughness on hydraulic resistance decrease with increasing flow depth, which implies that highly varying flow depths further limit the possibility to relate sediment transport in rills to general network characteristics. The ephemeral nature of flow in rills and gullies can furthermore result in a development of **substrate hydraulic and mechanical properties** that differ considerably from that in beds of perennial stream because of processes of pedogenesis acting during the dry periods. It can further lead to complex **interactions of fluvial erosion processes** in periods of high flow and **processes of mass wasting and diffusive erosion** affecting rill geometry in dry periods; and to interactions between fluvial erosion and stabilization by vegetation cover development in dry periods. **Vegetation** has been shown to affect drainage network development across a wide range of scales (Gurnell, 2013); however, effects cannot necessarily be transferred across scales (Phillips, 1995). As shear stress increases with increasing flow depth in larger drainage networks, vegetation effects become restricted to the influence of species with higher shear resistance and tolerance for immersion under flowing water. The hydrological and geomorphic effects of vegetation are mainly controlled by the critical shear stress and the roughness of the vegetation cover, its rooting depth and its effects on infiltration, and by the growth rates and thus the time spans needed for the development of an erosion-resistant vegetation cover; and can markedly differ between plant communities (Abrahams et al., 1995; Collins et al., 2004).

In addition to general questions of scaling, the **subsurface and surface geometry** of the sediment body in the Hühnerwasser catchment can have resulted in specific patterns of surface development that are not transferable to other sites. Transferability of observations on drainage network development in the Hühnerwasser catchment might be limited because of the characteristic **technogenic surface and subsurface structures**, which can affect surface and subsurface flow (as discussed in this work and by Hölzel et al. (2013)) and can thus result in different patterns of hydro-geomorphic development as compared with sites with sediment structures resulting from natural sediment deposition processes or a different anisotropy of technogenic structures in relation to the main drainage direction. Hydro-geomorphic patterns in the catchment are furthermore influenced by catchment size and geometry, the thickness of the water storage layer, and the geometry of the underlying bedrock or vertical barrier for seepage water. In the Hühnerwasser catchment, unique flow patterns might result from the fact that the exact catchment area was pre-defined by the delineation with ramparts, so that a re-orientation of erosion rills to the side slopes of the catchment was restricted. Flow patterns are also affected by the specific elongated shape of the catchment area, and surface flow is affected by the specific shaping of the surface, as further discussed

in Chapter 9.3. Unique patterns of subsurface flow can result from the specific geometry of the clay liner in the lower slope areas, where the clay wall perpendicular to the slope concentrates subsurface flow towards the center of the slope and retards subsurface flow to the lowest slope areas, as shown by Hofer et al. (2011).

9.2.2 Processes of initial landform development in the Hühnerwasser catchment

Observations in the Hühnerwasser catchment showed that linear erosion resulting from concentrated surface flow was the dominant process affecting the development of surface morphology during the initial development period (Elmer et al., 2013; Gerwin et al., 2009b; Gerwin et al., 2011; Schaaf et al., 2012). The dominance of processes of **fluvial sediment redistribution** in the formation of the drainage network is affirmed by the relatively good agreement of observed patterns to patterns resulting from simulations with a LEM that mainly represents fluvial processes. Simulations with the Wind Erosion Prediction System (WEPS) by Maurer and Gerke (2011) suggested effects of **aeolian sediment redistribution** on the catchment's sediment mass balance for the first years of development. Maurer and Gerke (2011) also described several field observations of effects of aeolian erosion and sedimentation, including patchy accumulations of wind-blown sediments, and aeolian ripple structures of such accumulations; and suggested that interaction effects between wind and water emerged from the sedimentation of wind-blown sediments in wind-sheltered areas in erosion rills. However, major effects of aeolian sediment redistribution on the formation of drainage network patterns are not assumable, since the observed wind erosion intensity was most probably not sufficient to completely infill erosion rills and since sediment accumulated in rills as a result of wind erosion can be expected to be relatively fine and loosely bedded and thus susceptible to re-entrainment by water.

Effects of **diffusive processes** of sediment redistribution could not be assessed in the DEM time series analyses. However, sediment erosion and deposition by diffusive processes for some areas of the slope was suggested by field observations, and was described from observations for specific locations by Badorreck et al. (2013) and Biemelt et al. (2011). The relatively dense spacing of erosion rills and the relatively low width and steep slopes of most rills observed especially for the first years of development suggest a low intensity of diffusive erosion in the interrill areas. The landscape evolution model simulations described in Chapter 8 resulted in patterns of low-intensity alternating elevation decrease and increase distributed over all areas of the slope (see Fig. 8.10), which are resulting from diffusive erosion processes simulated by a constant rate in the model. LEM simulations with differing rates for this representation of diffusive soil erosion processes resulted in considerably different geometry of simulated linear incisions (see Tables 8.6 and 8.7), which suggests that diffusive sediment redistribution has occurred and affected drainage network development

in the catchment; and that lower soil erosion would have resulted in narrower and deeper rills, while higher soil erosion would have resulted in broader, shallower and less connected linear incisions. The actual interactions of diffusive and advective erosion by water, however, need to be assumed to be more complex than represented in the model. Diffusive erosion by water is not represented in runoff-event-based resolution in the CAESAR model, but is simulated for daily time steps and depending on the drainage area of a model cell. Additional effects might also result from seasonal variations in the relative intensities of diffusive and advective processes, which can considerably affect drainage network development, as described by Bryan (2000). Furthermore, the relation of advective to diffusive processes of water erosion can be influenced by effects of structural and biological soil crusts, which can affect the generation and routing of surface runoff by several mechanisms that were assumed to occur on the Hühnerwasser catchment but that are not yet understood (Badorreck et al., 2013; Fischer et al., 2010; Spröte et al., 2010). **Groundwater sapping** occurred for the rills in the lowest slope area of the Hühnerwasser catchment, beginning with the state of development when rill incision in this area had encountered the rising groundwater table. The emergence of effects of groundwater sapping on drainage network development in lower slope areas after a certain time of development can affect drainage network development, as conceptualized by Dunne (1980). Because of the relatively low base flow in these rills and because these effects emerged only after the major flow patterns had developed, the effects on drainage network development are considered to be relatively small (see the discussion in Chapter 7). Field observations, the monitoring of parts of the rill network with a web cam (Biemelt and Nenov, 2010) and a photographic documentation of rill geometry development for specific parts of the network (Räpple et al., 2010) suggested that rill geometry development was affected by **mass wasting processes**, e.g., by bank failures following undercutting of the rill walls. These processes were observed along the central erosion rill and in the downslope parts of the major rills. They most probably contributed to the widening of these rills as observed during the later development phases analysed in this work (see Fig. 4.4, Table 4.2), as suggested by changes in rill geometry documented in daily web cam images (Fig. 9.1).

The elevation of the catchment's surface could also have been affected by processes of **subsidence** of the not yet consolidated mine spoil material underlying the clay and water storage layer. Subsidence can affect the total catchment area or cause local decreases in elevation. Effects of subsidence on the quantification of mass balances were discussed in Chapters 4 and 6. Locally concentrated subsidence could affect rill network development by modifying the rill slope and thus the erosion susceptibility at specific locations of the network during its development; and subsidence around the catchment's border could result in a reduction of the surface catchment area and thus of the drainage area of erosion rills. Repeated record-

ing of the elevations of the monitoring points in the 20 m by 20 m grid in the catchment indicates elevation change not attributable to linear erosion for some of these points (Fig. 9.2); however, it cannot be distinguished if these points were affected by diffusive erosion processes or lowering due to subsidence.

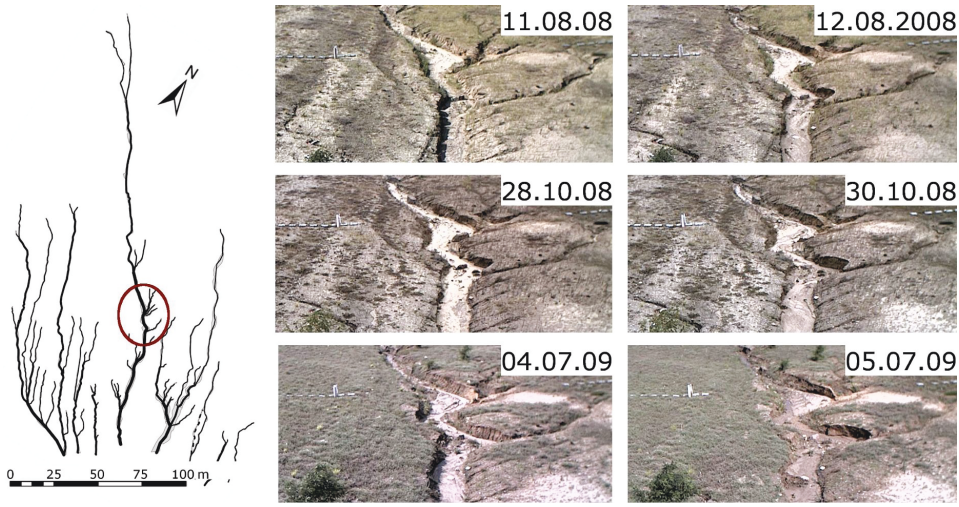

Figure 9.1: Indications of rill widening by mass wasting processes for a part of the central erosion rill recorded in webcam images (http://www.tu-cottbus.de/projekte/de/ecosystem/webcam.html). Left: the approximate location of the area depicted in the images, shown in the rill network map for July 1st, 2009 (see Fig. 7.4). Right: exemplary image pairs for August and October 2008 and July 2009, showing major changes in the geometry of the right part of the central erosion rill.

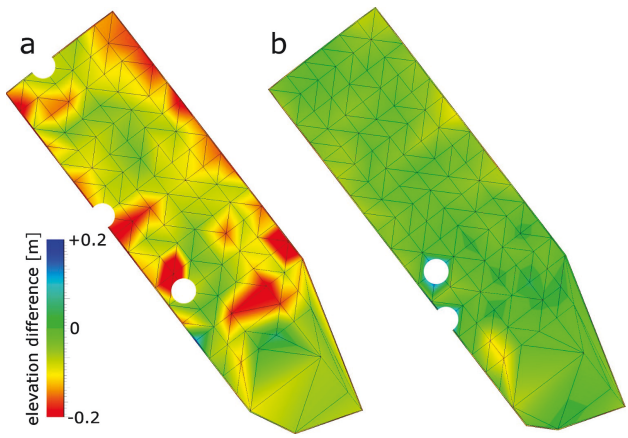

Figure 9.2: Elevation differences between d-GPS measurements for monitoring points, for the measurements of a) 10.08.2008 and 10.11.2009, and b) 10.11.2009 and 22.04.2010. Negative values denote a decrease and positive values denote an increase in measured elevation in the time period. Measurement points are at the nodes of the mesh depicted in the map, values for the area between the measurement points are interpolated. White circles mark raster points that are known to have be moved in their location (Rossen Nenov, personal communication, 11.11.2009 and 26.04.2010).

9.2.3 Patterns of hydro-geomorphic surface development in the Hühnerwasser catchment and effects of initial and boundary conditions

The analysis of DEM and aerial photograph time series (Chapter 7) showed that processes of erosion by concentrated surface flow, affected by changing boundary conditions and internal feedbacks, resulted in growth and subsequent contraction of the erosion rill network. The observed development of network geometry and surface geometry towards increased connectivity agrees with most other experiments. Effects of **overall initial morphology and small-scale surface irregularities** were assumed to have affected rill network development, as suggested by comparisons of maps of morphometric parameters and of aerial photographs of initial surface irregularities remaining from the construction works with the mapped erosion rill network development stages (see Fig. 7.17). The strong influence of initial morphology was affirmed by LEM simulations, which reproduced the spatial distribution of major erosion rills and allowed for an improved simulation of rill network patterns when elevations along the initial irregularities observed in the photographs were lowered. Simulation results affirm that overall morphology primarily controlled the location of major erosion rills, but that the small-scale irregularities resulted in slightly modified angles of the erosion rills in relation to the overall slope direction and in closer spacing and higher parallelism of the rills on the SW part of the catchment. In accordance to this interpretation, Hofer et al. (2012), based on two approaches of modeling rill network development in the catchment, concluded that the initial topography was the key factor that determined the location of major rills in the catchment. As further described in Chapter 7, the erosion rills in the Hühnerwasser catchment were initiated at different areas of the slope. This observation is different to those described in other experimental and modeling studies and conceptual approaches, which emphasize a dominant effect of headward erosion at knickpoints on drainage network development. The dominance of headward rill growth in many laboratory experiments, however, can be related to the external forcing by a very low base level set at the beginning of experiments or by the repeated lowering of the base level that is applied in many experiments, as also supposed by Gordon et al. (2012). In relation to the reconstruction of network development from remotely-sensed data, a clearer concentration of rill initiation to the lower slope areas was observed in LEM simulations, however, these simulations also showed the formation of isolated linear incisions and their subsequent connection to the drainage network (Chapter 8). This indicates that the formation of these incisions is not only controlled by spatially varying sediment erodibility and infiltration characteristics, which are not represented in the simulations, but is at least to a certain extent affected by the initial morphology. The fact that these effects were not observable in simulations for an initial surface with reduced roughness allows for the assumption that effects of general surface roughness, in addition to the linear technogenic structures, con-

tributed to the initiation of rill incision in upper slope areas. Experiments (Savat and De Ploey, 1982) have shown that rills develop more rapidly for surfaces with higher roughness. However, it has also been shown that rills can be initiated without the effects of initial surface irregularities by a emergence of convergent flow from circulations in sheet flow (Moss et al., 1982).

The development of the rills' **cross-sectional geometry** could not be reconstructed for time intervals because rill depths could not be quantified with sufficient accuracy from differential elevation models. However, the high-resolution aerial photographs allowed for mapping rill widths (see Chapter 7), and field observations and a spatially-distributed quantification of rill depths for September 2010 allow for a basic characterization of rill depths. While rills were relatively shallow and broad in September 2006, they became straighter and more deeply incised until 2007. Until 2008 and 2009, no considerable changes in the cross-sectional geometry of smaller rills were observed, while the central erosion rill and its main tributaries developed towards a wider cross-section and a higher sinuosity. This was, as suggested by field observations and photographic documentation, to a high extent due to major bank failures at the rill walls.

Drainage network development through **growth and subsequent contraction** is described in the conceptual model of Glock (1931). Drainage network contraction after a phase of headward growth of channels was also described for the experiments of Parker (1977) and was observed to be mainly due to rearrangement of the network and a shift of channels in this study. Generally, drainage network contraction during longer-term network development is mainly related to effects of micro-piracy and cross-grading (Horton, 1945); while for the initial period of network development in the Hühnerwasser catchment a reduction of the area of active erosion by stabilization of peripheral and upslope sections of the erosion rills was observed. Although LEM simulations included a representation of most of the effects that were discussed as potential drivers for the observed reduction of the actively eroding area (i.e., a concentration of flow accumulation to the central part of the stream network, effects of increasing vegetation cover and decreasing peak precipitation intensity); ongoing headward growth of the network was observed in the simulation results. This indicates that the development was affected by boundary conditions that are not or not sufficiently represented in the model. The strong increase of **vegetation cover** in the catchment over the first years of development has certainly contributed to the stabilization of parts of the rill network and has, furthermore, most probably affected the geometry of specific rills. Aerial photographs show a clear concentration of vegetation colonization within the rill areas, which, as suggested by Elmer et al. (2013), most probably results from higher moisture within these areas or sediment structure of the stream bed. The available datasets do not allow distinguishing whether the stabilization of these areas was due to vegetation

cover development or if vegetation could colonize these areas after a decrease of flow and shear stress in the rills that was due to reduced surface flow. Both effects most probably affected the co-evolution of vegetation and hydro-geomorphic patterns. It can be assumed that the reduction of the eroding rill area was affected by a decrease in overland flow due to increased infiltration capacity of the sediment. Vegetation, besides stabilizing the sediment, has most probably indirectly affected sediment erosion by increasing infiltration and buffering precipitation by leaf interception and therefore decreasing the intensities of fast surface runoff. Furthermore, an increase in infiltration over time with soil structure formation, the development of preferential flow paths in the sediment affected by soil fauna (Badorreck et al., 2012) and changes in biological soil crust cover from a dominance of crusts limiting infiltration to a dominance of crusts enhancing infiltration (Fischer et al.; Spröte et al., 2010) can be assumed. These effects would lead to lower generation of fast runoff for similar precipitation characteristics over time. This hypothesis is affirmed by a comparison of precipitation rates, pond inflow data and discharge simulated with the CAESAR landscape evolution model (Fig. 8.4c). Peak pond-inflow values decrease from 2007 to 2008 and 2009, with similar peak precipitation intensities for 2008 and 2009. However, simulated peak discharge increases from 2007 to 2008 and 2009, and clearly overestimates pond inflow, while an underestimation of pond inflow prevails for 2006 and 2007.

A comparison of meteorological monitoring data and rill network geometry development (Chapter 7) suggested that the **meteorological conditions** in 2007, when high-intensity rainstorms alternated with dry periods in spring and early summer, where considerably favorable for the formation of the relatively dense erosion rill network. LEM simulations that used different modifications of precipitation records affirmed that higher drainage density can develop when higher peak precipitation intensities occur during the first two development years, as compared with scenarios where such events occur in later development phases. Because effects of overall increasing surface runoff due to increasing infiltration are not represented by the LEM, this effect can be explained by an interaction of precipitation intensity and morphology. LEM simulations further suggest that the concentration of high drainage density to the lower slope areas in the catchment was affected by the relatively low precipitation intensities in 2006, which limited rill initiation to the areas of highest relative flow accumulation. Both the analysis of rill network maps and the analysis of morphometric patterns suggested that the period of rill network growth, as observed until 2007, was formative for runoff and erosion patterns in the catchment. Model simulations affirmed that those flow paths that had once been subject to incision prevailed as major flow paths in subsequent runoff events. Results of rill network mapping, aerial photographs and field observations show that differences in the rills' cross-sectional geometry, which can be assumed to be affected by the initial sediment properties, are decreasing over time, but

generally persist through network development, although overall network parameters are becoming increasingly similar. Based on the results of laser scanner measurements, Schaaf et al. (2012) affirmed that rills remained narrower and more deeply incised on the SW part and wider and shallower on the NE part of the catchment after five years of development. Also the LEM simulations suggested that after five years of development, erosion patterns still differ for differing initial surface roughness, however, differences in the final simulated erosion and sedimentation patterns were comparably small in relation to the differences in temporal development observed during the simulations, i.e., differences in drainage density distribution for differing initial surface roughness were decreasing with time.

9.3 A concept of hydro-geomorphic pattern formation in initial phases of ecosystem development

Combining the results of this work, a characterization of phases of hydro-geomorphic surface development during initial phases of hydro-geomorphic development and of development patterns in the Hühnerwasser catchment can be attempted. Observations from the catchment show that the organization of drainage patterns on the catchment's surface was constitutive for the development of surface morphology. The organization of surface drainage patterns was shown to be oriented towards a higher connectivity, which results, e.g., from a shortening of the lengths of overland flow paths towards the sedimentation-dominated area. This development implies a spatial differentiation of surface runoff concentration and therefore the incision of erosion rills, which again enforces flow concentration; so that development leads to a higher efficiency of the system to transport water, solutes, and solids towards the outlet. With the differentiation of hydro-geomorphic surface structures due to rill incision, areas of different development trajectories emerge.

Generally, incision by water erosion for the areas of highest flow accumulation in a catchment results in an increased gradient at the location of the incisions, so that the incision propagates in upslope direction by knick-point migration and headward channel erosion. Vertical incision can result in additional lateral erosion of the channel, and headward and lateral erosion continue until the gradient is reduced by sediment accumulation in downslope areas. A specific section of a channel network is affected by negative feedbacks when the gradient to areas further upslope increases, which increases erosivity of flow from upslope areas and results in increased sediment transport to and deposition in the channel section. These principles are the basis of concepts of stream channel stability under equilibrium conditions (Lane, 1955; Simon and Rinaldi, 2006). However, during the initial phase of development, the organization of surface flow can result in positive feedbacks between incision and flow accumulation, so that erosivity is increased in lower slope areas and decreased

in the more peripheral, upslope parts of a drainage network. Furthermore, a stabilization of erosion channels in areas of relatively low flow accumulation, i.e., the upslope areas, by vegetation development and a general decrease in overland flow by increasing infiltration can limit headward erosion, sediment discharge to lower slope areas, aggradation in these areas and the reduction of gradients. It can therefore be assumed that drainage network development in an ecosystem developing from the initial phase differs from network development under constant biotic and pedogenic boundary conditions; and that drainage network development for initial land surfaces differs from drainage network development on surfaces with established surface flow paths for which drainage network development or growth is induced by base level lowering.

Observations for the Hühnerwasser catchment affirm that the temporal dynamics of boundary conditions need to be considered to characterize initial drainage network development (see Fig. 9.3). Sediment erodibility is depending on the sediment mechanical properties at the initial state and is generally decreasing with pedogenesis and vegetation development, i.e., the threshold shear stress for sediment erosion generally increases. The erosivity of runoff is largely depending on precipitation intensity for the initial state. During ecosystem development, overland flow depth and erosivity are, one the one hand, decreasing, as surface runoff generation is decreased by a general increase in infiltration. On the other hand, flow path organization results in relative decrease or increase of flow accumulation for specific areas, so that the development of erosivity differs for different areas. Development is furthermore affected by the temporal distribution of precipitation intensity and by effects of soil crust development or modifications of sediment structure by biota, which can result in a highly nonlinear development of sediment erodibility, of infiltration and runoff generation and thus of erosivity. Three major phases of hydro-geomorphic surface development as affected by flow path organization and the development of boundary conditions can be described (Fig. 9.3):

Phase I

Initial surface development during a first development phase is dominated by the initial formation of preferential flow paths. Surface runoff is affected by abiotic initial conditions in this phase, i.e., runoff generation is affected by the hydraulic properties of the initial sediment and runoff routing is affected by initial morphology. When flow structures emerge, the microtopography of the sediment surface is altered so that a differentiation into areas of flow divergence and flow convergence develops, which, in areas of relatively high flow concentration, results in the incision of erosion rills. Specific location and geometry of these incisions can further be affected by initial sediment mechanic properties. The initiation of incisions is not necessarily restricted to the area closest to the base level for erosion, but

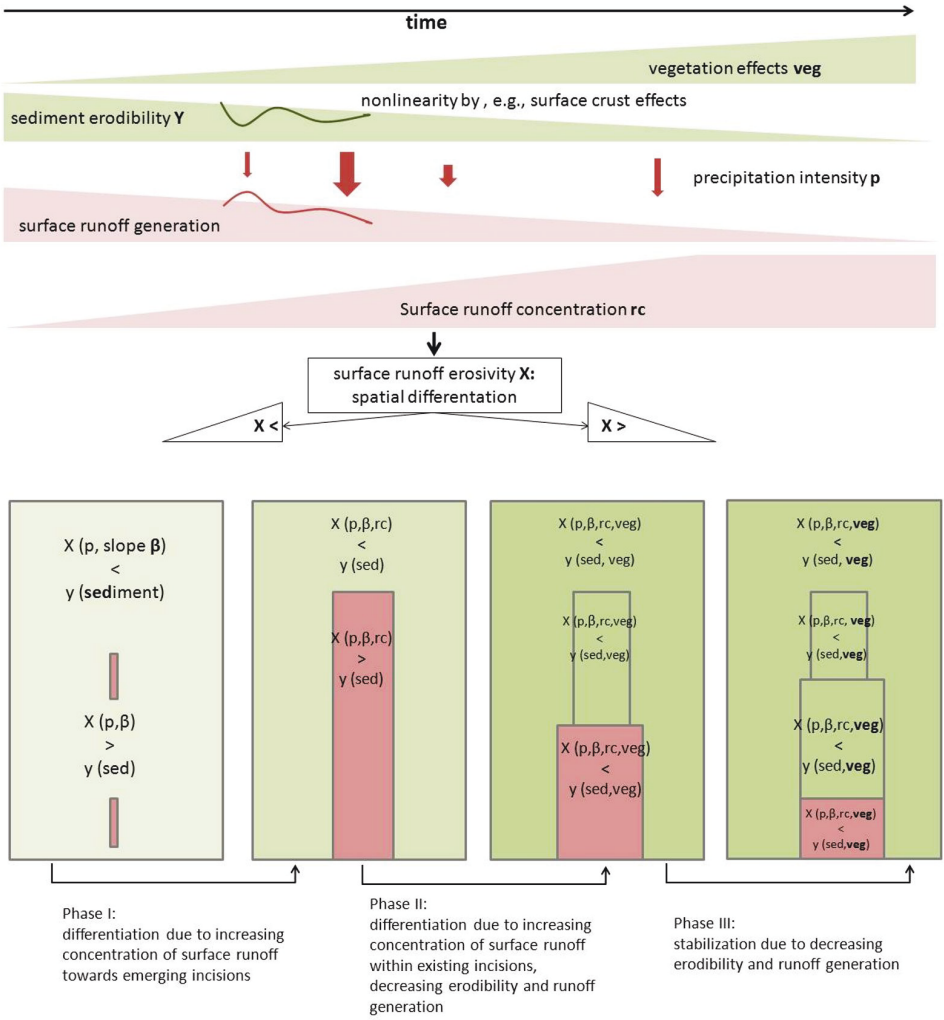

Figure 9.3: Schematic illustration of phases of surface morphologic development affected by water erosion during initial phases of ecosystem development by combined effects of the organization of surface flow paths and of the development of stabilizing boundary conditions.

can commence in any area over the slope for that a critical threshold of flow accumulation is exceeded due to the effects of overall and local morphology. The local erosion results in an increase of flow accumulation and in higher slope in the incised areas. Flow pattern development in this phase is characterized by a concentration of flow towards a developing erosion rill network.

The formation of linear incisions on the surface of the Hühnerwasser catchment was already observable in the first aerial photograph that was available for the documentation of surface development, i.e., the photograph of November 26, 2005. Rill incision started from the lowest areas of the slope and from local incisions on different areas of the slope, and incisions became connected to form linear erosion features. Hydro-geomorphic surface development was then dominated by a growing areal extent of the erosion rill network and of the sedimentation areas. The growth of the erosion rill network in this phase was most probably favored by high intensity rainfall events and high amounts of infiltration excess overland flow due to low infiltration rates and the presence of biological and structural surface crusts. Rill incision was most probably accelerated by increasing runoff concentration, which also resulted in a higher spatial concentration of erosion in narrower rill areas. The organization of surface flow towards a concentration in the developing erosion rills is reflected in flow accumulation maps based on DEMs for the phase from November 2005 to November 2007 (Fig. 9.4).

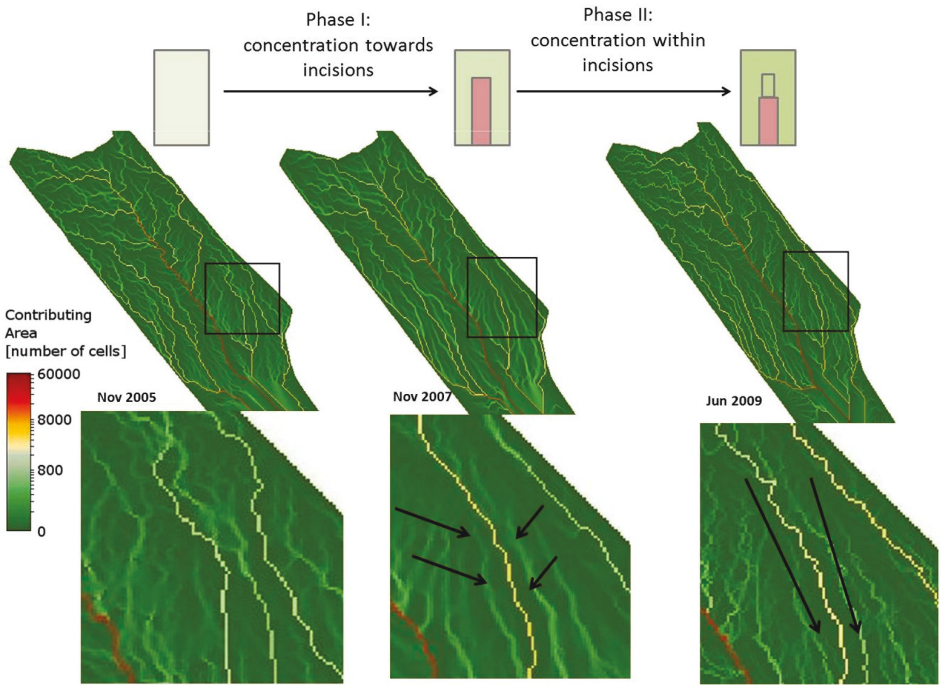

Figure 9.4: Indications of surface flow organization by concentration towards erosion rills (Phase I) and organization within erosion rills (Phase II) in maps of cells' contributing areas for DEMs of the Hühnerwasser catchment of November 2005, November 2007 and June 2009.

Phase II

In a next development phase, flow organization is characterized by a concentration of flow towards the lower slope and central parts of the drainage network. The resulting increase of flow accumulation and erosivity in the central parts of the network and decrease in the more peripheral parts can counteract the effects of headward erosion of the incisions. Furthermore, effects of vegetation cover development and initial pedogenic processes begin to decrease erodibility of the sediment and erosivity of surface runoff; so that the critical shear stress for erosion is increasing, while surface runoff shear stress is decreasing for most areas. The combination of effects of drainage network internal organization and stabilization by development of other ecosystem components can result in a decrease of drainage density and channel lengths and a further differentiation of the surface into stabilized and unstable areas.

Lower rates of volume change, decreasing spatial extents of the rill network and minor change in the area of alluvial sedimentation were observed for a next development phase in the Hühnerwasser catchment. The decreasing spatial extent of the rill network most probably reflects the effects of lower erosive power of surface flow, increased infiltration and increased surface stabilization by vegetation cover and by roots. Furthermore, effects of flow concentration in the central parts of the rill network were shown. High erosion rates became more and more restricted to these areas and to confluences of tributaries and higher-order rills, where sidewall erosion and bank collapse occurred episodically. Flow organization within the rill network towards those parts of the network in the lower and central slope areas is reflected in flow accumulation maps based on DEMs from November 2007 and June 2009 (Fig. 9.4).

Phase III

The following development phase is characterized by dominant influences of decreased erodibility and erosivity due to vegetation cover development. These effects can result in a stabilization of major parts of the catchment area, so that sediment redistribution is limited to erosion, transport and resedimentation over short distances within the rill network and that sediment discharge from the network only occurs for considerably high-intensity precipitation events. For the Hühnerwasser catchment, this phase was most probably only reached at the end of the study period of this work or later. No considerable change of flow accumulation patterns was observed for DEMs of 2009 and 2010. Aerial photographs for dates after 2009 did not allow for a mapping of erosion rills because most parts of the rill network were covered by dense vegetation. These photographs still show indications of sediment redistribution within the major rills and rill widening by lateral erosion around tributary confluences to the major erosion rill.

This characterization of hydro-geomorphic surface development during the initial phase is centrally based on the organization of surface flow towards a spatial concentration along preferential flow paths. The development of preferential flow paths is a formative process in initial structural development of sediments, not only at the sediment's surface but also in the vadose zone (Lin, 2010). Because the formation of preferential flow paths implies a differentiation into areas of relatively low and relatively high flow accumulation, it can induce a differentiation into unstable and stable areas. Morphologic surface differentiation can therefore emerge in the development of a hydro-geomorphic system in the absence of biota influences. Vegetation or other biotic effects can, however, increase the differentiation. A differentiation of landscapes into geomorphically stable and unstable patches is frequently described for water limited systems (e.g., Saco et al., 2007). For these systems, the differentiation was described to be affected by stability thresholds that locally cause a transition from positive feedback cycles between vegetation cover and surface stability to negative feedback cycles, so that divergent landform development is ongoing and does not pass over to a phase of dominant stabilization. In other studies, a threshold-induced differentiation into stable and unstable areas has been supposed to occur before the establishment of higher vegetation, i.e., with the surface colonization by biological soil crusts Lázaro et al., 2008). Concepts of bio-geomorphic succession often describe a state of complete stabilization for a final development state. It depends on the spatial and temporal development scales of morphologic and vegetation patterns if vegetation effects can completely stabilize a land surface. These concepts and the results of this study show that the transition from non-equilibrium conditions to disequilibrium or equilibrium conditions can hardly be attributed to specific phases or states of landform and ecosystem development, but that these conditions can only occur for specific units within a landscape, e.g., for a section of a stream channel. This is in accordance to Renwick (1992), who discusses the question of equilibrium in cascading systems and concludes that "the outputs of a geomorphic system may appear to be equilibrium-dominated in some cases but exhibit nonequilibrium behavior in others, depending on the relative influence of equilibrium and nonequilibrium landforms on the system".

10 Conclusions

10.1 Synthesis of key questions and results

The central aim of this work was to describe the development of mass balances of the sediment solid phase during initial phases of ecosystem development in 3D spatial and temporal resolution. Taking into account the possibilities and limitations of the project context, this aim was approached using remotely-sensed data, methods of quantitative soil-landscape modeling and geomorphic change detection, and the application of a numerical landscape evolution model.

A review on the integration of the initial development phase in geomorphologic systems theory (Chapter 1) showed that detailed conceptual models for the initial phase of geomorphic development have hardly been formulated. The classic geomorphologic concepts of landform evolution, which do not explicitly address the role of interactions with other processes of ecosystem development, have hardly been discussed in relation to concepts of ecosystem development founded in other disciplines. The conceptualization of landform development in geomorphology mainly focused on considerably larger spatial and temporal scales as compared with those considered in ecological theory. Interdisciplinary concepts for, e.g., bio-geomorphic landscape development have been established during the last decades.

The overview on field and experimental studies that focus on initial landform development (Chapter 2) suggested that the limited consideration of the initial development phase in geomorphologic theory is to some extent due to the lack of possibilities to carry out empirical studies on the relevant scales and capturing relevant processes. A research gap between studies on small and large spatial and temporal scales was shown up, which has also been identified for other aspects of initial ecosystem development and is currently approached in the Hühnerwasser project and in other research projects. The overview on the state of the art of landform development modeling (Chapter 2) suggested that a GIS-based 3D soil landscape model can be suitable to describe and analyze the initial landform development phase. However, the review has also shown that methods of GIS-based 3D soil landscape modeling have not yet been developed to a stage where they can routinely be applied. The application of numerical soil erosion or landscape evolution models to improve the understanding of the initial landform development phase is promising, but still requires critical evaluation;

and methods to integrate GIS-based soil landscape modeling and process-explicit numerical landscape evolution modeling still need to be developed.

In Chapter 4, the construction of a 3D volume model of the Hühnerwasser catchment's water storage layer was described, and possibilities for the quantification of sediment mass balances from DEM time series were discussed exemplarily for three DEMs. The 3D volume model allowed for quantifying the volume of the sediment body with an uncertainty that is depending on the accuracy of the delineating DEMs. For the initial sediment body of the catchment, a sediment volume of 122600 m^3 was calculated with an uncertainty of ± 12300 m^3. Assigning sediment property information to the model by interpolation from sampling points allowed for a depiction of large scale variations of sediment properties, i.e., differences between the SW and NE part of the catchment. Limitations to sediment budget quantification from DEM time series for the Hühnerwasser catchment were suggested by the relatively high uncertainty of the available DEMs in relation to the magnitude of changes in sediment volume, and were affirmed by imbalances in the calculated sediment budgets. These results showed that there is the need for a detailed evaluation of DEM resolution and errors and of their effects on sediment budget quantification (Chapter 6). Similarities in the spatial distribution of morphometric parameter values and of erosion and deposition patterns were observed and suggested that morphometric analysis of the DEM time series is suitable for characterizing the effects of initial surface structures on sediment mass balance development.

In Chapter 5, a method to implement a description of sediment mass balance development in a 3D volume model of the sediment body based on a DEM time series was described for the example of nine specific stages of surface development in the Hühnerwasser catchment. The transfer of data between the 3D volume model and simulations with a numerical sediment redistribution model was exemplarily described for a simulation of erosion and alluvial fan sedimentation using the CAESAR landscape evolution model. It was shown that models of boundary surfaces between sediment layers accumulated in specific time intervals can be derived from surface DEMs by locally modifying elevation values based on logical principles. Using this method, a 3D volume model including a representation of sediment layers deposited in time intervals can be constructed from a surface elevation data time series. For the 3D volume model of the Hühnerwasser catchment, the method allowed for a visualization of sediment accumulation in the alluvial fan area; although the quantitative interpretation of the model was limited because of DEM uncertainty. It was further shown that datasets describing 3D spatial distribution of sediment properties could be transferred between a 3D volume model and a numerical sediment redistribution simulation model. Limitations arose from discrepancies between simulated elevation change and elevation change reconstructed from DEMS, and from limitations to the resolution of

the 3D volume model. These observations gave the impetus for a more detailed evaluation of the applicability of the CAESAR landscape evolution model for initial landform development phases on the scale of a small catchment (Chapter 8).

The detailed evaluation of DEMs regarding their suitability for the quantification of sediment mass balances was approached for elevation data based on photogrammetry, airborne and terrestrial laser scanning in Chapter 6. Furthermore, methods for the modification of DEMs based on plausibility rules and hydro-geomorphic principles and for the construction of a multi-source elevation model to improve mass balance quantification were described and evaluated. It was shown that none of the three methods of elevation data acquisition alone is best suited for mass balance quantification, but that the suitability of measurement methods is depending on vegetation cover and morphologic characteristics; that mass balance quantification can be moderately improved by modifying DEM based on hydro-geomorphic principles; and that mass balance quantification can be considerably improved by constructing a multi-source DEM combining best-suited data sources for regions of differing vegetation and geomorphic structures. Modification of DEMs based on hydro-geomorphic principles, which reduces the obstruction of flow within rill areas by DEM artefacts, can further improve the suitability of DEMs for the derivation of surface flow paths by flow routing algorithms.

A detailed analysis of hydro-geomorphic development in the catchment, as suggested in Chapter 4 and using photogrammetry-based DEMs evaluated in Chapter 5, was described in Chapter 7. The combined analysis of the DEM time series and aerial photographs showed that hydro-geomorphic development was characterized by a differentiation of geomorphic structures, i.e., the growth of an erosion rill network along with relatively high variations in flow paths and morphometric parameters, during the first two years of development; and by a spatial concentration of the area of active erosion along with higher stability in flow paths and morphometric parameters during the following development phase. Based on aerial photographs, meteorological monitoring data and field observations, effects of precipitation characteristics, vegetation cover development, and initial surface irregularities on hydro-geomorphic development were shown. The combined analysis of aerial photographs and DEMs further suggested an influence of rill network internal dynamics on surface development, i.e., showed that flow accumulation increased in the central areas of the rill network and slightly decreased in interrill areas and peripheral areas of the rill network; which can lead to proceeding erosion in central parts of the network and enforce the stabilization of peripheral areas. Limitations to the delineation of development phases and the characterization of effects of specific initial and boundary conditions were due to the relatively low temporal and spatial resolution of the DEM time series and to the limited possibility to distinguish specific processes and causal relations between boundary conditions

and processes by inferring to them from the resulting patterns.

In Chapter 8, the landscape evolution model CAESAR was evaluated for its suitability to simulate initial phases of surface development on the scale of the small catchment, as suggested in Chapter 5; and the model was applied for a further examination of the effects of specific initial and boundary conditions on hydro-geomorphic surface development, as encouraged by the results described in Chapter 7. Results showed that water discharge, the locations of major flow paths and the distribution of drainage density over the slope can be well reproduced by simulations with the model, although only the most important processes affecting surface development in the catchment are represented. However, an underestimation of drainage density and an overestimation of suspended sediment discharge showed limitations to the quantification of erosion for small spatial scales and the initial period with the model. Results affirmed the effect of initial surface irregularities on rill network formation that was suggested in Chapter 7. Simulation results further affirmed that the considerably high variability of precipitation intensities for the second year of surface development in the Hühnerwasser catchment has contributed to the development of the relatively dense rill network; and revealed that low precipitation intensity during the first year has affected the concentration of high drainage density to the lowest slope areas.

The integrative discussion of results (Chapter 9) showed up that for the Hühnerwasser catchment, the sediment body's surface was mainly affected by processes of erosion by concentrated water runoff on the catchment's surface, which resulted in a diversification of the surface structure. With the formation of linear incisions, a diversification of local slopes and aspects and of distances of the surface to the groundwater body emerged, which induced a diversification of local boundary conditions for soil and biota development. While this development was affected by sediment characteristics for the initial state, interactions of geomorphic structures and biotic structures emerged and became more important during ecosystem development. Feedbacks between hydro-geomorphic surface structures and processes of water erosion are reflected in a concentration of the erosive power of overland flow to central parts of the erosion rill network, which is probably induced by a development of surface flow paths towards higher connectivity and spatial organization.

10.2 General Conclusions

The results of 3D model construction and evaluation in this work showed that a 3D geological model of the sediment body of a small catchment can allow for the quantification and improved visualization of the catchment's geometry. The described methods of 3D volume model construction allow for the establishment of a virtual catchment model that integrates a representation of the results of hydro-geomorphic development in the form of accumu-

lated sediment layers. Such a model can be used for the visualization and analysis of 3D spatial soil, sediment and morphologic structures. Results suggest that the quantification of sediment redistribution during the initial phase of development in a small catchment using 3D modeling approaches requires elevation data in considerably high spatial and temporal resolution, which can hardly be provided using commonly available remote-sensing data; but that a combination of data from different sources for regions of different morphologic and vegetation cover structures can allow for an improved sediment mass balance quantification. Results of drainage network development analysis by combining aerial photography and DEMs suggest that this method can allow for critical comparisons of flow accumulation and erosion patterns and therefore for improved analyses of the dynamic evolution of runoff and erosion patterns. The observed patterns of flow concentration affirm the importance of the implementation of a dynamic adaptation of topography in numerical models of landform evolution.

Results of the analyses of surface development showed that the main morphologic patterns in the Hühnerwasser catchment were formed during the first development phase, i.e., during the phase of flow organization towards the rill network, which affirms the critical importance of the earliest phase of surface development. Results further suggest that the initial surface morphology and precipitation characteristics were formative for morphologic pattern evolution in the initial phase and indicate a lasting influence of the initial phase on morphologic development. Results allowed for a description of major steps in erosion-affected surface development in the Hühnerwasser catchment, and for a general conceptual description of phases of hydro-geomorphic development for the initial phase of ecosystem development, i.e., the concentration of surface flow towards a developing erosion rill network in a first phase, the concentration of flow within this network in a second phase, and the stabilization of the rill network mainly due to vegetation effects in a third phase.

Based on the results of this work, the hypotheses of Chapter 3.1 can be discussed as follows:

- **During the initial phase of ecosystem development, the evolution of geomorphic patterns is affected by initial structures of the sediment's solid phase.**
  Results of DEM and aerial photograph time series and LEM simulations suggest that the overall morphology and small irregularities of the initial surface have affected the overall geometry of the developing erosion rill network and have contributed to the high drainage density observed in parts of the Hühnerwasser catchment. Effects of the spatial structure of sediment hydraulic and mechanical characteristics could not be reconstructed based on available information, however, are indicated by developing rill network patterns.

- **Geomorphic development during the initial phase leads to a diversification of surface structures.**
  Results clearly showed that in the Hühnerwasser catchment, geomorphic development during the initial phase has resulted in a diversification of morphometry, e.g., of local slopes and of areas of lower and higher flow accumulation. This diversification of stable and unstable areas induces a diversification of 'surface ages', i.e. of the progress of pedogenesis on different areas of the catchment. Observations in the Hühnerwasser catchment further show that the development of morphologic structures has considerably affected patterns of vegetation development. Results therefore affirm that initial landform development can result in a diversification of geomorphic and biotic structures of the surface.

- **Geomorphic patterns established during the initial development phase are constitutive for structures of the developing ecosystem.**
  Results of DEM and aerial photograph analysis showed that hydro-geomorphic patterns established during the first two years of development in the catchment remained relatively stable the development period analysed in this study. LEM simulations suggested that this stability of established patterns can also be assumed for a different initial surface roughness and for other meteorological influences acting during the initial development phase. However, results also showed that the rill network develops towards an equally-distributed density over the slope cross section for differing initial sediment characteristics and surface roughness. Results therefore affirm that overall statistical characteristics of surface structures develop towards more similarity for different initial conditions; however, that initial conditions can have a lasting effect on the geometry of specific landscape elements.

Appendix A - Technical description of DEM modification

The digital elevation models used in this work were modified using different methods, based on the results of DEM evaluation described in Chapters 4 and 6. To reduce overall systematic errors, DEMs were referenced to d-GPS data. The referenced datasets were employed for all analyses described in this dissertation. To reduce imprecise representation of elevation in erosion rill and alluvial fan areas, elevation values within rills were modified based on hydro-geomorphic principles, i.e., by removing increases of elevation along rills in downslope direction. DEMs modified based on this method were employed for the construction of the 3D volume model described in Chapter 5 and for morphometric analyses described in Chapter 7. To reduce artefacts resulting from vegetation cover recording in interrill areas, elevation values were modified based on logical comparison by replacing elevation values in areas that showed an implausible development of elevation over time by elevation values from other DEMs of the time series. DEMs modified based on this method were employed for the construction of the 3D volume model described in Chapter 5. These modifications are evaluated and discussed in detail for the DEM of June 2009 in Chapter 6. Technical descriptions of the modification methods, which could not be included in each chapter, are provided here.

A.1 Referencing of photogrammetry-based DEMs to d-GPS data

The following material was published as online supplementary material to Schneider, A., Gerke, H.H., Maurer, T., Nenov, R., (2013). Initial hydro-geomorphic development and rill network evolution in an artificial catchment. Earth Surface Processes and Landforms 38 (13), 1496-1512. doi: 10.1002/esp.3384.

In our study, we used d-GPS reference data to evaluate and reference elevation datasets based on automated digital photogrammetry, which were provided by the mine surveying department of Vattenfall Europe Mining AG (Cottbus, Germany). In the following, we provide additional information on the referencing and its effects on the DEMs.

A.1.1 Problems and aims

Visual assessment of elevation data showed that, while relative topographic characteristics (e.g., the increasing incision of erosion rills) were observable in the DEMS, there were fluctuations in general elevations of the elevation data time series which could not be explained by processes of surface development or sediment settling. For instance, elevations in the data for June 2009 are, despite of some outliers, generally higher compared to those in the data for March 2010 (Fig. A.1). This indicated the presence of systematic errors in the datasets, which might result from several factors of aerial image acquisition or digital photogrammetric processing (Hunter and Goodchild, 1995). It was therefore attempted to better assess and reduce this type or errors by comparing and referencing datasets to d-GPS data.

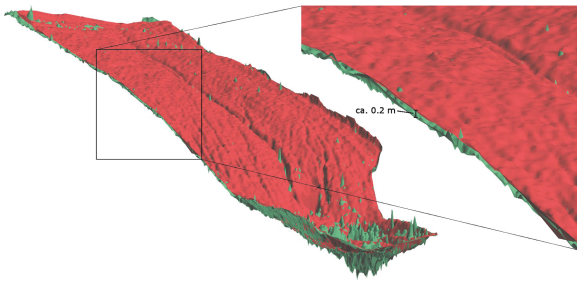

Figure A.1: Elevation data in the catchment area for June 2009 (green) and March 2010 (red).

A.1.2 Assessment of errors and referencing

We compared elevation datasets to reference data recorded in a 20 m by 20 m grid in the monitoring area of the catchment. As reference data were only recorded beginning in October 2008, we used only a selection of reference data which we assumed to be stable in elevation to reference older photogrammetry-based elevation data. Selections of reference data were made based on comparison of reference points to aerial photographs, from which morphodynamic activity between the recording of reference data and DEMs was assessed. A similar approach has been applied by Betts and DeRose (1999). For the selection of reference data from the dataset recorded on 20.08.2008, we used aerial photographs taken on 26.11.2005, 01.05.2006, 03.11.2006, 21.11.2007, and 18.08.2008. Reference data from the dataset of 10.11.2009 were selected using aerial photographs recorded on 13.06.2009, 01.07.2009, and 05.12.2009; and for selecting reference data recorded on 22.04.2010 we used photographs taken in 04.03.2010 and 24.04.2010. The reference data that were assumed to be morphologically stable were not equally distributed across the catchment area (Fig. A.2).

The assignment of reference data to elevation datasets and the number of reference data used for the processing of each dataset are given in Table 5.2. Deviations between reference data and elevation datasets were computed, statistical criteria were calculated and elevation datasets were fitted to reference data as described in Chapter 5 of this work. Distances between reference data were not equally distributed across the catchment (Fig. A.3).

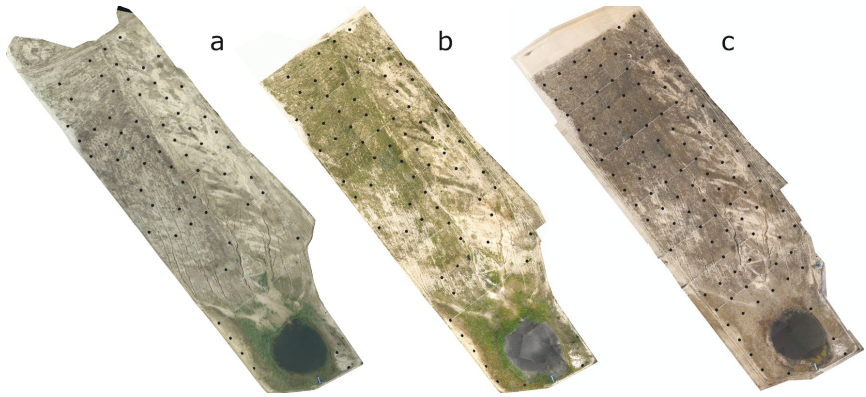

Figure A.2: Locations of d-GPS data (black dots) used to reference elevation models. a) 61 d-GPS points recorded on 09.10.2008, displayed on an aerial photograph of 18.08.2008 (© VEM AG). b) 74 d-GPS points recorded on 10.11.2009, displayed on an aerial photograph mosaic of 01.07.2009. c) 114 d-GPS points recorded on 22.04.2010, displayed on an aerial photograph mosaic of 24.04.2010.

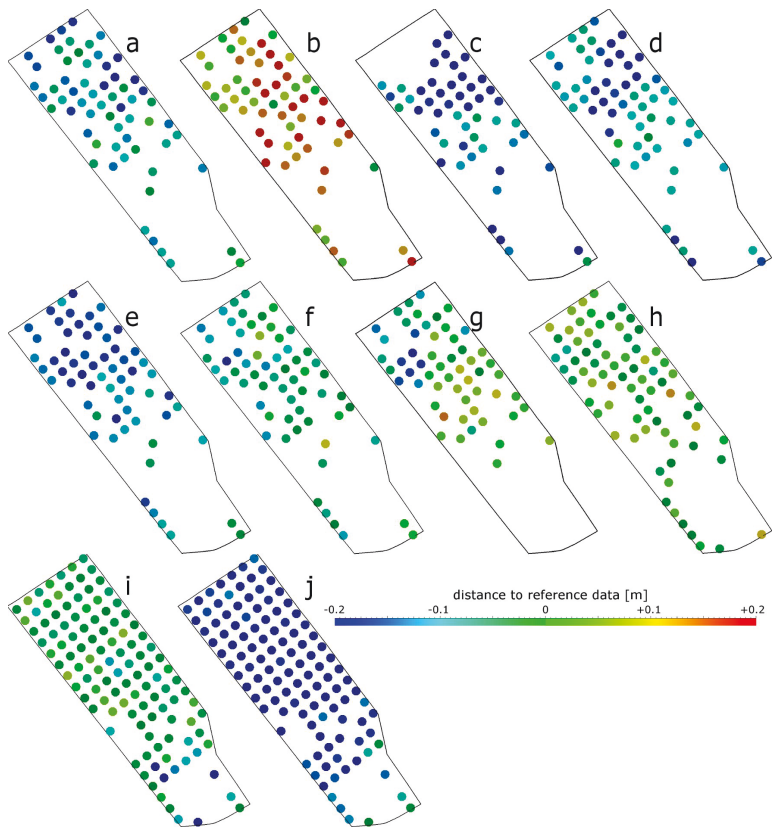

Figure A.3: Distribution of the vertical deviations between reference data points and DEM data at the location of reference points for DEMs of a) 26.11.2005, b) 01.05.2006, c) 03.11.2006, d) 21.11.2007, e) 24.04.2008, f) 18.08.2008, g) 04.12.2008, h) 13.06.2009, i) 05.12.2009, and j) 04.03.2010.

A.1.3 Results

As a result of the fitting procedure, elevation data at locations of reference points were shifted to the elevation of GPS points and elevation data between reference points were modified (Fig. A.4).

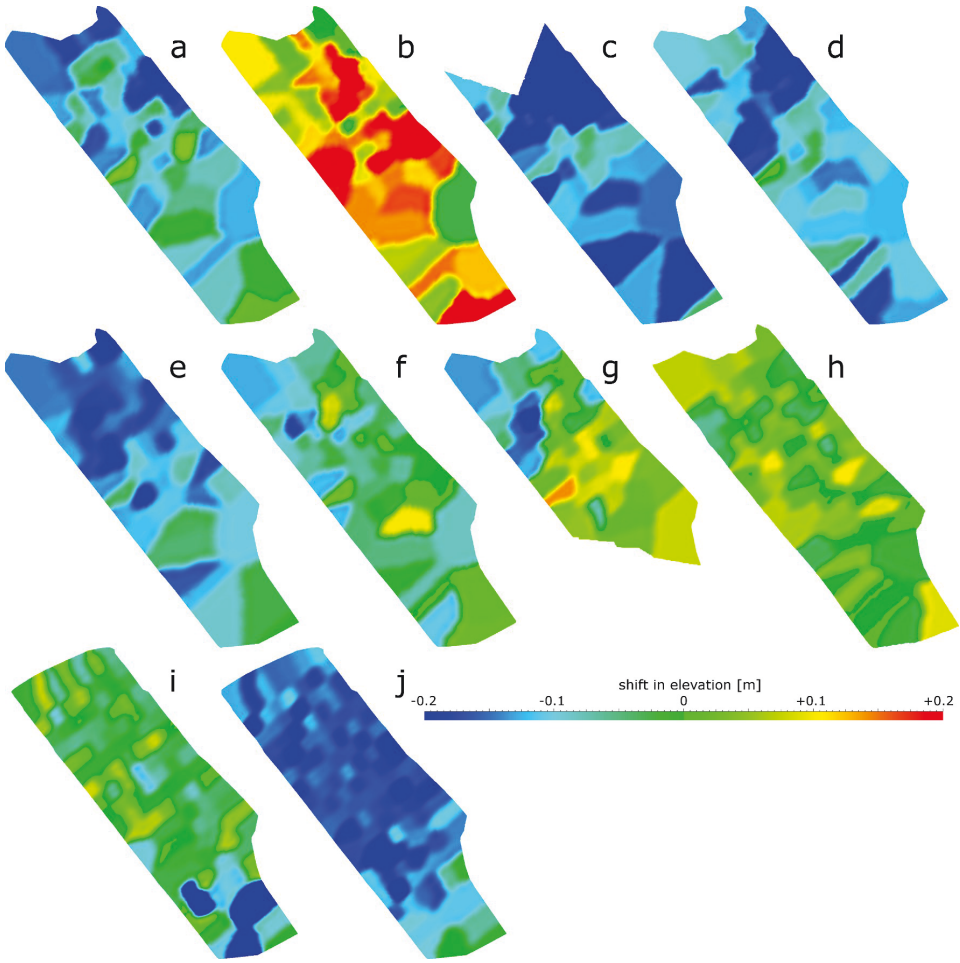

Figure A.4: Spatial distribution of vertical elevation shift as a result of referencing for DEMs of a) 26.11.2005, b) 01.05.2006, c) 03.11.2006, d) 21.11.2007, e) 24.04.2008, f) 18.08.2008, g) 04.12.2008, h) 13.06.2009, i) 05.12.2009, and j) 04.03.2010.

A.2 Modification based on hydro-geomorphic principles in rill areas

A.2.1 Problems and aims

The evaluation of photogrammetry-based DEMs in comparison to other DEMs and GPS reference data (Chapter 6) showed that elevations were mainly overestimated within rill areas, probably because of shadowing effects; and in alluvial fan areas, probably because of the relatively dense vegetation cover in this area.

DEM modification in rill areas and alluvial fans therefore aimed at improving the representation of erosion rill areas for an improved quantification of sediment mass balances (Chapter 6) and at improving DEMs for the application of flow routing algorithms to derive DEM cells' contributing areas and other morphometric parameters based on the contributing areas (Chapter 7).

A.2.2 Methods

Based on the results of the DEM evaluation, it was assumed that the lower elevation values in the DEMs give better representations of the actual elevation within erosion rills, and that higher elevation values result from imprecise recording of the surface within rills. DEM modification was therefore based on preserving the lower elevation values within the rill areas and suppressing all elevations that were higher than any elevation values further upslope. To carry out this modification, the drainage network's longitudinal profiles as represented in the DEMs were extracted from elevation models as described under 'Modifications in rill and alluvial areas' in Chapter 6. The rill networks digitized for 2006, 2007, 2008 and 2009 were used for modification of the DEMs of 05/06 - 11/06, of 11/07, of 04/08 - 12/08, and of 06/09 - 03/10, respectively. For modifying the ALS- and TLS-based DEMs described in Chapter 6, the rill network map for July 2009 was used. To each node of the resulting polylines (see Fig. A.5a), the values of the Stream Order and the width of the rill segment around this point was assigned based on the rill network polygon datasets. For each node, the x-, y- , and z-coordinate, the Stream Order and rill width values and an index number identifying each rill segment were then exported to an ASCII file. An additional index number was added to identify each node. These files were processed in Microsoft Excel using the attached VBA-scripts. Additional variables were calculated and written to data sheets for verification. The number of nodes in each segment was determined (Sub I) to sort nodes for each segment in upslope direction (Sub II). Modified elevation values (*hoehekorr*) and the x- and y-coordinates of two additional coordinates left and right from the node and perpendicular to the polyline in a distance of 0.75 · the rill widths (*rwnorm1, hwnorm1, rwnorm2, hwnorm2*) were calculated (Sub III). These coordinates were imported to GOCAD as point data (see Fig. A.5b), assigning the modified elevation of each rill node to the two additional coordinates left and right of the node. The auxiliary surface, as described in Chapter 6 (see Fig. A.5c), was constructed from these data points by triangulation, and elevation values

within the rills were replaced by elevation values of the auxiliary surface. Triangulation between the modified data points was optimized using the option to switch triangles, i.e., to change from one to the other possible way to construct two triangles between four points, in order to obtain a minimum curvature, and by using the option to manually switch triangles in GOCAD.

```
Sub I()

Dim nid, id(9250), nextid(9250)

      Worksheets("1").Cells(1, 1).Value = "id"
      Worksheets("1").Range("B1").Value = "nextid"
      Worksheets("1").Range("C1").Value = "nrnid"
      Worksheets("1").Range("D1").Value = "sumnid"
      Worksheets("1").Range("E1").Value = "sumnid2"

For x = 0 To 9247
For nid = 1 To 76

 id(x) = Worksheets("0").Cells(2 + x, 1).Value
 nextid(x) = Worksheets("0").Cells(3 + x, 1).Value
 If IsEmpty(Worksheets("0").Cells(3 + x, 1)) Then
 nextid(x) = id(x) + 1
 End If

 If id(x) = nid Then
      Dim spalteid As Range
      Dim sumnid(9250), nrnid(9250), sumnid2, sumnid1
      Set spalteid = Worksheets("0").Range("a:a")
      nrnid(x) = Application.WorksheetFunction.CountIf(spalteid, nid)
      sumnid(x) = Application.WorksheetFunction.CountIf(spalteid, "<" & nid)
      sumnid2 = sumnid(x) + 2
      Worksheets("1").Cells(2 + x, 1).Value = id(x)
      Worksheets("1").Cells(2 + x, 2).Value = nextid(x)
      Worksheets("1").Cells(2 + x, 3).Value = nrnid(x)
      Worksheets("1").Cells(2 + x, 4).Value = sumnid(x)
      Worksheets("1").Cells(2 + x, 5).Value = sumnid2
      Worksheets("1").Cells(1 + x, 6).Value = sumnid1
End If

Next nid
Next
Worksheets("1").Range("F1").Value = "sumnext1"
MsgBox " enter last value for sumnid1"
End Sub

Sub II()

Dim id(9250), nextid(9250), erstezelle(9250), letztezelle(9250), erstehoehe, letztehoehe

For y = 0 To 9247
For ynid = 1 To 76

id(y) = Worksheets("1").Cells(2 + y, 1).Value
nextid(y) = Worksheets("1").Cells(2 + y, 2).Value
erstezelle(y) = Worksheets("1").Cells(2 + y, 5).Value
letztezelle(y) = Worksheets("1").Cells(2 + y, 6).Value
erstehoehe = Worksheets("0").Cells(erstezelle(y), 5).Value
letztehoehe = Worksheets("0").Cells(letztezelle(y), 5).Value

 If id(y) = ynid And nextid(y) = ynid + 1 And erstehoehe < letztehoehe Then
   Range(Worksheets("0").Cells(erstezelle(y), 1), Worksheets("0").Cells(letztezelle(y), 7)).Select
   Selection.sort Key1:=Range("G2"), Order1:=xlDescending, Header:=xlGuess, _
   OrderCustom:=1, MatchCase:=False, Orientation:=xlTopToBottom, _
   DataOption1:=xlSortNormal
End If

Next ynid
Next y
MsgBox "check last segment"
End Sub
```

```
Sub III()

Dim rw, hw, rwstart, hwstart, hoehe, drw, dhw, dupsl, ddownsl, hoehemin, hoehedownls, hoehekorr, rwvor, hwvor,
rwnach, hwnach, nid, nextid, lastid, rwnorm1, hwnorm1, rwnorm2, hwnorm2, diffrw, diffhw, betrag, diffhwein,
diffrwein, breite, halbebreite11 As Double
Dim id(9250)

Worksheets("2").Cells(1, 1).Value = "id"
Worksheets("2").Range("B1").Value = "anzahl mit id kleiner"
Worksheets("2").Range("C1").Value = "rwstart"
Worksheets("2").Range("D1").Value = "hwstart"
Worksheets("2").Range("E1").Value = "rw"
Worksheets("2").Range("F1").Value = "hw"
Worksheets("2").Range("G1").Value = "dupsl"
Worksheets("2").Range("H1").Value = "hoehe"
Worksheets("2").Range("I1").Value = "hoehekorr"

For nid = 1 To 76

   For x = 0 To 9247
      id(x) = Worksheets("0").Cells(2 + x, 1).Value
      Worksheets("2").Cells(2 + x, 1).Value = id(x)

    If id(x) = nid Then
      Dim sumnid(9250), nrnid(9250), sumnid2
      nrnid(x) = Worksheets("1").Cells(2 + x, 3).Value
      sumnid(x) = Worksheets("1").Cells(2 + x, 4).Value
      Worksheets("2").Cells(2 + x, 2).Value = nrnid(x)
      sumnid2 = Worksheets("1").Cells(2 + x, 5).Value
      rwstart = Worksheets("0").Cells(sumnid2, 3).Value
      Worksheets("2").Cells(2 + x, 3).Value = rwstart
      hwstart = Worksheets("0").Cells(sumnid2, 4).Value
      Worksheets("2").Cells(2 + x, 4).Value = hwstart
      rw = Worksheets("0").Cells(2 + x, 3).Value
      drw = rw - rwstart
      Worksheets("2").Cells(2 + x, 5).Value = rw
      hw = Worksheets("0").Cells(2 + x, 4).Value
      dhw = hw - hwstart
      Worksheets("2").Cells(2 + x, 6).Value = hw
      dupsl = Sqr(drw ^ 2 + dhw ^ 2)
      Worksheets("2").Cells(2 + x, 7).Value = dupsl
      hoehe = Worksheets("0").Cells(2 + x, 5).Value
      Worksheets("2").Cells(2 + x, 8).Value = hoehe
          hoehemin = Application.WorksheetFunction.Min(Range(Worksheets("2").Cells(sumnid(x) + 2, 8),
Worksheets("2").Cells(2 + x, 8)))

      If hoehe < hoehemin Then hoehekorr = hoehe Else: hoehekorr = hoehemin
      Worksheets("2").Cells(2 + x, 9).Value = hoehekorr
      lastid = Worksheets("1").Cells(1 + x, 2).Value
      nextid = Worksheets("1").Cells(3 + x, 2).Value

      If lastid < id(x) Then
         rwvor = Worksheets("0").Cells(2 + x, 3).Value
         hwvor = Worksheets("0").Cells(2 + x, 4).Value

      Else
      rwvor = Worksheets("0").Cells(1 + x, 3).Value
      hwvor = Worksheets("0").Cells(1 + x, 4).Value
      End If

      If nextid > id(x) Then
         rwnach = Worksheets("0").Cells(2 + x, 3).Value
         hwnach = Worksheets("0").Cells(2 + x, 4).Value

      Else
      rwnach = Worksheets("0").Cells(3 + x, 3).Value
```

```
            hwnach = Worksheets("0").Cells(3 + x, 4).Value
        End If

      breite = Worksheets("0").Cells(2 + x, 6).Value
      halbebreite11 = (breite / 2) * 1.5
        diffrw = rwnach - rwvor
        diffhw = hwnach - hwvor
        betrag = Sqr(diffrw ^ 2 + diffhw ^ 2)
        diffhwein = (diffhw / betrag) * halbebreite11
        diffrwein = (diffrw / betrag) * halbebreite11
         rwnorm1 = rw - diffhwein
         hwnorm1 = hw + diffrwein
         rwnorm2 = rw + diffhwein
         hwnorm2 = hw - diffrwein

      Worksheets("2").Cells(1, 10).Value = "rwnorm1"
      Worksheets("2").Cells(1, 11).Value = "hwnorm1"
      Worksheets("2").Cells(1, 12).Value = "rwnorm2"
      Worksheets("2").Cells(1, 13).Value = "hwnorm2"
      Worksheets("2").Cells(2 + x, 10).Value = rwnorm1
      Worksheets("2").Cells(2 + x, 11).Value = hwnorm1
      Worksheets("2").Cells(2 + x, 12).Value = rwnorm2
      Worksheets("2").Cells(2 + x, 13).Value = hwnorm2
End If

      Next x
      Next nid

End Sub
```

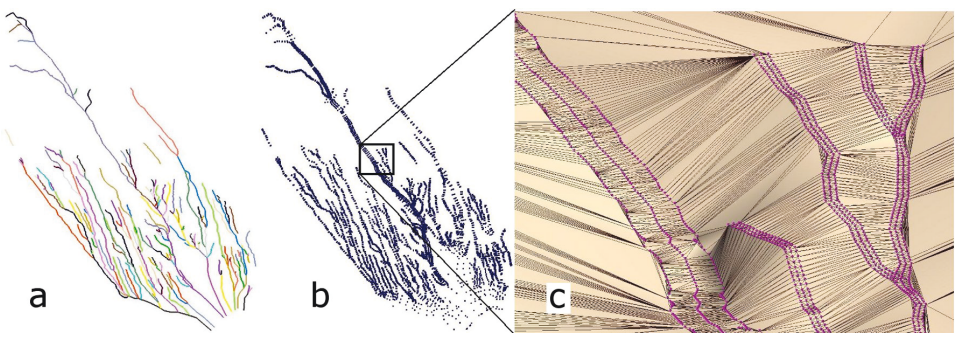

Figure A.5: Construction steps for obtaining the auxiliary surface representing the rill beds, a) segments of the rill network as exported from GOCAD (colors denote the specific segments), b) point dataset generated by the VBA-script, c) detail of the auxiliary surface constructed from the generated point dataset.

A.2.3 Results

As a result of the modification, elevation data for nodes in rill and alluvial fan areas with higher elevation values as compared with upslope values were reduced to values of the upslope nodes (Fig. A.6).

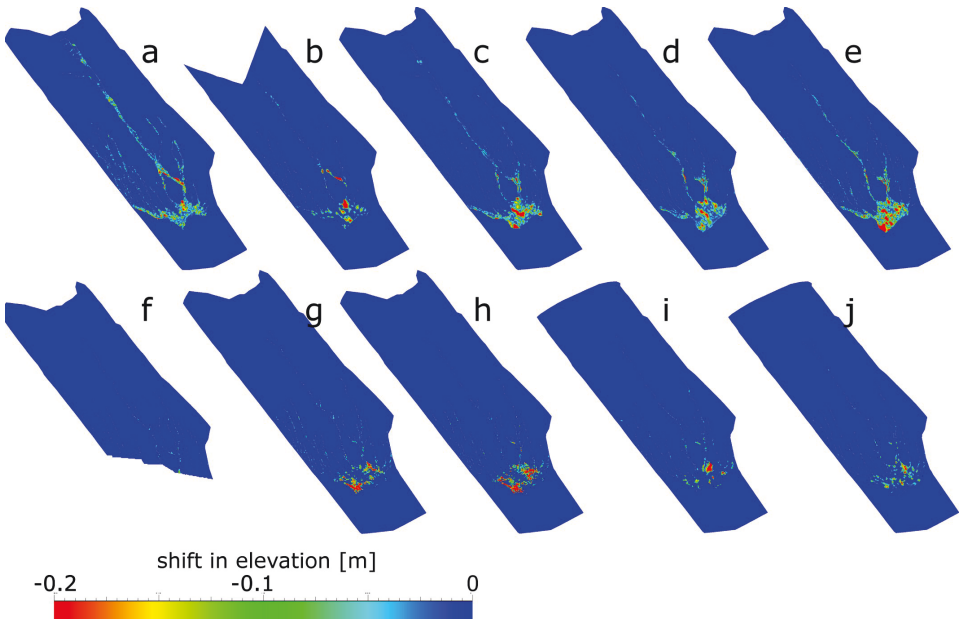

Figure A.6: Spatial distribution of vertical elevation shift as a result of referencing for DEMs of a) 01.05.2006, b) 03.11.2006, c) 21.11.2007, d) 24.04.2008, e) 18.08.2008, f) 04.12.2008, g) 13.06.2009 with 1 m node spacing, h)13.06.2009 with 0.5 m node spacing, i) 05.12.2009, and j) 04.03.2010.

A.3 Modification based on plausibility rules and logical comparison in interrill areas

A.3.1 Problems and aims

The evaluation of photogrammetry-based DEMs (Chapters 4 and 6) showed a misestimation of elevation values in the interrill areas due to artefacts in the elevation models resulting from the erroneous recording of vegetation cover, and due to random errors. DEM modification in interrill areas therefore aimed at identifying areas with a high probability of DEM artefacts due to vegetation cover recording and random errors; and at replacing elevations in these areas with elevations from other DEMs of the time series.

A.3.2 Methods

Morphometric analysis for the DEM time series (Chapters 4 and 6) affirmed the assumption that the density of vegetation artefacts, resulting in increased surface roughness (i.e., a higher small-scale spatial variation of elevation values), is higher in DEMs recorded during the growing season and is lower in DEMs recorded at dates outside of the growing season. The comparison of elevation change between pairs of DEMs showed alternating decrease and increase of elevation in different areas of the catchment. It was presumed that such an alternating elevation development can occur in erosion rill or alluvial fan areas; but that alternating elevation change does not occur in a magnitude that can be captured in the photogrammetry-based elevation data in the relatively stable interrill areas. Therefore, when all elevation differences for nodes of a TIN DEM to nodes of DEMs for previous and for subsequent dates were found to be either negative or positive; this was assumed to be indicative of implausible elevation development due to DEM errors. For nodes that met these criteria, elevation values were replaced by elevations of the DEM recorded with the smallest time lag to the processed DEM.

In a first step, the polygon datasets representing the rills' and alluvial fan's outline (Chapters 5 and 6) were used to delineate the interrill areas, i.e., the areas outside of the rills and alluvial fan in the TIN elevation models. Rill network and alluvial fan polygons were assigned to the DEMs as listed in Table A.1. Elevation differences as compared with the previous and subsequent DEMs of the time series were calculated in GOCAD. Using the 'Properties Script Editor' in GOCAD, indices were then assigned to nodes for that all elevation differences to the two previous and two subsequent DEMs were either positive or negative. Only one previous and only one subsequent DEM were used for processing the DEMs of May 2006 and December 2009, respectively. DEM nodes were then assigned to GOCAD model regions according to the indices, and elevations were replaced by those of the other DEM using the option 'Edit Remove Crossings'.

Table A.1: Rill and alluvial fan polygons and DEMs used for logical comparison and modification.

processed DEM	rill maps used to delineate the interrill area	DEMs used to calculate disttop2, disttop, distton, distto2n	DEM used to replace elevation values
May 1, 2006	Sep 22, 2006	Nov 26, 2005, Nov 3, 2006, Nov 21, 2007	Nov 26, 2005
Nov 3, 2006	Sep 22, 2006	Nov 26, 2005, May 1, 2006, Nov 21, 2007, Apr 24, 2008	May 1, 2006
Nov 21, 2007	Jun 14, 2007	May 1, 2006, Nov 3, 2006, Apr 24, 2008, Aug 18, 2008	Apr 24, 2008
Apr 24, 2008	Jul 10, 2008	Nov 3, 2006, Nov 21, 2007, Aug 18, 2008, Jun 13, 2009	Aug 18, 2008
Aug 18, 2008	Jul 10, 2008	Nov 21, 2007, Apr 24, 2008, Jun 13, 2009, Dec 5, 2009	Apr 24, 2008
Jun 13, 2009	Jul 1, 2009	Apr 24, 2008, Aug 18, 2008, Dec 5, 2009, Mar 4, 2010	Dec 5, 2009
Dec 5, 2009	Jul 1, 2009	Aug 18, 2008, Jun 13, 2009, Mar 4, 2010	Mar 3, 2010

A.3.3 Results

As a result of the modification, elevation data for nodes in interrill areas that met the inconsistency criteria were reduced or increased to the elevation of other DEMs, as listed in Table A.1 (Fig. A.7).

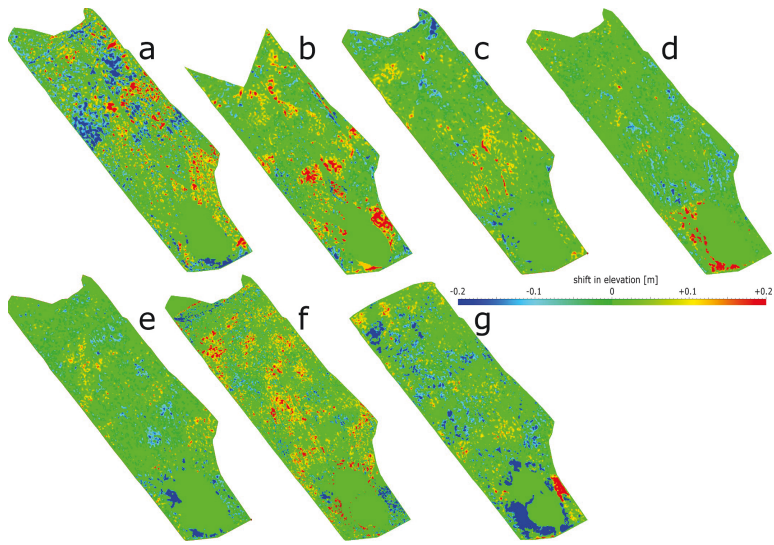

Figure A.7: Spatial distribution of vertical elevation shift as a result of DEM modification in interrill areas for the DEMs of a) 01.05.2006, b) 03.11.2006, c) 21.11.2007, d) 24.04.2008, e) 18.08.2008, f) 13.06.2009, and g) 05.12.2009.

Appendix B - List of own thematically related publications

peer reviewed publications

Gerke, H.H., Maurer, T., Schneider, A., (accepted). A 3D structure and process model for integrated hydro-geo-pedologic analysis of a constructed hydrological catchment. Vadose Zone Journal. doi: 10.216/vzj2013.02.0040

Maurer, T., Schneider, A., Gerke , H.H., 2011. A structure generator for modelling the initial sediment distribution of an artificial hydrologic catchment. Hydrology and Earth System Sciences 15: 3617-3638. doi: 10.5194/hess-15-3617-2011

Raab, T., Krümmelbein, J., Schneider, A., Gerwin, W., Maurer, T., Naeth, M. 2012. Initial Ecosystem Processes as Key Factors of Landscape Development - A Review. Physical Geography 33 (4): 305-343. doi: 10.2747/0272-3646.33.4.305

Schneider, A., Gerke, H.H., Maurer, T., Nenov, R., (2013) . Initial hydro-geomorphic development and rill network evolution in an artificial catchment. Earth Surface Processes and Landforms 38 (13), 1496-1512. doi: 10.1002/esp.3384

Schneider, A., Gerke, H.H., Maurer, T., Seifert, S., Nenov, R., Hüttl, R.F., 2012: Evaluation of remotely-sensed DEMs and modification based on plausibility rules and initial sediment budgets of an artificially-created catchment. Earth Surface Processes and Landforms, 37 (7): 708-725. doi: 10.1002/esp.2274

Schneider, A., Gerke, H.H., Maurer, T., 2011. 3D initial sediment distribution and quantification of mass balances of an artificially-created hydrological catchment based on DEMs from aerial photographs using GOCAD. Physics and Chemistry of the Earth (Special Issue: Hydrological Observations) 36 (1-4), 87-100. doi: 10.1016/f.pce.2010.03.023

other publications (first author, chronologically)

Schneider, A., Maurer, T., Gerke, H.H., 2009.Quantification of initial 3D sediment mass balance components in an artificially-created hydrologic catchment using GOCAD. Geophysical Research Abstracts, 11, A-8700.

Schneider, A., Maurer, T., Gerke, H.H., 2009. Bilanzierung der Sedimentmassen eines künstlichen Wassereinzugsgebiets mit einem 3D- Strukturmodell. Böden - eine endliche Ressource, September 2009, Bonn. available online at http://eprints.dbges.de/252/.

Schneider, A., Maurer, T., Gerke, H.H., 2010. 3D sediment mass balances of an artificially-created catchment using multi-temporal digital elevation data and GOCAD. – Geophysical Research Abstracts 12, A-2621.

Schneider, A., Gerke, H.H., Maurer, T., Nenov, R., Seifert, S., 2010. Evaluation of surface models for improving descriptions of initial changes in the 3D structure of the "'Huehnerwasser'" catchment. Proceedings of the 1st International Conference "Structures and Processes of initial ecosystem development", 20.-24.09.2010, Cottbus, Germany. pp. 17 - 18.

Schneider, A., Gerke, H.H., Maurer, T., Nenov, R., Seifert, S., 2011. Quantification of initial sediment redistribution in an artificially-created catchment using a time series of digital elevation models. Geophysical Research Abstracts 13, EGU2011-4686.

Schneider, A., Maurer, T., Gerke, H.H., 2011. 3D-räumliche Beschreibung initialer Sedimentumverteilung in einem künstlichen Einzugsgebiet. In: Böden verstehen - Böden nutzen - Böden fit machen, 3. - 9. September 2011, Berlin. available online at http://eprints.dbges.de/546/.

Schneider, A., Maurer, T. Gerke, H.H., 2011. Aspects of initial surface development. In: M. Elmer, W. Schaaf, D. Biemelt, W. Gerwin and R.F. Hüttl (Editors), The artificial catchment 'Chicken Creek' – initial ecosystem development 2005-2010. Ecosystem Development 3, pp. 11-32. urn:nbn:de:kobv:co1-opus-23730.

Schneider, A., Gerke, H.H., Maurer, T., Nenov, R., Raab, T., 2011.Hydro-geomorphic differentiation of an artificial catchment during the initial phase of ecosystem development, AGU Fall Meeting, San Francisco, California, H31A-1134.

Schneider, A., Gerke, H.H., 2013. Initial phases of surface development in a constructed hydrological catchment using the CAESAR landscape evolution model. Geophysical Research Abstracts 15, EGU2013-5293.

Schneider, A., Gerke, H.H., Maurer, T., Nenov, R., Raab, T., 2013. Analysis of initial drainage network evolution from aerial photography and a DEM time series. Geophysical Research Abstracts 15, EGU2013-5264.

Bibliography

Abdul-Rahman, A. and Pilouk, M., 2008. Spatial Data Modelling for 3D GIS. Springer, Berlin, Heidelberg, New York, 289 pp.

Aber, J.S., Marzolff, I. and Ries, J.B., 2010. Small-format aerial photography - principles, techniques and geoscience applications. Elsevier Science, Amsterdam, 266 pp.

Abrahams, A.D., Li, G. and Parsons, A.J., 1996. Rill hydraulics on a semiarid hillslope, southern Arizona. Earth Surface Processes and Landforms 21(1): 35-47.

Abrahams, A.D., Parsons, A.J. and Wainwright, J., 1995. Effects of vegetation change on interrill runoff and erosion, Walnut Gulch, southern Arizona. Geomorphology 13(1-4): 37-48.

Adams, J. and Chandler, J., 2002. Evaluation of Lidar and Medium Scale Photogrammetry for Detecting Soft-Cliff Coastal Change. The Photogrammetric Record 17(99): 405-418.

Ahnert, F., 1994. Equilibrium, scale and inheritance in geomorphology. Geomorphology 11 (2): 125-140.

Aksoy, H. and Kavvas, M.L., 2005. A review of hillslope and watershed scale erosion and sediment transport models. CATENA 64(2-3): 247-271.

Alms, R., Balovnev, O., Breunig, M., Cremers, A.B., Jentzsch, T. and Siehl, A., 1998. Space-time modelling of the Lower Rhine Basin supported by an object-oriented database. Physics and Chemistry of The Earth 23(3): 251-260.

Anderson, S.P., Bales, R.C. and Duffy, C.J., 2008. Critical Zone Observatories: Building a network to advance interdisciplinary study of Earth surface processes. Mineralogical Magazine 72(1): 7-10.

Armstrong, M.J. and Bragg, N.C., 1984. Soil physical parameters and earthworm populations associated with opencast coal working and land restoration. Agriculture Ecosystems & Environment 11(2): 131-143.

Auzet, A.V., Poesen, J. and Valentin, C., 2004. Editorial: Soil surface characteristics: Dynamics and impacts on soil erosion. Earth Surface Processes and Landforms 29(9): 1063-1064.

Baas, A.C.W., 2002. Chaos, fractals and self-organization in coastal geomorphology: simulating dune landscapes in vegetated environments. Geomorphology 48(1-3): 309-328.

Badorreck, A., Gerke, H.H. and Hüttl, R.F., 2012. Effects of Ground-Dwelling Beetle Burrows on Infiltration Patterns and Pore Structure of Initial Soil Surfaces. Vadose Zone Journal 11(1).

Badorreck, A., Gerke, H.H. and Hüttl, R.F., 2013. Morphology of physical soil crusts and infiltration patterns in an artificial catchment. Soil and Tillage Research 129(0): 1-8.

Baetz, N., 2010. Predicting ecological diversity of floodplains using a hydromorphic model (CAESAR) : a reduced complexity approach on reach scale for the Tagliamento River. Master Thesis Thesis, Wageningen University, 110 pp. http://library.wur.nl/WebQuery/clc/-1959681.

Baily, B., Collier, P., Farres, P., Inkpen, R. and Pearson, A., 2003. Comparative assessment of analytical and digital photogrammetric methods in the construction of DEMs of geomorphological forms. Earth Surface Processes and Landforms 28(3): 307-320.

Ballantyne, C.K., 2002. Paraglacial geomorphology. Quaternary Science Reviews 21(18-19): 1935-2017.

Baltsavias, E.P., 1999. A comparison between photogrammetry and laser scanning. ISPRS Journal of Photogrammetry and Remote Sensing 54(2-3): 83-94.

Bar, K., Arndt, D., Fritsche, J.G., Gotz, A.E., Kracht, M., Hoppe, A. and Sass, I., 2011. 3D modeling of the deep geothermal Potential of Hesse - Input data and Potential expulsion. Zeitschrift Der Deutschen Gesellschaft Fur Geowissenschaften 162(4): 371-388.

Barneveld, R.J., Seeger, M. and Maalen-Johansen, I., 2013. Assessment of terrestrial laser scanning technology for obtaining high-resolution DEMs of soils. Earth Surface Processes and Landforms 38(1): 90-94.

Baruch, A. and Filin, S., 2011. Detection of gullies in roughly textured terrain using airborne laser scanning data. ISPRS Journal of Photogrammetry and Remote Sensing 66(5): 564-578.

Benda, L., 2008. Confluence Environments at the Scale of River Networks. In: S.P. Rice, A.G. Roy and B.L. Rhoads (Editors), River Confluences, Tributaries and the Fluvial Network. John Wiley & Sons, Ltd, pp. 271-300.

Berger, C., Schulze, M., Rieke-Zapp, D. and Schlunegger, F., 2010. Rill development and soil erosion: a laboratory study of slope and rainfall intensity. Earth Surface Processes and Landforms 35(12): 1456-1467.

Betts, H.D. and DeRose, R.C., 1999. Digital elevation models as a tool for monitoring and measuring
gully erosion. International Journal of Applied Earth Observation and Geoinformation 1(2): 91-101.

Betts, H.D., Trustrum, N.A. and De Rose, R.C., 2003. Geomorphic changes in a complex gully system measured from sequential digital elevation models, and implications for management. Earth Surface Processes and Landforms 28(10): 1043-1058.

Beven, K., 1996. Equifinality and uncertainty in geomorphological modelling. In: B.L. Rhoads and C.E. Thorn (Editors), The Scientific Nature of Geomorphology: Proceedings of the 27th Binghamton Symposium in Geomorphology. Wiley, Chichester, U.K., pp. 289-314.

Beven, K., 1997. TOPMODEL: A critique. Hydrological Processes 11(9): 1069-1085.

Beven, K. and Kirkby, M., 1979. A Physically Based, Variable Contributing Area Model of Basin Hydrology. Hydrological Sciences Bulletin 24(1): 43-69.

Biber, P., Seifert, S., Zaplata, M., Schaaf, W., Pretzsch, H. and Fischer, A., 2013. Relationships between substrate, surface characteristics, and vegetation in an initial ecosystem. Biogeosciences Discusssions 10: 4733-4780.

Biemelt, D. and Nenov, R., 2010. Meteorology. In: W. Schaaf, D. Biemelt and R.F. Hüttl (Editors), Initial development of the artificial catchment 'Chicken Creek' – monitoring program and survey 2005-2008. Ecosystem Development 2, pp. 9-19.

Biemelt, D., Schaaf, W. and Mazur, K., 2011. Water budget components. In: M. Elmer, W. Schaaf, D. Biemelt, W. Gerwin and R.F. Hüttl (Editors), The artificial catchment 'Chicken Creek' - initial ecosystem development 2005 - 2010. Ecosystem Development 3, pp. 33-54.

Biemelt, D., Schapp, A., Kleeberg, A. and Grünewald, U., 2005. Overland flow, erosion, and related phosphorus and iron fluxes at plot scale: a case study from a non-vegetated lignite mining dump in Lusatia. Geoderma 129(1-2): 4-18.

Bird, S., Hogan, D. and Schwab, J., 2010. Photogrammetric monitoring of small streams under a riparian forest canopy. Earth Surface Processes and Landforms 35(8): 952-970.

Birkeland, P.W., 1984. Soils and Geomorphology. Oxford University Press, New York, N.Y., 372 pp.

Birkeland, P.W., 1990. Soil-geomorphic research - a selective overview. Geomorphology 3 (3-4): 207-224.

Bishop, J.G., 2002. Early primary succession on Mount St. Helens: Impact of insect herbivores on colonizing lupines. Ecology 83(1): 191-202.

Bistacchi, A., Griffith, W.A., Smith, S.A.F., Di Toro, G., Jones, R. and Nielsen, S., 2011. Fault Roughness at Seismogenic Depths from LIDAR and Photogrammetric Analysis. Pure and Applied Geophysics 168(12): 2345-2363.

Bistacchi, A., Massironi, M., Dal Piaz, G.V., Dal Piaz, G., Monopoli, B., Schiavo, A. and Toffolon, G., 2008. 3D fold and fault reconstruction with an uncertainty model: An example from an Alpine tunnel case study. Computers & Geosciences 34(4): 351-372.

Bogena, H., Kunkel, R., Puetz, T., Vereecken, H., Krueger, E., Zacharias, S., Dietrich, P., Wollschlaeger, U., Kunstmann, H., Papen, H., Schmid, H.P., Munch, J.C., Priesack, E., Schwank, M., Bens, O., Brauer, A., Borg, E. and Hajnsek, I., 2012. TERENO - Long-term monitoring network for terrestrial environmental research. Hydrologie Und Wasserbewirtschaftung 56(3): 138-143.

Borselli, L., Cassi, P. and Torri, D., 2008. Prolegomena to sediment and flow connectivity in the landscape: A GIS and field numerical assessment. CATENA 75(3): 268-277.

Bowman, D., Devora, S. and Svoray, T., 2011. Drainage organization on the newly emerged Dead Sea bed, Israel. Quaternary International 233(1): 53-60.

Brasington, J., Langham, J. and Rumsby, B., 2003. Methodological sensitivity of morphometric estimates of coarse fluvial sediment transport. Geomorphology 53(3-4): 299-316.

Brasington, J., Rumsby, B.T. and R. A. McVey, R.A., 2000. Monitoring and modelling morphological change in a braided gravel-bed river using high resolution GPS-based survey. Earth Surface Processes and Landforms 25(9): 973-990.

Brasington, J. and Smart, R.M.A., 2003. Close range digital photogrammetric analysis of experimental drainage basin evolution. Earth Surface Processes and Landforms 28(3): 231-247.

Braun, J. and Sambridge, M., 1997. Modelling landscape evolution on geological time scales: a new method based on irregular spatial discretization. Basin Research 9(1): 27-52.

Breunig, M. and Zlatanova, S., 2011. 3D geo-database research: Retrospective and future directions. Computers & Geosciences 37(7): 791-803.

Brown, A.G., Carey, C., Erkens, G., Fuchs, M., Hoffmann, T., Macaire, J.-J., Moldenhauer, K.-M. and Walling, D.E., 2009. From sedimentary records to sediment budgets: Multiple approaches to catchment sediment flux. Geomorphology 108(1-2): 35-47.

Brunsden, D. and Thornes, J.B., 1979. Landscape sensitivity and change. Transactions of the Institute of British Geographers 4(4): 463-484.

Brunton, D.A. and Bryan, R.B., 2000. Rill network development and sediment budgets. Earth Surface Processes and Landforms 25(7): 783-800.

Bryan, R.B., 2000. Soil erodibility and processes of water erosion on hillslope. Geomorphology 32(3-4): 385-415.

Bryan, R.B. and Jones, J.A.A., 1997. The significance of soil piping processes: inventory and prospect. Geomorphology 20(3-4): 209-218.

Bryan, R.B. and Rockwell, D.L., 1998. Water table control on rill initiation and implications for erosional response. Geomorphology 23(2-4): 151-169.

Buczko, U. and Gerke, H.H., 2005. Estimating spatial distributions of hydraulic parameters for a two-scale structured heterogeneous lignitic mine soil. Journal of Hydrology 312(1-4): 109-124.

Buczko, U., Gerke, H.H. and Hüttl, R.F., 2001. Spatial distributions of lignite mine spoil properties for simulating 2-D variably saturated flow and transport. Ecological Engineering 17(2-3): 103-114.

Bull, W.B., 1997. Discontinuous ephemeral streams. Geomorphology 19(3-4): 227-276.

Bürgi, M., Hersperger, A. and Schneeberger, N., 2004. Driving forces of landscape change - current and new directions. Landscape Ecology 19(8): 857-868.

Burnett, M.R., August, P.V., Brown, J.H., Jr and Killingbeck, K.T., 1998. The Influence of Geomorphological Heterogeneity on Biodiversity I. A Patch-Scale Perspective. Conservation Biology 12(2): 363-370.

Callow, J.N., Van Niel, K.P. and Boggs, G.S., 2007. How does modifying a DEM to reflect known hydrology affect subsequent terrain analysis? Journal of Hydrology 332(1-2): 30-39.

Carbonneau, P., Fonstad, M.A., Marcus, W.A. and Dugdale, S.J., 2012. Making riverscapes real. Geomorphology 137(1): 74-86

Casalí, J., Loizu, J., Campo, M.A., De Santisteban, L.M. and Álvarez-Mozos, J., 2006. Accuracy of methods for field assessment of rill and ephemeral gully erosion. CATENA 67(2): 128-138.

Cavazzi, S., Corstanje, R., Mayr, T., Hannam, J. and Fealy, R., 2013. Are fine resolution digital elevation models always the best choice in digital soil mapping? Geoderma 195-196(0): 111-121.

Cazorzi, F., Fontana, G.D., Luca, A.D., Sofia, G. and Tarolli, P., 2013. Drainage network detection and assessment of network storage capacity in agrarian landscape. Hydrological Processes 27(4): 541-553.

Chandler, J., 1999. Effective application of automated digital photogrammetry for geomorphological research. Earth Surface Processes and Landforms 24(1): 51-63.

Chandler, J., Ashmore, P., Paola, C., Gooch, M. and Varkaris, F., 2002. Monitoring river-channel change using terrestrial oblique digital imagery and automated digital photogrammetry. Annals of the Association of American Geographers 92(4): 631-644.

Chapin, F.S., Walker, L.R., Fastie, C.L. and Sharman, L.C., 1994. Mechamisms of primary succession following deglaciation at Glacier Bay, Alaska. Ecological Monographs 64(2): 149-175.

Chong, S.K. and Cowsert, P.T., 1997. Infiltration in reclaimed mined land ameliorated with deep tillage treatments. Soil & Tillage Research 44(3-4): 255-264.

Chorley, R., 1962. Geomorphology and general systems theory. Geological Survey professional paper 500-B, Washington, 10 pp.

Chorley, R. and Kennedy, B., 1971. Physical Geography. A Systems Approach. Prentice-Hall International, London, 370 pp.

Church, M., 2003. What is a Geomorphological Prediction? In: P.R. Wilcock and R.M. Iverson (Editors), Prediction in Geomorphology. Geophysical Monograph 135, American Geophysical Union, Washington, DC, pp. 183-194.

Church, M. and Ashmore, P., 1998. Sediment transport and river morphology: a paradigm for study. In: K. P.C., R.L. Beschta, P.D. Komar and J.B. Bradley (Editors), Gravel-Bed Rivers in the Environment. Water Resources Publications, LLC, Highlands Ranch, CO, pp. 115-148.

Church, M. and Ryder, J.M., 1972. Paraglacial Sedimentation: A Consideration of Fluvial Processes Conditioned by Glaciation. Geological Society of America Bulletin 83(10): 3059-3072.

Cohen, S., Svoray, T., Laronne, J.B. and Alexandrov, Y., 2008. Fuzzy-based dynamic soil erosion model (FuDSEM): Modelling approach and preliminary evaluation. Journal of Hydrology 356(1-2): 185-198.

Collins, B.D., Brown, K.M. and Fairley, H.C., 2008. Evaluation of terrestrial LIDAR for monitoring geomorphic change at archaeological sites in Grand Canyon National Park, Arizona. U.S. Geological Survey, Open-File Report 2008-1384, 60 pp.

Collins, D.B.G., Bras, R.L. and Tucker, G.E., 2004. Modeling the effects of vegetation-erosion coupling on landscape evolution. Journal of Geophysical Research - Earth Surface. 109 (F3).

Coors, V. and Zipf, A. (Editors), 2005. 3D-Geoinformationssysteme. Grundlagen und Anwendungen. Wichmann, Heidelberg, 522 pp.

Corenblit, D., Baas, A.C.W., Bornette, G., Darrozes, J., Delmotte, S., Francis, R.A., Gurnell, A.M., Julien, F., Naiman, R.J. and Steiger, J., 2011. Feedbacks between geomorphology and biota controlling Earth surface processes and landforms: A review of foundation concepts and current understandings. Earth-Science Reviews 106(3-4): 307-331.

Corenblit, D., Tabacchi, E., Steiger, J. and Gurnell, A.M., 2007. Reciprocal interactions and adjustments between fluvial landforms and vegetation dynamics in river corridors: A review of complementary approaches. Earth-Science Reviews 84(1-2): 56-86.

Cosandey, A.-C., Guenat, C., Bouzelboudjen, M., Maître, V. and Bovier, R., 2003. The modelling of soil-process functional units based on three-dimensional soil horizon cartography, with an example of denitrification in a riparian zone. Geoderma 112(1-2): 111-129.

Coulthard, T.J., 2001. Landscape evolution models: a software review. Hydrological Processes 15(1): 165-173.

Coulthard, T.J., 2005. Entry in the CAESAR discussion board. http://www.coulthard.org.uk/discus/messages/3/16.html?1183973364, last update: 09.07. 2007. accessed 22.03.2013.

Coulthard, T.J., 2010. Entry in the CAESAR discussion board. http://www.coulthard.org.uk/discus/messages/45/129.html?1288550405, last update: 31.10. 2010. accessed 22.03.2013.

Coulthard, T.J., Hancock, G.R. and Lowry, J.B.C., 2012. Modelling soil erosion with a downscaled landscape evolution model. Earth Surface Processes and Landforms 37(10): 1046-1055.

Coulthard, T.J., Hicks, D.M. and Van De Wiel, M.J., 2007. Cellular modelling of river catchments and reaches: Advantages, limitations and prospects. Geomorphology 90(3-4): 192-207.

Coulthard, T.J., Macklin, M.G. and Kirkby, M.J., 2002. A cellular model of Holocene upland river basin and alluvial fan evolution. Earth Surface Processes and Landforms 27(3): 269-288.

Coulthard, T.J. and Wiel, M.J.V.D., 2006. A cellular model of river meandering. Earth Surface Processes and Landforms 31(1): 123-132.

Croke, J., Mockler, S., Fogarty, P. and Takken, I., 2005. Sediment concentration changes in runoff pathways from a forest road network and the resultant spatial pattern of catchment connectivity. Geomorphology 68(3-4): 257-268.

Culling, W.E.H., 1957. Multicyclic streams and the equilibrium theory of grade. Journal of Geology 65(3): 259-274.

Culling, W.E.H., 1987. Equifinality - modern approaches to dynamic-systems and their potential for geographical thought. Transactions of the Institute of British Geographers 12(1): 57-72.

Curry, A.M., Cleasby, V. and Zukowskyj, P., 2006. Paraglacial response of steep, sediment-mantled slopes to post-'Little Ice Age' glacier recession in the central Swiss Alps. Journal of Quaternary Science 21(3): 211-225.

Cutler, N.A., Belyea, L.R. and Dugmore, A.J., 2008. The spatiotemporal dynamics of a primary succession. Journal of Ecology 96(2): 231-246.

Davis, W.M., 1899. The geographical cycle. Geography Journal 14: 481-504.

Day, S.S., Gran, K.B., Belmont, P. and Wawrzyniec, T., 2012. Measuring bluff erosion part 1: terrestrial laser scanning methods for change detection. Earth Surface Processes and Landforms: in press, available online. doi: 10.1002/esp.3353.

De Oro, L.A. and Buschiazzo, D.E., 2009. Threshold wind velocity as an index of soil susceptiblility to wind erosion under variable climatic conditions. Land Degradation & Development 20(1): 14-21.

Delarue, F., Cornu, S., Daroussin, J., Salvador-Blanes, S., Bourennane, H., Albéric, P., Vennink, A., Bruand, A. and King, D., 2009. 3D representation of soil distribution: An approach for understanding pedogenesis. Comptes Rendus Geosciences 341(6): 486-494.

DeRoo, A.P.J., Wesseling, C.G., Jetten, V.G. and Ritsema, C.J., 1996. LISEM: A physically-based hydrological and soil erosion model incorporated in a GIS. In: K. Kovar and H.P. Nachtnebel (Editors), Conference on the Application of Geographic Information Systems in Hydrology and Water Resources Management (HydroGIS 96), Vienna, Austria, pp. 395-403.

Derose, R.C., Gomez, B., Marden, M. and Trustrum, N.A., 1998. Gully erosion in Mangatu Forest, New Zealand, estimated from digital elevation models. Earth Surface Processes and Landforms 23(11): 1045-1053.

Desir, G. and Marín, C., 2007. Factors controlling the erosion rates in a semi-arid zone (Bardenas Reales, NE Spain). CATENA 71(1): 31-40.

Desmet, P.J.J. and Govers, G., 1997. Two-dimensional modelling of the within-field variation in rill and gully geometry and location related to topography. CATENA 29(3-4): 283-306

Dietrich, W.E., Bellugi, D.G., Sklar, L.S., Stock, J.D., Heimsath, A.M. and Roering, J.J., 2003. Geomorphic Transport Laws for Predicting Landscape Form and Dynamics. In: P. Wilcock and R.M. Iverson (Editors), Prediction in Geomorphology. Geophysical Monograph Series 135, AGU, Washington D.C., pp. 103-132.

Dietrich, W.E. and Dunne, T., 1978. Sediment budget for a small catchment in mountainous terrain Zeitschrift für Geomorphologie N.F. Supplement-Band 29: 191-206.

Dietrich, W.E., Wilson, C.J., Montgomery, D.R., McKean, J. and Bauer, R., 1992. Erosion thresholds and land surface morphology. Geology 20(8): 675-679.

Dominik, R., 2007. Multitemporale Analyse Digitaler Geländemodelle - Rekonstruktion des inneren Aufbaus des künstlichen Einzugsgebiets "'Hühnerwasser"' (Multi-temporal Analysis of Digital Elevation Models). Master Thesis, Chair of Soil Protection and Recultivation, BTU Cottbus (in German).

Douglass, J. and Schmeeckle, M., 2007. Analogue modeling of transverse drainage mechanisms. Geomorphology 84(1-2): 22-43.

Dunne, T., 1980. Formation and controls of channel networks. Progress in Physical Geography 4(2): 211-239.

Einstein, H.A., 1950. The bed-load function for sediment transport on open channel flows. USDA, Soil Conservation Service, Technical Bulletin 1026.

Elmer, M., Gerwin, W., Schaaf, W., Zaplata, M., Hohberg, K., Nenov, R., Bens, O. and Hüttl, R., 2013. Dynamics of initial ecosystem development at the artificial catchment Chicken Creek, Lusatia, Germany. Environmental Earth Sciences: 1-15.

Elshorbagy, A. and Barbour, S.L., 2007. Probabilistic approach for design and hydrologic performance assessment of reconstructed watersheds. Journal of Geotechnical and Geoenvironmental Engineering 133(9): 1110-1118.

Erdoğan, S., 2010. Modelling the spatial distribution of DEM error with geographically weighted regression: An experimental study. Computers & Geosciences 36(1): 34-43.

Evans, K.G. and Willgoose, G.R., 2000. Post-mining landform evolution modelling: 2. Effects of vegetation and surface ripping. Earth Surface Processes and Landforms 25(8): 803-823.

Evans, M. and Lindsay, J., 2010. High resolution quantification of gully erosion in upland peatlands at the landscape scale. Earth Surface Processes and Landforms 35(8): 876-886.

Evans, R. and Taylor, J., 1995. Some methods of directly assessing water erosion of cultivated land - a comparison of measurements made on plots and in fields. Progress in Physical Geography 19(1): 115-129.

FAO, 1965. Soil Erosion by Water: Some Measures for its Control on Cultivated Lands. FAO/UNESCO, Rome, 288 pp.

Fath, B.D., Jørgensen, S.E., Patten, B.C. and Straškraba, M., 2004. Ecosystem growth and development. Biosystems 77(1-3): 213-228.

Faulkner, H., 2008. Connectivity as a crucial determinant of badland morphology and evolution. Geomorphology 100(1-2): 91-103.

Favis-Mortlock, D., 1998. A self-organizing dynamic systems approach to the simulation of rill initiation and development on hillslopes. Computers & Geosciences 24(4): 353-372.

Favis-Mortlock, D.T., Boardman, J., Parsons, A.J. and Lascelles, B., 2000. Emergence and erosion: a model for rill initiation and development. Hydrological Processes 14(11-12): 2173-2205.

Feine, S.C., 2007. Neandertal - three-dimensional analysis of the sediments containing finds with GoCAD and typological description of the Upper Palaeolithic inventory. Archäologisches Korrespondenzblatt 37(3): 347-363.

Fischer, T., Veste, M., Schaaf, W., Dümig, A., Kögel-Knabner, I., Wiehe, W., Bens, O. and Hüttl, R., 2010. Initial pedogenesis in a topsoil crust 3 years after construction of an artificial catchment in Brandenburg, NE Germany. Biogeochemistry 101(1): 165-176.

Fischer, T., Veste, M., Wiehe, W. and Lange, P., Water repellency and pore clogging at early successional stages of microbiotic crusts on inland dunes, Brandenburg, NE Germany. CATENA 80(1): 47-52.

Fisher, P.E. and Tate, N.J., 2006. Causes and consequences of error in digital elevation models. Progress in Physical Geography 30(4): 467-489.

Fisher, S.G., Heffernan, J.B., Sponseller, R.A. and Welter, J.R., 2007. Functional ecomorphology: Feedbacks between form and function in fluvial landscape ecosystems. Geomorphology 89(1-2): 84-96.

Florinsky, I.V., 1998. Combined analysis of digital terrain models and remotely sensed data in landscape investigations. Progress in Physical Geography 22(1): 33-60.

Förster, H. and Wunderlich, J., 2009. Holocene sediment budgets for upland catchments: The problem of soilscape model and data availability. CATENA 77(2): 143-149.

Foufoula-Georgiou, E. and Vuruputur, V., 2000. Patterns and Organisation in Precipitation. In: R. Grayson and G. Blöschl (Editors), Spatial Patterns in Catchment Hydrology - Observations and Modelling. Cambridge University Press, Cambridge, pp. 82-104.

Freeman, T.G., 1991. Calculating catchment-area with divergent flow based on a regular grid. Computers & Geosciences 17(3): 413-422.

Fridriksson, S., 1987. Plant Colonization of a volcanic island, Surtsey, Iceland. Arctic and Alpine Research 19(4): 425-431.

Fryer, J.G., Chandler, J.H. and Cooper, M.A.R., 1994. On the accuracy of heighting from aerial photographs and maps - implications to process modellers. Earth Surface Processes and Landforms 19(6): 577-583.

Fuller, I.C., Large, A.R.G., Charlton, M.E., Heritage, G.L. and Milan, D.J., 2003. Reach-scale sediment transfers: an evaluation of two morphological budgeting approaches. Earth Surface Processes and Landforms 28(8): 889-903.

Gallart, F., Marignani, M., Pérez-Gallego, N., Santi, E. and Maccherini, S., 2013. Thirty years of studies on badlands, from physical to vegetational approaches. A succinct review. CATENA 106: 4-11.

Gascuel-Odoux, C., Weiler, M. and Molenat, J., 2010. Effect of the spatial distribution of physical aquifer properties on modelled water table depth and stream discharge in a headwater catchment. Hydrology and Earth System Sciences 14(7): 1179-1194.

Gaucherel, C. and Houet, T., 2009. Preface to the selected papers on spatially explicit landscape modelling: Current practices and challenges. Ecological Modelling 220(24): 3477-3480.

Gauthier, M.J., Camporese, M., Rivard, C., Paniconi, C. and Larocque, M., 2009. A modeling study of heterogeneity and surface water-groundwater interactions in the Thomas Brook catchment, Annapolis Valley (Nova Scotia, Canada). Hydrology and Earth System Sciences 13(9): 1583-1596.

Gerke, H.H., Maurer, T. and Schneider, A., 2013. A 3D structure and process model for integrated hydro-geo-pedologic analysis of a constructed hydrological catchment. accepted for publication in Vadose Zone Journal.

Gerwin, W., Raab, T., Biemelt, D., Bens, O. and Hüttl, R.F., 2009a. The artificial water catchment "Chicken Creek" as an observatory for critical zone processes and structures. Hydrol. Earth Syst. Sci. Discuss. 6: 1769 - 1795.

Gerwin, W., Schaaf, W., Biemelt, D., Elmer, M., Maurer, T. and Schneider, A., 2010. The artificial catchment 'Hühnerwasser' (Chicken Creek): construction and intial properties. Ecosystem Development 1.

Gerwin, W., Schaaf, W., Biemelt, D., Fischer, A., Winter, S. and Hüttl, R.F., 2009b. The artificial catchment "Chicken Creek" (Lusatia, Germany) - A landscape laboratory for interdisciplinary studies of initial ecosystem development. Ecological Engineering 35(12): 1786-1796.

Gerwin, W., Schaaf, W., Biemelt, D., Winter, S., Fischer, A., Veste, M. and Hüttl, R.F., 2011. Overview and first results of ecological monitoring at the artificial watershed Chicken Creek (Germany). Physics and Chemistry of the Earth, Parts A/B/C 36(1-4): 61-73.

Gessler, P.E., Chadwick, O.A., Chamran, F., Althouse, L. and Holmes, K., 2000. Modeling soil-landscape and ecosystem properties using terrain attributes. Soil Science Society of America Journal 64(6): 2046-2056.

Gilbert, G.K., 1877. Report on the Geology of the Henry Mountains. U.S. Geolographical and Geological Survey, Washington D.C., 160 pp.

Gilley, J.E., Kottwitz, E.R. and Simanton, J.R., 1990. Hydraulic charactersitics of rills. Transactions of the Asae 33(6): 1900-1906.

Gimenez, R., Marzolff, I., Campo, M.A., Seeger, M., Ries, J.B., Casali, J. and Alvarez-Mozos, J., 2009. Accuracy of high-resolution photogrammetric measurements of gullies with contrasting morphology. Earth Surface Processes and Landforms 34(14): 1915-1926.

Glock, W.S., 1931. The development of drainage systems: a synoptic view. Geographical Review 21: 475-482.

Gomez, B. and Church, M., 1989. An assessment of bed load sediment transport formulae for gravel bed rivers. Water Resources Research 25(6): 1161-1186.

Gómez, J.A., Darboux, F. and Nearing, M.A., 2003. Development and evolution of rill networks under simulated rainfall. Water Resour. Res. 39(6): 1148.

Gordon, L.M., Bennett, S.J. and Wells, R.R., 2012. Response of a soil-mantled experimental landscape to exogenic forcing. Water Resour. Res. 48(10): W10514.

Govers, G., 1992. Relationship between discharge, velocity and flow area for rills eroding loose, non-layered materials. Earth Surface Processes and Landforms 17(5): 515-528.

Govers, G., Giménez, R. and Van Oost, K., 2007. Rill erosion: Exploring the relationship between experiments, modelling and field observations. Earth-Science Reviews 84(3-4): 87-102.

Grayson, R. and Blöschl, G., 2000. Spatial Processes, Organisation and Patterns. In: R. Grayson and G. Blöschl (Editors), Spatial Patterns in Catchment Hydrology - Observations and Modelling. Cambridge University Press, Cambridge, pp. 3-16.

Greene, R.S.B. and Hairsine, P.B., 2004. Elementary processes of soil-water interaction and thresholds in soil surface dynamics: a review. Earth Surface Processes and Landforms 29(9): 1077-1091.

Grunwald, S., 2009. Multi-criteria characterization of recent digital soil mapping and modeling approaches. Geoderma 152(3-4): 195-207.

Grunwald, S., Barak, P., McSweeney, K. and Lowery, B., 2000. Soil landscape models at different scales portrayed in virtual reality modeling language. Soil Science 165(8): 598-615.

Gurnell, A., 2013. Plants as river system engineers. Earth Surface Processes and Landforms: in press, available online. doi: 10.1002/esp.3397.

Hack, J.T., 1960. Interpretation of erosional topography in humid temperate regions. American Journal of Science 258: 80-97.

Haigh, M.J., 1980. Slope retreat and gullying on revegetated surface mine dumps, Waun Hoscyn, Gwent. Earth Surface Processes 5(1): 77-79.

Hancock, G. and Willgoose, G., 2001. The interaction between hydrology and geomorphology in a landscape simulator experiment. Hydrological Processes 15(1): 115-133.

Hancock, G.R., 2005. The use of digital elevation models in the identification and characterization of catchments over different grid scales. Hydrological Processes 19(9): 1727-1749.

Hancock, G.R., 2009. A catchment scale assessment of increased rainfall and storm intensity on erosion and sediment transport for Northern Australia. Geoderma 152(3-4): 350-360.

Hancock, G.R. and Coulthard, T.J., 2012. Channel movement and erosion response to rainfall variability in southeast Australia. Hydrological Processes 26(5): 663-673.

Hancock, G.R., Coulthard, T.J., Martinez, C. and Kalma, J.D., 2011. An evaluation of landscape evolution models to simulate decadal and centennial scale soil erosion in grassland catchments. Journal of Hydrology 398(3-4): 171-183.

Hancock, G.R., Crawter, D., Fityus, S.G., Chandler, J. and Wells, T., 2008. The measurement and modelling of rill erosion at angle of repose slopes in mine spoil. Earth Surface Processes and Landforms 33(7): 1006-1020.

Hancock, G.R. and Evans, K.G., 2006. Gully position, characteristics and geomorphic thresholds in an undisturbed catchment in Northern Australia. Hydrological Processes 20(14): 2935-2951.

Hancock, G.R., Martinez, C., Evans, K.G. and Moliere, D.R., 2006a. A comparison of SRTM and high-resolution digital elevation models and their use in catchment geomorphology and hydrology: Australian examples. Earth Surface Processes and Landforms 31(11): 1394-1412.

Hancock, G.R., Nuake, J. and Fityus, S.G., 2006b. Modelling of sediment dynamics in a laboratory-scale experimental catchment. Hydrological Processes 20(1): 67-84.

Hancock, G.R., Willgoose, G.R. and Evans, K.G., 2002. Testing of the SIBERIA landscape evolution model using the Tin Camp Creek, Northern Territory, Australia, field catchment. Earth Surface Processes and Landforms 27(2): 125-143.

Hasbargen, L.E. and Paola, C., 2000. Landscape instability in an experimental drainage basin. Geology 28(12): 1067-1070.

Helming, K., Römkens, M.J.M., Prasad, S.N. and Sommer, H., 1999. Erosional development of small scale drainage networks. In: S. Hergarten and H. Neugebauer (Editors), Process Modelling and Landform Evolution. Lecture Notes in Earth Sciences Springer Berlin Heidelberg, pp. 123-145.

Hesp, P., 2002. Foredunes and blowouts: initiation, geomorphology and dynamics. Geomorphology 48(1-3): 245-268.

Hinderer, M., 2012. From gullies to mountain belts: A review of sediment budgets at various scales. Sedimentary Geology 280(0): 21-59.

Hofer, M., Lehmann, P., Biemelt, D., Stähli, M. and Krafczyk, M., 2011. Modelling subsurface drainage pathways in an artificial catchment. Physics and Chemistry of the Earth, Parts A/B/C 36(1-4): 101-112.

Hofer, M., Lehmann, P., Stähli, M., Seifert, S. and Krafczyk, M., 2012. Two approaches to modeling the initiation and development of rills in a man-made catchment. Water Resour. Res. 48(1): W01531.

Holländer, H.M., Blume, T., Bormann, H., Buytaert, W., Chirico, G.B., Exbrayat, J.-F., Gustafsson, D., Hölzel, H., Kraft, P., Stamm, C., Stoll, S., Blöschl, G. and Flühler, H., 2009. Comparative predictions of discharge from an artificial catchment (Chicken Creek) using sparse data. Hydrology and Earth System Sciences 13: 2069 - 2094.

Hölzel, H., Diekkrüger, B., Biemelt, D. and Gädeke, A., 2013. Impact of dumped sediment structures on hydrological modelling in the artificial Chicken Creek catchment, Germany. Journal of Hydrology 477(0): 189-202.

Hopp, L., Harman, C., Desilets, S.L.E., Graham, C.B., McDonnell, J.J. and Troch, P.A., 2009. Hillslope hydrology under glass: confronting fundamental questions of soil-water-biota coevolution at Biosphere 2. Hydrology and Earth System Sciences 13(11): 2105-2118.

Horton, R.E., 1945. Erosional development of streams and their drainage basins; hydrophysical approach to quantitative morphology. Geological Society of America Bulletin 56(3): 275-370.

Houben, P., Hoffmann, T., Zimmermann, A. and Dikau, R., 2006. Land use and climatic impacts on the Rhine system (RheinLUCIFS): Quantifying sediment fluxes and human impact with available data. CATENA 66(1-2): 42-52.

Howard, A.D., 1971. Simulation of stream networks by headward growth and branching. Geographical Analysis 3(1): 29-50.

Huggett, R., 2007. A history of the systems approach in geomorphology. Geomorphologie-Relief Processus Environnement(2): 145-157.

Hunter, G.J. and Goodchild, M.F., 1995. Dealing with Error in Spatial Databases: A Simple Case Study. Photogrammetric Engineering & Remote Sensing 61(5): 529 - 537.

Hüttl, R. and Weber, E., 2001. Forest ecosystem development in post-mining landscapes: a case study of the Lusatian lignite district. Naturwissenschaften 88(8): 322-329.

Hüttl, R.F. and Gerwin, W., 2005. Disturbed landscapes - development of ecosystems. Geoderma 129(1-2): 1-3.

Hutton, C., Nicholas, A. and Brazier, R., 2013. Sub-grid scale parameterisation of hillslope runoff and erosion processes for catchment scale models of semi-arid landscapes. Hydrological Processes: in press, available online. doi: 10.1002/hyp.9712.

Ijjász-Vásquez, E.J., Bras, R.L., Rodríguez-Iturbe, I., Rigon, R. and Rinaldo, A., 1993. Are river basins optimal channel networks? Advances in Water Resources 16(1): 69-79.

Innes, J.L., 1985. Lichenometric dating of debris-flow deposits on alpine colluvial fans in south-west Norway. Earth Surface Processes and Landforms 10(5): 519-524.

Istanbulluoglu, E., Tarboton, D.G., Pack, R.T. and Luce, C., 2002. A probabilistic approach for channel initiation. Water Resources Research 38(12): 61-1 - 61-14.

Istanbulluoglu, E., Tarboton, D.G., Pack, R.T. and Luce, C., 2003. A sediment transport model for incision of gullies on steep topography. Water Resources Research 39(4): 1103 - 1117.

James, A.L., McDonnell, J.J., Tromp-van Meerveld, I. and Peters, N.E., 2010. Gypsies in the palace: experimentalist's view on the use of 3-D physics-based simulation of hillslope hydrological response. Hydrological Processes 24(26): 3878-3893.

James, L.A., Hodgson, M.E., Ghoshal, S. and Latiolais, M.M., 2012. Geomorphic change detection using historic maps and DEM differencing: The temporal dimension of geospatial analysis. Geomorphology 137(1): 181-198.

James, L.A., Watson, D.G. and Hansen, W.F., 2007. Using LiDAR data to map gullies and headwater streams under forest canopy: South Carolina, USA. CATENA 71(1): 132-144.

Jenny, H., 1941. Factors of Soil Formation. McGraw-Hill, New York, 281 pp.

Jetten, V., de Roo, A. and Favis-Mortlock, D., 1999. Evaluation of field-scale and catchment-scale soil erosion models. CATENA 37(3-4): 521-541.

Jetten, V., Poesen, J., Nachtergaele, J. and van de Vlag, D., 2006. Spatial modelling of ephemeral gully incision: a combined empirical and physical approach. In: P.N. Owens and A.J. Collins (Editors), Soil erosion and sediment redistribution in river catchments: measurement, modelling and management. Cabi Publishing, Wallingford, Cambridge MA, pp. 195-206.

Joerg, P.C., Morsdorf, F. and Zemp, M., 2012. Uncertainty assessment of multi-temporal airborne laser scanning data: A case study on an Alpine glacier. Remote Sensing of Environment 127(0): 118-129.

Jones, C.G., Lawton, J.H. and Shachak, M., 1994. Organisms as ecosystem engineers. Oikos 69(3): 373-386.

Jones, J.A.A., 1987. The initiation of natural drainage networks. Progress in Physical Geography 11(2): 207-245.

Jones, R.R., Wawrzyniec, T.F., Holliman, N.S., McCaffrey, K.J.W., Imber, J. and Holdsworth, R.E., 2008. Describing the dimensionality of geospatial data in the earth sciences - Recommendations for nomenclature. Geosphere 4(2): 354-359.

Jorgensen, S.E., Patten, B.C. and Straskraba, M., 2000. Ecosystems emerging: 4. growth. Ecological Modelling 126(2-3): 249-284.

Kendall, C., McDonnell, J.J. and Gu, W.Z., 2001. A look inside 'black box' hydrograph separation models: a study at the Hydrohill catchment. Hydrological Processes 15(10): 1877-1902.

Kendzia, G., Reißmann, R. and Neumann, T., 2008. Targeted development of wetland habitats for nature conservation fed by natural inflow in the post-mining landscape of Lusatia. World of Mining - Surface & Underground 60(2): 88 - 95.

Kinnell, P.I.A., 2010. Event soil loss, runoff and the Universal Soil Loss Equation family of models: A review. Journal of Hydrology 385(1-4): 384-397.

Kirkby, M., 1995. Modelling the links between vegetation and landforms. Geomorphology 13(1-4): 319-335.

Kleeberg, A., 2011. Sediment accumulation and impact of aquatic macrophyte decomposition on sediment nutrient and metal mobilizaton in initial ecosystem development. In: M. Elmer, W. Schaaf, D. Biemelt, W. Gerwin and R.F. Hüttl (Editors), The artificial catchment 'Chicken Creek' - initial ecosystem development 2005 - 2010. Ecosystem Development 3, pp. 129-144.

Kleeberg, A., Herzog, C., Jordan, S. and Hupfer, M., 2010. What drives the evolution of the sedimentary phosphorus cycle? Limnologica - Ecology and Management of Inland Waters 40(2): 102-113.

Kleinhans, M.G., Bierkens, M.F.P. and van der Perk, M., 2010. HESS Opinions. On the use of laboratory experimentation: 'Hydrologists, bring out shovels and garden hoses and hit the dirt'. Hydrology and Earth System Sciences 14(2): 369-382.

Knox, J.C., 1972. Valley Alluvation in southwestern Wisconsin. Annals of the Association of American Geographers 62(3): 401-410.

Kohake, D.J., Hagen, L.J. and Skidmore, E.L., 2010. Wind Erodibility of Organic Soils Soil Sci. Soc. Am. J. 74(1): 250-257.

Kostic, B., Becht, A. and Aigner, T., 2005. 3-D sedimentary architecture of a Quaternary gravel delta (SW-Germany): Implications for hydrostratigraphy. Sedimentary Geology 181(3-4): 147-171.

Kuhn, N.J. and Yair, A., 2004. Spatial distribution of surface conditions and runoff generation in small arid watersheds, Zin Valley Badlands, Israel. Geomorphology 57(3-4): 183-200.

Laflen, J.M., Elliot, W.J., Flanagan, D.C., Meyer, C.R. and Nearing, M.A., 1997. WEPP - predicting water erosion using a process-based model. Journal of Soil and Water Conservation 52(2): 96-102.

Lagacherie, P., 2008. Digital Soil Mapping: A State of the Art. In: A. Hartemink, A. McBratney and M.L. Mendonça-Santos (Editors), Digital Soil Mapping with Limited Data. Springer Netherlands, pp. 3-14.

Lane, E.W., 1955. The importance of fluvial morphology in hydraulic engineering. American Society of Civil Engineering, Proceedings 81: paper 745: 1-17.

Lane, S.N., James, T.D. and Crowell, M.D., 2000. Application of Digital Photogrammetry to Complex Topography for Geomorphological Research. The Photogrammetric Record 16(95): 793-821.

Lane, S.N., Richards, K.S. and Chandler, J.H., 1994. Developments in monitoring and modelling small-scale river bed topography. Earth Surface Processes and Landforms 19(4): 349-368.

Lane, S.N., Richards, K.S. and Chandler, J.H., 1996. Discharge and sediment supply controls on erosion and deposition in a dynamic alluvial channel. Geomorphology 15(1): 1-15.

Lane, S.N., Westaway, R.M. and Murray Hicks, D., 2003. Estimation of erosion and deposition volumes in a large, gravel-bed, braided river using synoptic remote sensing. Earth Surface Processes and Landforms 28(3): 249-271.

Lang, J., Winsemann, J., Steinmetz, D., Polom, U., Pollok, L., Bohner, U., Serangeli, J., Brandes, C., Hampel, A. and Winghart, S., 2012. The Pleistocene of Schoningen, Germany: a complex tunnel valley fill revealed from 3D subsurface modelling and shear wave seismics. Quaternary Science Reviews 39: 86-105.

Larsen, L.G. and Harvey, J.W., 2010. How Vegetation and Sediment Transport Feedbacks Drive Landscape Change in the Everglades and Wetlands Worldwide. American Naturalist 176(3): E66-E79.

Lawrence, D.S.L., 1996. Physically Based Modelling and the Analysis of Landscape Development. In: B.L. Rhoads and C.E. Thorn (Editors), The Scientific Nature of Geomorphology: Proceedings of the 27th Binghamton Symposium in Geomorphology. John Wiley & Sons, pp. 273-288.

Lázaro, R., Cantón, Y., Solé-Benet, A., Bevan, J., Alexander, R., Sancho, L.G. and Puigdefábregas, J., 2008. The influence of competition between lichen colonization and erosion on the evolution of soil surfaces in the Tabernas badlands (SE Spain) and its landscape effects. Geomorphology 102(2): 252-266.

Leopold, L.B. and Langbein, W.B., 1962. The concept of entropy in landscape evolution. US Geological Survey Professional Paper 500-A: 20 pp.

Leopold, L.B., Wolman, M.G. and Miller, J.P., 1964. Fluvial Processes in Geomorphology. W.H. Freeman and Co, San Francisco, 522 pp.

Leopold, M. and Völkel, J., 2007. Colluvium: Definition, differentiation, and possible suitability for reconstructing Holocene climate data. Quaternary International 162-163(0): 133-140.

Lin, H., 2010. Linking principles of soil formation and flow regimes. Journal of Hydrology 393(1-2): 3-19.

Losier, L.M., Pouliot, J. and Fortin, M., 2007. 3D geometrical modeling of excavation units at the archaeological site of Tell 'Acharneh (Syria). Journal of Archaeological Science 34(2): 272-288.

Lubowe, J.K., 1964. Stream junction angles in the dendritic drainage pattern. American Journal of Science 262(3): 325-339.

Luhmann, T., 2000. Nahbereichsphotogrammetrie: Grundlagen, Methoden und Anwendungen. Wichmann, Heidelberg, 571 pp.

Mallet, J.-L., 1989. Discrete smooth interpolation. ACM Transactions on Graphics 8(2): 121-144.

Mallet, J.-L., 1997. Discrete modeling for natural objects. Mathematical Geology 29(2): 199-219.

Mallet, J.-L., 2004. Space-time mathematical framework for sedimentary geology. Mathematical Geology 36(1): 1-32.

Marston, R.A., 2010. Geomorphology and vegetation on hillslopes: Interactions, dependencies, and feedback loops. Geomorphology 116(3-4): 206-217.

Marston, R.A. and Pearson, M., 2004. Sediment budgets. In: A. Goudie (Editor), Encyclopedia of Geomorphology. Routledge, London, pp. 927-930.

Martin, Y., 2000. Modelling hillslope evolution: linear and nonlinear transport relations. Geomorphology 34(1-2): 1-21.

Martin, Y. and Church, M., 1997. Diffusion in Landscape Development Models: On The Nature of Basic Transport Relations. Earth Surface Processes and Landforms 22(3): 273-279.

Martinez-Casasnovas, J.A., Anton-Fernandez, C. and Ramos, M.C., 2003. Sediment production in large gullies of the Mediterranean area (NE Spain) from high-resolution digital elevation models and geographical information systems analysis. Earth Surface Processes and Landforms 28(5): 443-456.

Martinez, C., Hancock, G.R., Kalma, J.D., Wells, T. and Boland, L., 2010. An assessment of digital elevation models and their ability to capture geomorphic and hydrologic properties at the catchment scale. International Journal of Remote Sensing 31(23): 6239-6257.

Marzolff, I. and Poesen, J., 2009. The potential of 3D gully monitoring with GIS using high-resolution aerial photography and a digital photogrammetry system. Geomorphology 111(1-2): 48-60.

Marzolff, I., Ries, J.B. and Poesen, J., 2011. Short-term versus medium-term monitoring for detecting gully-erosion variability in a Mediterranean environment. Earth Surface Processes and Landforms 36(12): 1604-1623.

Maurer, T., Bartsch, R., Schneider, A., Buczko, U. and Gerke , H.H., 2011a. Modellierung der strukturellen Heterogenität in einem künstlichen Wassereinzugsgebiet und Ableitung von hydraulischen Eigenschaften mittels Pedotransferfunktionen. Böden verstehen - Böden nutzen - Böden fit machen, 3.-9.September 2011, Berlin. Berichte der DBG: ID-Code 705.

Maurer, T. and Gerke, H.H., 2008. Modelling of aeolian sediment translocation on the soil surface of a small catchment area using WEPS. Geophysical Research Abstracts, pp. EGU-2008-A-03636.

Maurer, T. and Gerke, H.H., 2011. Modelling aeolian sediment transport during initial soil development on an artificial catchment using WEPS and aerial images. Soil and Tillage Research 117(0): 148-162.

Maurer, T., Schneider, A., Buczko, U. and Gerke, H.H., 2009. A 3Dmodel describing the initial structure of an artificial hydrological catchment. Geophysical Research Abstracts, pp. EGU2009-4877-3.

Maurer, T., Schneider, A. and Gerke , H.H., 2011b. A structure generator for modelling the initial sediment distribution of an artificial hydrologic catchment. Hydrology and Earth System Sciences 15: 3617-3638.

McGuire, L.A., Pelletier, J.D., Gómez, J.A. and Nearing, M.A., 2013. Controls on the spacing and geometry of rill networks on hillslopes: Rain splash detachment, initial hillslope roughness, and the competition between fluvial and colluvial transport. Journal of Geophysical Research: Earth Surface 118(1): 241-256.

Meinsen, J., Winsemann, J., Weitkamp, A., Landmeyer, N., Lenz, A. and Dölling, M., 2011. Middle Pleistocene (Saalian) lake outburst floods in the Münsterland Embayment (NW Germany): impacts and magnitudes. Quaternary Science Reviews 30(19-20): 2597-2625.

Mendonca Santos, M.L., Guenat, C., Bouzelboudjen, M. and Golay, F., 2000. Three - dimensional GIS cartography applied to the study of the spatial variation of soil horizons in a Swiss floodplain. Geoderma 97(3-4): 351-366.

Mercier, D., Étienne, S., Sellier, D. and André, M.-F., 2009. Paraglacial gullying of sediment-mantled slopes: a case study of Colletthøgda, Kongsfjorden area, West Spitsbergen (Svalbard). Earth Surface Processes and Landforms 34(13): 1772-1789.

Merritt, W.S., Letcher, R.A. and Jakeman, A.J., 2003. A review of erosion and sediment transport models. Environmental Modelling & Software 18(8-9): 761-799.

Michael, H.A., Li, H., Boucher, A., Sun, T., Caers, J. and Gorelick, S.M., 2010. Combining geologic-process models and geostatistics for conditional simulation of 3-D subsurface heterogeneity. Water Resources Research 46 (5): W05527.

Milan, D.J., Heritage, G.L. and Hetherington, D., 2007. Application of a 3D laser scanner in the assessment of erosion and deposition volumes and channel change in a proglacial river. Earth Surface Processes and Landforms 32(11): 1657-1674.

Milan, D.J., Heritage, G.L., Large, A.R.G. and Fuller, I.C., 2010. Filtering spatial error from DEMs: Implications for morphological change estimation. Geomorphology 125(1): 160-171.

Milledge, D.G., Lane, S.N. and Warburton, J., 2009. The potential of digital filtering of generic topographic data for geomorphological research. Earth Surface Processes and Landforms 34(1): 63-74.

Milne, G., 1935. Some suggested units of classification and mapping particularly for East African soils. Soil Research 4: 183-198.

Milne, J.A. and Sear, D.A., 1997. Modelling river channel topography using GIS. International Journal of Geographical Information Science 11(5): 499-519.

Minasny, B. and McBratney, A.B., 2006. Mechanistic soil-landscape modelling as an approach to developing pedogenetic classifications: Advances in landscape-scale soil research. Geoderma 133(1-2): 138-149.

Minasny, B. and McBratney, A.B., 2007. Spatial prediction of soil properties using EBLUP with the Matérn covariance function. Geoderma 140(4): 324-336.

Minasny, B., McBratney, A.B. and Salvador-Blanes, S., 2008. Quantitative models for pedogenesis - A review: Antarctic Soils and Soil Forming Processes in a Changing Environment. Geoderma 144(1-2): 140-157.

Molina, A., Govers, G., Cisneros, F. and Vanacker, V., 2009. Vegetation and topographic controls on sediment deposition and storage on gully beds in a degraded mountain area. Earth Surface Processes and Landforms 34(6): 755-767.

Moller, P., Stubdrup, O.P. and Kronborg, C., 1995. Late Weichselian to early Holocene sedimentation in a steep fjord valley setting, Visdalen, Edgeoya, eastern svalbard: Glacial deposits, alluvial colluvial-fan deltas and spit-platforms. Polar Research 14(2): 181-203.

Montgomery, D.R., 1994. Road surface drainage, channel initiation, and slope instability. Water Resources Research 30(6): 1925-1932.

Montgomery, D.R. and Dietrich, W.E., 1989. Source Areas, Drainage Density, and Channel Initiation. Water Resources Research 25(8): 1907-1918.

Moore, I.D., Gessler, P.E., Nielsen, G.A. and Peterson, G.A., 1993. Soil Attribute Predictions Using Terrain Analysis. Soil Science Society of America Journal 57(6): 1548-1548.

Moore, I.D., Grayson, R.B. and Ladson, A.R., 1991. Digital terrain modeling - a review of hydrological, geomorphological, and biological applications. Hydrological Processes 5(1): 3-30.

Morisawa, M., 1964. Development of drainage systems on an upraised lake floor. American Journal of Science 262(3): 340-354.

Moss, A.J., Green, P. and Hutka, J., 1982. Small channels: Their experimental formation, nature, and significance. Earth Surface Processes and Landforms 7(5): 401-415.

Murray, A.B., Lazarus, E., Ashton, A., Baas, A., Coco, G., Coulthard, T., Fonstad, M., Haff, P., McNamara, D., Paola, C., Pelletier, J. and Reinhardt, L., 2009. Geomorphology, complexity, and the emerging science of the Earth's surface. Geomorphology 103(3): 496-505.

Nachtergaele, J. and J. Poesen, 1999. Assessment of soil losses by ephemeral gully erosion using high-altitude (stereo) aerial photographs. Earth Surface Processes and Landforms 24(8): 693-706.

Nearing, M.A., Norton, L.D., Bulgakov, D.A., Larionov, G.A., West, L.T. and Dontsova, K.M., 1997. Hydraulics and Erosion in Eroding Rills. Water Resour Res 33(33): 865-876.

Nichols, W.F., Killingbeck, K.T. and August, P.V., 1998. The Influence of Geomorphological Heterogeneity on Biodiversity II. A Landscape Perspective. Conservation Biology 12(2): 371-379.

Nicolau, J.M., 2002. Runoff generation and routing on artificial slopes in a Mediterranean-continental environment: the Teruel coalfield, Spain. Hydrological Processes 16(3): 631-647.

Notebaert, B., Verstraeten, G., Rommens, T., Vanmontfort, B., Govers, G. and Poesen, J., 2009. Establishing a Holocene sediment budget for the river Dijle. CATENA 77(2): 150-163.

Nouwakpo, S.K. and Huang, C.-h., 2012. The Role of Subsurface Hydrology in Soil Erosion and Channel Network Development on a Laboratory Hillslope. Soil Sci. Soc. Am. J. 76(4): 1197-1211.

Nyssen, J. and Vermeersch, D., 2010. Slope aspect affects geomorphic dynamics of coal mining spoil heaps in Belgium. Geomorphology 123(1-2): 109-121.

O'Callaghan, J.F. and Mark, D.M., 1984. The extraction of drainage networks from digital elevation data. Computer Vision, Graphics, and Image Processing 28(3): 323-344.

Odum, E.P., 1969. Strategy of ecosystem development. Science 164(3877): 262.

Otto, J.-C., Schrott, L., Jaboyedoff, M. and Dikau, R., 2009. Quantifying sediment storage in a high alpine valley (Turtmanntal, Switzerland). Earth Surface Processes and Landforms 34(13): 1726-1742.

Paik, K. and Kumar, P., 2010. Optimality approaches to describe characteristic fluvial patterns on landscapes. Philosophical Transactions of the Royal Society B-Biological Sciences 365(1545): 1387-1395.

Paola, C., Straub, K., Mohrig, D. and Reinhardt, L., 2009. The "unreasonable effectivenes" of stratigraphic and geomorphic experiments. Earth-Science Reviews 97(1-4): 1-43.

Papritz, A., Dümig, A., Zimmermann, C., Gerke, H.H., Felderer, B., Kögel-Knabner, I., Schaaf, W. and Schulin, R., 2011. Uncertainty of variance component estimates in nested sampling: a case study on the field-scale spatial variability of a restored soil. European Journal of Soil Science 62(3): 479-495.

Park, S.J. and Vlek, P.L.G., 2002. Environmental correlation of three-dimensional soil spatial variability: a comparison of three adaptive techniques. Geoderma 109(1-2): 117-140.

Parker, R.S., 1977. Experimental study of drainage basin evolution and its hydrologic implications. Hydrology Papers, Colorado State University 90, 58 pp.

Passalacqua, P., Do Trung, T., Foufoula-Georgiou, E., Sapiro, G. and Dietrich, W.E., 2010. A geometric framework for channel network extraction from lidar: Nonlinear diffusion and geodesic paths. Journal of Geophysical Research - Earth Surface 115: F01002.

Pazzaglia, F.J., 2003. Landscape evolution models. In: A.R. Gillespie, S.C. Porter and B.F. Atwater (Editors), Developments in Quaternary Sciences. Elsevier, pp. 247-274.

Pearson, S.M. and Gardner, R.H., 1997. Neutral Models: Useful Tools for Understanding Landscape Patterns. In: J.A. Bissonette (Editor), Wildlife and Landscape Ecology. Effects of Pattern and Scale. Springer, New York, Berlin, Heidelberg, Barcelona, Budapest, Hong Kong, London, Milan, Paris, Santa Clara, Singapore, Tokyo, pp. 215-230.

Pelletier, J.D., 2003. Drainage basin evolution in the Rainfall Erosion Facility: dependence on initial conditions. Geomorphology 53(1-2): 183-196.

Pelletier, J.D., 2013. A robust, two-parameter method for the extraction of drainage networks from high-resolution digital elevation models (DEMs): Evaluation using synthetic and real-world DEMs. Water Resources Research 49(1): 75-89.

Penck, W. and Penck, A., 1924. Die morphologische Analyse. Ein Kapitel der physikalischen Geologie. Engelhorn's Nachf., Stuttgart, 283 pp.

Perron, T.J. and Fagherazzi, S., 2012. The legacy of initial conditions in landscape evolution. Earth Surface Processes and Landforms 37(1): 52-63.

Perroy, R.L., Bookhagen, B., Asner, G.P. and Chadwick, O.A., 2010. Comparison of gully erosion estimates using airborne and ground-based LiDAR on Santa Cruz Island, California. Geomorphology 118(3-4): 288-300.

Phillips, J.D., 1992. The end of equilibrium? Geomorphology 5(3-5): 195-201

Phillips, J.D., 1995. Biogeomorphology and landscape evolution: The problem of scale. Geomorphology 13(1-4): 337-347.

Phillips, J.D., 2003. Sources of nonlinearity and complexity in geomorphic systems. Progress in Physical Geography 27(1): 1-23.

Phillips, J.D., 2006. Evolutionary geomorphology: thresholds and nonlinearity in landform response to environmental change. Hydrology and Earth System Sciences 10(5): 731-742.

Phillips, J.D., 2011. Emergence and pseudo-equilibrium in geomorphology. Geomorphology 132(3-4): 319-326.

Pike, R.J., Evans, I.S. and Hengl, T., 2009. Geomorphometry: A Brief Guide. In: T. Hengl and H.I. Reuter (Editors), Geomorphometry. Concepts, Software, Applications. Developments in Soil Science 33, Elsevier, pp. 3-30.

Planchon, O. and Darboux, F., 2002. A fast, simple and versatile algorithm to fill the depressions of digital elevation models. CATENA 46(2-3): 159-176.

Poesen, J., Vandaele, K. and Van Wesemael, B., 1996. Contribution of gully erosion to sediment production in cultivated lands and rangelands. In: D.E. Walling and B.W. Webb (Editors), Erosion and Sediment Yield: Global and Regional Perspectives (Proceedings of the Exeter Symposium, July 1996). IAHS Publication 236, pp. 251-266.

Prosser, I.P., Dietrich, W.E. and Stevenson, J., 1995. Flow resistance and sediment transport by concentrated overland flow in a grassland valley. Geomorphology 13(1-4): 71-86.

Raab, T., Krümmelbein, J., Schneider, A., Gerwin, W., Maurer, T. and Naeth, M., 2012. Initial Ecosystem Processes as Key Factors of Landscape Development - A Review. Physical Geography 33(4): 305-343.

Raff, D.A., Ramirez, J.A. and Smith, J.L., 2004. Hillslope drainage development with time: a physical experiment. Geomorphology 62(3-4): 169-180.

Raff, D.A., Smith, J.L. and Trlica, M.J., 2003. Statistical descriptions of channel networks and their shapes on non-vegetated hillslopes in Kemmerer, Wyoming. Hydrological Processes 17(10): 1887-1897.

Ramos, M.I., Feito, F.R., Gil, A.J. and Cubillas, J.J., 2008. A study of spatial variability of soil loss with high resolution DEMs: A case study of a sloping olive grove in southern Spain. Geoderma 148(1): 1-12.

Räpple, B., Hovy, I., Meyer, J., Giesen, R., Meier, P. and Mutz, M., 2010. Dissecting the surface - stream corridor structure in a newly created landscape, 1st International Conference on Structures and Processes of the Initial Ecosystem Development, Cottbus, Germany, p. 92.

Reid, L.M. and Dunne, T., 2003. Sediment budgets as an organizing framework in fluvial geomorphology. In: M.G. Kondolf and H. Piégay (Editors), Tools in Fluvial Geomorphology. Wiley, New York, pp. 463-500.

Reinhardt, L., Jerolmack, D., Cardinale, B.J., Vanacker, V. and Wright, J., 2010. Dynamic interactions of life and its landscape: feedbacks at the interface of geomorphology and ecology. Earth Surface Processes and Landforms 35(1): 78-101.

Renard, P. and Courrioux, G., 1994. Three-dimensional geometric modeling of a faulted domain: The Soultz Horst example (Alsace, France). Computers & Geosciences 20(9): 1379-1390.

Renwick, W.H., 1992. Equilibrium, disequilibrium, and nonequilibrium landforms in the landscape. Geomorphology 5(3-5): 265-276.

Rieke-Zapp, D.H. and Nearing, M.A., 2005. Slope shape effects on erosion: A laboratory study. Soil Science Society of America Journal 69(5): 1463-1471.

Rinaldo, A., Rodriguez-Iturbe, I., Rigon, R., Bras, R.L., Ijjasz-Vasquez, E. and Marani, A., 1992. Minimum energy and fractal structures of drainage networks. Water Resour. Res. 28(9): 2183-2195.

Risser, P.G., Karr, J.R. and Forman, R.T.T., 1983. Landscape Ecology: Directions and Approaches. . In: J.A. Wiens, M.R. Moss, M.G. Turner and D.J. Mladenoff (Editors), Foundation Papers in Landscape Ecology. Columbia Unversity Press, Chichester, West Sussex, pp. 254-264.

Ritter, J.B. and Gardner, T.W., 1993. Hydrologic evolution of drainage basins disturbed by surface mining, central Pennsylvania. Geological Society of America Bulletin 105(1): 101-115.

Robinson, G.J., 1994. The accuracy of digital elevation models derived from digitized contour data. Photogrammetric Record 14(83): 805-814.

Rodríguez-Iturbe, I., Rinaldo, A., Rigon, R., Bras, R.L., Marani, A. and Ijjász-Vásquez, E., 1992. Energy dissipation, runoff production, and the three-dimensional structure of river basins. Water Resour. Res. 28(4): 1095-1103.

Rohdenburg, H., 1971. Einführung in die klimagenetische Geomorphologie anhand eines Systems von Modellvorstellungen am Beispiel des fluvialen Abtragungsreliefs. Lenz, Giessen, 350pp.

Rommens, T., Verstraeten, G., Poesen, J., Govers, G., Van Rompaey, A., Peeters, I. and Lang, A., 2005. Soil erosion and sediment deposition in the Belgian loess belt during the Holocene: establishing a sediment budget for a small agricultural catchment. Holocene 15(7): 1032-1043.

Russell, A.J., Knight, P.G. and Van Dijk, T.A.G.P., 2001. Glacier surging as a control on the development of proglacial, fluvial landforms and deposits, Skeiðarársandur, Iceland. Global and Planetary Change 28(1-4): 163-174.

Ryder, J.M., 1971. The Stratigraphy and Morphology of Para-glacial Alluvial Fans in South-central British Columbia. Canadian Journal of Earth Sciences 8(2): 279-298.

Saco, P.M., Willgoose, G.R. and Hancock, G.R., 2007. Eco-geomorphology of banded vegetation patterns in arid and semi-arid regions. Hydrology and Earth System Sciences 11(6): 1717-1730.

Salvany, T., Lahitte, P., Nativel, P. and Gillot, P.-Y., 2012. Geomorphic evolution of the Piton des Neiges volcano (Réunion Island, Indian Ocean): Competition between volcanic construction and erosion since 1.4 Ma. Geomorphology 136(1): 132-147.

Savat, J. and De Ploey, J., 1982. Sheetwash and rill development by surface flow. In: R.B. Bryan and A. Yair (Editors), Badland Geomorphology and Piping. Geo Abstracts, Norwich, pp. 113-126.

Schaaf, W., 2001. What can element budgets of false-time series tell us about ecosystem development on post-lignite mining sites? Ecological Engineering 17(2-3): 241-252.

Schaaf, W., Elmer, M., Fischer, A., Gerwin, W., Nenov, R., Pretzsch, H., Seifert, S., Winter, S. and Zaplata, M., 2012. Monitoring the formation of structures and patterns during initial development of an artificial catchment. Environmental Monitoring and Assessment: 1-22.

Schaaf, W., Gerwin, W., Koegel-Knabner, I., Munch, J.C., Grunewald, U. and Huttl, R.F., 2008. Patterns and processes of initial ecosystem development in an artificial catchment. Geochimica et Cosmochimica Acta 72(12): A827-A827.

Scheffer, F., Schachtschabel, P. and Blume, H., 2008. Lehrbuch der Bodenkunde. 15. Aufl. Spektrum Akademischer Verlag, Heidelberg, 953 pp.

Schiefer, E. and Gilbert, R., 2007. Reconstructing morphometric change in a proglacial landscape using historical aerial photography and automated DEM generation. Geomorphology 88(1-2): 167-178.

Schindewolf, M. and Schmidt, J., 2012. Parameterization of the EROSION 2D/3D soil erosion model using a small-scale rainfall simulator and upstream runoff simulation. CATENA 91(0): 47-55.

Schlichting, E., 1993. Einführung in die Bodenkunde (Introduction into Soil Science). Parey, Hamburg, 131 pp.

Schmidt, J., Werner, M.v. and Michael, A., 1999. Application of the EROSION 3D model to the CATSOP watershed, The Netherlands. CATENA 37(3-4): 449-456.

Schmidt, S. and Götze, H.J., 1999. Integration of data constraints and potential field modelling - an example from southern lower saxony, Germany. Physics and Chemistry of the Earth, Part A: Solid Earth and Geodesy 24(3): 191-196.

Schneider, A., Gerke, H.H. and Maurer, T., 2011. 3D initial sediment distribution and quantification of mass balances of an artificially-created hydrological catchment based on DEMs

from aerial photographs using GOCAD. Physics and Chemistry of the Earth, Parts A/B/C 36(1-4): 87-100.

Schneider, A., Gerke, H.H., Maurer, T., Seifert, S., Nenov, R. and Hüttl, R.F., 2012. Evaluation of remotely-sensed DEMs and modification based on plausibility rules and initial sediment budgets of an artificially-created catchment. Earth Surface Processes and Landforms 37(7): 708-725.

Schob, A., Schmidt, J. and Tenholtern, R., 2006. Derivation of site-related measures to minimise soil erosion on the watershed scale in the Saxonian loess belt using the model EROSION 3D. CATENA 68(2-3): 153-160.

Schober, A. and Exner, U., 2011. 3D Structural modelling of an outcrop-scale fold train using photogrammetry and GPS mapping. Austrian Journal of Earth Sciences 104(2): 73-79.

Schoorl, J.M., Veldkamp, A. and Bouma, J., 2002. Modeling Water and Soil Redistribution in a Dynamic Landscape Context. Soil Sci. Soc. Am. J. 66(5): 1610-1619.

Schumm, S.A., 1956. Evolution of drainage systems and slopes in badlands at Perth-Amboy, New Jersey. Geological Society of America Bulletin 67(5): 597-646.

Schumm, S.A., 1998. To interpret the earth. Ten ways to be wrong. Cambridge University Press, Cambridge, 133 pp.

Schumm, S.A., Mosley, M.P. and Weaver, W., 1987. Experimental fluvial geomorphology. John Wiley and Sons Inc., New York, 416 pp.

Schwanghart, W. and Coulthard, T.J., 2007. Entries in the CAESAR discussion board. http://www.coulthard.org.uk/discus/messages/3/78.html?1185374112, last update: 25.07.2007. accessed 22.03.2013.

Sciuto, G. and Diekkrueger, B., 2010. Influence of Soil Heterogeneity and Spatial Discretization on Catchment Water Balance Modeling. Vadose Zone Journal 9(4): 955-969.

Seeger, M., Marzolff, I. and Ries, J.B., 2009. Identification of gully-development processes in semi-arid NE-Spain. Zeitschrift für Geomorphologie, NF 53(4): 417-431.

Seidel, J. and Mäckel, R., 2007. Holocene sediment budgets in two river catchments in the Southern Upper Rhine Valley, Germany. Geomorphology 92(3-4): 198-207.

Shaw, J.N., West, L.T., Bosch, D.D., Truman, C.C. and Leigh, D.S., 2004. Parent material influence on soil distribution and genesis in a Paleudult and Kandiudult complex, southeastern USA. CATENA 57(2): 157-174.

Sidorchuk, A., 1999. Dynamic and static models of gully erosion. CATENA 37(3-4): 401-414.

Simon, A. and Rinaldi, M., 2006. Disturbance, stream incision, and channel evolution: The roles of excess transport capacity and boundary materials in controlling channel response. Geomorphology 79(3-4): 361-383.

Slaymaker, O., 2003. The sediment budget as conceptual framework and management tool. Hydrobiologia 494(1-3): 71-82.

Smith, R.E., Goodrich, D.C. and Quinton, J.N., 1995. Dynamic, distributed simulation of watershed erosion - the KINEROS2 and EUROSEM models. Journal of Soil and Water Conservation 50(5): 517-520.

Smith, T.R. and Bretherton, F.P., 1972. Stability and the conservation of mass in drainage basin evolution. Water Resour. Res. 8(6): 1506-1529.

Soil Science Glossary Terms Committee, 2008. Glossary of soil science terms. Soil Science Society of America, 92 pp.

Sommer, M., 2006. Influence of soil pattern on matter transport in and from terrestrial biogeosystems–A new concept for landscape pedology. Geoderma 133(1-2): 107-123.

Sommer, M., Gerke, H.H. and Deumlich, D., 2008. Modelling soil landscape genesis - A "time split" approach for hummocky agricultural landscapes: Modelling Pedogenesis. Geoderma 145(3-4): 480-493.

Sprague, K., de Kemp, E., Wong, W., McGaughey, J., Perron, G. and Barrie, T., 2006. Spatial targeting using queries in a 3-D GIS environment with application to mineral exploration. Computers & Geosciences 32(3): 396-418.

Spröte, R., Fischer, T., Veste, M., Raab, T., Wiehe, W., Lange, P., Bens, O. and Huettl, R.F., 2010. Biological topsoil crusts at early successional stages on Quaternary substrates dumped by mining in Brandenburg, NE Germany. Geomorphologie-Relief Processus Environnement (4): 359-370.

Stallins, J.A., 2006. Geomorphology and ecology: Unifying themes for complex systems in biogeomorphology. Geomorphology 77(3-4): 207-216.

Stevenson, J.A., Sun, X.F. and Mitchell, N.C., 2010. Despeckling SRTM and other topographic data with a denoising algorithm. Geomorphology 114(3): 238-252.

Strahler, A.N., 1957. Quantitative analysis of watershed geomorphology. Transactions of the American Geophysical Union 8(6): 913-920.

Stroosnijder, L., 2005. Measurement of erosion: Is it possible? CATENA 64(2-3): 162-173.

Swanson, F.J., Kratz, T.K., Caine, N. and Woodmansee, R.G., 1988. Landform Effects on Ecosystem Patterns and Processes. Bioscience 38(2): 92-98.

Takken, I., Govers, G., Jetten, V., Nachtergaele, J., Steegen, A. and Poesen, J., 2001. Effects of tillage on runoff and erosion patterns. Soil and Tillage Research 61(1-2): 55-60.

Tal, M. and Paola, C., 2010. Effects of vegetation on channel morphodynamics: results and insights from laboratory experiments. Earth Surface Processes and Landforms 35(9): 1014-1028.

Tarboton, D.G., 1997. A new method for the determination of flow directions and upslope areas in grid digital elevation models. Water Resources Research 33(2): 309-319.

Taylor, J., 1997. An Introduction to Error Analysis: the Study of Uncertainties in Physical Measurements. University Science Books, Sausalito, C.A., pp. 327.

Temme, A.J.A.M., Heuvelink, G.B.M., Schoorl, J.M. and Claessens, L., 2008. Geostatistical Simulation and Error Propagation in Geomorphometry. In: T. Hengl and H.I. Reuter (Editors), Geomorphometry: Concepts, Software, and Applications. Developments in Soil Science 33, Elsevier, pp. 121-140.

Temmerman, S., Bouma, T.J., Van de Koppel, J., Van der Wal, D., De Vries, M.B. and Herman, P.M.J., 2007. Vegetation causes channel erosion in a tidal landscape. Geology 35(7): 631-634.

Thompson, J.A., Bell, J.C. and Butler, C.A., 2001. Digital elevation model resolution: effects on terrain attribute calculation and quantitative soil-landscape modeling. Geoderma 100(1-2): 67-89.

Thompson, J.A., Pena-Yewtukhiw, E.M. and Grove, J.H., 2006. Soil-landscape modeling across a physiographic region: Topographic patterns and model transportability: Advances in landscape-scale soil research. Geoderma 133(1-2): 57-70.

Thompson, J.A., Roecker, S., Grunwald, S. and Owens, P.R., 2012. Digital Soil Mapping: Interactions with and Applications for Hydropedology. In: H. Lin (Editor), Hydropedology. Academic Press, Boston, pp. 665-709.

Thornes, J.B., 1983. Evolutionary geomorphology. Geography 68(300): 225-235.

Thornes, J.B., 1985. The ecology of erosion. Geography 70(308): 222-235.

Tucker, G.E., Arnold, L., Bras, R.L., Flores, H., Istanbulluoglu, E. and Sólyom, P., 2006. Headwater channel dynamics in semiarid rangelands, Colorado high plains, USA. Geological Society of America Bulletin 118(7-8): 959-974.

Tucker, G.E. and Hancock, G.R., 2010. Modelling landscape evolution. Earth Surface Processes and Landforms 35(1): 28-50.

Tucker, G.E., Lancaster, S.T., Gasparini, N.M. and Bras, R.L., 2001. The Channel-Hillslope Integrated Landscape Development Model (CHILD). In: R.S. Harmon and W.W. Doe III (Editors), Landscape Erosion and Evolution Modeling. Kluwer Academic / Plenum Publishers, New York, pp. 349-388.

Tucker, G.E. and Slingerland, R., 1997. Drainage basin responses to climate change. Water Resour. Res. 33(8): 2031-2047.

Van De Wiel, M.J. and Coulthard, T.J., 2010. Self-organized criticality in river basins: Challenging sedimentary records of environmental change. Geology 38(1): 87-90

Van De Wiel, M.J., Coulthard, T.J., Macklin, M.G. and Lewin, J., 2007. Embedding reach-scale fluvial dynamics within the CAESAR cellular automaton landscape evolution model. Geomorphology 90(3-4): 283-301.

van Schaik, N.L.M.B., 2009. Spatial variability of infiltration patterns related to site characteristics in a semi-arid watershed. CATENA 78(1): 36-47.

Vandaele, K., Vanommeslaeghe, J., Muylaert, R. and Govers, G., 1996. Monitoring soil redistribution patterns using sequential aerial photographs. Earth Surface Processes and Landforms 21(4): 353-364.

Vandekerckhove, L., Poesen, J., Wijdenes, D.O. and Gyssels, G., 2001. Short-term bank gully retreat rates in Mediterranean environments. CATENA 44(2): 133-161.

Vanwalleghem, T., Giráldez, J.V., Jiménez-Hornero, F.J. and Laguna, A., 2009. Evaluating a general sediment transport model for linear incisions under field conditions. Earth Surface Processes and Landforms 34(14): 1852-1857.

Verstraeten, G., Rommens, T., Peeters, I., Poesen, J., Govers, G. and Lang, A., 2009. A temporarily changing Holocene sediment budget for a loess-covered catchment (central Belgium). Geomorphology 108(1-2): 24-34.

Veste, M., Seiffert, T. and Nenov, R., 2010. Microdrone-based aerial monitoring. In: W. Schaaf, D. Biemelt and R.F. Hüttl (Editors), Initial development of the artificial catchment 'Chicken Creek' - monitoring program and survey 2005-2008. Ecosystem Development 2, pp. 177-188.

Viles, H.A., 1988. Perspectives. In: H.A. Viles (Editor), Biogeomorphology. Blackwell, Oxford, pp. 351-355.

Vogel, H.-J. and Ippisch, O., 2008. Estimation of a Critical Spatial Discretization Limit for Solving Richards' Equation at Large Scales. Vadose Zone Journal 7(1): 112-114.

von Elverfeldt, K., 2012. Systemtheorie in der Geomorphologie. Problemfelder, erkenntnistheoretische Konsequenzen und praktische Implikationen. Erdkundliches Wissen 151. Franz Steiner Verlag, Stuttgart, 168 pp.

von Elverfeldt, K. and Glade, T., 2011. Systems theory in Geomorphology A challenge. Zeitschrift für Geomorphologie, Supplementbände 55(3): 87-108.

Wang, L. and Liu, H., 2006. An efficient method for identifying and filling surface depressions in digital elevation models for hydrologic analysis and modelling. International Journal of Geographical Information Science 20(2): 193-213.

Wheaton, J.M., Brasington, J., Darby, S.E. and Sear, D.A., 2010. Accounting for uncertainty in DEMs from repeat topographic surveys: improved sediment budgets. Earth Surface Processes and Landforms 35(2): 136-156.

Wiens, J.A., 2002. Riverine landscapes: taking landscape ecology into the water. Freshwater Biology 47(4): 501-515.

Wilcock, P. and Crowe, J., 2003. Surface-based Transport Model for Mixed-Size Sediment. Journal of Hydraulic Engineering 129(2): 120-128.

Willgoose, G., 1994. A physical explanation for an observed area-slope-elevation relationship for catchments with declining relief. Water Resour. Res. 30(2): 151-159.

Willgoose, G., 2005. Mathematical modeling of whole landscape evolution. Annual Review of Earth and Planetary Sciences 33: 443-459.

Willgoose, G., Bras, R.L. and Rodriguez-Iturbe, I., 1991. A coupled channel network growth and hillslope evolution model: 1. Theory. Water Resour. Res. 27(7): 1671-1684.

Willgoose, G., Bras, R.L. and Rodriguez-Iturbe, I., 1992. The relationship between catchment and hillslope properties: implications of a catchment evolution model. Geomorphology 5(1-2): 21-37.

Willgoose, G.R. and Riley, S., 1998. The long-term stability of engineered landforms of the Ranger Uranium Mine, Northern Territory, Australia: application of a catchment evolution model. Earth Surface Processes and Landforms 23(3): 237-259.

Wilson, J.P., 2012. Digital terrain modeling. Geomorphology 137(1): 107-121.

Wirtz, S., Seeger, M., Remke, A., Wengel, R., Wagner, J.F. and Ries, J.B., 2013. Do deterministic sediment detachment and transport equations adequately represent the process-interactions in eroding rills? An experimental field study. CATENA 101: 61-78.

Wirtz, S., Seeger, M. and Ries, J.B., 2010. The rill experiment as a method to approach a quantification of rill erosion process activity. Zeitschrift für Geomorphologie, NF 54(1): 47-64.

Wirtz, S., Seeger, M. and Ries, J.B., 2012. Field experiments for understanding and quantification of rill erosion processes. CATENA 91(0): 21-34.

Wise, S., 2000. Assessing the quality for hydrological applications of digital elevation models derived from contours. Hydrological Processes 14(11-12): 1909-1929.

Wise, S.M., 1998. The Effect of GIS Interpolation Errors on the Use of Digital Elevation Models in Geomorphology. In: S.N. Lane, K.S. Richards and J.H. Chandler (Editors), Landform monitoring, modelling and analysis. Wiley, Chichester, pp. 139-164

Wu, J.G. and Loucks, O.L., 1995. From balance of nature to hierarchical patch dynamics: A paradigm shift in ecology. Quarterly Review of Biology 70(4): 439-466.

Wu, S., Bras, R.L. and Barros, A.P., 2006. Sensitivity of channel profiles to precipitation properties in mountain ranges. Journal of Geophysical Research: Earth Surface 111(F1): F01024.

Wu, Y., Zheng, Q., Zhang, Y., Liu, B., Cheng, H. and Wang, Y., 2008. Development of gullies and sediment production in the black soil region of northeastern China. Geomorphology 101(4): 683-691.

Wysocki, D.A., Schoeneberger, P.J. and LaGarry, H.E., 2005. Soil surveys: a window to the subsurface. Geoderma 126(1-2): 167-180.

Yair, A., Bryan, R.B., Lavee, H., Schwanghart, W. and Kuhn, N.J., 2013. The resilience of a badland area to climate change in an arid environment. CATENA 106: 12-21.

Yoo, K., Amundson, R., Heimsath, A.M., Dietrich, W.E. and Brimhall, G.H., 2007. Integration of geochemical mass balance with sediment transport to calculate rates of soil chemical weathering and transport on hillslopes. Journal of Geophysical Research: Earth Surface 112(F2): F02013.

Zanchi, A., Francesca, S., Stefano, Z., Simone, S. and Graziano, G., 2009. 3D reconstruction of complex geological bodies: Examples from the Alps. Computers & Geosciences 35(1): 49-69.

Zanchi, A., Francesca, S., Stefano, Z., Simone, S. and Graziano, G., 2009. 3D reconstruction of complex geological bodies: Examples from the Alps. Computers & Geosciences 35(1): 49-69.

Zevenbergen, L.W. and Thorne, C.R., 1987. Quantitative analysis of land-surface topography. Earth Surface Processes and Landforms 12(1): 47-56.

Zimmermann, A., Schinn, D.S., Francke, T., Elsenbeer, H. and Zimmermann, B., 2013. Uncovering patterns of near-surface saturated hydraulic conductivity in an overland flow - controlled landscape. Geoderma 195-196(0): 1-11.

Acknowledgements

I want to thank Prof. Dr. Dr. h.c. Reinhard F. Hüttl for the opportunity to do my PhD project under his supervision, for providing the primary assessment of the dissertation, and for creating the necessary framework to carry out the work on this thesis within the CRC 38.

I thank my doctoral advisor, PD Dr. Horst H. Gerke, for the opportunity to work in the project, for his constant encouragement and advice on my work, and for his great support in preparing the publications contained in this dissertation. I am highly grateful for his supervision, which provided guidance to keep me focused on the essentials of this work, and at the same time gave me the freedom to make the topic of this dissertation my own.

I thank asst. Prof. Dr. Matthias Leopold for his willingness to act as a co-examiner of this dissertation.

I thank Prof. Dr. Thomas Raab for providing the opportunity to continue and finish the work on this dissertation at BTU Cottbus. I am even more grateful to him for making me feel welcome at BTU when I started this work, and for his constant support and encouragement through the years.

I want to thank my colleague Dr. Thomas Maurer for the valuable collaboration in the project, for fruitful discussions and for always giving an optimistic view on our work.

It would not have been possible to accomplish this dissertation without the data and information provided by Hühnerwasser catchment monitoring project. I owe thanks to many people involved in this project, who have contributed on maintaining the site and providing data over the years. I especially want to thank

- Rossen Nenov, who contributed fundamental data for this work by recording and processing GPS data and microdrone-based aerial photographs, by carrying out the mapping of erosion rills, and by providing thorough information on these and other monitoring data.
- Dr. Werner Gerwin, Michael Elmer, and apl. Prof. Dr. Wolfgang Schaaf, for making the information on the site available and accessible, and for providing helpful support with questions on site construction and monitoring.
- Dr. Detlef Biemelt and Kai Mazur, for providing most of the meteorological and hydrological monitoring data and for valuable information on the data.
- Silvio Vogt, Marin Dimitrov, and Thomas Seiffert, for carrying out field work and contributing to the processing of drone-based aerial photographs.

I thank Dr. Stefan Seifert for providing the TLS-based elevation data, and for the fruitful collaboration in the analysis of the datasets; and Dr. Alexander Dümig for providing bulk density data for the Hühnerwasser catchment.

I thank Prof. Dr. Tom J. Coulthard for helpful support with the CAESAR model application.

Working on this dissertation was made much better by the good atmosphere in the group at BTU and by the scientific and non-scientific support, encouragement, and also distraction, offered by my colleagues. Thank you all for making the office a place I enjoy to be at!

For financial support, I thank BTU Cottbus and the Transregional Collaborative Research Centre 38 (SFB/TRR 38), which is financially supported by the German Research Foundation (DFG, Bonn) and the Brandenburg Ministry of Science, Research and Culture (MWFK, Potsdam). I would also like to thank Vattenfall Europe Mining AG for providing the research site, elevation data and aerial photographs.

In dieser Reihe bereits erschienen

Raab, T., Raab, A., Gerwin, W., Schopper, F. (Hrsg., 2013): Landschaftswandel - *Landscape Change*. - GeoRS Vol. 01.

Raab, T., Hirsch, F., Raab, A., Schopper, F., Freytag, K. (Hrsg., 2013): Arbeitskreis Geoarchäologie - Jahrestagung 2013, 2. - 4.5.2013, BTU Cottbus. Tagungsband und Exkursionsführer. - GeoRS Vol. 02.